



# Development and Characterization of Selective Immunoproteasome Inhibitors

**Christian Dubiella**

Vollständiger Abdruck der von der Fakultät für Chemie der Technischen Universität München zur Erlangung des akademischen Grades eines Doktors der Naturwissenschaften (Dr. rer. nat.) genehmigten Dissertation.

Vorsitzende: Univ.-Prof. Dr. Corinna R. Hess

Prüfer der Dissertation:

1. Univ.-Prof. Dr. Michael Groll
2. Univ.-Prof. Dr. Tobias A. M. Gulder
3. Univ.-Prof. Dr. Dr. h.c. Bernhard Rieger  
(mündliche Prüfung)  
Univ.-Prof. Dr. Markus Kaiser,  
Universität Duisburg-Essen  
(schriftliche Beurteilung)

Die Dissertation wurde am 02.12.2015 bei der Technischen Universität München eingereicht und durch die Fakultät für Chemie am 17.12.2015 angenommen.



---

## Summary

20S proteasome core particles (CPs) represent the central proteolytic elements in the non-lysosomal breakdown of intracellular proteins. Based on their participation in disease-associated processes, including cell survival and the immune response, CPs emerged as validated drug-targets in the therapy of blood cancers. Clinically applied proteasome inhibitors trigger cell death by blocking both the constitutive (cCP) as well as the immunoproteasome (iCP). The resulting cytotoxicity creates the basis for the treatment of hematological malignancies. At the same time, however, it strictly limits the clinical utility of isoform unselective CP inhibitors to chemotherapy. In contrast, selective inhibition of iCPs induces cytotoxicity to a far lesser extent and has the potential to modulate chronic inflammations and autoimmune diseases, as shown previously in mouse models of rheumatoid arthritis and multiple sclerosis. However, the therapeutic window of iCP inhibitors as inflammatory agents depends entirely on their isoform selectivity. So far, the only strategy to enhance specificity focuses on the optimization of the peptide backbone of already existing inhibitors. The lack of alternative concepts is aggravated by the limited understanding of the principles underlying selective iCP blockage.

In this thesis three new concepts of selective iCP inhibition have been investigated:

- Structure-based ligand design by targeting an iCP-specific non-catalytic cysteine led to the development of the first iCP inhibitor that binds independently from the active site. This new class of peptide  $\alpha$ -chloroacetamides is highly isoform selective (> 150-fold), exhibits low cytotoxicity and suppresses the production of inflammatory cytokines in monocytes, thereby displaying anti-inflammatory agent properties. X-ray analysis of the binding mode provides a rationale for the further enhancement of specificity (Chapter 3).
- Structural and mass spectrometric analyses uncovered the binding mode of peptido sulfonyl fluorides whose action results in polarity inversion and ultimately intramolecular crosslinking of the active site. For the first time, a pharmacophore was shown to enhance iCP selectivity (28-fold) apart from the peptide backbone of the inhibitor compared to  $\alpha',\beta'$ -epoxyketone counterparts (Chapter 4).
- The development of peptide sulfonate esters as inhibitors of the cCP and iCP allowed the detection and quantification of active proteasome types. This compound class represents the first CP inhibitors whose potency is tunable by exchange of the leaving group (Chapter 5).



## Zusammenfassung

20S Proteasom Kernpartikel (KPs) stellen die zentralen, proteolytischen Elemente des nicht-lysosomalen Abbaus von intrazellulären Proteinen dar. Aufgrund ihrer Beteiligung an krankheitsassoziierten Prozessen wie dem Zellüberleben und der Immunantwort haben sich KPs zu einer etablierten Zielstruktur für Wirkstoffe in der Therapie von Blutkrebs entwickelt. Hierbei lösen klinisch angewandte Proteasom-Inhibitoren Zelltod aus indem sie das konstitutive (kKP) sowie das Immunproteasom (iKP) in gleichem Maße hemmen. Die daraus resultierende Zytotoxizität bildet die Grundlage für die Behandlung von Leukämien, jedoch beschränkt sie den klinischen Nutzen von Isoform-unspezifischen KP-Inhibitoren auf die Chemotherapie. Im Gegensatz dazu ist selektive iKP-Inhibition in geringerem Maße toxisch und hat das Potenzial chronische Entzündungen und Autoimmunkrankheiten zu beeinflussen, wie bereits für rheumatoide Arthritis und Multiple Sklerose im Mausmodell gezeigt wurde. Jedoch hängt das therapeutische Fenster von iKP-Inhibitoren als Entzündungshemmer vollständig von deren Spezifität für das Immunproteasom ab. Bisher konzentrieren sich sämtliche Strategien zur Erhöhung der Spezifität von Isotyp-selektiven Liganden auf das Optimieren des Peptidrückgrates von schon bestehenden Inhibitoren. Dabei wird das Fehlen alternativer Konzepte durch das unvollständige Verständnis der Grundprinzipien der selektiven iKP-Inhibition verschärft.

In dieser Arbeit wurden drei neue Konzepte für die spezifische iKP-Inhibition aufgeklärt:

- Struktur-basiertes Liganden-Design durch Wahl eines nicht-katalytischen Cysteins als Angriffspunkt führte zur Entwicklung des ersten iKP-Inhibitors der nicht an das aktive Zentrum bindet. Diese neue Klasse von  $\alpha$ -Chloracetamiden ist hoch Isoform-selektiv (150-fach), zeigt geringe Zytotoxizität, unterdrückt die Produktion von inflammatorischen Zytokinen von Monozyten und weist somit anti-inflammatorische Eigenschaften auf. Röntgenstrukturanalysen liefern ein Erklärungsmodell für die weitere Spezifitätserhöhung (Kapitel 3).
- Kristallographische und massenspektrometrische Analysen offenbarten den Bindemechanismus von peptidischen Sulfonylfluoriden die eine Umpolung und Quervernetzung des aktiven Zentrums des Proteasoms induzieren. Erstmals konnte gezeigt werden, dass ein Pharmakophor die iKP-Spezifität (28-fach) neben dem peptidischen Rückgrats erhöhen kann, verglichen mit ihren  $\alpha',\beta'$ -Epoxyketon-Äquivalenten (Kapitel 4).
- Die Entwicklung von peptidischen Sulfonatestern als Inhibitoren des kKP und iKP erlaubten die Detektion und Quantifizierung aktiver Proteasomisoformen, die mittels Wahl der Abgangsgruppe eingestellt werden kann (Kapitel 5).



---

## List of publications & patents

Parts of this dissertation have been published as listed below:

### *Publications in peer-reviewed journals:*

- “Selective Inhibition of the Immunoproteasome by Structure-Based Targeting of a Non-Catalytic Cysteine”  
Christian Dubiella, Regina Baur, Haissi Cui, Eva-Maria Huber & Michael Groll.  
*Angew. Chem. Int. Ed.* **2015**, doi: 10.1002/anie.201506631.
- “Selective Inhibition of the Immunoproteasome by Ligand-Induced Crosslinking of the Active Site”  
Christian Dubiella, Haissi Cui, Malte Gersch, Arwin J. Brouwer, Stephan A. Sieber, Achim Krüger, Rob M. J. Liskamp & Michael Groll.  
*Angew. Chem. Int. Ed.* **2014**, 53 (44), 11969-11973; *Angew. Chem.* **2014**, 126 (44), 12163-12167.
- “Covalent and Non-Covalent Reversible Proteasome Inhibition”  
Philipp Beck, Christian Dubiella & Michael Groll.  
*Biological Chemistry* **2012**, 393 (10), 1101-1120.
- “A Mass Spectrometry Platform for a Streamlined Investigation of Proteasome Integrity, Posttranslational Modifications, and Inhibitor Binding”  
Malte Gersch, Mathias W. Hackl, Christian Dubiella, Alexander Dobrinevski, Michael Groll & Stephan A. Sieber.  
*Chemistry & Biology* **2015**, 22 (3), 404-411.

### *Publications in progress:*

- “Tunable Inhibitors of the 20S Proteasome with Quantifiable Fluorescence Feedback”  
Christian Dubiella, Regina Baur & Michael Groll.  
manuscript in preparation.
- “Elucidation of the Binding Mode of a Selective, Non-Covalent Immunoproteasome Inhibitor”  
Regina Baur, Haissi Cui, Camille Le Chapelain, Christian Dubiella, Eva-Maria Huber, Wolfgang Heinemeyer & Michael Groll.  
manuscript in preparation.

### *Patent applications:*

- “Proteasome Inhibitor Comprising a Signal-Emitting Moiety”  
Christian Dubiella & Michael Groll.  
European Patent Application, **2015**, EP15182683.1 - 1453.

*Conferences:*

- 50<sup>th</sup> Winter Seminar on Biophysical Chemistry, Molecular Biology and Cybernetics of Cell Functions, Klosters (Switzerland), January 2015, poster presentation.
- 32<sup>nd</sup> Winter School on Proteinases and Inhibitors, Tiers (Italy), February 2015, oral presentation.

*Publications not highlighted in this work:*

- Macyranones: Structure, Biosynthesis, and Binding Mode of an Unprecedented Epoxyketone that Targets the 20S Proteasome”  
Lena Keller, Alberto Plaza, Christian Dubiella, Michael Groll, Marcel Kaiser & Rolf Müller.  
*J. Am. Chem. Soc.* **2015**, 137 (25), 8121-8130.
- “Systematic Comparison of Peptidic Proteasome Inhibitors Highlights the  $\alpha$ -Ketoamide Electrophile as an Auspicious Reversible Lead Motif”  
Martin L. Stein, Haissi Cui, Philipp Beck, Christian Dubiella, Constantin Voss, Achim Krüger, Boris Schmidt & Michael Groll.  
*Angew. Chem. Int. Ed.* **2014**, 53 (6), 1679-1683; *Angew. Chem.* **2014**, 126 (6), 1705-1709.

The present thesis has been conducted from January 2012 till December 2015 under the supervision of Prof. Dr. Michael Groll at the Chair of Biochemistry (Department of Chemistry) at the Technische Universität München.



*Meinen Eltern gewidmet*

## Table of contents

<b>Summary</b> .....	<b>iii</b>
<b>Zusammenfassung</b> .....	<b>v</b>
<b>List of publications &amp; patents</b> .....	<b>vii</b>
<b>Table of contents</b> .....	<b>x</b>
<b>1 Introduction</b> .....	<b>1</b>
1.1 Proteolysis and antigen presentation by the UPS.....	1
1.2 Structure and functions of 20S proteasomes.....	3
1.2.1 Composition and types of 20S proteasomes .....	3
1.2.2 Catalytic principle of 20S proteasomes .....	3
1.3 20S proteasomes as drug targets in cancer treatment .....	5
1.4 20S proteasome inhibitors in the clinic .....	5
1.5 $\beta$ 5i-selective inhibitors and their possible applications .....	8
1.6 References .....	10
<b>2 Objective and summary of results</b> .....	<b>13</b>
2.1 Objective .....	13
2.2 Contents .....	13
2.3 Structural rationales for the design of $\beta$ 5i-selective inhibitors.....	16
2.3.1 Peptidic $\beta$ 5i-selective inhibitors with C-terminal electrophiles .....	17
2.3.2 Peptidic $\beta$ 5i-selective inhibitors without C-terminal electrophiles .....	21
2.4 References .....	24
<b>3 Targeting a non-catalytic cysteine of subunit <math>\beta</math>5i</b> .....	<b>25</b>
3.1 Supporting information.....	33
3.1.1 Supplementary schemes .....	34
3.1.2 Supplementary figures.....	35
3.1.3 Supplementary tables.....	39
3.1.4 Supplementary in vitro methods .....	42
3.1.5 Supplementary cell culture methods.....	44
3.1.6 Supplementary chemical synthesis .....	45
3.1.7 Supplementary references.....	61
<b>4 Ligand-induced active site crosslinking of subunit <math>\beta</math>5i</b> .....	<b>63</b>
4.1 Supporting information.....	69
4.1.1 Supplementary schemes .....	70
4.1.2 Supplementary figures.....	70

---

4.1.3	Supplementary tables .....	75
4.1.4	Supplementary in vitro methods .....	77
4.1.5	Supplementary cell culture methods.....	78
4.1.6	Supplementary chemical synthesis.....	79
4.1.7	Supplementary references.....	88
<b>5</b>	<b>20S Proteasome inhibitors with fluorescent feedback .....</b>	<b>89</b>
5.1	Introduction .....	89
5.2	Results and discussion .....	90
5.3	Methods .....	95
5.4	References.....	113
<b>6</b>	<b>Abbreviations .....</b>	<b>114</b>
<b>7</b>	<b>Danksagung .....</b>	<b>117</b>
<b>8</b>	<b>Declaration .....</b>	<b>119</b>



## 1 Introduction

### 1.1 Proteolysis and antigen presentation by the UPS

Intracellular protein homeostasis constitutes an essential equilibrium between the ribosomal biosynthesis and the subsequent degradation of proteins at the end of their life cycle.<sup>[1]</sup> In cells of vertebrates, about 10% of intracellular proteins are unselectively degraded via the lysosomal pathway. The resulting peptide fragments provide building blocks and antigens for the presentation on major histocompatibility complexes (MHC) class II receptors at the cell surface of professional antigen-presenting cells.<sup>[2]</sup> In contrast, 90% of intracellular proteins are selectively degraded by the ubiquitin-proteasome system (UPS) of the non-lysosomal pathway (Figure 1.1).<sup>[3]</sup>

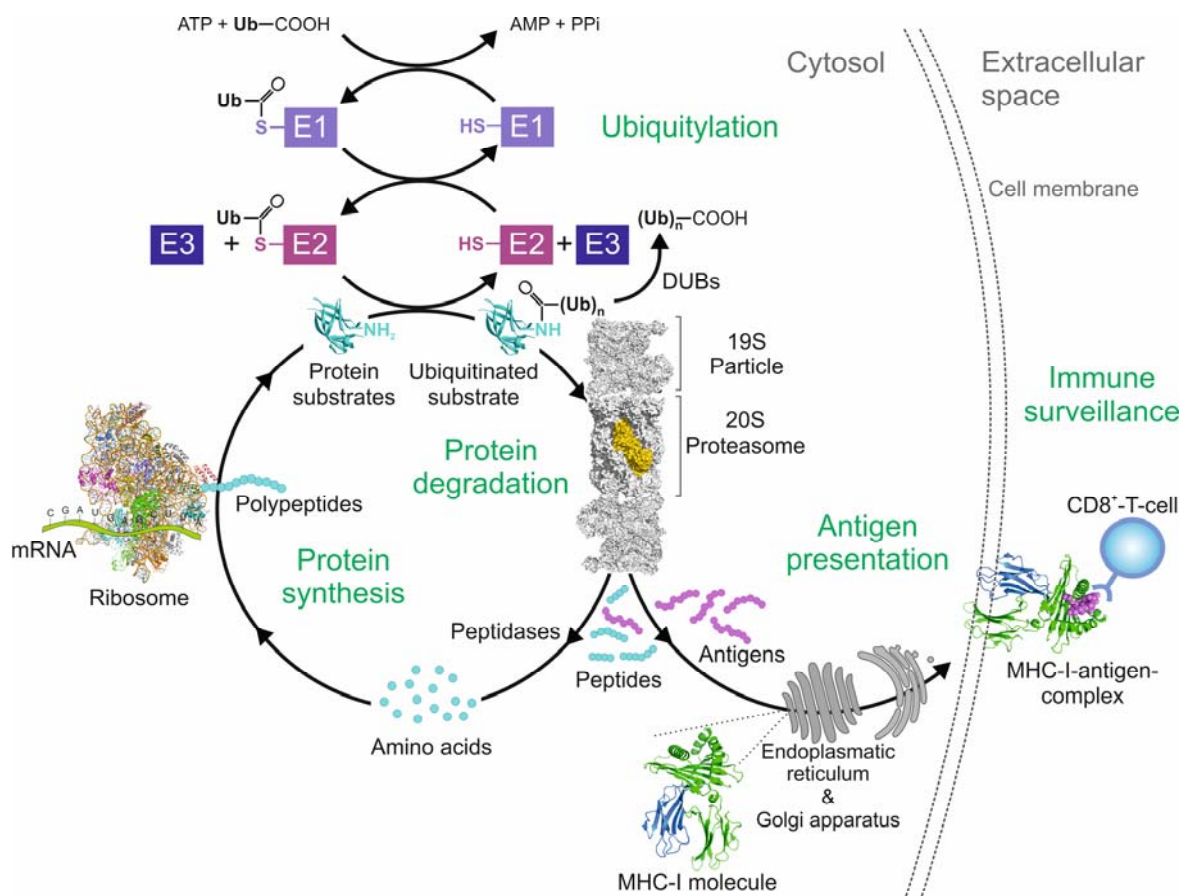


**Figure 1.1** Life cycle of proteins and degradation via the UPS. Ubiquitin (Ub) is activated in an ATP-dependent manner (E1), conjugated (E2) and ligated (E3) to a protein substrate by Ub-chain formation. Subsequent recognition by the 26S proteasome leads to substrate capture, deubiquitination by deubiquitinating enzymes (DUBs) and proteasomal degradation. The resulting oligopeptide fragments provide peptide building blocks and antigens for immune surveillance via antigen presentation on MHC-class I receptors.<sup>[4]</sup>

The UPS is strictly regulated since its substrates include not only damaged and misfolded proteins, but also mediators that are involved in cell proliferation, signal transduction and the immune response.<sup>[1]</sup> Hence, a sequential cascade of enzymes (E1-E3) ensures that only dispensable proteins are tagged with degradation signals for their breakdown by posttranslational elongation with a polyubiquitin fusion tag (Figure 1.1).<sup>[3]</sup> In the first step, ubiquitin-activating enzymes (E1) catalyze the C-terminal acyl adenylation of ubiquitin (Ub). Subsequently, the activated-thioester is transferred to a Ub-conjugating enzyme (E2) via transthioesterification. In the final step, Ub ligases (E3) covalently attach Ub to the substrate by forming an isopeptide bond between lysine side chains of the substrate and the C-terminus of Ub.<sup>[5,6]</sup> This step is of particular importance as it confers substrate specificity to the ubiquitinylation process.<sup>[7]</sup> The repetition of this procedure leads to the linear or dendrimeric polyubiquitinylation of substrates, since each Ub has seven modifiable lysine residues.<sup>[8]</sup> Consequently, the multitude of possible polyUb-tags mediates various signaling functions in the cell. Importantly, linear Ub-polymers with at least five Lys48-linked Ub-molecules serve as a signal for final degradation, which is recognized by the 26S proteasome.<sup>[3]</sup>

The 26S proteasome is a 2.5 MDa multifunctional complex, which is located in both the nucleus and the cytosol, thereby representing the proteolytic key element of the UPS.<sup>[9]</sup> It is composed of the cylindrical 20S proteasome core particle (CP) and two associated 19S regulatory particles, which are responsible for substrate recognition,<sup>[10]</sup> deubiquitination,<sup>[11,12]</sup> unfolding and translocation into the CP<sup>[13]</sup>. Inside the CP, three different proteolytic activities execute the hydrolysis of substrates into fragments with diverse lengths ranging from three to 25 amino acids.<sup>[14]</sup> While the majority of peptides produced is further digested and recycled to single amino acids by downstream peptidases, a certain fraction is used for antigen presentation.<sup>[4]</sup> These oligopeptides are transported into the endoplasmic reticulum (ER) via transporters associated with antigen processing 1 and 2 (TAP-1 & 2).<sup>[15,16]</sup> Amino-terminal trimming to a chain length of 8-11 amino acids by ER aminopeptidases ERAP1 & 2<sup>[17,18]</sup> and loading onto MHC-I receptors leads to their migration through the Golgi apparatus and, eventually, to the plasma membrane.<sup>[19]</sup> At the cell surface, cytotoxic T lymphocytes can interact with the MHC-I-antigen-complex via CD8 receptors, while scanning for antigens derived from viral and bacterial infection or neoplastic cells.<sup>[19]</sup> In the case of positive antigen recognition, the CD8<sup>+</sup>-T-cell initiates an immune response. Based on their involvement in shaping the antigen repertoire and immune signaling pathways such as nuclear factor  $\kappa$ -light-chain-enhancer of activated B cells (NF- $\kappa$ B),<sup>[20]</sup> the 20S proteasome is of utmost importance for cell survival, stress response and the adaptive immune system.<sup>[21]</sup>

## 1.2 Structure and functions of 20S proteasomes

### 1.2.1 Composition and types of 20S proteasomes

The eukaryotic 20S proteasome core particle is an approximately 720 kDa, barrel-shaped, multicatalytic complex consisting of 14 different  $\alpha$  and  $\beta$ -subunits, which are stacked to form four heptameric rings following an  $\alpha_{1-7}\beta_{1-7}\beta'_{1-7}\alpha'_{1-7}$  stoichiometry.<sup>[22]</sup> The  $\alpha$ -subunits ( $\alpha$ 1-7) are arranged to form the toroidal entry gate of the inner cavity and provide the contact surface for interactions with the 19S particle.<sup>[23,24]</sup> Similarly, the central compartment is formed by seven different  $\beta$ -subunits ( $\beta$ 1-7) arranged as a circle that includes the proteolytically active subunits  $\beta$ 1,  $\beta$ 2 and  $\beta$ 5.<sup>[22]</sup>

In vertebrates, three different proteasome types are present: the constitutive proteasome (cCP), which is expressed ubiquitously and represents the major CP type in all kind of cells, the immunoproteasome (iCP), which is primarily present in cells of hematopoietic origin like mono and lymphocytes,<sup>[21]</sup> and the thymoproteasome (tCP) found exclusively in cortical thymic epithelial cells.<sup>[25]</sup> In line with their specialized functions, their subunit composition only differs in the proteolytically relevant subunits  $\beta$ 1,  $\beta$ 2 and  $\beta$ 5, which significantly alters the substrate cleavage patterns.<sup>[26,27]</sup> The cCP features the catalytically active subunits  $\beta$ 1c (PSMB6),  $\beta$ 2c (PSMB7) and  $\beta$ 5c (PSMB5). In contrast, iCPs incorporate the subunits  $\beta$ 1i (PSMB9, LMP2),  $\beta$ 2i (PSMB10, MECL-1) and  $\beta$ 5i (PSMB8, LMP7) upon stimulation with the pro-inflammatory cytokines tumor necrosis factor  $\alpha$  (TNF- $\alpha$ ) and/or interferon gamma (IFN $\gamma$ ).<sup>[28,29]</sup> In contrast to  $\beta$ 1c,  $\beta$ 2c and  $\beta$ 5c, these cytokine-inducible  $\beta$ -subunits are predominantly expressed after stimulus exposure and are preferentially incorporated during the neosynthesis of iCPs.<sup>[30,31]</sup> However, CPs with mixed and irregular  $\beta$ -subunit composition have been described.<sup>[32,33]</sup> Apart from cCPs and iCPs, a third specialized CP type is exclusively expressed in cortical thymic epithelial cells: the tCP which contains the subunit  $\beta$ 5t (PSMB11) in addition to the subunits  $\beta$ 1i and  $\beta$ 2i.<sup>[34]</sup> It is assumed that this CP-type plays a crucial role in the positive selection of CD8<sup>+</sup>-T-cells.<sup>[25]</sup>

### 1.2.2 Catalytic principle of 20S proteasomes

The 20S proteasome belongs to the small superfamily of N-terminal nucleophile (Ntn) hydrolases.<sup>[35]</sup> Each catalytically active subunit contains a threonine (Thr1), which is embedded in a network of hydrogen bond-linked active site residues (Figure 1.2).<sup>[22]</sup> As an endoprotease, the proteasome consists of distinct substrate binding channels which contain specificity pockets in front of (S1-S4) and following (primed S1'-S4') the scissile

## 1. Introduction

peptide bond.<sup>[36]</sup> These are occupied by the corresponding side chains (P1-P4 and P1'-P2'-sites, respectively) of a peptide (Figure 1.2). During substrate binding, the peptide backbone is stabilized by hydrogen bonding, thereby forming an antiparallel  $\beta$ -sheet at the non-primed sites and prolonging the residence time at the active site.<sup>[36]</sup> Hydrolysis of the peptide bond is initiated by the nucleophilic attack of the hydroxyl group of Thr1 (Thr1O $\gamma$ ) on the carbonyl carbon of the peptide bond. An acyl-enzyme intermediate is formed, which is stabilized by the oxyanion hole Gly47NH. Subsequently, a water molecule liberates the C-terminus and restores the initial state of the active site.<sup>[37]</sup>

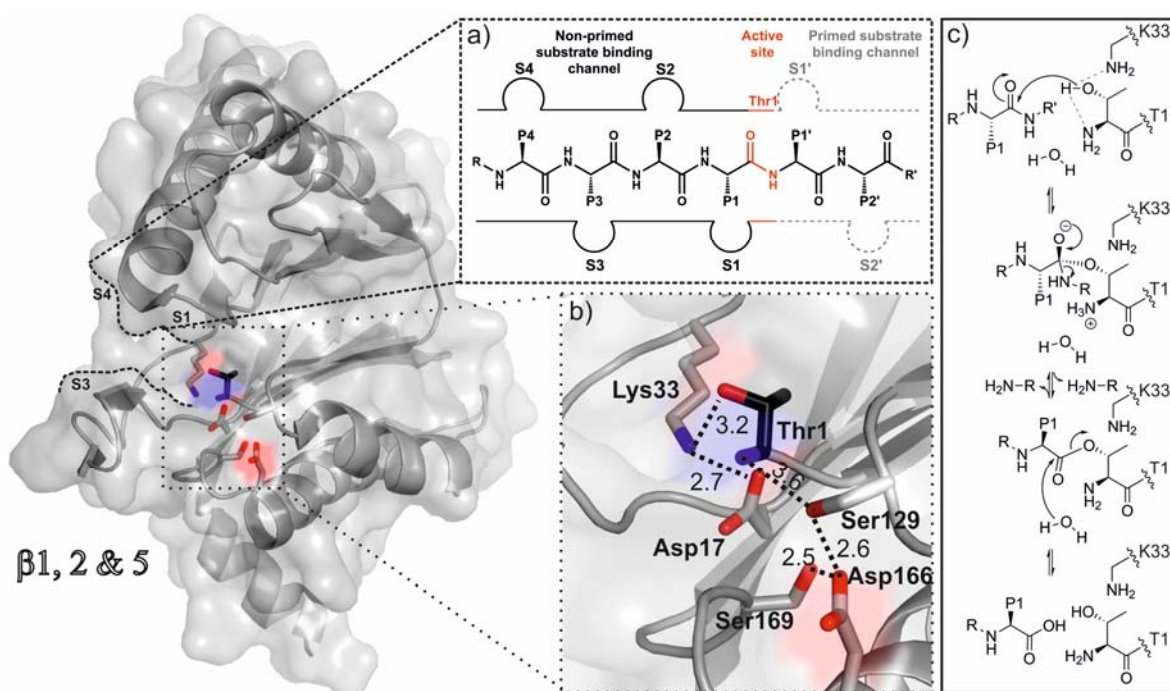


**Figure 1.2** General structure of catalytic  $\beta$ -subunits, their substrate binding channel and the active site with Thr1 (black). a) Schematic representation of the substrate binding channel with specificity pockets (S1-S4) occupying the side chains (P1-P4) of a peptide substrate, adapted from Beck et al.<sup>[38]</sup> The scissile peptide bond is highlighted in red. b) Active site with the nucleophile Thr1 (black) and the surrounding network of hydrogen bonding partners is depicted as dashed lines with distances in Å. c) Simplified catalytic mechanism of peptide bond hydrolysis by the CP. ThrN as well as Lys33 (K33) might act as base in the deprotonation (grey dashed lines) of Thr1O $\gamma$ .<sup>[37]</sup>

The turnover rate of an individual substrate depends on the degree of stabilization that is achieved by occupation of the specificity pockets. Analyses of cleavage products and digestion profiles of fluorogenic 7-amino-4-methylcoumarin (AMC) substrates revealed that each of the different  $\beta$ -subunits has a distinct substrate cleavage pattern and thus a defined specificity.<sup>[39]</sup> Therefore, the activity of subunit  $\beta$ 1c is comparable with a caspase-like activity (Z-LLE-AMC),  $\beta$ 2c with a trypsin-like activity (Ac-KQL-AMC) and  $\beta$ 5c displays a small neutral amino acid preferring (SnAAP) activity (Ac-WLA-AMC).<sup>[36]</sup> Similarly, the



activity of  $\beta$ 1i can be described as a branched chain amino acid preferring (BrAAP) activity (Ac-PAL-AMC),<sup>[40]</sup> while  $\beta$ 2i has a trypsin-like activity (Ac-KQL-AMC) and  $\beta$ 5i shows a chymotrypsin-like (ChTL) activity (Ac-ANW-AMC).<sup>[41]</sup> Notably, the exchange of the catalytic subunit  $\beta$ 1c with  $\beta$ 1i in iCPs enhances the generation of peptides with hydrophobic C-termini that are particularly suitable antigens for MHC-I presentation.<sup>[27]</sup> The exchange of  $\beta$ 5c with  $\beta$ 5i broadens the spectrum of produced peptide fragments with hydrophobic C-terminus, since  $\beta$ 5i, which is in contrast to  $\beta$ 5c, also accepts bulky hydrophobic residues besides Leu in P1 (Phe, Trp).<sup>[42]</sup> In tCPs, only subunit  $\beta$ 5t is exchanged which was shown to result in 60-70% decreased ChTL activity due to a more hydrophilic S1 pocket.<sup>[25]</sup> This exchange influences the pool of generated antigens which play an important role in the positive selection of T-cells.<sup>[21]</sup>

### 1.3 20S proteasomes as drug targets in cancer treatment

The 20S proteasome is involved in a multitude of fundamental and disease-associated processes including cell proliferation, apoptosis and the immune response. In non-transformed cells, proteasome inhibition leads to the accumulation of its entire substrate portfolio, thereby triggering unfolded protein response, cell-cycle arrest or apoptosis, depending on the degree of blockage.<sup>[43–45]</sup> In contrast, rapidly proliferating cancer cells heavily rely on protein degradation since their accelerated metabolism requires consistently high rates of protein turnover.<sup>[46]</sup> Therefore, these cells are especially susceptible to proteasome inhibition. In particular, multiple myeloma cells, a type of blood cancer derived from plasma cells, display constitutively elevated CP expression levels due to their chromosomal instability and biosynthetic burden resulting from immunoglobulin synthesis.<sup>[39,47]</sup> In addition, the accumulation of pro-apoptotic factors such as cyclin-dependent kinase inhibitor 1B (p27<sup>Kip1</sup>)<sup>[48]</sup> and pro-inflammatory mediators of NF- $\kappa$ B signaling induce apoptosis primarily in transformed plasma cells.<sup>[49]</sup> This discrepancy creates a therapeutic window which provides the basis for the clinical treatment of hematological malignancies such as multiple myeloma and mantle cell lymphoma with proteasome inhibitors. Since 2003, this alternative therapeutic approach has developed into a full first-line treatment of blood cancers, which is currently evaluated for broader applications in solid tumors.

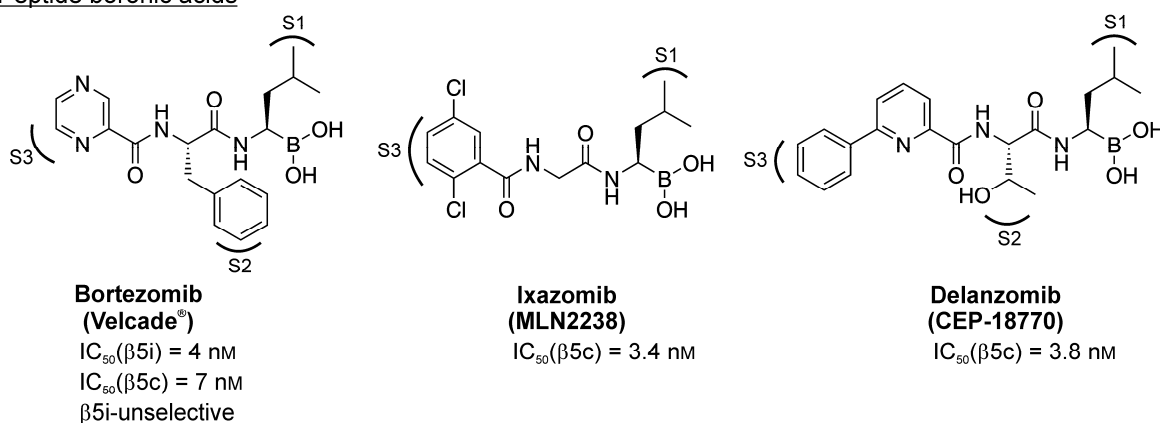
### 1.4 20S proteasome inhibitors in the clinic

The first generation of CP inhibitors was originally developed to serve as a research tool to investigate the implications of proteasomes in the UPS.<sup>[50]</sup> Their design comprises a di-, tri- or tetrapeptide backbone with an electrophilic warhead attached to the C-terminus,

## 1. Introduction

thereby mimicking the carbonyl electrophile of peptide bonds in natural substrates. The electrophile covalently reacts with the proteasomal active site nucleophile Thr1O<sup>γ</sup> in a single-step mechanism.<sup>[39]</sup> MG132, a tripeptide aldehyde,<sup>[50,51]</sup> became the most prominent representative of this class along with vinyl sulfones<sup>[52]</sup> and boronic acids<sup>[53]</sup>. In 2003, the dipeptide boronic acid bortezomib (Velcade<sup>®</sup>, former PS-341, Millennium (Takeda), Figure 1.3) was approved by the US Food and Drug Administration (FDA) for the treatment of multiple myeloma and refractory mantle cell lymphoma.<sup>[54–56]</sup> Bortezomib is administered intravenously and binds covalently but slowly-reversibly to Thr1 of the β5-subunits of both cCP and iCP ( $IC_{50}(\beta5c) = 7 \text{ nM}$ ,  $IC_{50}(\beta5i) = 4 \text{ nM}$ ), thereby inducing sustained cytotoxicity in malignant cells.<sup>[57,47]</sup> In addition, bortezomib co-inhibits the proteasomal subunit β1c ( $IC_{50}(\beta1c) = 74 \text{ nM}$ ) and was reported to also target the activity of β1i.<sup>[58–60]</sup>

### Peptide boronic acids



### Mechanism of action of peptide boronic acids

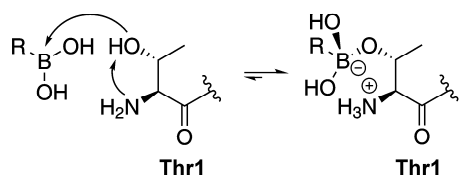
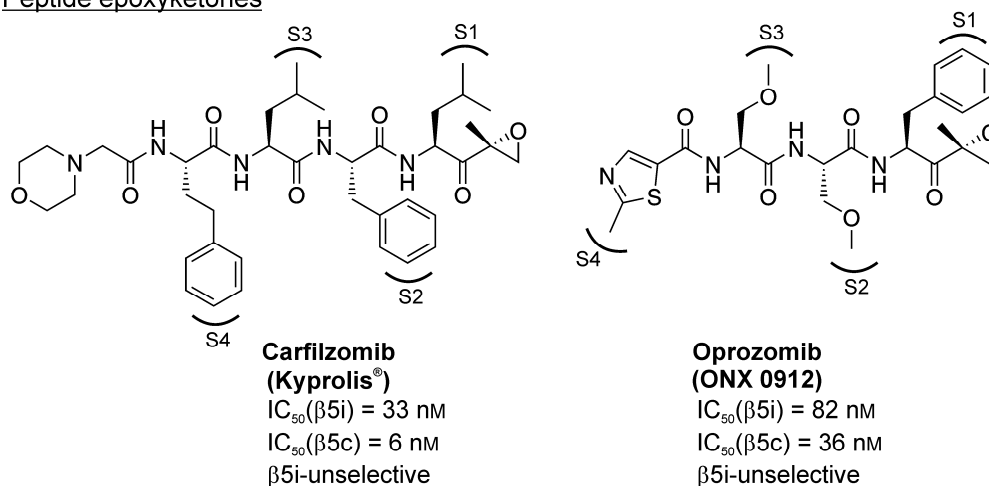


**Figure 1.3** Structures of the FDA-approved peptide boronic acid bortezomib (Velcade<sup>®</sup>) and the clinical candidates ixazomib (MLN2238) and delanzomib (CEP-18770). Mechanism of action of peptide boronic acids at the active site nucleophile Thr1 (bottom): a serine boronate tetrahedral transition state is formed that is stabilized by hydrogen bonding to Thr1N.<sup>[61]</sup>

However, despite the clinical success of bortezomib, its design is responsible for several drawbacks, which can even lead to therapies being interrupted prematurely. More than 30% of patients treated with bortezomib suffer from severe peripheral neuropathy which could be correlated with off-target activity towards serine proteases involved in neuronal cell survival.<sup>[62,63]</sup> Furthermore, emerging resistance towards bortezomib treatment restricts the therapeutic success and requires the development of improved CP inhibitors.<sup>[64,65]</sup>

Next generation CP inhibitors have been developed in an effort to decrease off-target specificity and improve patient convenience. With respect to a more convenient application method, ixazomib (Ninlaro<sup>®</sup>, former MLN2238, Takeda, Figure 1.3) is the first orally administered CP inhibitor for the treatment of multiple myeloma approved by the FDA in 2015.<sup>[66]</sup> In addition, Delanzomib (CEP-18770, Cephalon (Teva), Figure 1.3) as orally available bortezomib derivative has entered clinical trials phase I/II and is evaluated for the treatment of multiple myeloma and solid tumors.<sup>[67]</sup> In 2012, the tetrapeptide  $\alpha'$ ,  $\beta'$ -epoxyketone inhibitor carfilzomib (Kyprolis<sup>®</sup>, former PR-171, Onyx Pharmaceuticals (Amgen), Figure 1.4) gained FDA-approval for the second-line treatment of relapsed or refractory multiple myelomas.<sup>[68]</sup>

#### Peptide epoxyketones



#### Mechanism of action of peptide epoxyketones

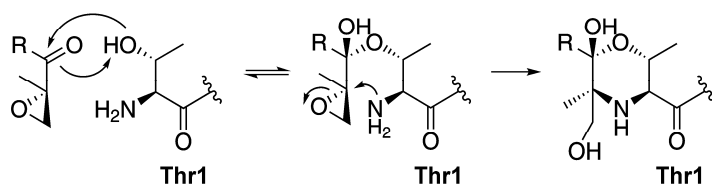


**Figure 1.4** Structures of the peptide epoxyketones carfilzomib and oprozomib. Mechanism of action of peptide epoxyketones at the active site nucleophile Thr1 (bottom): reversible hemiketal formation at Thr1 followed by nucleophilic attack of Thr1N on the second epoxide electrophile, thereby irreversibly forming a morpholine ring.<sup>[69,70]</sup>

Carfilzomib is derived from the natural product epoxomicin isolated from *Actinomycetes* and contains two electrophiles that involve Thr1N in addition to Thr1O<sup>γ</sup> in the mechanism. This enhances the compound's specificity for the proteasome as an Ntn-hydrolase.<sup>[57,69,70]</sup> Based on the bivalent reaction mechanism of the  $\alpha'$ ,  $\beta'$ -epoxyketone pharmacophore, the latter prevailed over the highly reactive boronic acid warhead. This can be correlated to the reduced record of side effects during the treatment with

carfilzomib.<sup>[62]</sup> Oprozomib (ONX 0912, Onyx Pharmaceuticals (Amgen), Figure 1.4), as an orally available advancement of the intravenously applied carfilzomib, is currently investigated for the treatment of hematological malignancies in Phase 1 studies.<sup>[71,72]</sup> Moreover, oprozomib was shown to be more selective for  $\beta 5c/\beta 5i$  by blocking  $\beta 1c$  and  $\beta 2c/\beta 2i$  only at concentrations in the micromolar range.<sup>[58]</sup> Apart from the general trend to improve subunit-specificity, current patent applications document the recent industrial research efforts to enhance the pharmacokinetic profile of CP inhibitors. The attachment of polyethylene glycol (PEG) polymer chains to the peptide backbone of carfilzomib increases the solubility and the distribution of the drug.<sup>[73]</sup> Furthermore, the utilization of activated diols as precursor warheads that form the epoxyketone pharmacophore in a pH-dependent intramolecular reaction might prolong the short half-life of less than 30 minutes, thereby enhancing plasma stability and tissue penetration.<sup>[73]</sup> Moreover, carfilzomib as a payload of antibody-drug conjugates and bortezomib combined to an octreotide conjugate for targeted drug delivery are currently investigated.<sup>[74]</sup> These prodrug and antibody-drug conjugate approaches might have the potential to broaden the clinical utility of CP inhibitors to the treatment of solid tumors.

### 1.5 $\beta 5i$ -selective inhibitors and their possible applications

ONX 0914 (PR-957; Onyx Pharmaceuticals (Amgen), Figure 1.5) represents the first iCP-selective inhibitor with at least nine-fold preference for  $\beta 5i$  versus  $\beta 5c$  ( $IC_{50}(\beta 5i) = 28$  nM,  $IC_{50}(\beta 5c) = 236$  nM).<sup>[75]</sup>

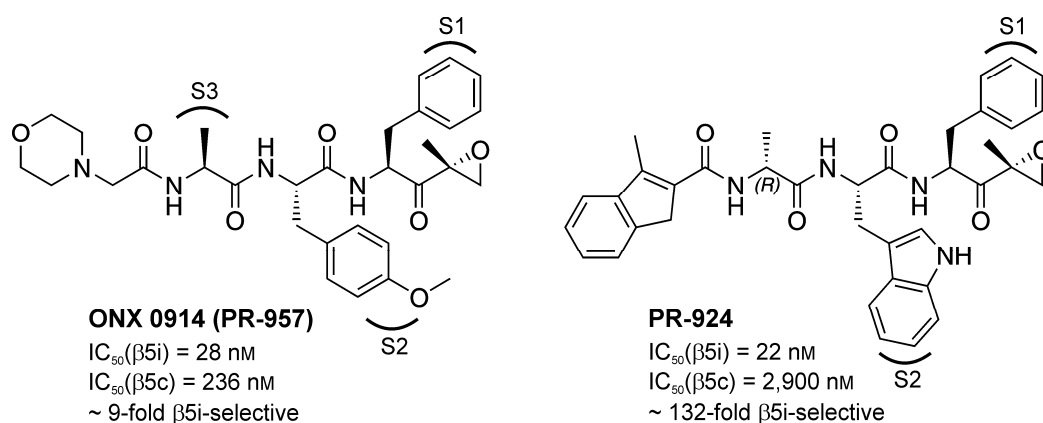


**Figure 1.5** Structures of the  $\beta 5i$ -selective peptide epoxyketones ONX 0914 (PR-957) and PR-924. The molecular basis for selectivity of these compounds is described in chapter 2 (2.3.1).

By selectively blocking the subunit  $\beta 5i$ , ONX 0914 downregulates the MHC class I cell surface expression by 50% without affecting the presentation of  $\beta 5i$ -independent epitopes, thereby modulating cytotoxic T-cell responses.<sup>[75]</sup> In addition, ONX 0914 was shown to suppress the production of pro-inflammatory cytokines, including IL-6, interleukin 23

(IL-23) and TNF- $\alpha$ , which play a crucial role in the development of T helper 17 (T<sub>h</sub>17) and 1 (T<sub>h</sub>1) cells. In contrast, regulatory T cells and T<sub>h</sub>2 cells remained unaffected.<sup>[75,76]</sup> Both T<sub>h</sub>17 and T<sub>h</sub>1 cells are associated with the pathogenesis of several autoimmune diseases such as inflammatory bowel disease,<sup>[77]</sup> rheumatoid arthritis and psoriasis.<sup>[78]</sup> Preclinical studies that evaluated ONX 0914 as an anti-inflammatory agent could show that the compound prevents the progression of chronic inflammations including rheumatoid arthritis,<sup>[75]</sup> systemic lupus erythematosus,<sup>[79]</sup> Hashimoto's thyroiditis,<sup>[80]</sup> experimental colitis<sup>[81]</sup> and autoimmune encephalomyelitis<sup>[82]</sup> in mouse models. Most importantly, ONX 0914 proved to have therapeutic effects at concentrations below the maximum tolerated dose in mice.<sup>[75]</sup> However, the therapeutic window of iCP selective agents depends entirely on their  $\beta$ 5i-selectivity that prevents cytotoxic effects resulting from co-inhibition of subunit  $\beta$ 5c or other combinations of simultaneously blocked subunits.<sup>[83–86]</sup> This is in contrast to unselective CP inhibitors that are applied for cancer treatment where cytotoxicity is an integral part of their anti-proliferative activity. Nevertheless, ONX 0914 displayed potent anti-leukemic activity during its preclinical evaluation for the possible application in hematological malignancies.<sup>[87]</sup> It was therefore hypothesized that iCPs, which are highly expressed in leukemic cells, might represent drug targets that can be blocked by selective iCP-inhibitors with low cytotoxicity. For this purpose, PR-924 (Onyx Pharmaceuticals (Amgen), Figure 1.5) was investigated, which offers a wider therapeutic window based on its 132-fold selectivity for  $\beta$ 5i ( $IC_{50}(\beta$ 5i) = 22 nM) versus  $\beta$ 5c ( $IC_{50}(\beta$ 5c) = 2,900 nM).<sup>[88]</sup> However, PR-924 displayed anti-proliferative activity towards leukemia cells only above concentrations that equally blocked  $\beta$ 5i and  $\beta$ 5c, indicating that the exclusive blockage of  $\beta$ 5i is insufficient as a therapeutic rationale for the treatment of blood cancer.<sup>[84]</sup> Consistently,  $\beta$ 5c-specific (PR-825 & PR-893) and  $\beta$ 5i-selective compounds exhibit neither anti-leukemic nor anti-inflammatory activity.<sup>[75,83]</sup> Taken together,  $\beta$ 5i-selective compounds represent promising agents for the treatment of chronic inflammations and autoimmune disorders.

## 1.6 References

- [1] A. Ciechanover, *EMBO J.* **1998**, *17*, 7151–7160.
- [2] A. L. Goldberg, K. L. Rock, *Nature* **1992**, *357*, 375–379.
- [3] A. Hershko, A. Ciechanover, *Annu. Rev. Biochem.* **1998**, *67*, 425–479.
- [4] K. L. Rock, A. L. Goldberg, *Annu. Rev. Immunol.* **1999**, *17*, 739–779.
- [5] A. Hershko, A. Ciechanover, H. Heller, A. L. Haas, I. A. Rose, *Proc. Natl. Acad. Sci.* **1980**, *77*, 1783–1786.
- [6] A. Ciechanover, H. Heller, S. Elias, A. L. Haas, A. Hershko, *Proc. Natl. Acad. Sci. U. S. A.* **1980**, *77*, 1365–1368.
- [7] M. H. Glickman, A. Ciechanover, *Physiol. Rev.* **2002**, *82*, 373–428.
- [8] C. M. Pickart, *Cell* **2004**, *116*, 181–190.
- [9] D. Finley, *Annu. Rev. Biochem.* **2009**, *78*, 477–513.
- [10] Q. Deveraux, V. Ustrell, C. Pickart, M. Rechsteiner, *J. Biol. Chem.* **1994**, *269*, 7059–7061.
- [11] Y. A. Lam, W. Xu, G. N. DeMartino, R. E. Cohen, *Nature* **1997**, *385*, 737–740.
- [12] Y. A. Lam, G. N. Demartino, C. M. Pickart, R. E. Cohen, J. B. Chem, *J. Biol. Chem.* **1997**, *272*, 28438–28446.
- [13] D. M. Rubin, M. H. Glickman, C. N. Larsen, S. Dhruvakumar, D. Finley, *EMBO J.* **1998**, *17*, 4909–4919.
- [14] L. Borissenko, M. Groll, *Chem. Rev.* **2007**, *107*, 687–717.
- [15] J. Neeffjes, F. Momburg, G. Hammerling, *Science* **1993**, *261*, 769–771.
- [16] R. N. Germain, D. H. Margulies, *Annu. Rev. Immunol.* **1993**, *11*, 403–450.
- [17] T. Saric, S.-C. Chang, A. Hattori, I. A. York, S. Markant, K. L. Rock, M. Tsujimoto, A. L. Goldberg, *Nat. Immunol.* **2002**, *3*, 1169–1176.
- [18] L. Saveanu, O. Carroll, V. Lindo, M. Del Val, D. Lopez, Y. Lepelletier, F. Greer, L. Schomburg, D. Fruci, G. Niedermann, et al., *Nat. Immunol.* **2005**, *6*, 689–697.
- [19] J. Neeffjes, M. L. Jongsma, P. Paul, O. Bakke, *Nat Rev Immunol* **2011**, *11*, 823–836.
- [20] T. J. Kalogeris, F. S. Laroux, A. Cockrell, H. Ichikawa, N. Okayama, T. J. Phifer, J. S. Alexander, M. B. Grisham, *Am.J.Physiol* **1999**, *276*, 856–864.
- [21] M. Groettrup, C. J. Kirk, M. Basler, *Nat. Rev. Immunol.* **2010**, *10*, 73–78.
- [22] M. Groll, L. Ditzel, J. Löwe, D. Stock, M. Bochtler, H. Bartunik, R. Huber, *Nature* **1997**, *386*, 463–471.
- [23] M. Groll, M. Bajorek, A. Köhler, L. Moroder, D. M. Rubin, R. Huber, M. H. Glickman, D. Finley, *Nat. Struct. Biol.* **2000**, *7*, 1062–1067.
- [24] F. G. Whitby, E. I. Masters, L. Kramer, J. R. Knowlton, Y. Yao, C. C. Wang, C. P. Hill, *Nature* **2000**, *408*, 115–120.
- [25] S. Murata, K. Sasaki, T. Kishimoto, S. Niwa, H. Hayashi, Y. Takahama, K. Tanaka, *Science* **2008**, *316*, 1349–1353.
- [26] M. Gaczynska, K. L. Rock, T. Spies, A. L. Goldberg, *Proc. Natl. Acad. Sci. U. S. A.* **1994**, *91*, 9213–9217.
- [27] J. Driscoll, M. Brown, D. Finley, *Nature* **1993**, *365*, 262–264.
- [28] M. Aki, N. Shimbara, M. Takashina, K. Akiyama, S. Kagawa, T. Tamura, N. Tanahashi, T. Yoshimura, K. Tanaka, a Ichihara, *J. Biochem.* **1994**, *115*, 257–269.
- [29] K. Tanaka, *J. Leukoc. Biol.* **1994**, *56*, 571–575.
- [30] B. B. Boes, H. Hengel, T. Ruppert, G. Multhaup, U. H. Koszinowski, P. Kloetzel, *J. Exp. Med.* **1994**, *179*, 901–909.
- [31] K. Akiyama, K. Yokota, S. Kagawa, N. Shimbara, T. Tamura, H. Akioka, H. G. Nothwang, C. Noda, K. Tanaka, A. Ichihara, *Science* **1994**, *265*, 1231–1234.
- [32] N. Klare, M. Seeger, K. Janek, P. R. Jungblut, B. Dahlmann, *J. Mol. Biol.* **2007**, *373*, 1–10.

- [33] B. Guillaume, J. Chapiro, V. Stroobant, D. Colau, B. Van Holle, G. Parvizi, M.-P. Bousquet-Dubouch, I. Théate, N. Parmentier, B. J. Van den Eynde, *Proc. Natl. Acad. Sci. U. S. A.* **2010**, *107*, 18599–604.
- [34] M. Groettrup, R. Kraft, S. Kostka, S. Standera, R. Stohwasser, P.-M. Kloetzel, *Eur. J. Immunol.* **1996**, *26*, 863–869.
- [35] E. Seemüller, A. Lupas, D. Stock, J. Löwe, R. Huber, W. Baumeister, *Science* **1995**, *268*, 579–582.
- [36] L. Borissenko, M. Groll, *Chem. Rev.* **2007**, *107*, 687–717.
- [37] M. Groll, T. Clausen, *Curr. Opin. Struct. Biol.* **2003**, *13*, 665–673.
- [38] P. Beck, C. Dubiella, M. Groll, *Biol. Chem.* **2012**, *393*, 1101–1120.
- [39] E. M. Huber, M. Groll, *Angew. Chemie Int. Ed.* **2012**, *51*, 8708–8720.
- [40] C. Cardozo, *J. Biol. Chem.* **1998**, *273*, 16764–16770.
- [41] E. M. Huber, M. Basler, R. Schwab, W. Heinemeyer, C. J. Kirk, M. Groettrup, M. Groll, *Cell* **2012**, *148*, 727–738.
- [42] H.-G. Rammensee, T. Friede, S. Stevanovic, *Immunogenetics* **1995**, *41*, 178–228.
- [43] S. Imajoh-Ohmi, T. Kawaguchi, S. Sugiyama, K. Tanaka, S. Omura, H. Kikuchi, *Biochem. Biophys. Res. Commun.* **1995**, *217*, 1070–1077.
- [44] G. Bianchi, L. Oliva, P. Cascio, N. Pengo, F. Fontana, F. Cerruti, A. Orsi, E. Pasqualetto, A. Mezghrani, V. Calbi, et al., *Blood* **2009**, *113*, 3040–9.
- [45] E. A. Obeng, L. M. Carlson, D. M. Gutman, W. J. Harrington, K. P. Lee, L. H. Boise, *Blood* **2006**, *107*, 4907–4916.
- [46] L. R. Dick, P. E. Fleming, *Drug Discov. Today* **2010**, *15*, 243–249.
- [47] T. Hideshima, P. Richardson, D. Chauhan, V. J. Palombella, P. J. Elliott, J. Adams, K. C. Anderson, *Cancer Res* **2001**, *61*, 3071–3076.
- [48] I. Nicleleit, S. Zender, F. Sasse, R. Geffers, G. Brandes, I. Sörensen, H. Steinmetz, S. Kubicka, T. Carlomagno, D. Menche, et al., *Cancer Cell* **2008**, *14*, 23–35.
- [49] M. Rape, S. Jentsch, *Nat. Cell Biol.* **2002**, *4*, 113–116.
- [50] D. H. Lee, A. L. Goldberg, *Trends Cell Biol.* **1998**, *8*, 397–403.
- [51] A. Vinitzky, C. Michaud, J. C. Powers, M. Orlowski, *Biochemistry* **1992**, *31*, 9421–9428.
- [52] M. Bogyo, J. S. McMaster, M. Gaczynska, D. Tortorella, a. L. Goldberg, H. Ploegh, *Proc. Natl. Acad. Sci. U. S. A.* **1997**, *94*, 6629–6634.
- [53] J. Adams, M. Behnke, S. Chen, A. a Cruickshank, L. R. Dick, L. Grenier, J. M. Klunder, Y.-T. Ma, L. Plamondon, R. L. Stein, *Bioorg. Med. Chem. Lett.* **1998**, *8*, 333–338.
- [54] R. C. Kane, P. F. Bross, A. T. Farrell, R. Pazdur, *Oncologist* **2003**, *8*, 508–513.
- [55] R. C. Kane, A. T. Farrell, R. Sridhara, R. Pazdur, *Clin. cancer Res.* **2006**, *12*, 2955–2960.
- [56] R. C. Kane, R. Dagher, A. Farrell, C. W. Ko, R. Sridhara, R. Justice, R. Pazdur, *Clin. Cancer Res.* **2007**, *13*, 5291–5294.
- [57] S. D. Demo, C. J. Kirk, M. A. Aujay, T. J. Buchholz, M. Dajee, M. N. Ho, J. Jiang, G. J. Laidig, E. R. Lewis, F. Parlati, et al., *Cancer Res.* **2007**, 6383–6391.
- [58] G. de Bruin, B. T. Xin, M. Kraus, M. van der Stelt, G. a. van der Marel, A. F. Kisselev, C. Driessen, B. I. Florea, H. S. Overkleeft, *Angew. Chemie Int. Ed.* **2015**, DOI 10.1002/anie.201509092.
- [59] M. Altun, P. J. Galaray, R. Shringarpure, T. Hideshima, R. LeBlanc, K. C. Anderson, H. L. Ploegh, B. M. Kessler, *Cancer Res.* **2005**, *65*, 7896–7901.
- [60] C. R. Berkers, M. Verdoes, E. Lichtman, E. Fiebigler, B. M. Kessler, K. C. Anderson, H. L. Ploegh, H. Ovaa, P. J. Galaray, *Nat. Methods* **2005**, *2*, 357–362.
- [61] M. Groll, C. R. Berkers, H. L. Ploegh, H. Ovaa, *Structure* **2006**, *14*, 451–456.
- [62] S. Arastu-Kapur, J. L. Anderl, M. Kraus, F. Parlati, K. D. Shenk, S. J. Lee, T. Muchamuel, M. K. Bennett, C. Driessen, A. J. Ball, et al., *Clin. Cancer Res.* **2011**, *17*, 2734–2743.
- [63] A. A. Argyriou, G. Cavaletti, J. Bruna, A. P. Kyritsis, H. P. Kalofonos, *Arch. Toxicol.* **2014**, *88*, 1669–1679.
- [64] E. M. Huber, W. Heinemeyer, M. Groll, *Structure* **2015**, *23*, 407–417.

- [65] A. M. Ruschak, M. Slassi, L. E. Kay, A. D. Schimmer, *J. Natl. Cancer Inst.* **2011**, *103*, 1007–1017.
- [66] E. Kupperman, E. C. Lee, Y. Cao, B. Bannerman, M. Fitzgerald, A. Berger, J. Yu, Y. Yang, P. Hales, F. Bruzzese, et al., *Cancer Res.* **2010**, *70*, 1970–1980.
- [67] R. Piva, B. Ruggeri, M. Williams, G. Costa, I. Tamagno, D. Ferrero, V. Giai, M. Coscia, S. Peola, M. Massaia, et al., *Blood* **2008**, *111*, 2765–2775.
- [68] T. M. Herndon, A. Deisseroth, E. Kaminskas, R. C. Kane, K. M. Koti, M. D. Rothmann, B. Habtemariam, J. Bullock, J. D. Bray, J. Hawes, et al., *Clin. cancer Res.* **2013**, *19*, 4559–4563.
- [69] M. Groll, K. B. Kim, N. Kairies, R. Huber, C. M. Crews, *J. Am. Chem. Soc.* **2000**, *122*, 1237–1238.
- [70] W. Harshbarger, C. Miller, C. Diedrich, J. Sacchettini, *Structure* **2015**, *23*, 418–424.
- [71] D. Chauhan, A. V Singh, M. Aujay, C. J. Kirk, M. Bandi, B. Ciccarelli, N. Raje, P. Richardson, K. C. Anderson, *Blood* **2010**, *116*, 4906–4915.
- [72] H. J. Zhou, M. a. Aujay, M. K. Bennett, M. Dajee, S. D. Demo, Y. Fang, M. N. Ho, J. Jiang, C. J. Kirk, G. J. Laidig, et al., *J. Med. Chem.* **2009**, *52*, 3028–3038.
- [73] P. Phiasivongsa, G. Luehr, *Prodrugs of Peptide Epoxy Ketone Protease Inhibitors*, **2014**, WO 2014/011695 A2.
- [74] P. Beck, H. Cui, J. D. Hegemann, M. a. Marahiel, A. Krüger, M. Groll, *ChemMedChem* **2015**, *10*, 1969–1973.
- [75] T. Muchamuel, M. Basler, M. A. Aujay, E. Suzuki, K. W. Kalim, C. Lauer, C. Sylvain, E. R. Ring, J. Shields, J. Jiang, et al., *Nat. Med.* **2009**, *15*, 781–787.
- [76] K. W. Kalim, M. Basler, C. J. Kirk, M. Groettrup, *J. Immunol.* **2012**, *189*, 4182–4193.
- [77] G. Bouma, W. Strober, *Nat. Rev. Immunol.* **2003**, *3*, 521–533.
- [78] W. Ouyang, J. K. Kolls, Y. Zheng, *Immunity* **2008**, *28*, 454–467.
- [79] H. T. Ichikawa, T. Conley, T. Muchamuel, J. Jiang, S. Lee, T. Owen, J. Barnard, S. Nevarez, B. I. Goldman, C. J. Kirk, et al., *Arthritis Rheum.* **2015**, *64*, 493–503.
- [80] Y. Nagayama, M. Nakahara, M. Shimamura, I. Horie, K. Arima, N. Abiru, *Clin. Exp. Immunol.* **2012**, *168*, 268–273.
- [81] M. Basler, M. Dajee, C. Moll, M. Groettrup, C. J. Kirk, *J. Immunol.* **2010**, *185*, 634–641.
- [82] M. Basler, S. Mundt, T. Muchamuel, C. Moll, J. Jiang, M. Groettrup, C. J. Kirk, *EMBO Mol. Med.* **2014**, *6*, 226–238.
- [83] F. Parlati, S. J. Lee, M. Aujay, E. Suzuki, K. Levitsky, J. B. Lorens, D. R. Micklem, P. Ruurs, C. Sylvain, Y. Lu, et al., *Blood* **2009**, *114*, 3439–3447.
- [84] D. Niewerth, J. van Meerloo, G. Jansen, Y. G. Assaraf, T. C. Hendrickx, C. J. Kirk, J. L. Anderl, S. Zweegman, G. J. L. Kaspers, J. Cloos, *Biochem. Pharmacol.* **2014**, *89*, 43–51.
- [85] A. C. Mirabella, A. A. Pletnev, S. L. Downey, B. I. Florea, T. B. Shabaneh, M. Britton, M. Verdoes, D. V Filippov, H. S. Overkleeft, A. F. Kisselev, *Chem. Biol.* **2011**, *18*, 608–618.
- [86] M. Britton, M. M. Lucas, S. L. Downey, M. Screen, A. A. Pletnev, M. Verdoes, R. A. Tokhunts, O. Amir, A. L. Goddard, P. M. Pelphrey, et al., *Chem. Biol.* **2009**, *16*, 1278–1289.
- [87] D. Niewerth, N. E. Franke, G. Jansen, Y. G. Assaraf, J. van Meerloo, C. J. Kirk, J. Degenhardt, J. Anderl, A. D. Schimmer, S. Zweegman, et al., *Haematologica* **2013**, *98*, 1896–1904.
- [88] A. V Singh, M. Bandi, M. a Aujay, C. J. Kirk, D. E. Hark, N. Raje, D. Chauhan, K. C. Anderson, *Br. J. Haematol.* **2011**, *152*, 155–163.



## 2 Objective and summary of results

### 2.1 Objective

Selective iCP inhibitors have the potential to modulate chronic inflammations and autoimmune diseases and thus represent promising anti-inflammatory agents.<sup>[1]</sup> However, their therapeutic window depends entirely on their isoform selectivity, which as a rule, prevents cytotoxic effects arising from simultaneous blockage of the cCP and the iCP.<sup>[2-5]</sup>

The aim of this thesis was to develop innovative strategies for the design of peptidic iCP inhibitors with high isoform-specificity and therefore potentially improved safety profiles. Extensive peptide backbone optimization, which to date represents the common approach to screen for peptidic iCP specific inhibitors, was avoided. Instead, this work was dedicated to the discovery of novel concepts for selective iCP inhibition and the understanding of their underlying principles. In this regard, structural information about the molecular differences between the cCP and the iCP played a key role in providing starting points for the rational design of specific inhibitors. This was pursued by following a multidisciplinary approach that combined structural bioinformatics, chemical synthesis, biochemical evaluation of compounds in vitro following cell-based assays and the rational optimization of promising candidates.

### 2.2 Contents

This thesis reports on both published and unpublished research that was dedicated to the development of isoform selective iCP inhibitors. Three new compound classes are described that might provide starting points for the design of selective iCP inhibitors as valuable research tools and potential anti-inflammatory agents.

Chapter 3 describes research that aimed to identify molecular differences between the cCP and the iCP, more precisely their proteolytically active subunits  $\beta$ 5c and  $\beta$ 5i, in order to exploit these for selective inhibitor design. Importantly, this study identified a non-catalytic cysteine as a subunit-specific nucleophile that can be targeted by side chain-electrophile containing decarboxylated peptides derived from carfilzomib. In an effort to screen for appropriate electrophiles for cysteine targeting,  $\alpha$ -chloroacetamides were shown to offer a balanced compromise between potency and stability in cell culture, which is consistent with current literature suggesting this warhead for specific probe and inhibitor design. Subsequent analysis of the binding mode via X-ray crystallography confirmed, for the first time, that an iCP inhibitor acts independently from the active site nucleophile Thr1. Moreover, the structural insights provided detailed input for the rational optimization

## 2. Objective and summary of results

---

of this compound class, which culminated in an at least 150-fold preferential binding to the subunit  $\beta 5i$  versus  $\beta 5c$ . In the process of elucidating the underlying rationale for  $\beta 5i$  selectivity, apart from the electrophile, the study uncovered the crucial role of the ligand's P3-side chain. This is in accordance with inhibitors containing C-terminal electrophiles, which primarily rely on P1-side chain stabilization for appropriate alignment of the warhead whereas the  $\alpha$ -chloroacetamides mainly depend on stabilization at the S3-site. By this means, selectivity can be generated by P3-side chains that are preferentially stabilized in the S3-pocket of subunit  $\beta 5i$ , as opposed to  $\beta 5c$ , resulting in strong irreversible binders to  $\beta 5i$  but only weak reversible binders to  $\beta 5c$ . Finally, the study once more proved that selective  $\beta 5i$  blockage is sufficient to suppress the production of inflammatory cytokines like TNF- $\alpha$  and IL-6 without inducing cytotoxicity.

Apart from the targeting of isoform-specific nucleophiles in order to achieve selectivity, Chapter 4 reports that also inhibitory mechanisms can contribute to specificity, even if the targeted nucleophile is present in both isoforms. The study was initially designed to clarify the binding mode of peptido sulfonyl fluorides (PSF) to the proteasomal active site via X-ray crystallographic and mass spectrometric analyses. It uncovered an unexpected mode of action comprising sulfonylation and subsequent polarity inversion of the nucleophile Thr1, ultimately leading to an intramolecular crosslinking of the active site. Moreover, comparison of PSFs with their  $\alpha',\beta'$ -epoxyketone counterparts revealed that the sulfonyl fluoride headgroup and its uncommon mechanism indeed contribute to iCP selectivity with 28-fold preference for subunit  $\beta 5i$  versus  $\beta 5c$ .

In an effort to further exploit the mechanism of action of the sulfonyl fluorides, Chapter 5 describes the discovery of sulfonate esters as tunable inhibitors of the cCP and the iCP. By exchanging the leaving group of the sulfonyl fluorides with highly fluorescent reporter molecules, this study gave insights into the kinetics of proteasomal inhibition. This new class of CP inhibitors allows the quantification of active CP in solution with high sensitivity.

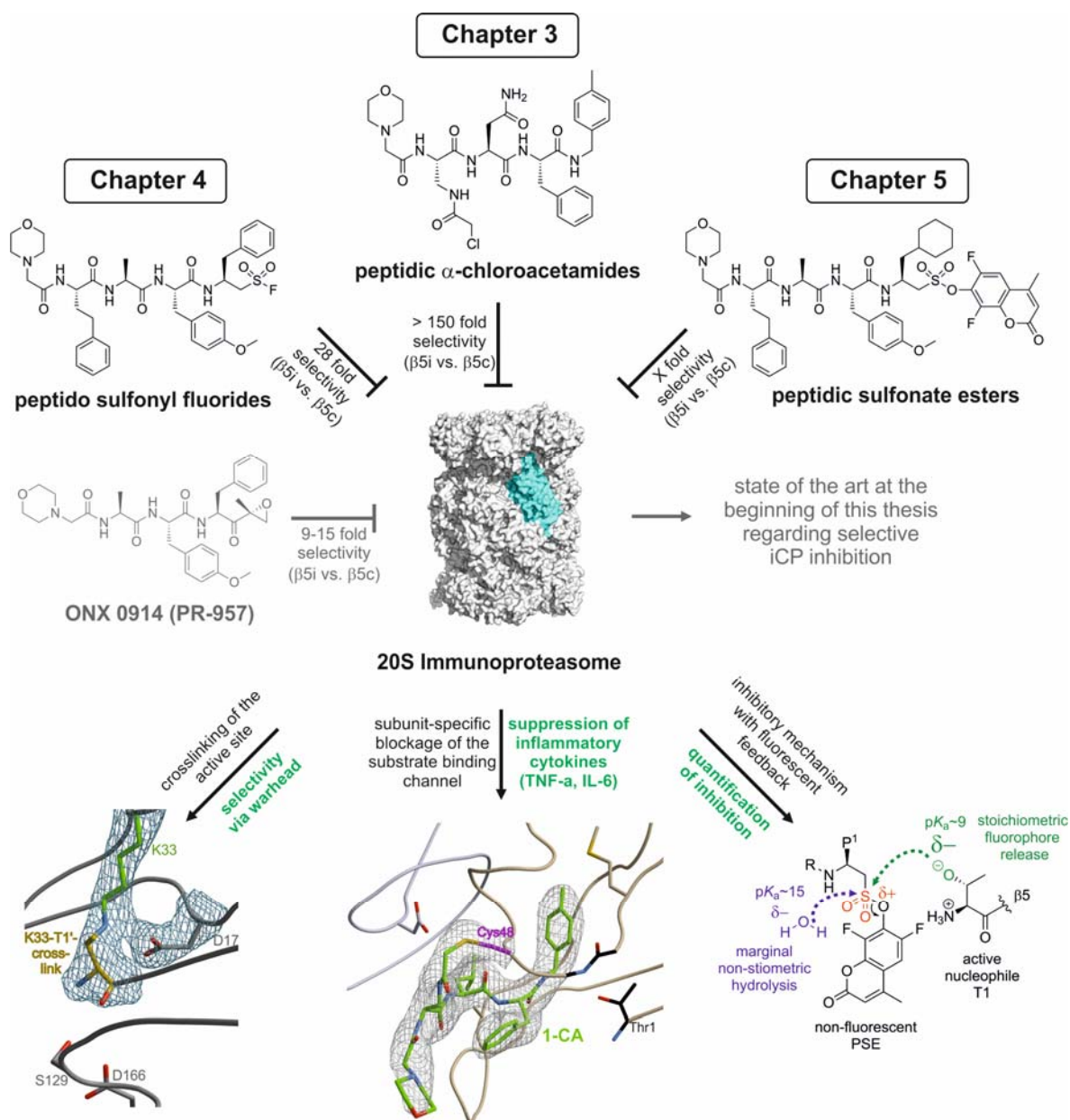


**Figure 2.1** Summary of the main achievements presented in this thesis. Chapter 3 (center): Rational design of peptidic  $\alpha$ -chloroacetamides that target the isoform-specific non-catalytic Cys48 of  $\beta 5i$ . The compounds suppressed cytokines (IL-6 & TNF- $\alpha$ ) and exhibited low cytotoxicity in cell culture. Structure-based optimization of the peptidic backbone led to over 150-fold  $\beta 5i$ -selectivity. Chapter 4 (left): Elucidation of the mechanism of action of peptido sulfonyl fluorides (PSFs) resulting in an intramolecular crosslinking of the active site. Combined with  $\beta 5i$ -specific peptide backbones, 28-fold  $\beta 5i$ -specificity was obtained. Chapter 5 (right): Peptide sulfonate esters (PSEs) were developed to quantify proteasomal inhibition by addition of a fluorogenic reporter leaving group.

### 2.3 Structural rationales for the design of $\beta$ 5i-selective inhibitors

A major challenge in the design of  $\beta$ 5i-selective proteasome inhibitors is the high sequence identity between human  $\beta$ 5c and  $\beta$ 5i of 72.4%, resulting in almost identical substrate binding channels, similar specificity pockets (S1-S4) and equal active site architectures. However, the structural superposition of murine  $\beta$ 5i (PDB ID: 3UNH)<sup>[6]</sup> and human  $\beta$ 5c (PDB ID: 4R3O)<sup>[7]</sup>, in combination with sequence alignments, reveal important differences (Figure 2.2). Among these distinctions only few residues directly affect the substrate binding channel and thus ligand binding. The most obvious change between  $\beta$ 5c and  $\beta$ 5i represents the strictly conserved exchange of Gly48 ( $\beta$ 5c) by Cys48 ( $\beta$ 5i) which extends the shallow S2 pocket and reduces the spacious S4 pocket.<sup>[6]</sup> In addition, Cys48 is located at a positively charged  $\alpha$ -helix dipole (N-terminal end), which has the potential to lower the  $pK_a$  value of the thiol group, thereby promoting interactions with substrates and ligands.<sup>[8]</sup> In particular, complex structures with  $\beta$ 5i-selective peptidic ligands (e.g. PDB ID: 3UNF)<sup>[6]</sup> provide a basis for understanding the individual contributions of each side chain, which sum up to significant observable  $\beta$ 5i-specific inhibition in activity assays.

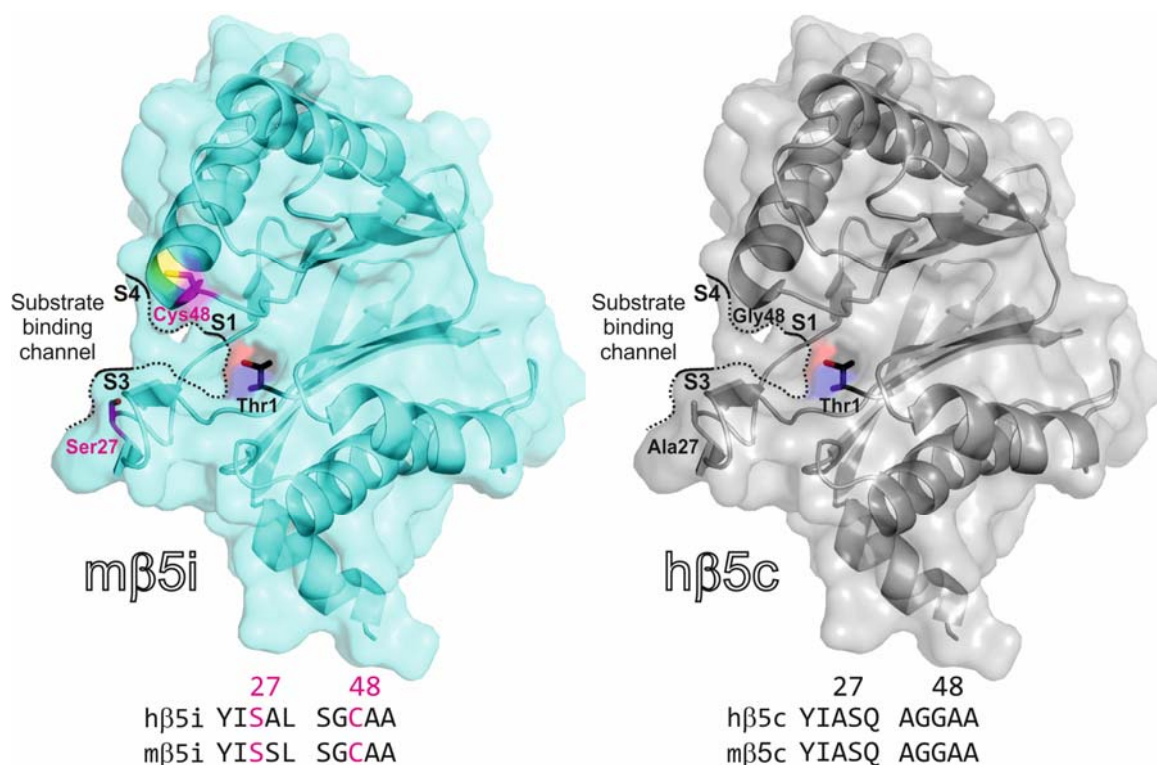


**Figure 2.2** Subunit m $\beta$ 5i of murine iCP (left, cyan, PDB ID: 3UNH)<sup>[6]</sup> and h $\beta$ 5c of human cCP (right, grey, PDB ID: 4R3O)<sup>[7]</sup>. The active site nucleophile Thr1 (black) and the specificity pocket (S1-S4) of the substrate binding channel (dashed line) are depicted, including the most prominent differences: Cys48 & Ser27 (magenta) of m $\beta$ 5i and Gly48 & Ala27 (black) of h $\beta$ 5c with sequence alignments (bottom).

### 2.3.1 Peptidic $\beta$ 5i-selective inhibitors with C-terminal electrophiles

The comparison of the  $\alpha',\beta'$ -epoxyketone carfilzomib and its  $\beta$ 5i-specific analog ONX 0914 reveals major reasons for target selectivity by discriminating between  $\beta$ 5c/ $\beta$ 5i, even though both inhibitors differ in their peptide backbone composition only (Figure 2.3).

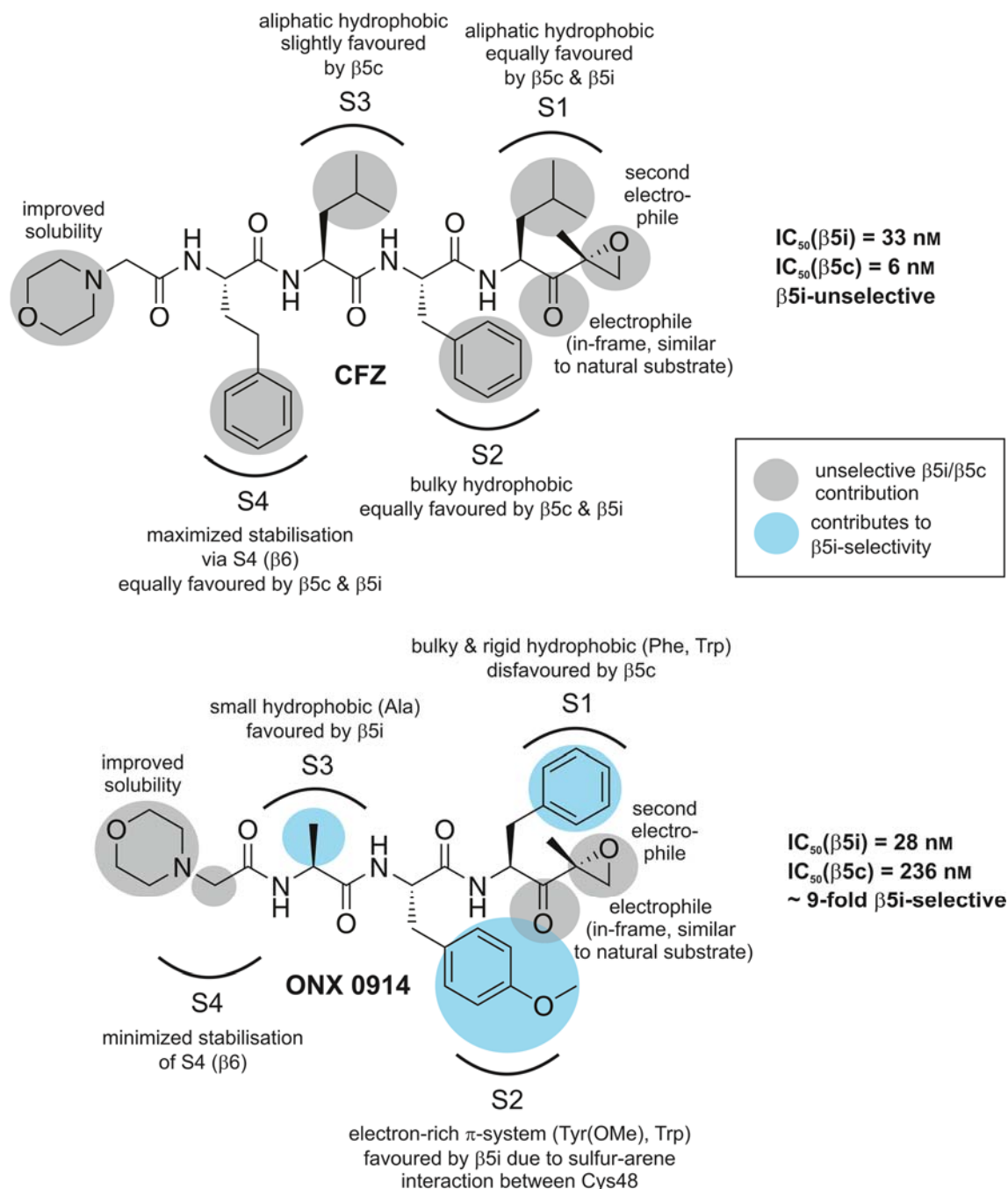


**Figure 2.3** Illustration of the  $\beta$ 5i/ $\beta$ 5c-unselective carfilzomib (CFZ, top) and the  $\beta$ 5i-selective ONX 0914 (bottom) with the contribution of each side chain (grey: unselective; blue: selective for  $\beta$ 5i). The  $IC_{50}$  values<sup>[1,9]</sup> against the ChTL activities of purified human iCP and cCP are given (right).

## 2. Objective and summary of results

In contrast to the unselective carfilzomib, ONX 0914 features side chain elements (P1-P4) that are preferentially occupied in the specificity pockets (S1-S4) of  $\beta 5i$ , thereby contributing to  $\beta 5i$ -selectivity:

- P1: the bulky and rigid Phe-side chain is favored by the more spacious S1 pocket of  $\beta 5i$  compared to the smaller one of  $\beta 5c$  (facilitated by the dislocation of Met45 and reorientation of Ile35).<sup>[6]</sup>
- P2: the electron-rich  $\pi$ -system of the Tyr(OMe)-side chain enhances sulfur-arene interactions with Cys48.
- P3: the small Ala-side chain preferentially occupies the smaller S3 pocket of  $\beta 5i$  (the substitution of Ala27 ( $\beta 5c$ ) by Ser27 ( $\beta 5i$ ) alters the polarity and the size of the S3 pocket of  $\beta 5i$ ).<sup>[6]</sup>

These findings are supported by the cleavage preferences of fluorogenic substrates specific for either  $\beta 5i$  or  $\beta 5c$ , which were investigated in kinetic experiments ( $\beta 5i$ : Ac-ANW-AMC;  $\beta 5c$ : Ac-WLA-AMC).<sup>[10]</sup> Recent efforts towards backbone optimization led to the development of PR-924 (132-fold  $\beta 5i$ -selectivity) and the derivative LU-035i (553-fold  $\beta 5i$ -selectivity).<sup>[11,12]</sup> The design of these compounds is based on a D-Ala in P3 that induces a sharp turn of the N-terminal 3-methyl-1*H*-indene cap, resulting in  $\beta 5i$ -selectivity (Figure 2.4). Moreover, LU-015i features the unnatural amino acid 3-Cyclohexyl-L-alanine in the P1-position, which impairs  $\beta 5c$  affinity twofold and improves  $\beta 5i$  potency by a factor of about 2 compared to PR-924.<sup>[12]</sup>

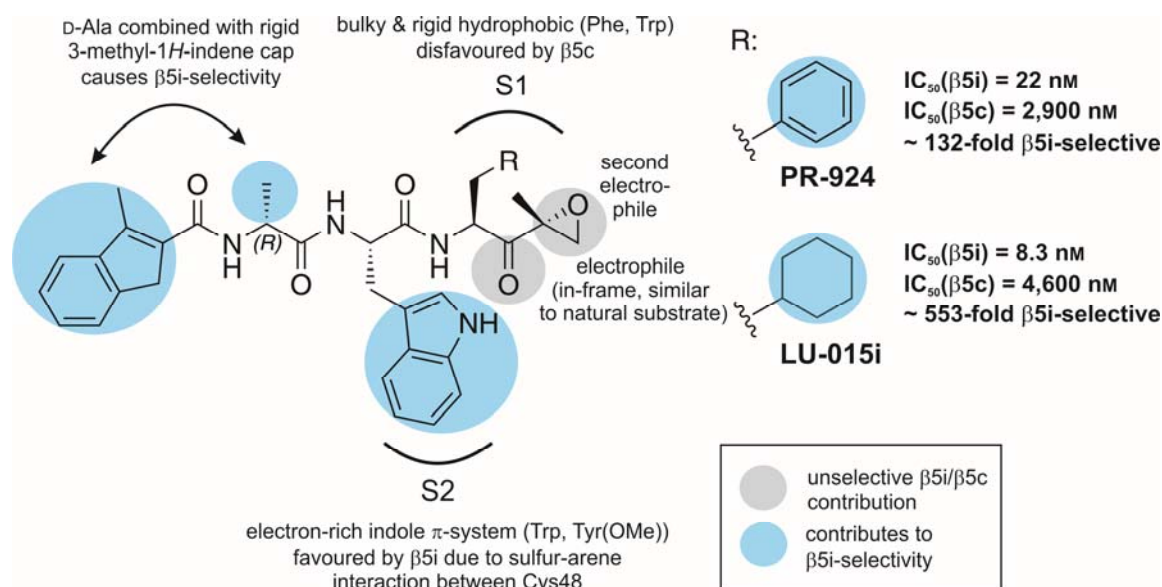


**Figure 2.4** Structures of PR-924 and LU-015i with the schematic depiction of the contributions of each side chain to the specificity pocket (S1-S2) stabilization resulting in  $\beta 5i$ -selectivity (grey: unselective; blue: selective for  $\beta 5i$ ). LU-015 contains 3-Cyclohexyl-L-alanine in the P1-position, which results in approximately fourfold enhanced  $\beta 5i$ -selectivity compared to PR-924.<sup>[12]</sup>



Taking all these factors into account, the design of  $\beta 5i$ -selective PSFs (Chapter 4) was initiated by the derivatization of the backbone of ONX 0914 with the sulfonyl fluoride warhead. Indeed, the resulting tripeptidic PSF **2** exhibited enhanced  $\beta 5i$ -selectivity (25-fold) compared to its  $\alpha',\beta'$ -epoxyketone counterpart ONX 0914 (~ nine-fold).<sup>[13]</sup> Since both compounds share an identical backbone, the shifted position of the sulfonyl fluoride electrophile, compared to the carbonyl electrophile of the epoxyketones, is responsible for the improved  $\beta 5i$ -selectivity (Figure 2.5). However, the inappropriate positioning of the electrophile diminishes the potency of PSF **2** against the ChTL activity of  $\beta 5i$  ( $IC_{50}(\beta 5i) = 1,134 \pm 146$  nM), indicating that PSFs require capped tetrapeptides for sufficient stabilization.<sup>[13]</sup> In order to improve potency, the backbone was extended with the P4-homophenylalanine derived from carfilzomib to yield PSF compound **3** (Figure 2.5). Interestingly, this improved the potency of compound **3** while fully retaining its  $\beta 5i$ -selectivity ( $IC_{50}(\beta 5i) = 139 \pm 34$  nM, 28-fold  $\beta 5i$ -selectivity).<sup>[13]</sup>

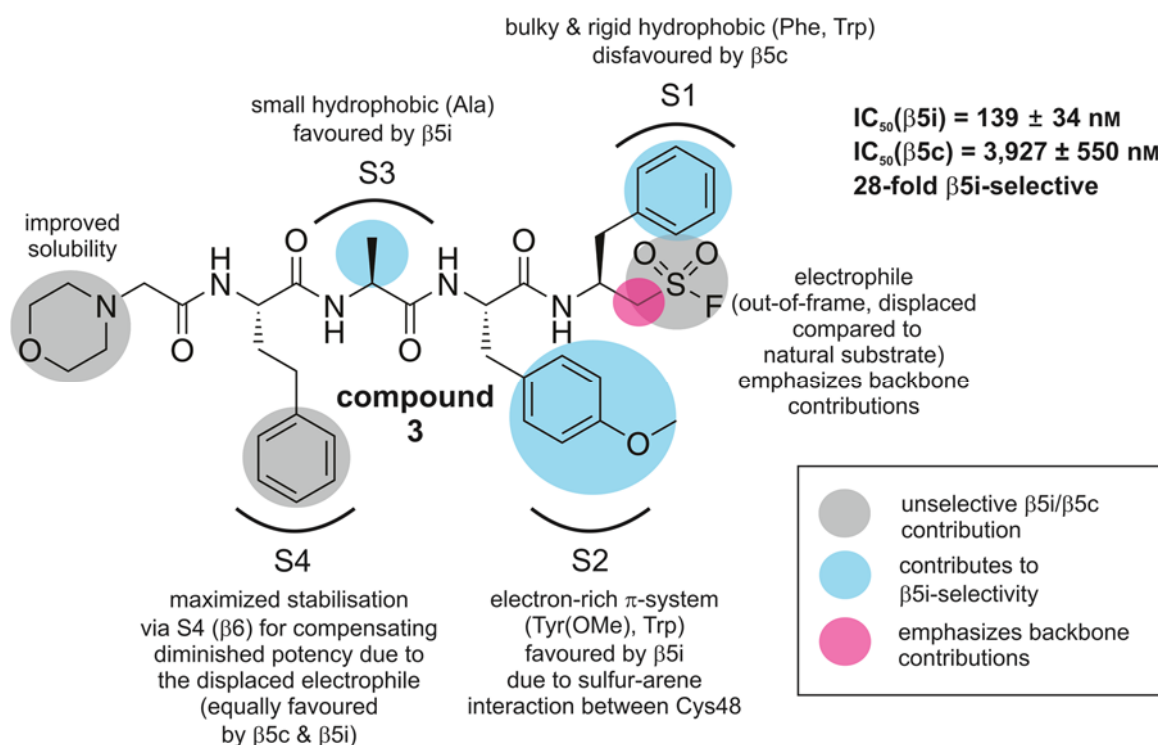


**Figure 2.5** Schematic representation of compound **3** (Chapter 4) with the contribution of each side chain to specificity pocket (S1-S4) stabilization resulting in  $\beta 5i$ -selectivity (grey: unselective; blue: selective for  $\beta 5i$ ; red: factor that emphasizes backbone contributions). The  $IC_{50}$  value against the ChTL activities of purified human iCP and cCP are given (right upper corner).<sup>[13]</sup>

## 2. Objective and summary of results

The same design principles were applied for the synthesis of peptidic sulfonate esters (Chapter 5), whereas the  $\beta 5i$ -selectivity was further improved by adapting the findings of de Bruin et al. 2014. It was shown that the side chain of 3-cyclohexyl-L-alanine in P1 disfavors binding to  $\beta 5c$ , thereby enhancing  $\beta 5i$ -selectivity compared to the phenylalanine moiety in P1 (Figure 2.6).<sup>[13]</sup>

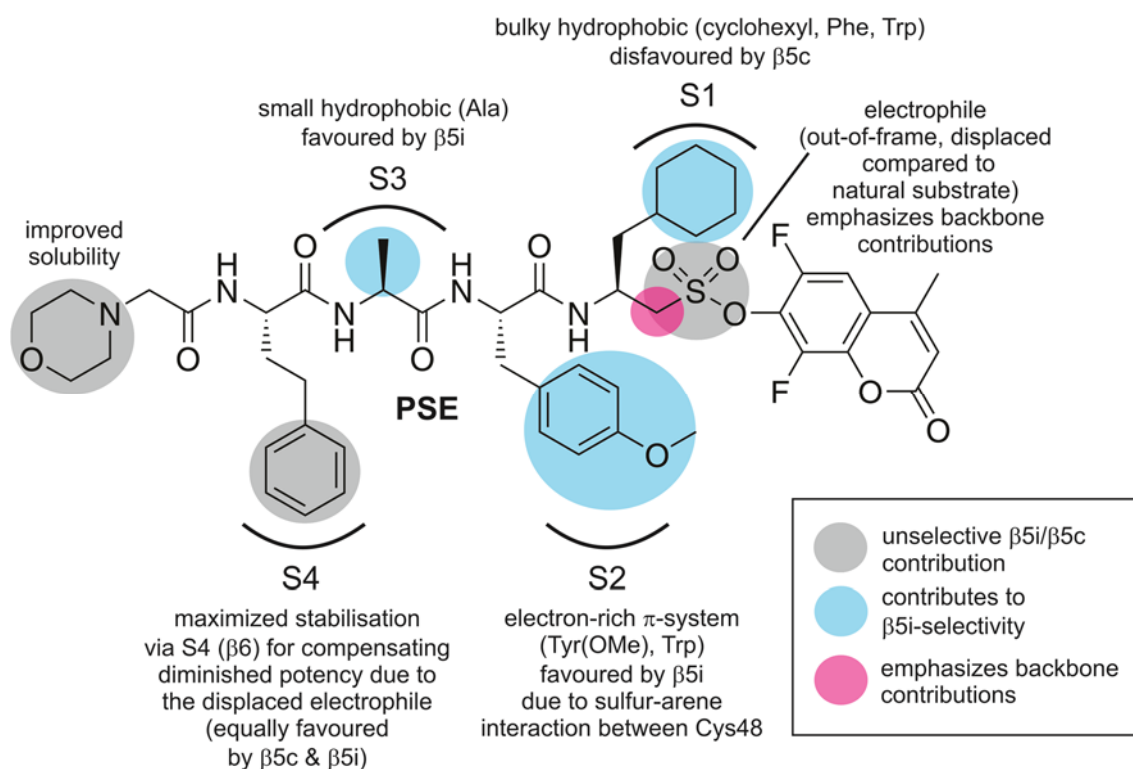


**Figure 2.6** Illustration of the PSE (Chapter 5) with the contributions of each side chain to specificity pocket (S1-S4) stabilization resulting in  $\beta 5i$ -selectivity (grey: unselective; blue: selective).

Lastly, it must be mentioned that the simplified dissection of individual side chain contributions should be regarded only as a guideline that insufficiently does justice to the complex nature of ligand binding. This is reflected in exceptional cases (e.g. oprozomib) and in the neglect of cooperative effects and the plasticity of specificity pockets during ligand binding which limit the validity of this model.



### 2.3.2 Peptidic $\beta 5i$ -selective inhibitors without C-terminal electrophiles

The ligand design described in the previous section was inspired by components of existing inhibitors, such as carfilzomib and ONX 0914, which had undergone extensive optimizations by Onyx Pharmaceuticals in terms of potency, selectivity and pharmacokinetic properties. This makes these agents a reliable source of inspiration for the development of similar peptidic inhibitors that employ a C-terminal warhead. However, the de novo design of new inhibitors requires a complete re-evaluation of each side chain contribution due to the altered binding mode in order to be able to pinpoint elements that generate  $\beta 5i$ -selectivity.

For the design of side chain-electrophiles containing decarboxylated peptides (Chapter 3) a 4-methylbenzyl amine<sup>[10,14]</sup> capped tetrapeptide derived from carfilzomib served as a starting point (see Figure 1.4 & 2.7). A screening for suitable electrophiles revealed that  $\alpha$ -chloroacetamides (**1-CA**) were potent ( $IC_{50}(\beta 5i) = 1.24 \mu M$ ) and selective inhibitors of subunit  $\beta 5i$  (nine-fold  $\beta 5i$ -selectivity), despite the unselective peptide backbone.<sup>[8]</sup>

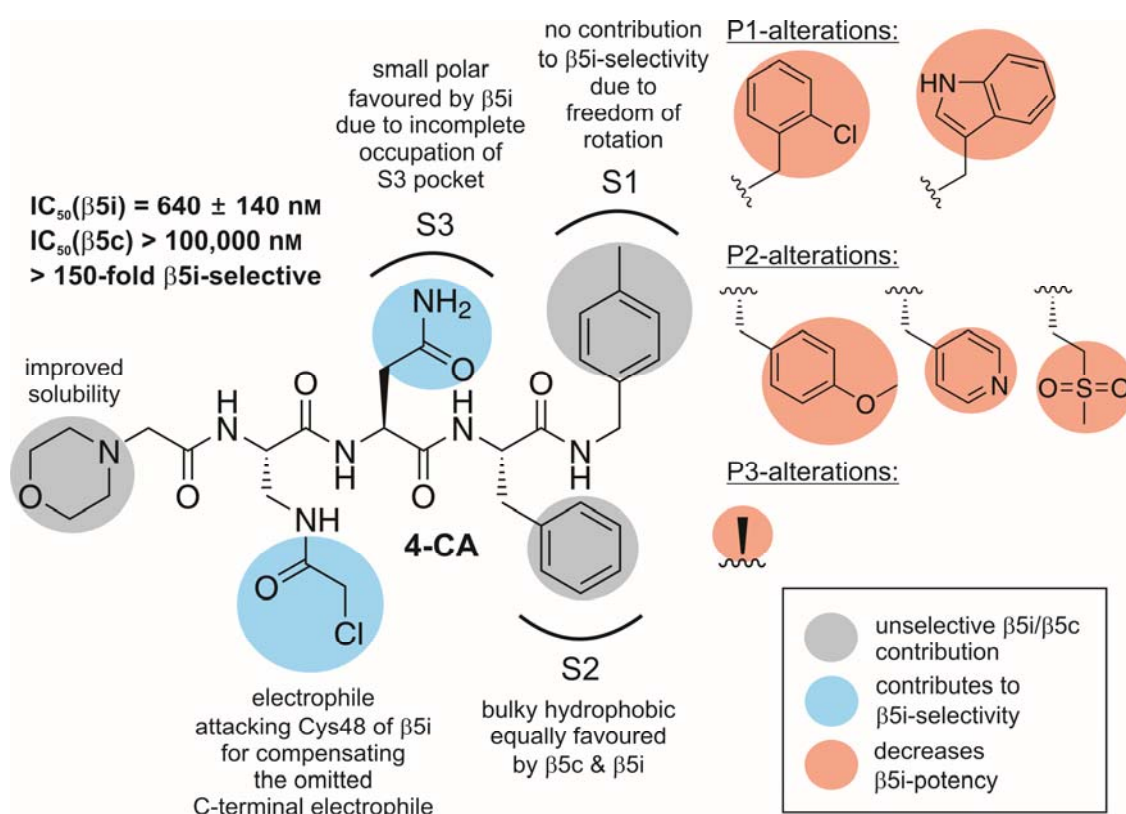


**Figure 2.7** Schematic depiction of **4-CA** (Chapter 3) with the contributions of each side chain to specificity pocket (S1-S3) stabilization resulting in  $\beta 5i$ -selectivity (grey: unselective; blue:  $\beta 5i$ -selective; red: decreases  $\beta 5i$ -potency). All described contributions apply only to  $\alpha$ -chloroacetamides containing decarboxylated peptides which are an exceptional case due to their special binding mode.

## 2. Objective and summary of results

In addition, an unreactive congener (**1-PA**) proved to have no  $\beta 5i$ -selectivity, revealing that it is solely the electrophile which generates nine-fold selectivity comparable to the optimized backbone of ONX 0914.<sup>[8]</sup> In an effort to enhance the  $\beta 5i$ -specificity via backbone optimization, the positions P1-P3 of **1-CA** were varied with the premise that these changes must not decrease potency but increase  $\beta 5i$ -specificity. Figure 2.7 summarizes important findings which emerged during the optimization process.

The failed attempts to generate selectivity by altering only the P1-site can be explained with the absence of a C-terminal electrophile and the resulting freedom of rotation of the toluoyl-cap (Figure 2.8).

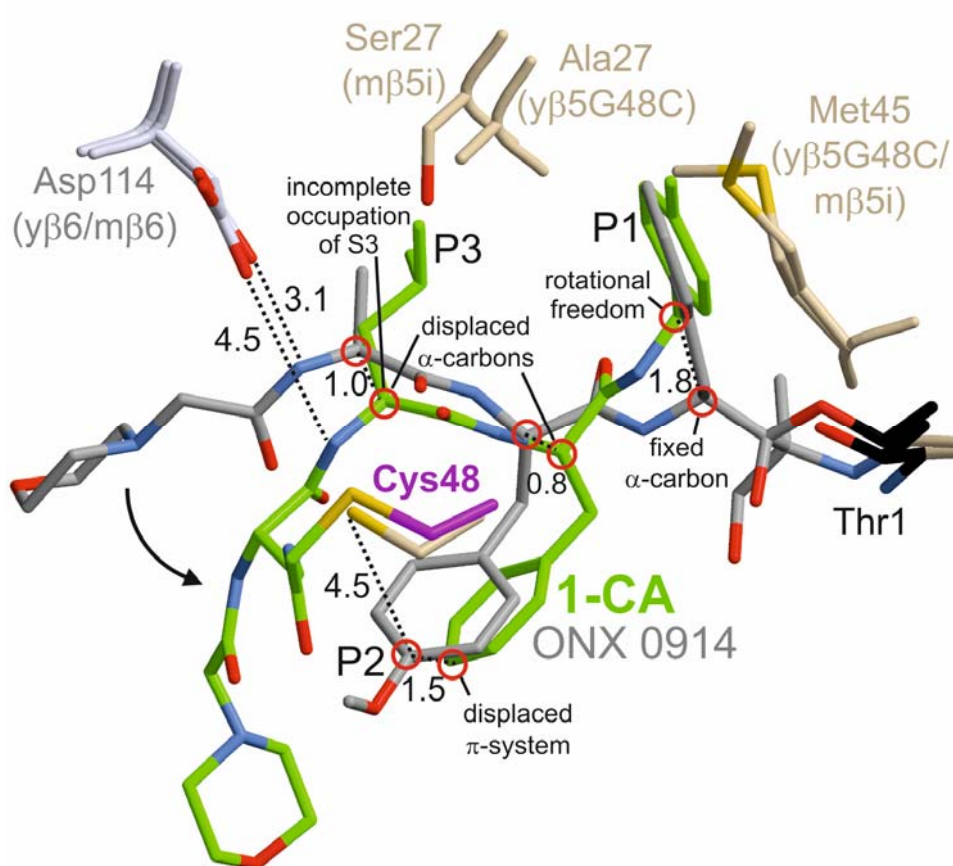


**Figure 2.8** Structural superposition of **1-CA** (green, PDB ID: 5CGG)<sup>[8]</sup> and ONX 0914 (grey, PDB ID: 5CGI)<sup>[8]</sup> bound to the  $\gamma\beta 5G48C$  mutant used as a model system and to  $m\beta 5i$ , respectively. The P1-P3-sites of the ligands and residues of subunits  $\gamma\beta 5G48C$  and  $m\beta 5i$  (beige) as well as  $\gamma\beta 6$  and  $m\beta 6$  (grey) are depicted including atomic distances in Å (black dashed lines). The movement of **1-CA** compared to ONX 0914 is illustrated by a black arrow. The resulting structural adjustments displace the  $\alpha$ -carbons and aromatic carbons of P2 (red circles) which has a substantial impact on the ligand-protein interactions. The figure is a modified adaption from Dubiella et al.<sup>[8]</sup>

This is supported by the finding that the unreactive congener **1-PA** is unselective, which strongly suggests that the P1-site plays no role in selectivity.<sup>[8]</sup> According to the structural

binding analysis, the P2-site is also not involved in generating specificity due to lacking sulfur-arene interactions with Cys48 of  $\beta 5i$  (Figure 2.8).<sup>[15,16]</sup> This was confirmed by introducing a Tyr(OMe) in the P2-position which diminished  $\beta 5i$ -potency.<sup>[8]</sup> Hence, variations of the P2-site were tested to improve solubility of the compounds but were shown to diminish  $\beta 5i$ -potency (Figure 2.7). Taken together these results imply that it is the P3-site that significantly contributes to  $\beta 5i$ -selectivity and potency. Since the P3-side chain of **1-CA** only partially occupies the S3-pocket due to a shift of the P3- $\alpha$ -carbon by 1.0 Å (Figure 2.8), the alanine residue in P3 offers insufficient stabilization of the ligand, explaining the reduced  $\beta 5i$ -potency.<sup>[8]</sup> Based on the fact that the S3-pocket of  $\beta 5i$  has a more hydrophilic character, due to Ser27 compared to Ala27 of  $\beta 5c$ , asparagine was chosen as a small and hydrophilic P3-residue to yield **4-CA** (Figure 2.8). Indeed, **4-CA** exhibited substantially improved potency against  $\beta 5i$  ( $IC_{50}(\beta 5i) = 640 \pm 140$  nM) versus  $\beta 5c$  ( $IC_{50}(\beta 5c) > 100$   $\mu$ M), with a  $\beta 5c/\beta 5i$ -selectivity of more than 150-fold.<sup>[8]</sup> Interestingly, the natural CP inhibitors TMC-95A-D, which were isolated from the fermentation broth of *Apiospora montagnei* Sacc. TC 1093, contain an Asn in the P3-position and employ a decarboxylated peptide backbone as well.<sup>[17]</sup> The crystal structure of yeast CP from *Saccharomyces cerevisiae* in complex with TMC-95A and synthetic replica<sup>[18,19]</sup> revealed a binding mode of the peptide backbone similar to linear peptide inhibitors.<sup>[20-22]</sup> Furthermore, the P3-Asn was identified as important hydrogen bonding partner with the amide group of Gln22 in subunit  $\gamma\beta 2$ .<sup>[20]</sup> However, the subunits  $\beta 5$  of human and murine iCPs bear Ala22 in this position, making it difficult to draw comparisons between the S3-stabilization of TMC-95A and **4-CA**, particularly in view of the incomplete occupation of the S3 pocket by **1-CA**. Nonetheless, natural products represent a valuable source of inspiration for the design of peptide CP inhibitors apart from synthetic compound.

In conclusion, structure-based inhibitor design identified the strictly conserved Cys48 of  $\beta 5i$  as a subunit-specific residue that is targetable by P4-electrophile-containing tetrapeptides. Structural investigations of the novel binding mode provided indications for their further rational optimization, while elucidating the key factors for  $\beta 5i$ -selectivity of this new compound class.

## 2.4 References

- [1] T. Muchamuel, M. Basler, M. A. Aujay, E. Suzuki, K. W. Kalim, C. Lauer, C. Sylvain, E. R. Ring, J. Shields, J. Jiang, et al., *Nat. Med.* **2009**, *15*, 781–787.
- [2] F. Parlati, S. J. Lee, M. Aujay, E. Suzuki, K. Levitsky, J. B. Lorens, D. R. Micklem, P. Ruurs, C. Sylvain, Y. Lu, et al., *Blood* **2009**, *114*, 3439–3447.
- [3] A. C. Mirabella, A. A. Pletnev, S. L. Downey, B. I. Florea, T. B. Shabaneh, M. Britton, M. Verdoes, D. V. Filippov, H. S. Overkleeft, A. F. Kisselev, *Chem. Biol.* **2011**, *18*, 608–618.
- [4] M. Britton, M. M. Lucas, S. L. Downey, M. Screen, A. A. Pletnev, M. Verdoes, R. A. Tokhunts, O. Amir, A. L. Goddard, P. M. Pelphrey, et al., *Chem. Biol.* **2009**, *16*, 1278–1289.
- [5] D. Niewerth, J. van Meerloo, G. Jansen, Y. G. Assaraf, T. C. Hendrickx, C. J. Kirk, J. L. Anderl, S. Zweegman, G. J. L. Kaspers, J. Cloos, *Biochem. Pharmacol.* **2014**, *89*, 43–51.
- [6] E. M. Huber, M. Basler, R. Schwab, W. Heinemeyer, C. J. Kirk, M. Groettrup, M. Groll, *Cell* **2012**, *148*, 727–738.
- [7] W. Harshbarger, C. Miller, C. Diedrich, J. Sacchettini, *Structure* **2015**, *23*, 418–424.
- [8] C. Dubiella, R. Baur, H. Cui, E. M. Huber, M. Groll, *Angew. Chem. Int. Ed.* **2015**, doi: 10.1002/anie.201506631.
- [9] S. D. Demo, C. J. Kirk, M. A. Aujay, T. J. Buchholz, M. Dajee, M. N. Ho, J. Jiang, G. J. Laidig, E. R. Lewis, F. Parlati, et al., *Cancer Res.* **2007**, *67*, 6383–6391.
- [10] C. Blackburn, K. M. Gigstad, P. Hales, K. Garcia, M. Jones, F. J. Bruzzese, C. Barrett, J. X. Liu, T. A. Soucy, D. S. Sappal, et al., *Biochem. J.* **2010**, *430*, 461–476.
- [11] A. V Singh, M. Bandi, M. a Aujay, C. J. Kirk, D. E. Hark, N. Raje, D. Chauhan, K. C. Anderson, *Br. J. Haematol.* **2011**, *152*, 155–163.
- [12] G. De Bruin, E. M. Huber, B.-T. Xin, E. J. van Rooden, K. Al-Ayed, K.-B. Kim, A. F. Kisselev, C. Driessen, M. Van Der Stelt, G. A. van der Marel, et al., *J. Med. Chem.* **2014**, *57*, 6197–6209.
- [13] C. Dubiella, H. Cui, M. Gersch, A. J. Brouwer, S. a. Sieber, A. Krüger, R. M. J. Liskamp, M. Groll, *Angew. Chem. Int. Ed.* **2014**, *53*, 11969–11973.
- [14] C. Blackburn, C. Barrett, J. L. Blank, F. J. Bruzzese, N. Bump, L. R. Dick, P. Fleming, K. Garcia, P. Hales, M. Jones, et al., *Medchemcomm* **2012**, *3*, 710–719.
- [15] L. M. Salonen, M. Ellermann, F. Diederich, *Angew. Chemie - Int. Ed.* **2011**, *50*, 4808–4842.
- [16] K. N. Daeffler, H. A. Lester, D. A. Dougherty, *J. Am. Chem. Soc.* **2012**, *134*, 14890–14896.
- [17] J. Kohno, Y. Koguchi, M. Nishio, K. Nakao, M. Kuroda, R. Shimizu, T. Ohnuki, S. Komatsubara, *J. Org. Chem.* **2000**, *65*, 990–995.
- [18] M. Kaiser, A. Milbradt, C. Siciliano, I. Assfalg-Machleidt, W. Machleidt, M. Groll, C. Renner, L. Moroder, *Chem. Biodiv.* **2004**, *1*, 161–173.
- [19] M. Kaiser, M. Groll, C. Renner, R. Huber, L. Moroder, *Angew. Chem. Int. Ed.* **2002**, *41*, 780–783.
- [20] M. Groll, Y. Koguchi, R. Huber, J. Kohno, *J. Mol. Biol.* **2001**, *311*, 543–548.
- [21] M. Kaiser, M. Groll, C. Siciliano, I. Assfalg-Machleidt, E. Weyher, J. Kohno, A. G. Milbradt, C. Renner, R. Huber, L. Moroder, *ChemBioChem* **2004**, *5*, 1256–1266.
- [22] M. Groll, M. Götz, M. Kaiser, E. Weyher, L. Moroder, *Chem. Biol.* **2006**, *13*, 607–614.

### 3 Targeting a non-catalytic cysteine of subunit $\beta 5i$

The research of this chapter was originally published in *Angewandte Chemie International Edition* **2015**, doi: 10.1002/anie.201506631, by Christian Dubiella, Regina Baur, Haissi Cui, Eva M. Huber and Michael Groll.

Copyright © 2015 Wiley-VCH Verlag GmbH & Co. KGaA, Weinheim, Germany. Reproduced with permission.

#### *Summary*

This publication reports a new strategy for the development of selective iCP inhibitors. We rationally designed decarboxylated peptides that covalently target an isoform-specific, non-catalytic cysteine of the iCP subunit  $\beta 5i$  via  $\alpha$ -chloroacetamide containing side chains. Structure-based optimization of the inhibitors led to over 150-fold selectivity towards subunit  $\beta 5i$  versus  $\beta 5c$ . The enhanced isoform-specificity decreased cytotoxic effects and suppressed the production of inflammatory cytokines which has the potential to modulate chronic inflammations and autoimmune diseases. This is in contrast to currently clinically applied proteasome inhibitors which induce apoptosis by the concomitant blockage of cCPs and iCPs. Hence, this new class of compounds provides a starting point for the development of selective iCP inhibitors as potential anti-inflammatory agents.

This summary is based on the above mentioned publication and is subject of copyright © 2015 Wiley-VCH Verlag GmbH & Co. KGaA, Weinheim, Germany.

#### *Author contributions*

C. Dubiella as first and corresponding author conceived the project including planning and execution. C. Dubiella performed all experiments unless noted otherwise including organic synthesis, activity assays and crystal soaking experiments. R. Baur as intern helped with the synthesis of compounds during a practical course. H. Cui performed cell-based activity and cytotoxicity assays. E. M. Huber provided the yeast mutant strain. M. Groll solved crystal structures and supervised the project. C. Dubiella wrote the manuscript with input of M. Groll and all involved authors.



# Selective Inhibition of the Immunoproteasome by Structure-Based Targeting of a Non-catalytic Cysteine

Christian Dubiella,\* Regina Baur, Haissi Cui, Eva M. Huber, and Michael Groll\*

Dedicated to Professor Luis Moroder on the occasion of his 75th birthday

**Abstract:** Clinically applied proteasome inhibitors induce cell death by concomitant blockage of constitutive and immunoproteasomes. In contrast, selective immunoproteasome inhibition is less cytotoxic and has the potential to modulate chronic inflammation and autoimmune diseases. In this study, we rationally designed decarboxylated peptides that covalently target a non-catalytic cysteine of the immunoproteasome subunit  $\beta 5i$  with  $\alpha$ -chloroacetamide-containing sidechains. The enhanced isoform specificity decreased cytotoxic effects and the compound suppressed the production of inflammatory cytokines. Structure-based optimization led to over 150-fold selectivity for subunit  $\beta 5i$  over  $\beta 5c$ . This new compound class provides a promising starting point for the development of selective immunoproteasome inhibitors as potential anti-inflammatory agents.

Core particles (CPs) of the proteasome degrade the majority of intracellular proteins and represent essential elements for cell function and survival.<sup>[1]</sup> While the constitutive proteasome (cCP) is expressed ubiquitously as a central proteolytic machinery, its immunomodulatory isoform, the immunoproteasome (iCP), is predominantly found in cells associated with the immune system.<sup>[2]</sup> During inflammatory states, iCPs influence the production of cytokines and alter antigen processing, thereby facilitating immune responses.<sup>[2]</sup> The FDA-approved CP inhibitors bortezomib and carfilzomib (CFZ) block the catalytically active  $\beta 5$  subunits of the cCP ( $\beta 5c$ ) and iCP ( $\beta 5i$ /LMP7) equally.<sup>[3]</sup> However, simultaneous inhibition of  $\beta 5c$  and  $\beta 5i$  or combined blockage of other proteolytic subunits ( $\beta 1i$ /LMP2,  $\beta 1c$ ,  $\beta 2i$ /MECL1,  $\beta 2c$ ) induces cytotoxicity, which limits the clinical application of both drugs to the treatment of blood cancer.<sup>[4]</sup> In contrast, the agent ONX 0914 (PR-957) avoids cytotoxic effects by predominantly blocking  $\beta 5i$ . This compound was shown to attenuate the progression of multiple sclerosis and rheumatoid arthritis in mouse models.<sup>[5,6]</sup>  $\beta 5i$  is thus a promising therapeutic target for chronic inflammation and autoimmune disorders.<sup>[7]</sup> ONX 0914 displays an approximately ten-fold preference for  $\beta 5i$  versus  $\beta 5c$  owing to an optimized peptide

backbone composition.<sup>[5]</sup> Enhanced binding affinity is achieved through an epoxyketone electrophile that reacts irreversibly with the active-site nucleophile Thr1 (Scheme S1).<sup>[8]</sup> However, reactive C-terminal warheads have the potential to co-inhibit  $\beta 5c$  as well, since the mechanism of proteolysis is the same for all proteasomal active sites. In an attempt to find new target residues that are independent from the proteasomal active site, we followed a structure-guided approach for the design of  $\beta 5i$ -specific inhibitors without a C-terminal warhead. By targeting a non-catalytic cysteine as a compensating anchor residue, we aimed to retain sustained covalent binding. The same concept is successfully exploited by inhibitors against various kinases,<sup>[9]</sup> G-proteins,<sup>[10]</sup> and the  $\gamma 2$  subunit<sup>[11]</sup> of the yeast proteasome (yCP). Structural superposition of the murine subunits  $m\beta 5c$  and  $m\beta 5i$  in combination with sequence alignments highlight Cys48 as a strictly conserved nucleophilic residue that is exclusively found in  $\beta 5i$  (Figure 1).<sup>[8]</sup>

Cys48 is located at a positively charged  $\alpha$ -helix dipole, which has the potential to lower the  $pK_a$  value of the thiol group, thereby increasing its nucleophilicity. Furthermore,

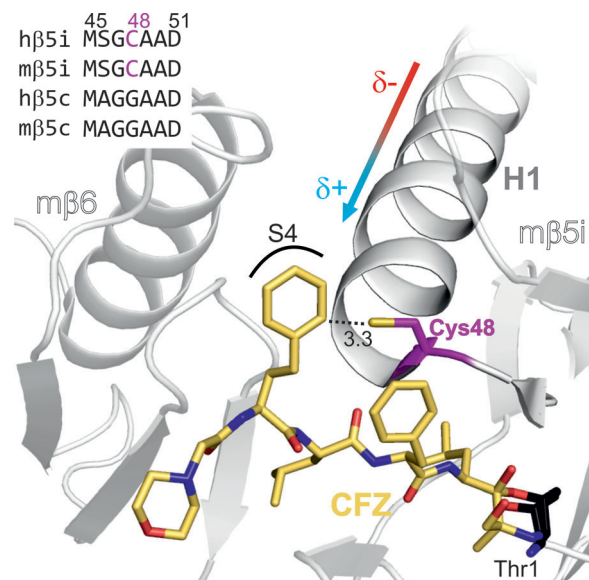


**Figure 1.** Structural superposition of the murine subunits  $m\beta 5i$  and  $m\beta 6$  (PDB ID: 3UNH)<sup>[8]</sup> with CFZ (yellow) bound to Thr1 (black) of subunit  $\gamma 5$  of yCP (PDB ID: 4QW4).<sup>[12]</sup> The homophenylalanine P4 residue of CFZ occupies the specificity pocket S4 and is positioned in proximity to Cys 48 (magenta, 3.3 Å) of  $m\beta 5i$ . The positively charged N-terminal end of the  $\alpha$ -helix dipole H1 points at Cys 48. The sequence alignment of  $\beta 5i$  and  $\beta 5c$  shows Cys 48 highlighted in magenta (h = human, m = mouse; upper left corner).

[\*] C. Dubiella, R. Baur, H. Cui, Dr. E. M. Huber, Prof. Dr. M. Groll  
 Center for Integrated Protein Science Munich (CIPSM)  
 Department of Chemistry, Technische Universität München  
 Lichtenbergstrasse 4, 85748 Garching (Germany)  
 E-mail: christian.dubiella@mytum.de  
 michael.groll@tum.de

Supporting information for this article is available on the WWW under <http://dx.doi.org/10.1002/anie.201506631>.



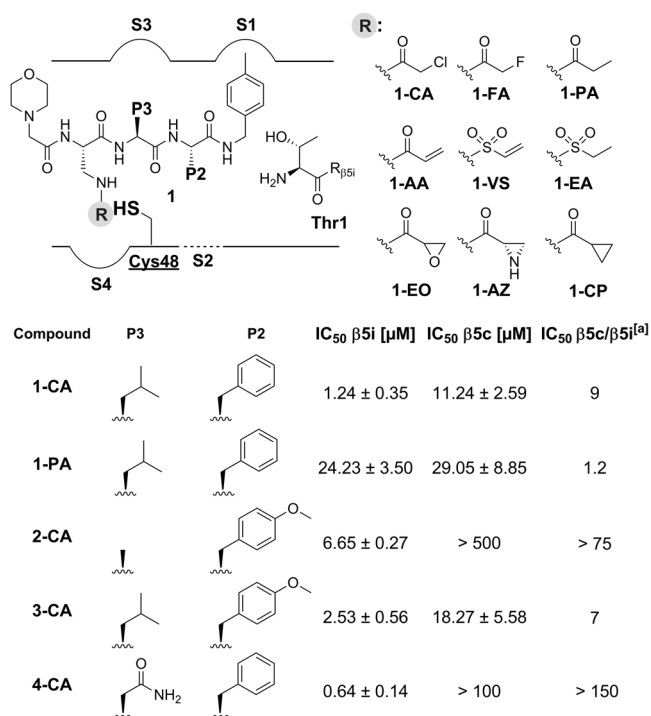


**Figure 2.** Schematic representation of the substrate binding channel of  $\beta 5i$  with the specificity pockets S1–S4 and Cys48 (underlined). The CFZ-derived decarboxylated peptides **1** contain distinct P4 side-chain electrophiles (R, gray):  $\alpha$ -chloroacetamide (**1-CA**),  $\alpha$ -fluoroacetamide (**1-FA**), acrylamide (**1-AA**), vinyl sulfonamide (**1-VS**), epoxide (**1-EO**), and aziridine (**1-AZ**). Corresponding non-reactive controls: propionamide (**1-PA**), ethylsulfonamide (**1-EA**), cyclopropanamide (**1-CP**). A complete list of compounds, including half-maximal inhibitory concentration (IC<sub>50</sub>) values, can be found in the supporting information (Tables ST1–3). The lower panel shows the  $\alpha$ -chloroacetamides **1-CA**–**4-CA** with their corresponding P2 and P3 residues and the control, **1-PA**. The in vitro IC<sub>50</sub> values were determined by using purified human iCP or cCP. [a] A high IC<sub>50</sub>  $\beta 5c/\beta 5i$  ratio indicates selectivity for  $\beta 5i$ .

Cys48 participates in forming the substrate binding channel of  $\beta 5i$  by partially shaping the S2 and S4 pockets. According to structural superpositions, it is accessible via the P4 side chains of tetrapeptides (Figure 1). Consequently, we initiated our inhibitor design by exchanging the P4 residue of CFZ with L-2,3-diaminopropionic acid (Dap). Dap suits the steric requirements of S4 and allows the late-stage introduction of electrophiles owing to its side-chain amino function (Figure 2).

The CFZ-inspired peptide backbone was prepared by solid-phase peptide synthesis using the Fmoc strategy and was C-terminally capped with the previously described 4-methylbenzyl amine.<sup>[13,14]</sup> In the final step, we introduced various electrophiles by utilizing the corresponding acid chlorides, *N*-hydroxysuccinimide esters, or carboxylic acids in amide coupling reactions. This straightforward synthesis was used to generate a set of decarboxylated peptides with diverse side-chain electrophiles that were shown to be suitable for targeting soft thiol nucleophiles (**1-CA**, **1-FA**, **1-AA**, **1-VS**, **1-EO**, and **1-AZ**; Figure 2).<sup>[9]</sup> As controls, we prepared their unreactive congeners **1-PA**, **1-EA**, and **1-CP** (Figure 2).

Our initial screening efforts using human iCP and cCP showed that sulfonamide compounds (**1-VS**, **1-EA**) are slightly selective for  $\beta 5c$ , whereas amide-bond-connected electro-

philes (**1-CA**, **1-FA**, **1-AA**, **1-EO**, **1-AZ**) displayed a preference for  $\beta 5i$  (Table ST1 and Figure S1 in the Supporting Information). The most potent electrophile in the screen was **1-CA**, which showed substantial activity against  $\beta 5i$  (IC<sub>50</sub> = 1.24  $\mu$ M, Figure 2). This is in agreement with studies that propose  $\alpha$ -chloroacetamides for sustained targeting of non-catalytic cysteines.<sup>[10,15]</sup> Despite the unselective peptide backbone of **1-CA**, it displayed nine-fold selectivity for  $\beta 5i$  ( $\beta 5c/\beta 5i = 9$ ), which is comparable to that of ONX 0914 ( $\beta 5c/\beta 5i \approx 10$ ).<sup>[5]</sup> Importantly, **1-CA** was inactive against the subunits  $\beta 1c$ ,  $\beta 1i$ ,  $\beta 2c$ , and  $\beta 2i$  (IC<sub>50</sub> > 100  $\mu$ M, Table ST2). The more stable **1-FA**, as well as the unreactive congener **1-PA**, showed significantly decreased IC<sub>50</sub> values compared to **1-CA**, and both blocked the activity of  $\beta 5i$  (IC<sub>50</sub> = 36.25  $\mu$ M and 24.23  $\mu$ M, respectively) and  $\beta 5c$  (IC<sub>50</sub> = 43.84  $\mu$ M and 29.05  $\mu$ M, respectively) to the same extent ( $\beta 5c/\beta 5i = 1.2$ , Figure 2 and Table ST1). These findings indicate that the  $\beta 5i$  binding affinity originates from the  $\alpha$ -chloroacetamide electrophile forming a covalent thioether with Cys48 (Scheme S2).

Next, we aimed to assess the covalent binding mode of **1-CA** by X-ray analysis. Since mammalian iCPs are challenging to crystallize, we mimicked the S4 pocket of  $\beta 5i$  by replacing Gly48 of the yeast proteasome subunit  $\gamma 5$  with Cys48 in a plasmid-shuffling procedure (Figure S3a). Subsequent crystallization and structure elucidation of the  $\gamma 5G48C$  mutant yCP (2.8 Å resolution,  $R_{\text{free}} = 20.1\%$ , PDB ID: 5CGF, Table ST4) revealed an orientation of Cys48 identical to that observed in iCP from mouse. In addition, elucidation of the  $\gamma 5G48C$ :ONX 0914 complex structure (2.8 Å resolution,  $R_{\text{free}} = 20.6\%$ , PDB ID: 5CGI) showed a conformation of the ligand analogous to that observed in m $\beta 5i$  (Figure S4, S5). Strikingly, soaking of  $\gamma 5G48C$  yCP crystals with **1-CA** followed by X-ray analysis (2.9 Å resolution,  $R_{\text{free}} = 23.1\%$ , PDB ID: 5CGG) displayed the ligand exclusively bound to the mutant  $\gamma 5$  subunit. **1-CA** occupied the substrate binding channel by adopting an antiparallel  $\beta$ -sheet in a similar manner to known inhibitors that are based on decarboxylated peptides.<sup>[13,14]</sup> In fact, the structure revealed continuous electron density connecting the acetamide function of the P4 side chain of **1-CA** to the thiol group of the introduced Cys48 (Figure 3a). This linkage confirms a covalent mode of action and explains the nine-fold selectivity of **1-CA** for  $\beta 5i$ . In contrast, soaking of wild-type yCP crystals as a model for cCP showed empty  $\gamma 5$  substrate channels, thus emphasizing the importance of Cys48 for **1-CA** binding.

Based on these results, we optimized the peptidic backbone to improve  $\beta 5i$  selectivity. As a starting point, we used the peptide composition of ONX 0914 as a molecular blueprint and generated **2-CA** (Figure 2 and Table ST2). Unexpectedly, **2-CA** showed decreased potency against human  $\beta 5i$  (IC<sub>50</sub> = 6.65  $\mu$ M) and did not bind to the  $\gamma 5G48C$  mutant in soaking experiments. To understand this drop in potency, we compared the binding mode of ONX 0914 with that of **1-CA** and found pronounced differences: the structure of ONX 0914 bound to  $\gamma 5G48C$  revealed a distinct orientation of the P2-TyrOMe that facilitates attractive sulfur–arene interactions with Cys48.<sup>[16,17]</sup> In contrast, the P2-Phe of **1-CA** is displaced by the P4 side chain, which covalently binds to Cys48, thereby restricting the S2 pocket. To probe the



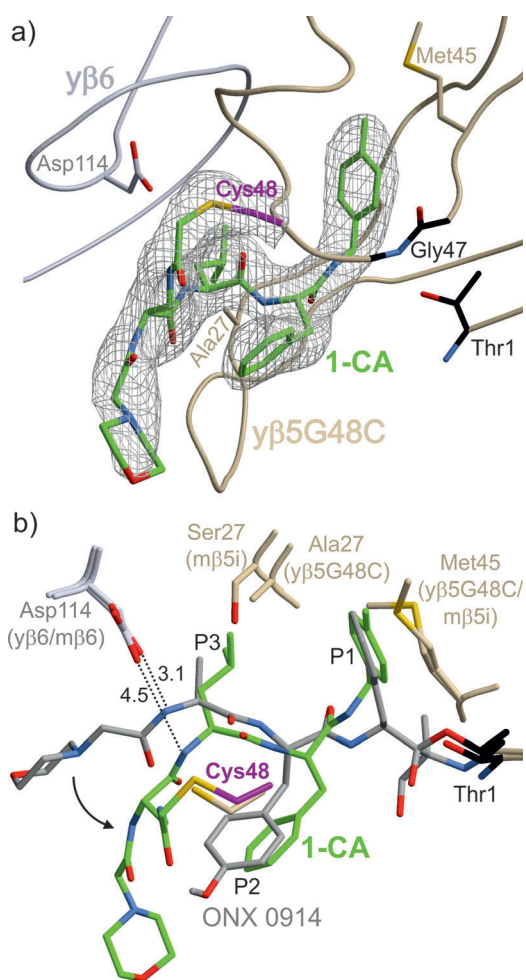


**Figure 3.** X-ray analysis for the binding of **1-CA** to the  $\gamma\beta 5G48C$  mutant (PDB ID: 5CGG). a) The  $2F_o - F_c$  electron density map (gray mesh, contoured at  $1\sigma$ , 2.9 Å resolution) depicts **1-CA** (green) bound to Cys48 (magenta) of subunit  $\gamma\beta 5G48C$  (beige) with the active-site nucleophile Thr1 (black), oxyanion hole amide of Gly47 (black), and Asp114 of  $\gamma\beta 6$  (gray). b) Structural superposition of **1-CA** (green) and ONX 0914 (gray) bound to  $\gamma\beta 5G48C$  and to  $m\beta 5i$  (PDB ID: 3UNF), respectively. The P1–P3 sites of the ligand and residues of subunits  $\gamma\beta 5$ ,  $m\beta 5i$  (beige), as well as  $\gamma\beta 6$  and  $m\beta 6$  (gray), are shown, including distances in Å (black dashed lines). The movement of **1-CA** compared to ONX 0914 is illustrated by a black arrow.

isolated impact of P2-TyrOMe of **2-CA**, we generated **3-CA** (Figure 2, Table ST2). This compound showed inferior  $\beta 5i$ -binding affinity ( $IC_{50} = 2.53 \mu M$ ) compared to that of **1-CA** ( $IC_{50} = 1.24 \mu M$ ), thus demonstrating a minor contribution from the S2 pocket. Taken together, these results suggest that the P3 site has a greater influence on potency. Remarkably, the P3-Leu of **1-CA** only incompletely occupies the S3 pocket, which displaces the residual backbone towards subunit  $\beta 5$  (Figure 3b). Therefore, the binding of **1-CA** solely depends on interactions with  $\beta 5$ , while the peptide backbone of ONX 0914 is additionally stabilized by Asp114 of  $\beta 6$  (Figure 3b and Figure S6). Since subunit  $\beta 6$  is identical in cCP and iCP, the design of **1-CA** is advantageous owing to an absence of interactions with  $\beta 6$ . To test whether the shift of **1-CA** towards  $\beta 5$  is caused by the short Dap spacer, we extended the P4 side chain by replacing Dap with the more

flexible L-2,4-diaminobutyric acid (Dab) to give **1-Dab-CA** (Table ST3). However, this resulted in a ten-fold decreased activity against  $\beta 5i$  ( $IC_{50} = 13.07 \mu M$ ), thus indicating that the conformationally constrained Dap already has the optimal linker size. Our findings imply that ligand stabilization in the S3 pocket is crucial for the correct positioning of the adjacent P4- $\alpha$ -chloroacetamide. In a similar fashion, the selectivity of ONX 0914 is mainly generated through interactions of the P1-Phe with the S1 pocket, which align the C-terminal warhead for nucleophilic attack of Thr1.<sup>[8]</sup>

As a result, we focused on the most prominent differences between the S3 pockets of human  $\beta 5i$  and  $\beta 5c$  by applying homology modelling combined with sequence alignments (Figure S3b). The strictly conserved substitution of Ala27 ( $\beta 5c$ ) by Ser27 ( $\beta 5i$ ) alters the polarity and size of the S3 pocket (Figure 3b).<sup>[8]</sup> To address this observation, we generated **4-CA** (Figure 2), in which an Asn in the P3 position allows enhanced hydrogen bonding to Ser27. Indeed, **4-CA** exhibited up to 150-fold selectivity for  $\beta 5i$  ( $IC_{50} = 0.64 \mu M$ ) over  $\beta 5c$ , whereas the unreactive congener **4-PA** proved to be only seven-fold selective for  $\beta 5i$ , with significantly decreased potency ( $IC_{50} = 29.29 \mu M$ ; Table ST2). These observations confirm that the nature of the P3 residue and its stabilization are crucial for appropriate ligand binding. We could achieve  $\beta 5i$  selectivity by exclusively modifying the P3 position. This is in contrast to Thr1-targeting inhibitors, which primarily rely on P1-residue stabilization.

Next, we aimed to examine the effect of **1-CA** and **4-CA** in cell-culture assays. Our prime focus was to analyze their inhibitory and cytotoxic profiles, as well as their impact on the production of inflammatory cytokines. By using a luminogenic substrate assay, we first determined the in vivo  $IC_{50}$  values with lysate from THP-1 cells, which constitutively express high levels of iCP.<sup>[18]</sup> Both **1-CA** ( $IC_{50} = 2.83 \mu M$ ) and **4-CA** ( $IC_{50} = 3.55 \mu M$ ) substantially blocked  $\beta 5$  activity compared to the unreactive control **1-PA** ( $IC_{50} = 36.69 \mu M$ ), which is in line with the in vitro data (Figure S7a). Second, we investigated the effects on cell viability. Concentrations of up to  $10 \mu M$  of **1-CA** and **4-CA** had no effect on the cells (Figure S7b). Finally, we evaluated the possible application of **1-CA** as an anti-inflammatory agent based on the favorable pharmacokinetics of the CFZ backbone. We examined its effect on the inflammation markers tumor necrosis factor alpha (TNF- $\alpha$ ) and interleukin 6 (IL-6) by using an enzyme-linked immunosorbent assay (ELISA). **1-CA** indeed suppressed the production of TNF- $\alpha$  and IL-6 in a dose-dependent manner.  $10 \mu M$  of **1-CA** reduced IL-6 levels substantially without causing cell death, and  $25 \mu M$  led to a reduction in TNF- $\alpha$  production (Figure 4, Figure S8). This reduction in cytokine production has similarly been described for ONX 0914.<sup>[5]</sup>

In summary, our study describes the first immunoproteasome inhibitor that acts independently of the active-site nucleophile Thr1. Commencing with structural bioinformatics, we identified Cys48 in  $\beta 5i$  as an isoform-specific nucleophilic residue that is accessible to tetrapeptides. For this purpose, we synthesized decarboxylated peptides and performed an electrophile screening procedure, which revealed the  $\alpha$ -chloroacetamide warhead of **1-CA** as the best option. In addition, we optimized the P3 site based on

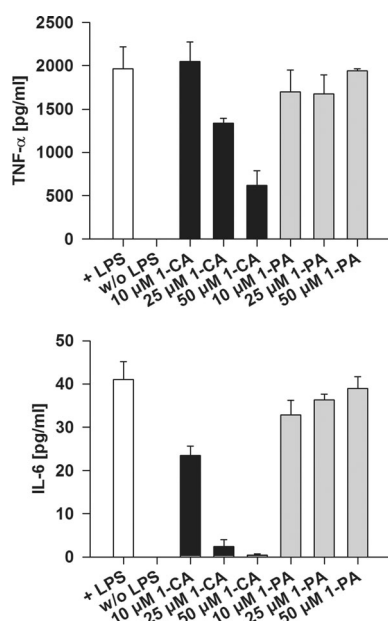


**Figure 4.** Quantification of the cytokines TNF- $\alpha$  and IL-6 produced by THP-1 cells after exposure to lipopolysaccharides (LPS, controls as white bars) and treatment with various concentrations (10–50  $\mu$ M) of **1-CA** (black bars) and **1-PA** (gray bars) as a negative control by ELISA. **1-CA** suppresses IL-6 and TNF- $\alpha$  production in a dose-dependent manner. Data are shown as the mean  $\pm$  standard error of the mean ( $n = 4$ ).

structural information, thereby underlining its impact on  $\beta$ 5i selectivity for this new concept of inhibition. Cell-based assays confirmed that **1-CA** blocks the activity of  $\beta$ 5 at concentrations below the induction of cytotoxicity, thereby suppressing the production of cytokines such as TNF- $\alpha$  and IL-6. Taken together, these properties highlight this new class of compounds as a starting point for the development of selective immunoproteasome inhibitors as potential anti-inflammatory agents.

## Acknowledgements

This work was funded by SFB 1035/A2. We thank Richard Feicht for experimental support and the staff of PXI of the Paul Scherrer Institute, Swiss Light Source (Villigen, Switzerland) for help with data collection.

**Keywords:** drug design · immunology · immunoproteasome · selective inhibitors · structure–activity relationships

- [1] A. Hershko, A. Ciechanover, *Annu. Rev. Biochem.* **1998**, *67*, 425–479.
- [2] M. Groettrup, C. J. Kirk, M. Basler, *Nat. Rev. Immunol.* **2010**, *10*, 73–78.
- [3] S. D. Demo, C. J. Kirk, M. A. Aujay, T. J. Buchholz, M. Dajee, M. N. Ho, J. Jiang, G. J. Laidig, E. R. Lewis, F. Parlati, et al., *Cancer Res.* **2007**, *67*, 6383–6391.
- [4] a) F. Parlati, S. J. Lee, M. Aujay, E. Suzuki, K. Levitsky, J. B. Lorens, D. R. Mickle, P. Ruurs, C. Sylvain, Y. Lu, et al., *Blood*

**2009**, *114*, 3439–3447; b) D. Niewerth, J. van Meerloo, G. Jansen, Y. G. Assaraf, T. C. Hendrickx, C. J. Kirk, J. L. Anderl, S. Zweegman, G. J. L. Kaspers, *Biochem. Pharmacol.* **2014**, *89*, 43–51; c) A. C. Mirabella, A. A. Pletnev, S. L. Downey, B. I. Florea, T. B. Shabaneh, M. Britton, M. Verdoes, D. V. Filippov, H. S. Overkleeft, A. F. Kisselev, *Chem. Biol.* **2011**, *18*, 608–618; d) M. Britton, M. M. Lucas, S. L. Downey, M. Screen, A. A. Pletnev, M. Verdoes, R. A. Tokhunts, O. Amir, A. L. Goddard, P. M. Pelphrey, et al., *Chem. Biol.* **2009**, *16*, 1278–1289.

- [5] T. Muchamuel, M. Basler, M. A. Aujay, E. Suzuki, K. W. Kalim, C. Lauer, C. Sylvain, E. R. Ring, J. Shields, J. Jiang, et al., *Nat. Med.* **2009**, *15*, 781–787.
- [6] M. Basler, S. Mundt, T. Muchamuel, C. Moll, J. Jiang, M. Groettrup, C. J. Kirk, *EMBO Mol. Med.* **2014**, *6*, 226–238.
- [7] A. F. Kisselev, M. Groettrup, *Curr. Opin. Chem. Biol.* **2014**, *23*, 16–22.
- [8] E. M. Huber, M. Basler, R. Schwab, W. Heinemeyer, C. J. Kirk, M. Groettrup, M. Groll, *Cell* **2012**, *148*, 727–738.
- [9] a) Q. Liu, Y. Sabnis, Z. Zhao, T. Zhang, S. J. Buhrlage, L. H. Jones, N. S. Gray, *Chem. Biol.* **2013**, *20*, 146–159; b) T. Zhang, F. Inesta-Vaquera, M. Niepel, J. Zhang, S. B. Ficarro, T. Machleidt, T. Xie, J. A. Marto, N. Kim, T. Sim, et al., *Chem. Biol.* **2012**, *19*, 140–154; c) M. Nacht, L. Qiao, M. P. Sheets, T. St. Martin, M. Labenski, H. Mazdiyasi, R. Karp, Z. Zhu, P. Chaturvedi, D. Bhavsar, et al., *J. Med. Chem.* **2013**, *56*, 712–721; d) M. Hagel, D. Niu, T. St Martin, M. P. Sheets, L. Qiao, H. Bernard, R. M. Karp, Z. Zhu, M. T. Labenski, P. Chaturvedi, et al., *Nat. Chem. Biol.* **2011**, *7*, 22–24; e) F. Solca, G. Dahl, A. Zoepfel, G. Bader, M. Sanderson, C. Klein, O. Kraemer, F. Himmelsbach, E. Haaksma, G. R. Adolf, *J. Pharmacol. Exp. Ther.* **2012**, *343*, 342–350; f) I. M. Serafimova, M. A. Pufall, S. Krishnan, K. Duda, M. S. Cohen, R. L. Maglathlin, J. M. McFarland, R. M. Miller, M. Frödin, J. Taunton, *Nat. Chem. Biol.* **2012**, *8*, 471–476.
- [10] S. M. Lim, K. D. Westover, S. B. Ficarro, R. A. Harrison, H. G. Choi, M. E. Pacold, M. Carrasco, J. Hunter, N. D. Kim, T. Xie, et al., *Angew. Chem. Int. Ed.* **2014**, *53*, 199–204; *Angew. Chem.* **2014**, *126*, 203–208.
- [11] G. Loidl, M. Groll, H.-J. Musiol, L. Ditzel, R. Huber, L. Moroder, *Chem. Biol.* **1999**, *6*, 197–204.
- [12] E. M. Huber, W. Heinemeyer, M. Groll, *Structure* **2015**, *23*, 407–417.
- [13] C. Blackburn, K. M. Gigstad, P. Hales, K. Garcia, M. Jones, F. J. Bruzzese, C. Barrett, J. X. Liu, T. A. Soucy, D. S. Sappal, et al., *Biochem. J.* **2010**, *430*, 461–476.
- [14] a) C. Blackburn, C. Barrett, J. L. Blank, F. J. Bruzzese, N. Bump, L. R. Dick, P. Fleming, K. Garcia, P. Hales, M. Jones, et al., *MedChemComm* **2012**, *3*, 710–719; b) M. Groll, N. Gallastegui, X. Maréchal, V. Le Ravalec, N. Basse, N. Richey, E. Genin, R. Huber, L. Moroder, J. Vidal, et al., *ChemMedChem* **2010**, *5*, 1701–1705.
- [15] a) C. Jöst, C. Nitsche, T. Scholz, L. Roux, C. D. Klein, *J. Med. Chem.* **2014**, *57*, 7590–7599; b) E. Weerapana, G. M. Simon, B. F. Cravatt, *Nat. Chem. Biol.* **2008**, *4*, 405–407; c) N. Brauckhoff, G. Hahne, J. T. H. Yeh, T. N. Grossmann, *Angew. Chem. Int. Ed.* **2014**, *53*, 4337–4340; *Angew. Chem.* **2014**, *126*, 4425–4429.
- [16] L. M. Salonen, M. Ellermann, F. Diederich, *Angew. Chem. Int. Ed.* **2011**, *50*, 4808–4842; *Angew. Chem.* **2011**, *123*, 4908–4944.
- [17] K. N. Daeffler, H. A. Lester, D. A. Dougherty, *J. Am. Chem. Soc.* **2012**, *134*, 14890–14896.
- [18] D. Niewerth, G. J. L. Kaspers, Y. G. Assaraf, J. van Meerloo, C. J. Kirk, J. Anderl, J. L. Blank, P. M. van de Ven, S. Zweegman, G. Jansen, et al., *J. Hematol. Oncol.* **2014**, *7*, 7.

Received: July 17, 2015

Revised: September 15, 2015

Published online: ■■■ ■■■, ■■■■■

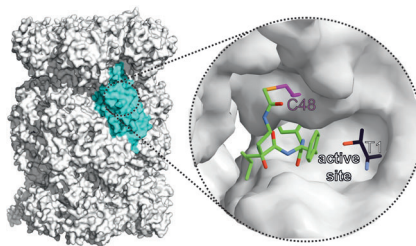
## Communications



### Immunoproteasome Inhibition

C. Dubiella,\* R. Baur, H. Cui, E. M. Huber,  
M. Groll\* ————— ■■■■—■■■■

Selective Inhibition of the  
Immunoproteasome by Structure-Based  
Targeting of a Non-catalytic Cysteine



**Blocking the channel:** Immunoproteasome inhibitors were designed that target an isoform-specific cysteine residue in the substrate binding channel instead of the active site. The compounds display a unique mode of action compared to commonly applied proteasome drugs. They are highly isoform selective and suppress the production of inflammatory cytokines. This new class of inhibitors provides a starting point for the development of anti-inflammatory agents.



### 3.1 Supporting information

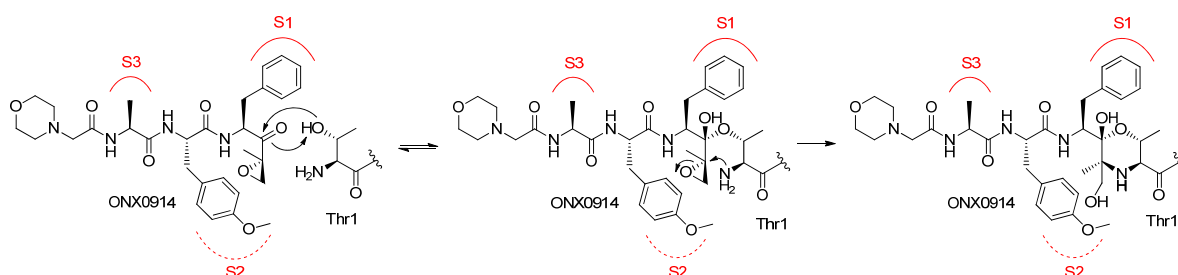
#### Selective Inhibition of the Immunoproteasome by Structure-Based Targeting of a Non-Catalytic Cysteine

C. Dubiella, R. Baur, H. Cui, E. M. Huber & M. Groll  
*Angewandte Chemie International Edition* **2015**,  
 doi: 10.1002/anie.201506631.

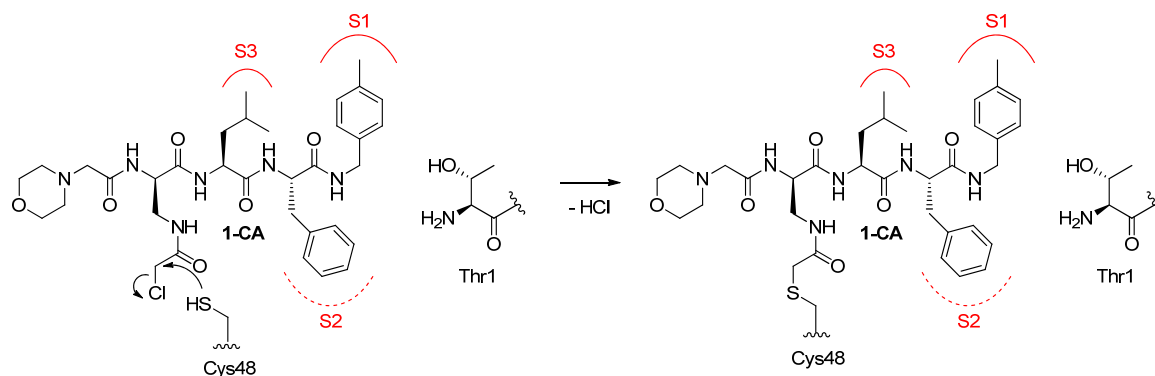
#### Supporting Information Table of Contents

3.1.1	Supplementary schemes .....	34
3.1.2	Supplementary figures .....	35
3.1.3	Supplementary tables .....	39
3.1.4	Supplementary in vitro methods .....	42
	Protein purification .....	42
	Point measurements for the inhibition of the activities of the subunits $\beta 1c$ , $\beta 1i$ , $\beta 2c$ , $\beta 2i$ .....	42
	IC <sub>50</sub> value determination of the proteasomal chymotrypsin-like activity.....	42
	Yeast mutagenesis.....	43
	Crystallization and structure elucidation.....	43
3.1.5	Supplementary cell culture methods.....	44
	IC <sub>50</sub> determination with Proteasome-Glo™ chymotrypsin-like cell-based assay .....	44
	LC <sub>50</sub> determination via AlamarBlue-based viability assay .....	44
	Quantification of cytokine production by enzyme-linked immunosorbent assay (ELISA) .....	44
3.1.6	Supplementary chemical synthesis.....	45
	General remarks .....	45
	General procedure for the synthesis of peptidic backbones.....	46
	General synthesis of C-terminal capped peptides.....	48
	Synthesis of C-terminal capped peptide inhibitors for electrophile screening .....	50
	Synthesis of C-terminal capped peptide inhibitors for backbone optimization.....	57
3.1.7	Supplementary references.....	61

### 3.1.1 Supplementary schemes



**Scheme S1** Binding of the  $\alpha,\beta$ -epoxyketone ONX 0914 to Thr1 at the proteasomal active site. The specificity pockets (S1, S3 and S4) are depicted in red and the shallow S2 pocket is illustrated as red dashed line.



**Scheme S2** Irreversible binding of the  $\alpha$ -chloroacetamide **1-CA** to Cys48 of subunit  $\beta 5i$  via thioether bond formation. The specificity pockets (S1, S3 and S4) are depicted in red and the shallow S2 pocket is illustrated as red dashed line.

## 3.1.2 Supplementary figures

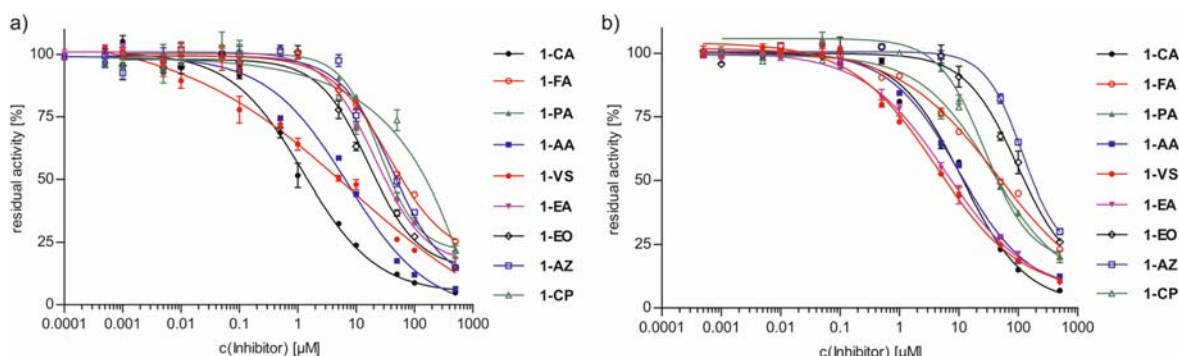


**Figure S1** In vitro  $IC_{50}$  assays against the ChTL activity of purified human iCP (a) and cCP (b) after 1 h incubation with various concentrations of side chain-electrophile containing compounds (right panel) using the fluorogenic Suc-LLVY-AMC-substrate assay. Data of three repetitions were normalized to DMSO-treated controls and are presented as relative activity with standard deviation.

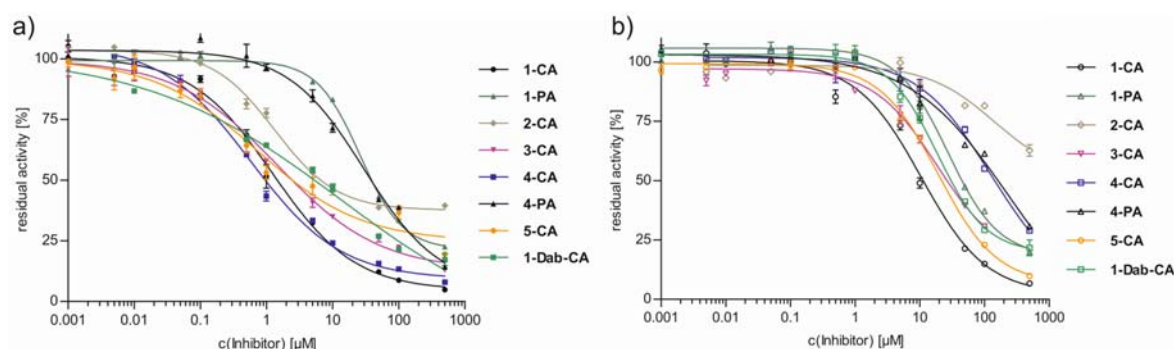


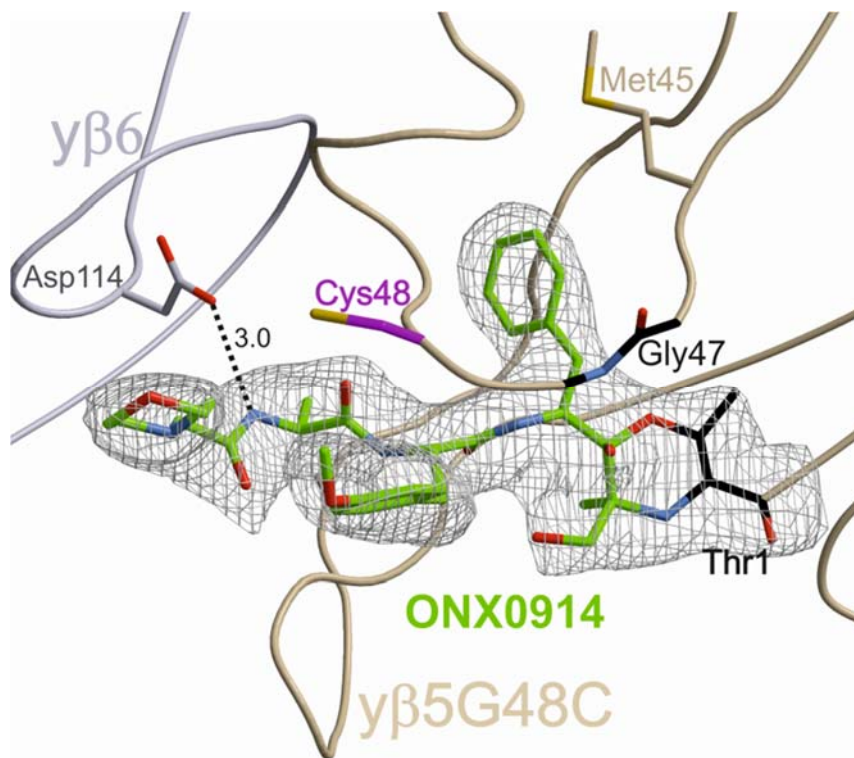
**Figure S2** In vitro  $IC_{50}$  assays against the ChTL activity of purified human iCP (a) and cCP (b) after 1 h incubation with various concentrations of  $\alpha$ -chloroacetamides **1-CA-5CA**, **1-Dab-CA** and **1-PA** as a control (right panel, Figure 2) using the fluorogenic Suc-LLVY-AMC-substrate assay. Data of three repetitions were normalized to DMSO-treated controls and are presented as relative activity with standard deviation.

a)	48	b)	27
h $\beta 5i$	TMSGCAADC	h $\beta 5i$	SYISALR
m $\beta 5i$	TMSGCAADC	m $\beta 5i$	SYISSLR
h $\beta 5c$	TMAGGAADC	h $\beta 5c$	AYIASQT
m $\beta 5c$	TMAGGAADC	m $\beta 5c$	AYIASQT
y $\beta 5G48C$	TMAGCAADC	y $\beta 5G48C$	NWVASQT
y $\beta 5$	TMAGGAADC	y $\beta 5$	NWVASQT

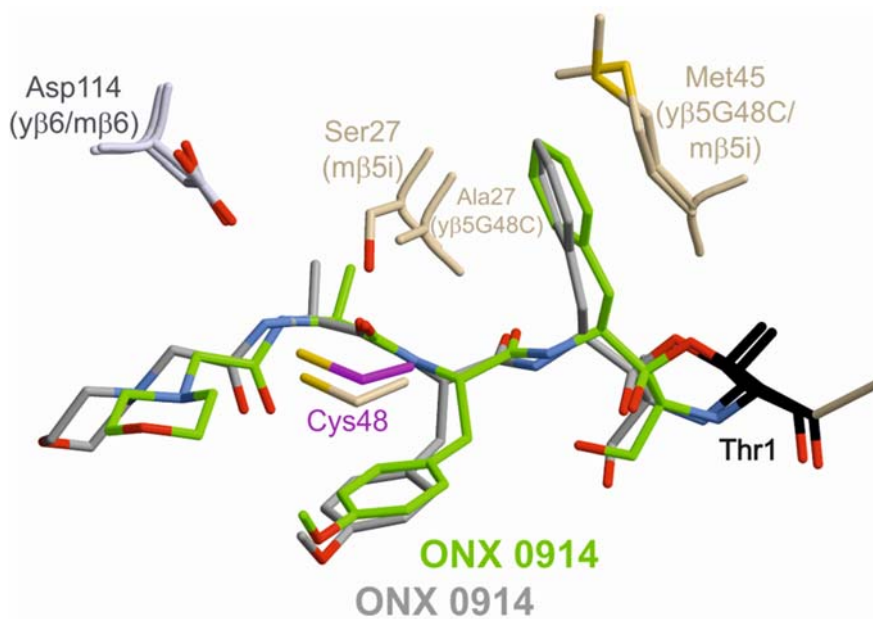
**Figure S3** Sequence alignments around the positions 48 (a) and 27 (b) of subunit  $\beta 5$  of various proteasome types (h = human, m = mouse, y = yeast). Cys48 and Ser27 are highlighted in magenta.



### 3. Targeting a non-catalytic cysteine of subunit $\beta 5i$

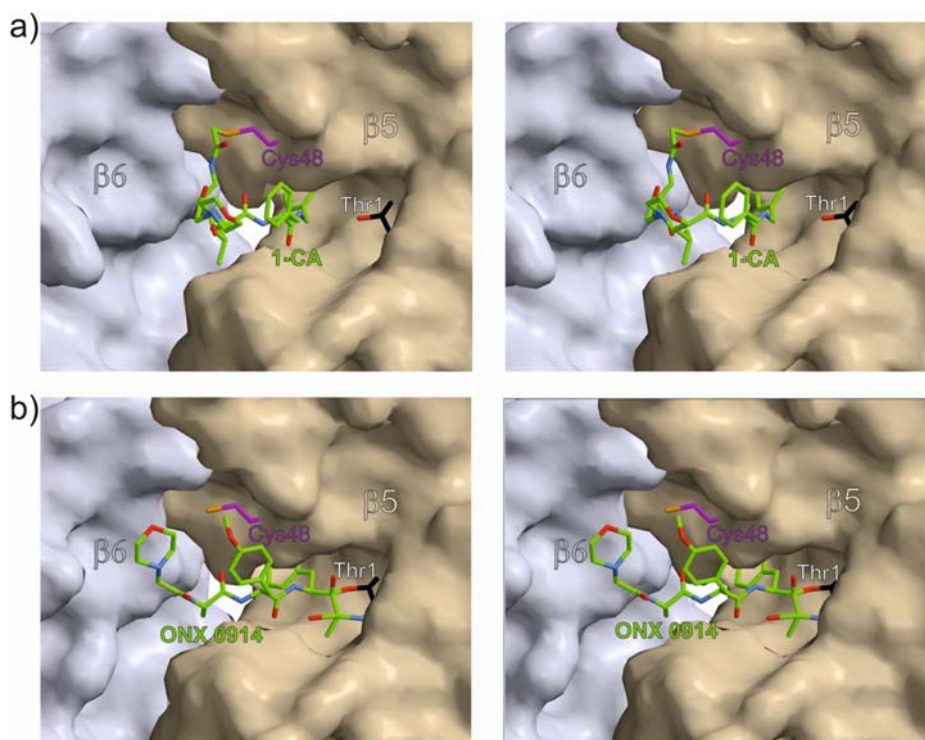


**Figure S4** The 2Fo-Fc electron density map (grey mesh, contoured at  $1\sigma$ , 2.8 Å resolution, PDB ID: 5CGI) shows ONX 0914 (green) bound to the active site nucleophile Thr1 (black) of the  $y\beta 5G48C$  mutant. ONX 0914 interacts via hydrogen-bonding with Asp114 of subunit  $y\beta 6$  (grey) and the oxyanion hole Gly47 (black) of subunit  $y\beta 5G48C$  (beige).



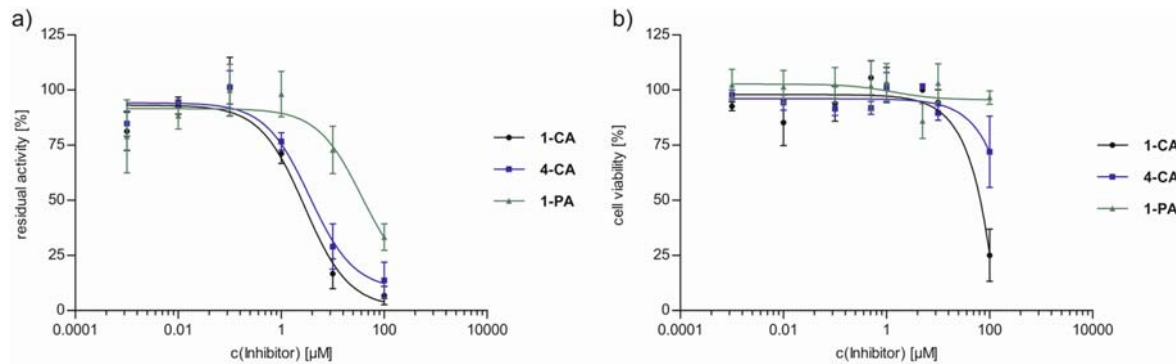
**Figure S5** Structural superposition of ONX 0914 (green) and ONX 0914 (grey) bound to Thr1 (black) of the  $y\beta 5G48C$  mutant and to  $m\beta 5i$  from mouse, respectively. Residues of the subunits  $\beta 5$  are depicted in beige and residues of  $\beta 6$  in grey. Cys48 of  $m\beta 5i$  is highlighted in magenta.



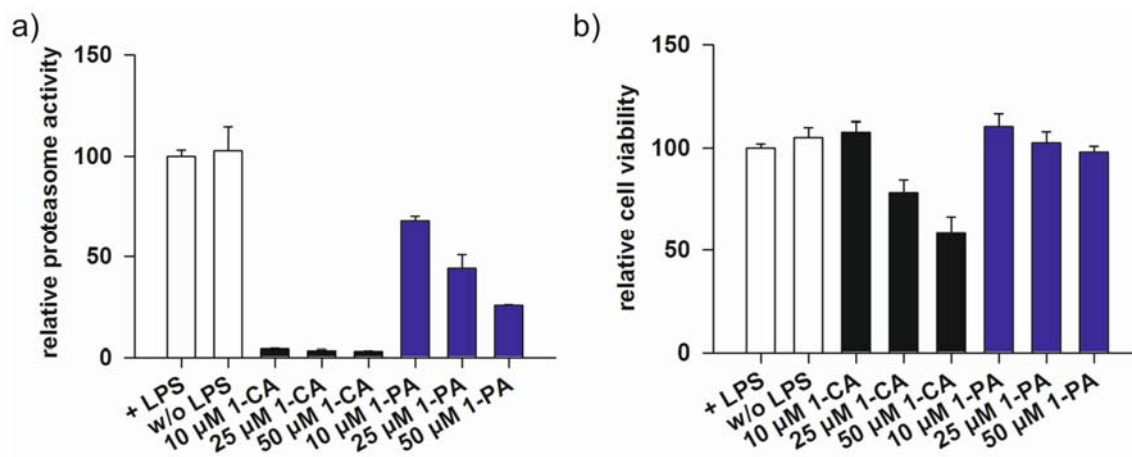


**Figure S6** Stereo views of **1-CA** (a) and ONX 0914 (b) bound to subunit  $\gamma\beta 5G48C$ . **1-CA** is bound to Cys48 (magenta) and solely interacts with residues of  $\gamma\beta 5G48C$  (beige) without making any contacts to  $\gamma\beta 6$  (grey). ONX 0914 is bound to the active site Thr1 (black) and interacts with residues of  $\gamma\beta 5G48C$  as well as  $\gamma\beta 6$ .

### 3. Targeting a non-catalytic cysteine of subunit $\beta 5i$



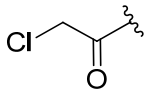
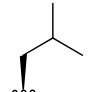
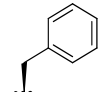
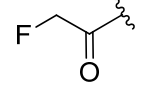
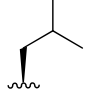
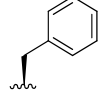
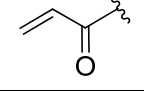
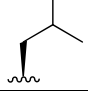
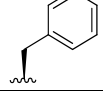
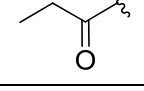
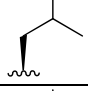
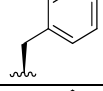
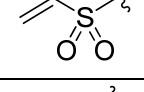
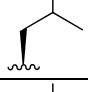
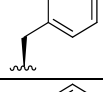
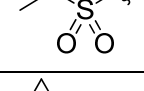
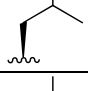
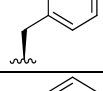
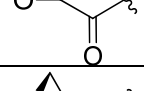
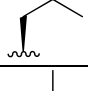
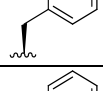
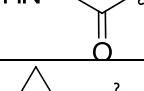
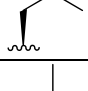
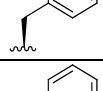
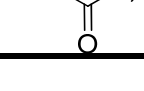
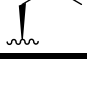
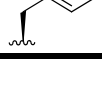
**Figure S7** a) In vivo  $\text{IC}_{50}$  assays against the ChTL activity in THP-1 cells after 105 min incubation at various concentrations of **1-CA**, **4-CA** and **1-PA** using a luminogenic substrate assay. Data of three biological repetitions (measurements performed as triplicates) were normalized to DMSO-treated controls and are presented as relative activity with standard deviation. b)  $\text{LC}_{50}$  against THP-1 cells after 48 h incubation with **1-CA**, **4-CA** and **1-PA** between 1 nM and 100  $\mu\text{M}$  using an AlamarBlue-based cell viability assay. Data of three biological repetitions (measurements performed as quadruplets) were normalized to DMSO-treated controls and are presented as relative viability with standard error of the mean.



**Figure S8** a) In vivo proteasome activity assay against the ChTL activity with cell lysate derived from LPS-stimulated THP-1 cells after 16 h incubation at various concentrations of **1-CA** or **1-PA** using a luminogenic substrate assay. Data of three replicates were normalized to DMSO-treated controls and are presented as relative activity with standard deviation. b) Cell viability of THP-1 cells after 16 h incubation with **1-CA** or **1-PA** in the presence of LPS using an AlamarBlue-based assay. Data of four replicates were normalized to DMSO-treated controls and are presented as relative viability with standard deviation. LPS: lipopolysaccharide, + LPS: positive control, w/o LPS: negative control.

## 3.1.3 Supplementary tables

**Table ST1** In vitro  $IC_{50}$  values of compounds in the electrophile screen against the ChTL activity of purified human iCP and cCP. A high  $IC_{50}$   $\beta 5c/\beta 5i$  ratio indicates selectivity for  $\beta 5i$ .

Comp.	R	P3	P2	$IC_{50}$ [ $\mu M$ ]		$IC_{50}$ $\beta 5c/\beta 5i$
				$\beta 5i$	$\beta 5c$	
1-CA				$1.24 \pm 0.35$	$11.24 \pm 2.59$	9
1-FA				$36.25 \pm 9.22$	$43.84 \pm 12.63$	1.2
1-AA				$7.13 \pm 2.88$	$10.00 \pm 2.19$	1.4
1-PA				$24.23 \pm 3.50$	$29.05 \pm 8.85$	1.2
1-VS				$7.98 \pm 17.59$	$4.26 \pm 1.22$	0.5
1-EA				$20.79 \pm 4.68$	$6.03 \pm 1.92$	0.3
1-EO				$16.19 \pm 5.06$	$95.88 \pm 59.80$	5.9
1-AZ				$41.19 \pm 17.16$	$117.7 \pm 34.34$	2.9
1-CP				> 50	$36.01 \pm 10.55$	< 0.7

### 3. Targeting a non-catalytic cysteine of subunit $\beta$ 5i

**Table ST2** In vitro  $IC_{50}$  values of compounds in the backbone optimization against the ChTL activity ( $\beta$ 5i,  $\beta$ 5c) and the activities of subunit  $\beta$ 1c,  $\beta$ 1i,  $\beta$ 2c,  $\beta$ 2i of purified human iCP and cCP. A high  $IC_{50}$   $\beta$ 5c/ $\beta$ 5i ratio indicates selectivity for  $\beta$ 5i.

Comp.	R	P3	P2	$IC_{50}$ [ $\mu$ M]						$IC_{50}$ $\beta$ 5c/ $\beta$ 5i
				$\beta$ 1i	$\beta$ 1c	$\beta$ 2i	$\beta$ 2c	$\beta$ 5i	$\beta$ 5c	
1-CA				> 100	> 100	> 100	> 100	1.24 $\pm$ 0.35	11.24 $\pm$ 2.59	9
1-PA				> 100	> 100	> 100	> 100	7.13 $\pm$ 2.88	10.00 $\pm$ 2.19	1.4
2-CA				> 100	> 100	> 100	> 100	6.65 $\pm$ 0.27	> 500	> 75
3-CA				> 100	> 100	> 100	> 100	2.53 $\pm$ 0.56	18.27 $\pm$ 5.58	7
4-CA				> 100	> 100	> 100	> 100	0.64 $\pm$ 0.14	> 100	> 150
4-PA				> 100	> 100	> 100	> 100	29.29 $\pm$ 9.60	> 200	> 7

**Table ST3** In vitro  $IC_{50}$  values of the compound **1-Dab-CA** against the ChTL activity ( $\beta$ 5i,  $\beta$ 5c) and the activities of subunit  $\beta$ 1c,  $\beta$ 1i,  $\beta$ 2c,  $\beta$ 2i of purified human iCP and cCP. A high  $IC_{50}$   $\beta$ 5c/ $\beta$ 5i ratio indicates selectivity for  $\beta$ 5i.

Comp.	$IC_{50}$ [ $\mu$ M]						$IC_{50}$ $\beta$ 5c/ $\beta$ 5i		
	$\beta$ 1i	$\beta$ 1c	$\beta$ 2i	$\beta$ 2c	$\beta$ 5i	$\beta$ 5c			
1-Dab-CA							13.07 $\pm$ 3.18	18.61 $\pm$ 4.52	1.4

**Table ST4** Crystallographic data collection and refinement statistics. Datasets were collected at the beamline X06SA at the Paul Scherrer Institute, Swiss Light Source, Villigen (Switzerland).

	<i>yCP <math>\beta 5G48C</math></i>	<i>yCP <math>\beta 5G48C:1-CA</math></i>	<i>yCP <math>\beta 5G48C:ONX 0914</math></i>
<b>Crystal parameters</b>			
Space group	P2 <sub>1</sub>	P2 <sub>1</sub>	P2 <sub>1</sub>
Cell constants	a= 135.5 Å b= 301.0 Å c= 143.9 Å $\beta$ = 112.9 °	a= 134.4 Å b= 300.5 Å c= 144.7 Å $\beta$ = 113.0 °	a= 136.2 Å b= 300.2 Å c= 145.9 Å $\beta$ = 113.0 °
CPs / AU <sup>a</sup>	1	1	1
<b>Data collection</b>			
Beam line	X06SA, SLS	X06SA, SLS	X06SA, SLS
Wavelength (Å)	1.0	1.0	1.0
Resolution range (Å) <sup>b</sup>	30-2.8 (2.9-2.8)	30-2.9 (3.0-2.9)	30-2.8 (2.9-2.8)
No. observations	786,086	677,285	804,869
No. unique reflections <sup>c</sup>	256,096	222,703	259,088
Completeness (%) <sup>b</sup>	98.5 (98.3)	95.5 (97.8)	98.6 (99.1)
R <sub>merge</sub> (%) <sup>b, d</sup>	7.3 (45.6)	9.4 (57.3)	6.7 (44.2)
I/ $\sigma$ (I) <sup>b</sup>	12.8 (2.8)	11.5 (2.4)	14.0 (3.1)
<b>Refinement (REFMAC5)</b>			
Resolution range (Å)	15-2.8	15-2.9	15-2.8
No. refl. working set	243,291	211,565	246,133
No. refl. test set	12,805	11,135	12,955
No. non hydrogen	49,776	49,734	49,886
No. of ligand atoms	-	92	252
Solvent (H <sub>2</sub> O, ions, MES)	439	335	326
R <sub>work</sub> /R <sub>free</sub> (%) <sup>e</sup>	18.6/20.1	20.4/23.1	18.6/20.6
r.m.s.d. bond (Å) / (°) <sup>f</sup>	0.004/0.883	0.004/0.846	0.004/0.904
Average B-factor (Å <sup>2</sup> )	59.8	62.1	66.1
Ramachandran Plot (%) <sup>g</sup>	97.8/1.9/0.3	97.7/2.1/0.3	97.3/2.4/0.3
PDB accession code	5CGF	5CGG	5CGI

<sup>[a]</sup> Asymmetric unit

<sup>[b]</sup> The values in parentheses for resolution range, completeness, R<sub>merge</sub> and I/ $\sigma$  (I) correspond to the highest resolution shell

<sup>[c]</sup> Data reduction was carried out with XDS and from a single crystal. Friedel pairs were treated as identical reflections

<sup>[d]</sup>  $R_{\text{merge}}(I) = \frac{\sum_{\text{hkl}} \sum_j |I(\text{hkl})_j - \langle I(\text{hkl}) \rangle|}{\sum_{\text{hkl}} \sum_j I(\text{hkl})_j}$ , where  $I(\text{hkl})_j$  is the  $j^{\text{th}}$  measurement of the intensity of reflection hkl and  $\langle I(\text{hkl}) \rangle$  is the average intensity

<sup>[e]</sup>  $R = \frac{\sum_{\text{hkl}} (|F_{\text{obs}}| - |F_{\text{calc}}|)}{\sum_{\text{hkl}} |F_{\text{obs}}|}$ , where R<sub>free</sub> is calculated without a sigma cut off for a randomly chosen 5% of reflections, which were not used for structure refinement, and R<sub>work</sub> is calculated for the remaining reflections

<sup>[f]</sup> Deviations from ideal bond lengths/angles

<sup>[g]</sup> Number of residues in favored region / allowed region / outlier region.

#### 3.1.4 Supplementary in vitro methods

##### *Protein purification*

20S proteasome from *Saccharomyces cerevisiae* (yCP) was purified as previously described.<sup>[1]</sup> Yeast cells were lysed in a continuous cell disruption system and centrifuged at 40,000 g. After precipitation in aqueous 40%  $(\text{NH}_4)_2\text{SO}_4$ , the suspension was applied to a phenyl sepharose HIC column. Eluted fractions displaying 20S proteasome activity were pooled and purified using FPLC with a hydroxyapatite column. Polishing was performed via a Resource-Q anion exchange column and a Superose 6 size exclusion chromatography. The pooled fractions were concentrated to 40 mg/mL in 20 mM MES (pH 6.8) and used for further crystallization trials and in vitro assays.

##### *Point measurements for the inhibition of the activities of the subunits $\beta 1c$ , $\beta 1i$ , $\beta 2c$ , $\beta 2i$*

In vitro proteasome inhibition point measurements were performed by fluorescence assays in 96-well plates. Assay mixtures contained 10  $\mu\text{g/mL}$  of freshly purified human cCP (Boston Biochem) or human iCP (Boston Biochem) in 100 mM Tris/HCl (pH 7.5) buffer. Inhibitors were dissolved in DMSO and added to yield a final concentration of 100  $\mu\text{M}$  with three repetitions each, thereby not surpassing a final concentration of 10% (v/v) DMSO. After an incubation time of 60 min at RT, the fluorogenic substrates Z-Leu-Leu-Glu-AMC ( $\beta 1c$ ), Ac-Lys-Gln-Leu-AMC ( $\beta 2c/\beta 2i$ ) and Ac-Pro-Ala-Leu-AMC ( $\beta 1i$ ) were added, respectively, to yield a final concentration of 333  $\mu\text{M}$  substrate. The assay mixture was incubated for another hour at RT and stopped by dilution with 300  $\mu\text{L}$  water. Afterwards fluorescence was determined on a Varian Cary Eclipse photofluorometer with excitation and emission wavelengths of  $\lambda_{\text{exc}} = 360 \text{ nm}$  and  $\lambda_{\text{em}} = 460 \text{ nm}$ , respectively.

##### *$IC_{50}$ value determination of the proteasomal chymotrypsin-like activity*

In vitro proteasome inhibition assays were performed by fluorescence assays in 96-well plates. Assay mixtures contained 10  $\mu\text{g/mL}$  purified human cCP (Boston Biochem) or human iCP (Boston Biochem) in 100 mM Tris/HCl (pH 7.5) buffer. Inhibitors were dissolved in DMSO and added at various concentrations with three repetitions each, thereby not surpassing a final concentration of 10% (v/v) DMSO. After an incubation time of 60 min at RT, the fluorogenic substrate Suc-Leu-Leu-Val-Tyr-AMC (Suc-LLVY-AMC, final concentration of 333  $\mu\text{M}$ ) was added to measure the residual activity of the chymotrypsin-like site. The assay mixture was incubated for another hour at RT and stopped by dilution with 300  $\mu\text{L}$  water. Afterwards fluorescence was determined on a

Varian Cary Eclipse photofluorometer with excitation and emission wavelengths of  $\lambda_{\text{exc}} = 360$  nm and  $\lambda_{\text{em}} = 460$  nm, respectively.

#### *Yeast mutagenesis*

The plasmid pRS315-PRE2 (*LEU2* selection marker),<sup>[2]</sup> encoding the wild type  $\beta 5$  subunit of the yeast proteasome, served as a template for mutagenesis. The *pre2-G48C* mutant allele was created by recombinant PCR techniques (Table ST2) and cloned into the *LEU2*-marked plasmid pRS315 via the restriction endonucleases *HindIII* and *BamHI* to yield pRS315-*pre2-G48C*. Introduction of the point mutation was verified by sequencing (GATC). The haploid yeast strain YWH20a (*pre2 $\Delta$ ::HIS3 [pRS316-PRE2]*),<sup>[3]</sup> expressing the wild type *PRE2* gene from an *URA3*-episome, was transformed by pRS315-*pre2-G48C*. Plasmid shuffling<sup>[4]</sup> based on counter-selection against the *URA3* marker with 5-fluoroorotic acid yielded a mutant strain that only expresses the G48C-mutant version of  $\gamma\beta 5$ . The  $\gamma\beta 5$ G48C mutant yeast strain was grown in 18 L YPD cultures for 2 days at 30 °C. Cells were harvested by centrifugation for 15 min at 5,000 g and frozen at -20 °C until further use.

#### *Crystallization and structure elucidation*

Crystals of  $\gamma$ CP were grown in hanging drop plates at 20 °C as previously described,<sup>[1,5]</sup> using a protein concentration of 40 mg/mL in MES (20 mM, pH 6.8). The drops contained 1  $\mu$ L of protein and 1  $\mu$ L of the reservoir solution consisting of 25 mM  $\text{MgAc}_2$ , 100 mM morpholino-ethane-sulfonic acid (MES) (pH 6.8) and 10% (v/v) 2-methyl-2,4-pentanediol. Crystals appeared after two days and were then soaked with inhibitor in DMSO at final concentrations of 25 mM for 12-24 h following complementation of the droplets with cryoprotecting buffer consisting of 30% (w/v) 2-methyl-2,4-pentanediol, 20 mM  $\text{MgAc}_2$ , 100 mM MES (pH 6.9). Crystals were supercooled in a stream of liquid nitrogen gas at 100 K (Oxford Cryo Systems). Datasets of  $\gamma$ CP:inhibitor structures were collected up to 2.5 Å resolution using synchrotron radiation ( $\lambda = 1.0$  Å) at the X06SA-beamline (Swiss Light Source, Villigen, Switzerland, Table ST4). X-ray intensities were assessed with the program XDS<sup>[6]</sup> and data reduction was carried out using XSCALE<sup>[6]</sup>. Molecular replacement started with the coordinates of  $\gamma$ CP (PDB ID: 1RYP)<sup>[1]</sup> and Translation/Libration/Screw (TLS) refinements were performed with REFMAC5 in the CCP4i suite<sup>[7]</sup>. Model building was carried out with the program package MAIN<sup>[8]</sup>.

### 3.1.5 Supplementary cell culture methods

#### *IC<sub>50</sub> determination with Proteasome-Glo™ chymotrypsin-like cell-based assay*

In vivo proteasome inhibition assays were performed with bioluminescence assays (Promega) in 96-well plates (Sigma Aldrich). THP-1 cells were plated at 10,000 cells per well, respectively, and incubated with various inhibitor concentrations for 90 min with three repetitions of each. 0.1% DMSO (v/v) was used as a control. The residual chymotrypsin-like activity was determined by the hydrolysis of the  $\beta 5$  specific substrate Suc-LLVY-aminoluciferin in the presence of luciferase using the Proteasome-Glo™ reagents according to the manufacturer's instructions. The resulting luminescence was detected with a PHERAstar Plus (BMG Labtech) plate-reader. THP-1 cells were cultured in RPMI medium (Sigma Aldrich) supplemented with 20% (v/v) FCS and 2 mM L-glutamine.

#### *LC<sub>50</sub> determination via AlamarBlue-based viability assay*

Viability of THP-1 cells was monitored in dependency of different CP inhibitor concentrations using an AlamarBlue-based assay.<sup>[9]</sup> 10,000 non-adherent THP-1 cells were seeded directly in the presence of **1-CA**, **4-CA** and **1-PA**, respectively. 0.1% (v/v) DMSO was used as a control. After 48 h, cells were washed with PBS (Sigma Aldrich) to remove dead cells and AlamarBlue (resazurin, AbD Serotech) was added in a 1:10 dilution for 2 h while AlamarBlue was directly added to THP-1 cells. Cell viability was monitored by measuring the reduction of resazurin to resorufin by metabolically active cells using fluorescence at 590 nm ( $\lambda_{exc} = 530$  nm) in PHERAstar Plus (BMG Labtech) plate-reader.

#### *Quantification of cytokine production by enzyme-linked immunosorbent assay (ELISA)*

THP-1 cells were used to evaluate the effect of  $\beta 5i$ -specific inhibitors on inflammatory cytokine production. 500,000 cells were seeded on 6-well plates 24 hours prior to treatment with **1-CA** or **1-PA** in a volume of 2 mL. 90 min following pre-incubation with inhibitor, cells were stimulated with 1  $\mu$ g/mL lipopolysaccharides (LPS) (Sigma Aldrich). Non-LPS treated cells were used as a negative control and DMSO was used as a vehicle control. Cells were incubated for 16 h and IL-6 and TNF- $\alpha$  content in conditioned supernatant was quantified using Human-IL-6 DuoSet ELISA or Human-TNF- $\alpha$  DuoSet ELISA (both R&D Systems) according to the manufacturer's instructions. Measurements were done in duplicates and three biological replicates were assessed. Data evaluation was done using a four parameter fit. Cell viability at the end of LPS-stimulation was determined by adding 10  $\mu$ L of AlamarBlue to 100  $\mu$ L of THP-1 cell suspension. The



measurements were done in quadruplets and carried out as described above. Proteasome inhibition was tested by the Proteasome-Glo™ chymotrypsin-like cell-based assay and samples were measured in triplicates prior to the addition of LPS at the end of stimulation for 14 h.

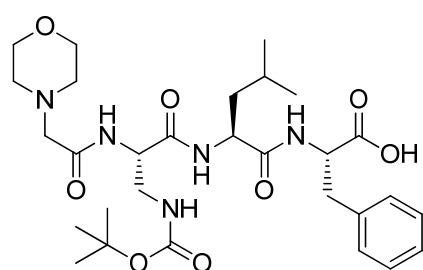
### 3.1.6 Supplementary chemical synthesis

#### *General remarks*

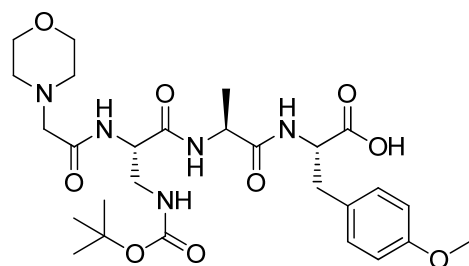
All chemicals and reagents were purchased in quality reagent grade or higher from commercial sources (Johnson Matthey Plc. (Alfa Aesar), Sigma-Aldrich Co. LLC, Merck KGaA, Iris Biotech GmbH, Protein Technologies Inc., Enamine Ltd, Santa Cruz Biotechnology Inc., Bachem Inc., AnaSpec (EGT group)) and used as received. Anhydrous solvents were purchased from Merck KGaA. Analytical thin-layer chromatography (TLC) was carried out on Merck silica gel 60 F<sub>254</sub> plates and compounds were visualized by UV light absorption ( $\lambda = 254$  nm) or common TLC stains (ninhydrin; KMnO<sub>4</sub>). Flash column chromatography was performed on a Reveleris® X1 Flash Chromatography System (W. R. Grace & Co.) using pre-packed GraceResolv™ silica cartridges 4-80 g (W. R. Grace & Co.). <sup>1</sup>H- and <sup>13</sup>C-NMR spectra were recorded on Bruker Avance III AVHD-300 (300 MHz), Bruker Avance I (360 MHz), Bruker AVHD-500 (500 MHz), or Bruker AV-500c NMR spectrometers and referenced to the residual proton or carbon signal of the deuterated solvent.<sup>[10]</sup> Chemical shifts are reported in parts per million (ppm) and coupling constants (*J*) are given in Hertz (Hz). High resolution mass spectra (HR-ESI-MS and RP-HPLC-HR-ESI-MS) were recorded with a Dionex UltiMate 3000 HPLC system eluting on a Waters XBridge C18 column (3.5  $\mu$ m, 4.6 x 100 mm; flow = 1.1 mL/min; column temperature = 30 °C), coupled with a Thermo Scientific LTQ-FT Ultra mass spectrometer and an ESI source. The applied buffers consisted of a gradient mixture of 0.1% (v/v) formic acid in H<sub>2</sub>O (buffer A) and 0.1% (v/v) formic acid in ACN:H<sub>2</sub>O 90:10 (v/v) (buffer B). ESI-MS and RP-HPLC-ESI-MS spectra were recorded with a Dionex UltiMate 3000 HPLC system coupled with a Thermo LCQ fleet. Reversed-phase HPLC purification was done using a system consisting of a Waters 1525 binary HPLC pump, X-Bridge™ Prep C18 column (5  $\mu$ m, 10 x 250 mm), Waters 2998 PDA detector and Waters Fraction Collector III (Waters Corp.). H<sub>2</sub>O with 0.1% TFA (v/v) (buffer A) and ACN with 0.1% TFA (v/v) (buffer B) were used as buffers. Lyophilization was performed on a Christ Alpha 2-4 LD plus.

*General procedure for the synthesis of peptidic backbones*

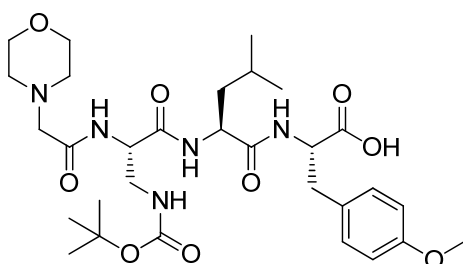
Peptidic backbones were prepared via solid-phase peptide synthesis (SPPS) using Fmoc-protected amino acids and a PS3 Peptide Synthesizer (Protein Technologies, Inc.). Preloaded L-Tyr(OMe)-2-Chlorotrityl-Cl resin (0.63 mmol/g loading) and L-Phe-2-Chlorotrityl-Cl resin (0.74 mmol/g loading) were used in a 0.2 mmol scale and Fmoc-protected amino acids (0.4 mmol, 2 eq.) were deprotected with 20% (v/v) piperidine in DMF. Activation of amino acids (0.4 mmol, 2 eq.) for coupling was performed using HCTU (0.4 mmol, 2 eq.) and 0.4 M DIPEA in DMF. Cleavage from the resin was performed with 20% 1,1,1,3,3,3-hexafluoro-2-propanol (v/v) in  $\text{CH}_2\text{Cl}_2$  following evaporation. The residual solid was dissolved in  $\text{H}_2\text{O}$  and lyophilized to yield the peptidic backbone quantitatively as white powdery free acid.

**MorphAc-Dap(Boc)-Leu-Phe-OH (1-a)**

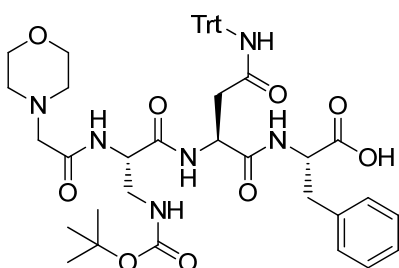
$^1\text{H NMR}$  (300 MHz,  $\text{DMSO-d}_6$ ):  $\delta$  = 8.16 (d,  $J$  = 7.7 Hz, 1H), 8.02 (d,  $J$  = 8.2 Hz, 1H), 7.88 (d,  $J$  = 7.9 Hz, 1H), 7.33 – 7.17 (m, 5H), 6.69 (t,  $J$  = 6.1 Hz, 1H), 4.47 – 4.25 (m, 3H), 3.61 (t,  $J$  = 4.6 Hz, 4H), 3.21 – 2.86 (m, 6H), 2.48 – 2.37 (m, 4H), 1.63 – 1.49 (m, 1H), 1.48 – 1.39 (m, 2H), 1.36 (s, 9H), 0.84 (dd,  $J$  = 13.7, 6.4 Hz, 6H) ppm.  $^{13}\text{C NMR}$  (75 MHz,  $\text{DMSO-d}_6$ ):  $\delta$  = 173.1, 172.4, 169.9, 169.6, 156.5, 137.9, 129.5, 128.6, 126.8, 78.5, 66.6, 61.9, 53.9, 53.7, 53.3, 51.4, 42.4, 36.9, 28.6, 24.5, 23.5, 22.0 ppm. **MS** (ESI):  $m/z$ : calcd. for  $\text{C}_{29}\text{H}_{46}\text{N}_5\text{O}_8$  [ $M+\text{H}^+$ ] 592.33; found 592.23.

**MorphAc-Dap(Boc)-Ala-Tyr(OMe)-OH (2-CA-a)**

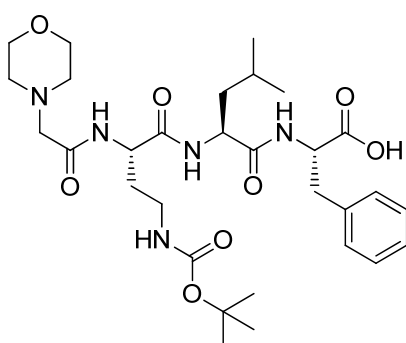
$^1\text{H NMR}$  (300 MHz,  $\text{DMSO-d}_6$ ):  $\delta$  = 8.09 (d,  $J$  = 7.3 Hz, 2H), 7.90 (d,  $J$  = 7.8 Hz, 1H), 7.15 (d,  $J$  = 8.4 Hz, 2H), 6.82 (d,  $J$  = 8.4 Hz, 2H), 6.73 (t,  $J$  = 6.1 Hz, 1H), 4.43 – 4.24 (m, 2H), 3.72 (s, 3H), 3.61 (t,  $J$  = 4.7 Hz, 3H), 3.47 – 3.14 (m, 3H), 3.04 – 2.79 (m, 4H), 2.44 (q,  $J$  = 5.0 Hz, 3H), 1.36 (s, 9H), 1.18 (d,  $J$  = 7.0 Hz, 3H) ppm.  $^{13}\text{C NMR}$  (75 MHz,  $\text{DMSO-d}_6$ ):  $\delta$  = 173.2, 172.6, 169.6, 169.6, 158.4, 156.5, 130.6, 129.7, 114.0, 78.5, 66.6, 61.9, 55.4, 54.4, 53.7, 53.2, 48.5, 42.4, 36.1, 28.6, 18.4 ppm. **MS** (ESI):  $m/z$ : calcd. for  $\text{C}_{27}\text{H}_{42}\text{N}_5\text{O}_9$  [ $M+\text{H}^+$ ] 580.30; found 580.07.

**MorphAc-Dap(Boc)-Leu-Tyr(OMe)-OH (3-CA-a)**

**$^1\text{H NMR}$**  (300 MHz,  $\text{DMSO-d}_6$ ):  $\delta$  = 8.05 (dd,  $J$  = 13.1, 7.9 Hz, 2H), 7.88 (d,  $J$  = 7.8 Hz, 1H), 7.13 (d,  $J$  = 8.5 Hz, 2H), 6.82 (d,  $J$  = 8.5 Hz, 2H), 6.69 (t,  $J$  = 6.0 Hz, 1H), 4.42 – 4.25 (m, 2H), 3.72 (s, 3H), 3.61 (t,  $J$  = 4.6 Hz, 4H), 3.48 – 3.12 (m, 3H), 3.05 – 2.81 (m, 4H), 2.49 – 2.35 (m, 4H), 1.64 – 1.51 (m, 1H), 1.51 – 1.40 (m, 2H), 1.36 (s, 9H), 0.84 (dd,  $J$  = 13.9, 6.4 Hz, 6H) ppm.  **$^{13}\text{C NMR}$**  (75 MHz,  $\text{DMSO-d}_6$ ):  $\delta$  = 173.2, 172.3, 169.9, 169.6, 158.4, 156.5, 130.6, 129.7, 114.0, 78.5, 66.6, 61.9, 55.4, 54.2, 53.7, 53.3, 51.4, 42.4, 36.1, 28.6, 24.5, 23.5, 22.0 ppm. **MS** (ESI):  $m/z$ : calcd. for  $\text{C}_{30}\text{H}_{48}\text{N}_5\text{O}_9$  [ $M+\text{H}^+$ ] 622.34; found 622.12.

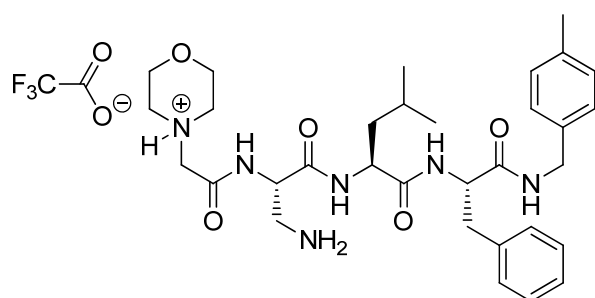
**MorphAc-Dap(Boc)-Asn(Trt)-Phe-OH (4-CA-a)**

**$^1\text{H NMR}$**  (300 MHz,  $\text{DMSO-d}_6$ ):  $\delta$  = 8.62 (s, 1H), 8.39 (d,  $J$  = 8.2 Hz, 1H), 8.06 (d,  $J$  = 7.5 Hz, 1H), 7.86 (d,  $J$  = 7.7 Hz, 1H), 7.33 – 7.12 (m, 20H), 6.71 (t,  $J$  = 6.1 Hz, 1H), 5.28 – 5.05 (m, 1H), 4.47 – 4.34 (m, 1H), 3.57 (t,  $J$  = 4.5 Hz, 4H), 3.48 – 3.31 (m, 2H), 3.30 – 3.19 (m, 1H), 3.12 – 2.89 (m, 4H), 2.77 – 2.65 (m, 2H), 2.47 – 2.35 (m, 4H), 1.37 (s, 9H) ppm.  **$^{13}\text{C NMR}$**  (75 MHz,  $\text{DMSO-d}_6$ ):  $\delta$  = 173.0, 171.5, 169.8, 169.5, 169.4, 156.5, 145.2, 137.9, 129.6, 129.0, 128.7, 127.9, 126.9, 126.8, 78.5, 69.8, 66.6, 61.8, 54.4, 53.7, 53.1, 50.3, 38.6, 36.9, 36.2, 28.6 ppm. **MS** (ESI):  $m/z$ : calcd. for  $\text{C}_{46}\text{H}_{55}\text{N}_6\text{O}_9$  [ $M+\text{H}^+$ ] 835.40; found 835.19.

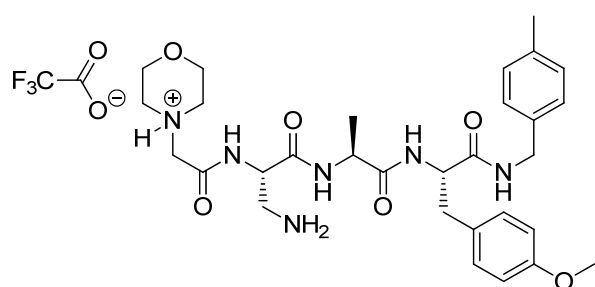
**MorphAc-Dab(Boc)-Leu-Phe-OH (Dab-CA-a)**

**$^1\text{H NMR}$**  (300 MHz,  $\text{DMSO-d}_6$ ):  $\delta$  = 8.19 (d,  $J$  = 7.7 Hz, 1H), 8.05 (d,  $J$  = 8.3 Hz, 1H), 7.79 (d,  $J$  = 8.3 Hz, 1H), 7.32 – 7.14 (m, 5H), 6.72 (t,  $J$  = 5.6 Hz, 1H), 4.48 – 4.24 (m, 3H), 3.60 (t,  $J$  = 4.6 Hz, 4H), 3.10 – 3.00 (m, 1H), 2.99 – 2.80 (m, 5H), 2.48 – 2.37 (m, 4H), 1.77 – 1.65 (m, 1H), 1.64 – 1.49 (m, 2H), 1.38 (s, 11H), 0.84 (dd,  $J$  = 15.3, 6.5 Hz, 6H) ppm.  **$^{13}\text{C NMR}$**  (75 MHz,  $\text{DMSO-d}_6$ ):  $\delta$  = 173.2, 172.2, 171.2, 169.3, 156.0, 138.0, 129.5, 128.6, 126.8, 78.1, 66.6, 65.4, 53.8, 53.6, 51.2, 50.2, 41.4, 37.0, 33.5, 28.7, 24.5, 23.5, 22.1 ppm. **MS** (ESI):  $m/z$ : calcd. for  $\text{C}_{30}\text{H}_{48}\text{N}_5\text{O}_8$  [ $M+\text{H}^+$ ] 606.35; found 605.80.

## General synthesis of C-terminal capped peptides

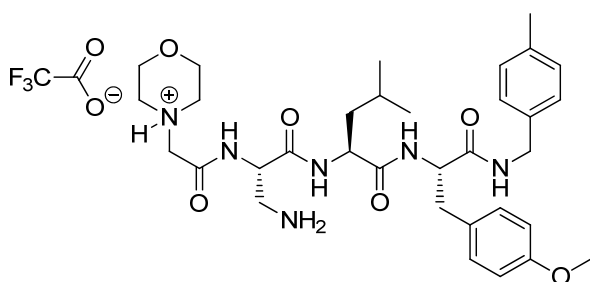
**MorphAc-Dap-Leu-Phe-4-methylbenzylamine · TFA (1)**

HATU (84 mg, 0.22 mmol, 1.1 eq.) was added to a solution of peptidic backbone **1-a** (118 mg, 0.2 mmol, 1 eq.) in  $\text{CH}_2\text{Cl}_2$  (1.2 mL) at 0 °C. The reaction mixture was stirred for 20 min before adding 4-methylbenzylamine (27.9  $\mu\text{L}$ , 0.22 mmol, 1.1 eq.). Afterwards, the reaction mixture was stirred for 10 min at 0 °C and DIPEA (77  $\mu\text{L}$ , 0.44 mmol, 2.2 eq.) was added dropwise. The reaction was then allowed to reach RT and was stirred overnight. After evaporation of the solvent, the residue was cooled to 0 °C and TFA (0.5 mL, 6.49 mmol) was added dropwise. The mixture was allowed to reach RT and was stirred for 30 min. Purification by RP-HPLC ( $t_{\text{R}} = 21$  min, linear gradient 20  $\rightarrow$  90% ACN/ $\text{H}_2\text{O}$  + 0.1% TFA in 80 min) and subsequent lyophilization yielded **1** (60.2 mg, 0.087 mmol, 44%) as a white powder.  **$^1\text{H}$  NMR** (500 MHz,  $\text{DMSO-d}_6$ ):  $\delta = 10.37$  (br s, 1H), 9.01 (br s, 1H), 8.47 (t,  $J = 5.9$  Hz, 1H), 8.35 – 8.26 (m, 2H), 8.05 (s, 3H), 7.29 – 7.18 (m, 5H), 7.08 (d,  $J = 7.8$  Hz, 2H), 7.00 (d,  $J = 7.9$  Hz, 2H), 4.66 – 4.59 (m, 1H), 4.56 – 4.49 (m, 1H), 4.29 (q,  $J = 7.7$  Hz, 1H), 4.25 - 4.14 (m, 2H), 3.79 (br s, 10H), 3.19 – 3.14 (m, 1H), 2.98 (dd,  $J = 13.7, 6.0$  Hz, 2H), 2.84 (dd,  $J = 13.7, 8.6$  Hz, 1H), 2.27 (s, 3H), 1.60 – 1.47 (m, 1H), 1.41 (t,  $J = 7.3$  Hz, 2H), 0.84 (dd,  $J = 16.6, 6.5$  Hz, 6H) ppm.  **$^{13}\text{C}$  NMR** (126 MHz,  $\text{DMSO-d}_6$ ):  $\delta = 172.1, 171.0, 158.8, 158.5, 138.0, 136.4, 136.2, 129.6, 129.2, 128.6, 127.5, 126.8, 63.6, 54.5, 52.5, 51.9, 50.8, 42.2, 41.0, 40.8, 38.1, 24.6, 23.5, 21.9, 21.1$  ppm. **MS** (ESI):  $m/z$ : calcd. for  $\text{C}_{32}\text{H}_{47}\text{N}_6\text{O}_5$  [ $\text{M}+\text{H}^+$ ] 595.36; found 595.32.

**MorphAc-Dap-Ala-Tyr(OMe)-4-methylbenzylamine · TFA (2-CA-b)**

Purification by RP-HPLC ( $t_{\text{R}} = 14$  min, linear gradient 20  $\rightarrow$  90% ACN/ $\text{H}_2\text{O}$  + 0.1% TFA in 80 min) and lyophilization yielded **2-CA-b** (75.3 mg, 0.111 mmol, 55%) as a white powder.  **$^1\text{H}$  NMR** (300 MHz,  $\text{DMSO-d}_6$ ):  $\delta = 8.95$  (br s, 1H), 8.44 (t,  $J = 5.9$  Hz, 1H), 8.37 (d,  $J = 7.1$  Hz, 1H), 8.20 (d,  $J = 8.1$  Hz, 1H), 8.16 – 8.02 (m, 3H), 7.18 – 7.05 (m, 4H), 7.00 (d,  $J = 8.1$  Hz, 2H), 6.81 (d,  $J = 8.7$  Hz, 2H), 4.72 – 4.58 (m, 1H), 4.52 – 4.40 (m, 1H), 4.32 - 4.15 (m, 3H), 3.82 (s, 6H), 3.72 (s, 3H), 3.31 – 3.02 (m, 6H), 2.87 – 2.72 (m, 2H),

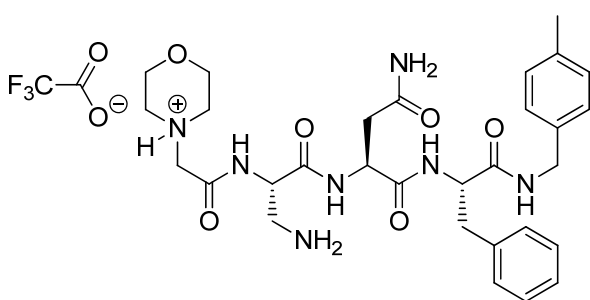
2.27 (s, 3H), 1.21 (d,  $J = 7.1$  Hz, 3H) ppm.  $^{13}\text{C}$  NMR (75 MHz, DMSO- $d_6$ ):  $\delta = 172.4$ , 171.1, 168.0, 161.4, 159.0, 158.3, 136.4, 136.2, 130.7, 129.2, 127.5, 114.0, 64.0, 55.4, 55.0, 52.6, 50.8, 49.1, 42.2, 37.4, 21.1, 18.4 ppm. MS (ESI):  $m/z$ : calcd. for  $\text{C}_{30}\text{H}_{43}\text{N}_6\text{O}_6$  [ $M+\text{H}^+$ ] 583.32; found 583.26.



**MorphAc-Dap-Leu-Tyr(OMe)-4-methylbenzylamine · TFA (3-CA-b)**

Purification by RP-HPLC ( $t_R = 26$  min, linear gradient 20  $\rightarrow$  90% ACN/ $\text{H}_2\text{O}$  + 0.1% TFA in 80 min) and lyophilization yielded **3-CA-b** (73 mg, 0.101 mmol, 51%) as a white powder.

$^1\text{H}$  NMR (300 MHz, DMSO- $d_6$ ):  $\delta = 8.96$  (br s, 1H), 8.42 (t,  $J = 6.1$  Hz, 1H), 8.33 (d,  $J = 7.8$  Hz, 1H), 8.20 (d,  $J = 8.2$  Hz, 1H), 8.12 (br s, 2H), 7.17 – 7.05 (m, 4H), 7.00 (d,  $J = 8.1$  Hz, 2H), 6.81 (d,  $J = 8.7$  Hz, 2H), 4.70 – 4.58 (m, 1H), 4.53 – 4.42 (m, 1H), 4.35 – 4.10 (m, 3H), 3.92 – 3.75 (m, 6H), 3.72 (s, 3H), 3.27 – 3.00 (m, 6H), 2.92 (dd,  $J = 13.7, 6.2$  Hz, 1H), 2.78 (dd,  $J = 13.6, 8.1$  Hz, 1H), 2.27 (s, 3H), 1.62 – 1.47 (m, 1H), 1.47 – 1.38 (m, 2H), 0.84 (dd,  $J = 10.1, 6.4$  Hz, 6H) ppm.  $^{13}\text{C}$  NMR (75 MHz, DMSO- $d_6$ ):  $\delta = 172.1$ , 171.1, 168.3, 159.1, 158.3, 136.4, 136.2, 130.7, 129.8, 129.2, 127.5, 114.0, 64.0, 55.4, 54.8, 52.6, 52.1, 50.9, 42.2, 37.3, 24.6, 23.5, 21.9, 21.1 ppm. MS (ESI):  $m/z$ : calcd. for  $\text{C}_{33}\text{H}_{49}\text{N}_6\text{O}_6$  [ $M+\text{H}^+$ ] 625.37; found 625.25.



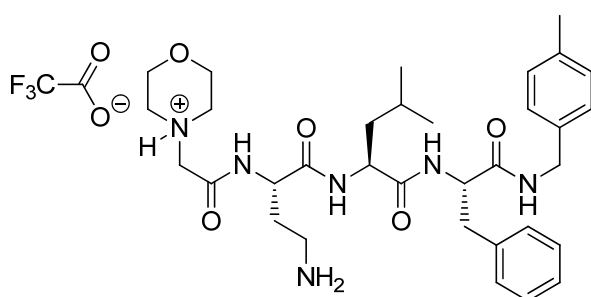
**MorphAc-Dap-Asn-Phe-4-methylbenzylamine · TFA (4-CA-b)**

Purification by RP-HPLC ( $t_R = 16$  min, linear gradient 20  $\rightarrow$  90% ACN/ $\text{H}_2\text{O}$  + 0.1% TFA in 80 min) and lyophilization yielded **4-CA-b** (57.5 mg, 0.087 mmol, 58%) as a white powder.

$^1\text{H}$  NMR (300 MHz, DMSO- $d_6$ ):  $\delta = 8.96$  (br s, 1H), 8.49 (t,  $J = 6.0$  Hz, 1H), 8.42 (d,  $J = 7.6$  Hz, 1H), 8.21 (d,  $J = 8.0$  Hz, 1H), 8.12 (s, 1H), 7.47 (s, 1H), 7.33 – 7.18 (m, 5H), 7.14 – 6.98 (m, 4H), 4.58 – 4.40 (m, 1H), 4.30 (d,  $J = 5.6$  Hz, 1H), 4.25 – 4.17 (m, 1H), 3.96 – 3.72 (m, 4H), 3.71 – 3.48 (m, 2H), 3.29 – 3.10 (m, 4H), 3.06 (dd,  $J = 13.9, 5.1$  Hz, 2H), 2.58 (dd,  $J = 15.7, 5.9$  Hz, 1H), 2.48 – 2.39 (m, 1H), 2.29 (s, 3H) ppm.  $^{13}\text{C}$  NMR (75 MHz, DMSO- $d_6$ ):  $\delta = 172.0$ , 171.0, 170.9, 168.1, 159.0, 158.6, 138.2, 136.5, 136.2, 129.7,

### 3. Targeting a non-catalytic cysteine of subunit $\beta 5i$

129.6, 129.2, 128.6, 127.6, 126.8, 64.0, 54.9, 52.6, 50.9, 50.4, 48.0, 42.4, 37.8, 37.2, 21.1 ppm. **MS** (ESI):  $m/z$ : calcd. for  $C_{30}H_{42}N_7O_6$  [ $M+H^+$ ] 596.32; found 596.25.

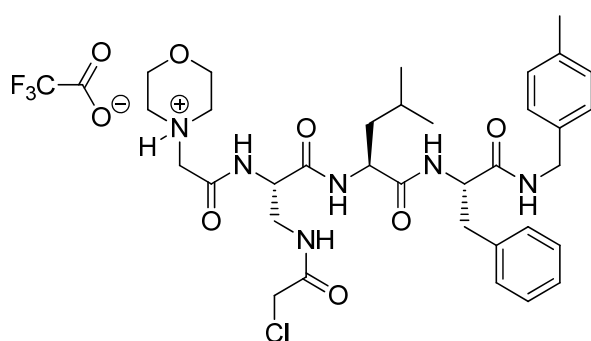


#### **MorphAc-Dab-Leu-Phe-4-methylbenzylamine · TFA (Dab-CA-b)**

Purification by RP-HPLC ( $t_R$  = 21 min, linear gradient 20 → 90% ACN/ $H_2O$  + 0.1% TFA in 80 min) and lyophilization yielded **Dab-CA-b** (64.4 mg, 0.091 mmol, 45%) as a white powder.

**$^1H$  NMR** (500 MHz,  $DMSO-d_6$ ):  $\delta$  = 10.33 (br s, 1H), 8.92 (br s, 1H), 8.44 (t,  $J$  = 5.9 Hz, 1H), 8.21 (d,  $J$  = 8.0 Hz, 2H), 7.95 – 7.80 (m, 3H), 7.29 – 7.20 (m, 5H), 7.08 (d,  $J$  = 7.8 Hz, 2H), 6.99 (d,  $J$  = 8.0 Hz, 2H), 4.56 – 4.47 (m, 1H), 4.43 (q,  $J$  = 7.1 Hz, 1H), 4.31 – 4.24 (m, 1H), 4.23 – 4.12 (m, 2H), 3.96 – 3.71 (m, 6H), 3.46 – 3.08 (m, 4H), 2.97 (dd,  $J$  = 13.7, 6.2 Hz, 1H), 2.91 – 2.80 (m, 3H), 2.27 (s, 3H), 2.00 – 1.79 (m, 2H), 1.62 – 1.50 (m, 1H), 1.40 (t,  $J$  = 7.3 Hz, 2H), 0.84 (dd,  $J$  = 24.0, 6.5 Hz, 6H) ppm.  **$^{13}C$  NMR** (126 MHz,  $DMSO-d_6$ ):  $\delta$  = 172.1, 171.1, 170.1, 158.7, 158.5, 138.0, 136.4, 136.2, 129.7, 129.2, 128.6, 127.5, 126.8, 63.6, 54.5, 52.3, 51.6, 50.7, 42.2, 41.2, 38.1, 36.2, 30.5, 24.6, 23.6, 21.8, 21.1 ppm. **MS** (ESI):  $m/z$ : calcd. for  $C_{32}H_{47}N_6O_5$  [ $M+H^+$ ] 595.36; found 595.32.

#### *Synthesis of C-terminal capped peptide inhibitors for electrophile screening*

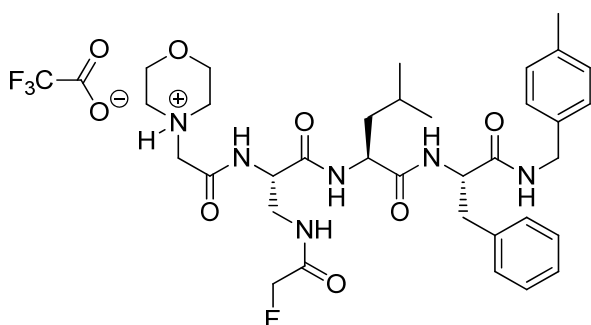


#### **MorphAc-Dap(N- $\beta$ -2-chloroacetyl)-Leu-Phe-4-methylbenzylamine · TFA (1-CA)**

*N*-(chloroacetoxy)succinimide (24.9 mg, 0.130 mmol) was added to a solution of capped peptidic backbone **1** (30 mg, 0.043 mmol) in  $CH_2Cl_2$  (0.3 mL) at 0 °C. After addition of DIPEA (15.2  $\mu$ L, 0.087 mmol) the reaction mixture was stirred for

15 min at 0 °C, then allowed to reach RT and was stirred for 30 min. After evaporation of the solvent, the residue was purified by RP-HPLC ( $t_R$  = 25 min, linear gradient 20 → 100% ACN/ $H_2O$  + 0.1% TFA in 80 min). Subsequent lyophilization yielded **1-CA** (28.7 mg, 0.037 mmol, 86%) as a white powder.  **$^1H$  NMR** (500 MHz,  $DMSO-d_6$ ):  $\delta$  = 10.22 (br s, 1H), 8.80 (br s, 1H), 8.47 (t,  $J$  = 5.9 Hz, 1H), 8.28 (d,  $J$  = 7.7 Hz, 1H), 8.19 (t,  $J$  = 6.0 Hz, 1H), 8.11 (d,  $J$  = 8.2 Hz, 1H), 7.32 – 7.15 (m, 5H), 7.08 (d,  $J$  = 7.8 Hz, 2H), 7.01 (d,  $J$  = 7.8 Hz, 2H), 4.64 – 4.52 (m, 1H), 4.48 (q,  $J$  = 6.7 Hz, 1H), 4.33 – 4.22 (m, 1H), 4.20 (t,  $J$  = 5.5 Hz, 2H),

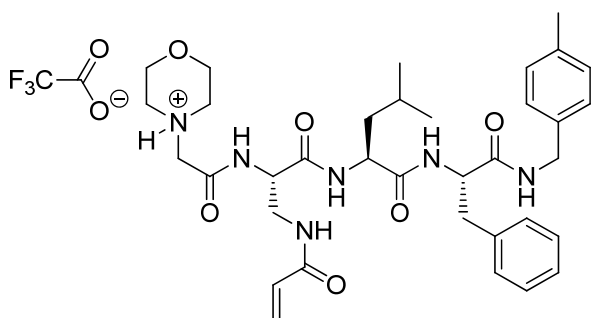
4.06 (d,  $J = 6.9$  Hz, 2H), 3.76 (s, 6H), 3.16 (s, 6H), 3.00 (dd,  $J = 13.7, 6.0$  Hz, 1H), 2.86 (dd,  $J = 13.7, 8.4$  Hz, 1H), 2.27 (s, 3H), 1.59 – 1.47 (m, 1H), 1.46 – 1.33 (m, 2H), 0.83 (dd,  $J = 22.4, 6.5$  Hz, 6H) ppm.  $^{13}\text{C NMR}$  (126 MHz, DMSO- $d_6$ ):  $\delta = 172.3, 171.1, 169.4, 166.9, 158.4, 158.1, 138.0, 136.4, 136.2, 129.6, 129.2, 128.5, 127.5, 126.8, 54.4, 52.7, 52.3, 52.0, 43.1, 42.3, 41.1, 40.9, 38.1, 24.6, 23.5, 21.8, 21.1$  ppm. **HRMS** (ESI):  $m/z$ : calcd. for  $\text{C}_{34}\text{H}_{48}\text{ClN}_6\text{O}_6$  [ $M+H^+$ ] 671.3318; found 671.3328.



**MorphAc-Dap(N- $\beta$ -fluoroacetyl)-Leu-Phe-4-methylbenzylamine · TFA (1-FA)**

2-Fluoroacetyl chloride (7.5  $\mu\text{L}$ , 0.087 mmol) was added to a solution of capped peptidic backbone **1** (20 mg, 0.029 mmol) in  $\text{CH}_2\text{Cl}_2$  (0.25 mL) at 0 °C. After addition of DIPEA (10.1  $\mu\text{L}$ , 0.058 mmol) the reaction mixture was stirred for 15 min at

0 °C, then allowed to reach RT and was stirred for 30 min. After evaporation of the solvent, the residue was purified by RP-HPLC ( $t_R = 23$  min, linear gradient 20  $\rightarrow$  100% ACN/ $\text{H}_2\text{O}$  + 0.1% TFA in 80 min). Subsequent lyophilization yielded **1-FA** (15.3 mg, 0.020 mmol, 70%) as a white powder.  $^1\text{H NMR}$  (300 MHz, DMSO- $d_6$ ):  $\delta = 10.23$  (br s, 1H), 8.72 (s, 1H), 8.41 (t,  $J = 6.0$  Hz, 1H), 8.25 (d,  $J = 7.7$  Hz, 1H), 8.15 – 8.00 (m, 2H), 7.29 – 7.18 (m, 5H), 7.08 (d,  $J = 8.1$  Hz, 2H), 7.01 (d,  $J = 8.1$  Hz, 2H), 4.79 (d,  $J = 46.9$  Hz, 2H), 4.59 – 4.46 (m, 2H), 4.30 – 4.18 (m, 3H), 3.82 (s, 6H), 3.50 – 3.13 (m, 6H), 3.00 (dd,  $J = 13.7, 6.1$  Hz, 1H), 2.87 (dd,  $J = 13.7, 8.4$  Hz, 1H), 2.27 (s, 3H), 1.62 – 1.48 (m, 1H), 1.43 – 1.34 (m, 2H), 0.83 (dd,  $J = 13.3, 6.5$  Hz, 6H) ppm.  $^{13}\text{C NMR}$  (75 MHz, DMSO- $d_6$ ):  $\delta = 172.2, 171.1, 169.4, 158.5, 158.1, 138.0, 136.4, 136.2, 129.6, 129.2, 128.5, 127.5, 126.7, 110.0, 81.6, 54.4, 52.9, 52.4, 52.1, 42.3, 38.1, 24.6, 23.5, 21.9, 21.1$  ppm. **HRMS** (ESI):  $m/z$ : calcd. for  $\text{C}_{34}\text{H}_{48}\text{FN}_6\text{O}_6$  [ $M+H^+$ ] 655.3614; found 655.3617.

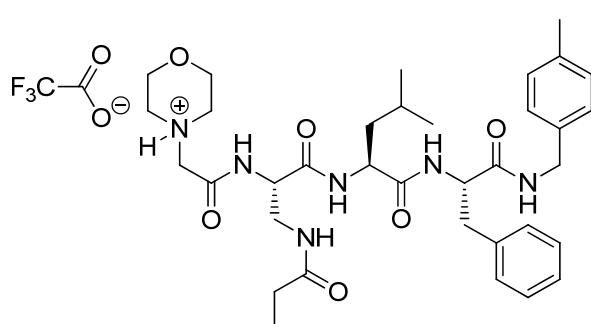


**MorphAc-Dap(N- $\beta$ -acryl)-Leu-Phe-4-methylbenzylamine · TFA (1-AA)**

Acryloyl chloride (8.1  $\mu\text{L}$ , 0.095 mmol) was added to a solution of capped peptidic backbone **1** (30 mg, 0.043 mmol) in  $\text{CH}_2\text{Cl}_2$  (0.3 mL) at 0 °C. After addition of DIPEA (16.7  $\mu\text{L}$ , 0.095 mmol) the reaction mixture was stirred for 15 min at 0 °C,

### 3. Targeting a non-catalytic cysteine of subunit $\beta 5i$

then allowed to reach RT and was stirred for 30 min. After evaporation of the solvent, the residue was purified by RP-HPLC ( $t_R = 23$  min, linear gradient 20  $\rightarrow$  100% ACN/H<sub>2</sub>O + 0.1% TFA in 80 min). Subsequent lyophilization yielded **1-AA** (16.8 mg, 0.023 mmol, 52%) as a white powder. **<sup>1</sup>H NMR** (500 MHz, DMSO-*d*<sub>6</sub>):  $\delta = 10.22$  (s, 1H), 8.80 (s, 1H), 8.47 (t,  $J = 5.9$  Hz, 1H), 8.31 (d,  $J = 7.7$  Hz, 1H), 8.21 – 8.08 (m, 2H), 7.29 – 7.16 (m, 5H), 7.08 (d,  $J = 7.9$  Hz, 2H), 7.01 (d,  $J = 8.1$  Hz, 2H), 6.23 (dd,  $J = 17.1, 10.1$  Hz, 1H), 6.10 (dd,  $J = 17.1, 2.2$  Hz, 1H), 5.59 (dd,  $J = 10.1, 2.2$  Hz, 1H), 4.62 – 4.52 (m, 1H), 4.47 (q,  $J = 6.7$  Hz, 1H), 4.30 – 4.15 (m, 3H), 4.01 – 3.71 (m, 6H), 3.49 – 3.39 (m, 2H), 3.27 (d,  $J = 114.4$  Hz, 4H), 3.00 (dd,  $J = 13.7, 5.9$  Hz, 1H), 2.87 (dd,  $J = 13.7, 8.6$  Hz, 1H), 2.26 (s, 3H), 1.58 – 1.48 (m, 1H), 1.44 – 1.34 (m, 2H), 0.82 (dd,  $J = 22.3, 6.6$  Hz, 6H) ppm. **<sup>13</sup>C NMR** (126 MHz, DMSO-*d*<sub>6</sub>):  $\delta = 172.4, 171.1, 169.6, 165.6, 158.4, 158.2, 138.0, 136.4, 136.2, 132.0, 129.6, 129.2, 128.5, 127.5, 126.8, 126.1, 63.7, 54.4, 53.2, 52.3, 52.0, 42.2, 40.9, 38.1, 24.5, 23.5, 21.8, 21.1$  ppm. **HRMS** (ESI):  $m/z$ : calcd. for C<sub>35</sub>H<sub>49</sub>N<sub>6</sub>O<sub>6</sub> [ $M+H^+$ ] 649.3708; found 649.3717.

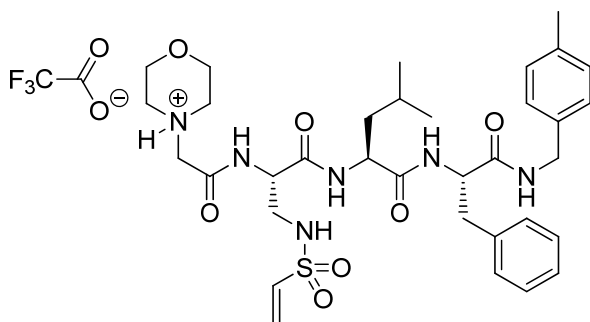


#### **MorphAc-Dap(*N*- $\beta$ -propionyl)-Leu-Phe-4-methylbenzylamine · TFA (1-PA)**

Propionyl chloride (7.7  $\mu$ L, 0.088 mmol) was added to a solution of capped peptidic backbone **1** (15.3 mg, 0.022 mmol) in CH<sub>2</sub>Cl<sub>2</sub> (0.1 mL) at 0 °C. After addition of DIPEA (11.6  $\mu$ L, 0.066 mmol) the reaction mixture was stirred for 15 min at 0 °C,

then allowed to reach RT and was stirred for 30 min. After evaporation of the solvent, the residue was purified by RP-HPLC ( $t_R = 25$  min, linear gradient 20  $\rightarrow$  100% ACN/H<sub>2</sub>O + 0.1% TFA in 80 min). Subsequent lyophilization yielded **1-PA** (8.5 mg, 0.011 mmol, 51%) as a white powder. **<sup>1</sup>H NMR** (500 MHz, DMSO-*d*<sub>6</sub>):  $\delta = 10.23$  (br s, 1H), 8.73 (br s, 1H), 8.46 (t,  $J = 5.9$  Hz, 1H), 8.26 (d,  $J = 7.6$  Hz, 1H), 8.09 (d,  $J = 8.2$  Hz, 1H), 7.79 (t,  $J = 6.0$  Hz, 1H), 7.27 – 7.18 (m, 5H), 7.08 (d,  $J = 7.9$  Hz, 2H), 7.01 (d,  $J = 7.8$  Hz, 2H), 4.59 – 4.51 (m, 1H), 4.42 (q,  $J = 6.7$  Hz, 1H), 4.28 – 4.15 (m, 3H), 4.02 – 3.65 (m, 6H), 3.41 – 3.12 (m, 6H), 3.00 (dd,  $J = 13.7, 5.9$  Hz, 1H), 2.87 (dd,  $J = 13.7, 8.6$  Hz, 1H), 2.27 (s, 3H), 2.12 – 2.02 (m, 2H), 1.59 – 1.48 (m, 1H), 1.44 – 1.32 (m, 2H), 0.97 (t,  $J = 7.6$  Hz, 3H), 0.82 (dd,  $J = 23.1, 6.6$  Hz, 6H) ppm. **<sup>13</sup>C NMR** (126 MHz, DMSO-*d*<sub>6</sub>):  $\delta = 174.1, 172.3, 171.1, 169.7, 158.5, 158.2, 138.0, 136.4, 136.2, 129.6, 129.2, 128.5, 127.5, 126.8, 63.6, 54.4, 53.2, 52.3, 52.0, 42.2, 40.9, 40.7, 38.1, 28.8, 24.6, 23.5, 23.3, 21.8, 21.1, 10.2$  ppm. **HRMS** (ESI):  $m/z$ : calcd. for C<sub>35</sub>H<sub>51</sub>N<sub>6</sub>O<sub>6</sub> [ $M+H^+$ ] 651.3865; found 651.3876.

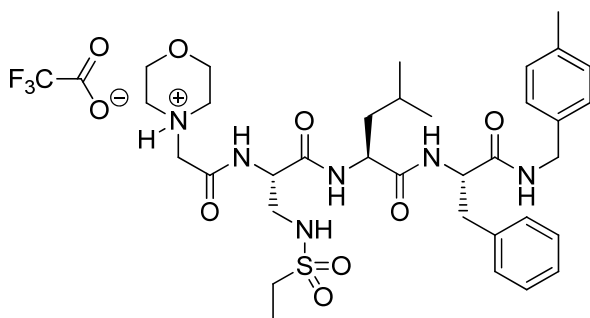




**MorphAc-Dap(N- $\beta$ -vinylsulfonyl)-Leu-Phe-4-methylbenzylamine · TFA (1-VS)**

Ethanesulfonyl chloride (13.8  $\mu$ L, 0.151 mmol) was added to a solution of capped peptidic backbone **1** (30 mg, 0.050 mmol) in  $\text{CH}_2\text{Cl}_2$  (0.4 mL) at 0  $^\circ\text{C}$ . After addition of DIPEA (17.6  $\mu$ L, 0.101 mmol) the reaction mixture was stirred for 15 min at

0  $^\circ\text{C}$ , then allowed to reach RT and was stirred for 30 min. After evaporation of the solvent, the residue was purified by RP-HPLC ( $t_R$  = 30 min, linear gradient 20  $\rightarrow$  90% ACN/ $\text{H}_2\text{O}$  + 0.1% TFA in 80 min). Subsequent lyophilization yielded **1-VS** (5.3 mg, 6.78  $\mu$ mol, 16%) as a white powder.  **$^1\text{H NMR}$**  (500 MHz,  $\text{DMSO-d}_6$ ):  $\delta$  = 10.24 (br s, 1H), 8.82 (d,  $J$  = 38.3 Hz, 1H), 8.46 (t,  $J$  = 5.9 Hz, 1H), 8.29 (d,  $J$  = 7.8 Hz, 0H), 8.09 (d,  $J$  = 8.2 Hz, 1H), 7.25 – 7.18 (m, 5H), 7.08 (d,  $J$  = 7.9 Hz, 2H), 7.01 (d,  $J$  = 7.9 Hz, 2H), 6.69 (dd,  $J$  = 16.5, 9.9 Hz, 1H), 6.02 (d,  $J$  = 16.6 Hz, 1H), 5.94 (d,  $J$  = 10.0 Hz, 1H), 4.59 - 4.44 (m, 2H), 4.30 – 4.16 (m, 3H), 4.09 – 3.68 (m, 6H), 3.35 – 3.03 (m, 6H), 2.98 (dd,  $J$  = 13.7, 5.9 Hz, 1H), 2.92 – 2.82 (m, 1H), 1.57 – 1.45 (m, 1H), 1.41 – 1.33 (m, 2H), 0.83 (dd,  $J$  = 21.0, 6.7 Hz, 6H) ppm.  **$^{13}\text{C NMR}$**  (126 MHz,  $\text{DMSO-d}_6$ ):  $\delta$  = 172.0, 171.1, 137.0, 136.5, 136.4, 136.2, 129.6, 129.2, 128.5, 127.5, 126.8, 126.2, 63.5, 54.4, 52.4, 51.8, 44.3, 42.2, 41.0, 38.1, 24.5, 23.5, 22.0, 21.1 ppm. **HRMS** (ESI):  $m/z$ : calcd. for  $\text{C}_{34}\text{H}_{49}\text{N}_6\text{O}_7\text{S}$  [ $M+\text{H}^+$ ] 685.3378; found 685.3382.



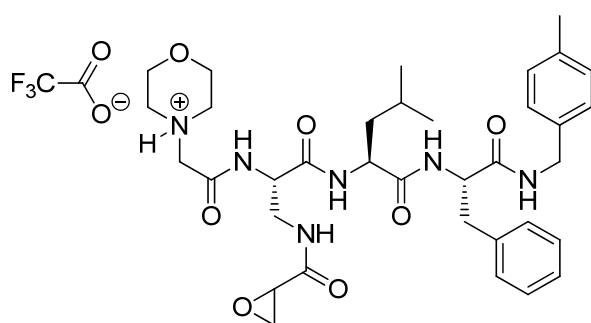
**MorphAc-Dap(N- $\beta$ -ethanesulfonyl)-Leu-Phe-4-methylbenzylamine · TFA (1-EA)**

Ethanesulfonyl chloride (12.3  $\mu$ L, 0.043 mmol) was added to a solution of capped peptidic backbone **1** (30 mg, 0.043 mmol) in  $\text{CH}_2\text{Cl}_2$  (0.3 mL) at 0  $^\circ\text{C}$ . After addition of DIPEA (15.2  $\mu$ L, 0.066 mmol) the reaction mixture was stirred for

15 min at 0  $^\circ\text{C}$ , then allowed to reach RT and was stirred overnight. After evaporation of the solvent, the residue was purified by RP-HPLC ( $t_R$  = 32 min, linear gradient 20  $\rightarrow$  90% ACN/ $\text{H}_2\text{O}$  + 0.1% TFA in 80 min). Subsequent lyophilization yielded **1-EA** (19.2 mg, 0.024 mmol, 57%) as a white powder.  **$^1\text{H NMR}$**  (500 MHz,  $\text{DMSO-d}_6$ ):  $\delta$  = 10.26 (br s, 1H), 8.76 (br s, 1H), 8.48 (t,  $J$  = 5.9 Hz, 1H), 8.34 (d,  $J$  = 7.9 Hz, 1H), 8.09 (d,  $J$  = 8.2 Hz, 1H), 7.29 - 7.17 (m, 5H), 7.08 (d,  $J$  = 7.8 Hz, 2H), 7.01 (d,  $J$  = 7.8 Hz, 2H), 4.61 – 4.43 (m, 2H),

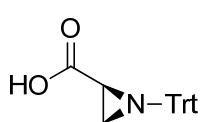
### 3. Targeting a non-catalytic cysteine of subunit $\beta 5i$

4.34 - 4.13 (m, 3H), 4.06 - 3.77 (m, 6H), 3.46 - 3.10 (m, 6H), 3.04 - 2.93 (m, 3H), 2.85 (dd,  $J = 13.7, 8.6$  Hz, 1H), 2.27 (s, 3H), 1.59 - 1.46 (m, 1H), 1.45 - 1.32 (m, 2H), 1.13 (t,  $J = 7.3$  Hz, 3H), 0.83 (dd,  $J = 21.5, 6.6$  Hz, 6H) ppm.  $^{13}\text{C}$  NMR (126 MHz, DMSO- $d_6$ ):  $\delta = 172.0, 171.2, 169.0, 158.5, 158.3, 138.0, 136.4, 136.2, 129.6, 129.2, 128.5, 127.5, 126.8, 63.6, 54.4, 53.4, 52.3, 51.9, 46.3, 44.4, 42.2, 41.1, 38.1, 24.5, 23.5, 22.0, 21.1, 8.5$  ppm. HRMS (ESI):  $m/z$ : calcd. for  $\text{C}_{34}\text{H}_{51}\text{N}_6\text{O}_7\text{S}$  [ $M+H^+$ ] 687.3534; found 687.3532.



#### MorphAc-Dap(*N*- $\beta$ -oxirane-2-carbonyl)-Leu-Phe-4-methylbenzylamine · TFA (1-EO)

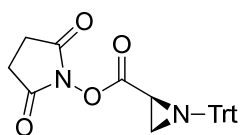
HATU (22 mg, 0.058 mmol) was added to a suspension of potassium oxirane-2-carboxylate (7.3 mg, 0.058 mmol) in  $\text{CH}_2\text{Cl}_2$  (0.4 mL) at 0 °C. The reaction mixture was stirred for 10 min before adding capped peptidic backbone **1** (40 mg, 0.058 mmol). Afterwards, the reaction mixture was stirred for 10 min at 0 °C and DIPEA (22.2  $\mu\text{L}$ , 0.127 mmol) was added dropwise. The reaction was then allowed to reach RT and was stirred overnight. After evaporation of the solvent, the residue was purified by RP-HPLC ( $t_R = 31$  min, linear gradient 20  $\rightarrow$  100% ACN/ $\text{H}_2\text{O}$  + 0.1% TFA in 80 min) and subsequent lyophilization yielded **1-EO** (8.7 mg, 0.011 mmol, 20%) as a white powder.  $^1\text{H}$  NMR (500 MHz, DMSO- $d_6$ ):  $\delta = 10.22$  (br s, 1H), 8.76 (br s, 1H), 8.48 - 8.40 (m, 1H), 8.27 (t,  $J = 8.0$  Hz, 1H), 8.11 (dd,  $J = 8.3, 3.9$  Hz, 1H), 8.03 - 7.96 (m, 1H), 7.29 - 7.17 (m, 5H), 7.08 (d,  $J = 7.8$  Hz, 2H), 7.00 (d,  $J = 7.8$  Hz, 2H), 4.62 - 4.51 (m, 1H), 4.47 (q,  $J = 6.6$  Hz, 1H), 4.32 - 4.23 (m, 1H), 4.22 - 4.13 (m, 2H), 4.06 - 3.67 (m, 6H), 3.41 - 3.13 (m, 6H), 3.05 - 2.96 (m, 1H), 2.93 - 2.83 (m, 2H), 2.81 - 2.75 (m, 1H), 2.26 (s, 3H), 1.60 - 1.49 (m, 1H), 1.44 - 1.34 (m, 2H), 0.83 (dd,  $J = 22.5, 6.5$  Hz, 5H) ppm.  $^{13}\text{C}$  NMR (126 MHz, DMSO- $d_6$ ):  $\delta = 172.2, 171.1, 169.4, 168.9, 158.5, 158.2, 138.0, 136.4, 136.2, 129.6, 129.2, 128.5, 127.5, 126.7, 63.5, 54.4, 52.9, 52.3, 52.0, 49.0, 49.0, 46.3, 42.2, 41.0, 38.1, 24.5, 23.5, 21.9, 21.1$  ppm. HRMS (ESI):  $m/z$ : calcd. for  $\text{C}_{35}\text{H}_{49}\text{N}_6\text{O}_7$  [ $M+H^+$ ] 665.3657; found 665.3658.



#### (S)-1-Trityl-aziridine-2-carboxylic acid (1-AZ-a)

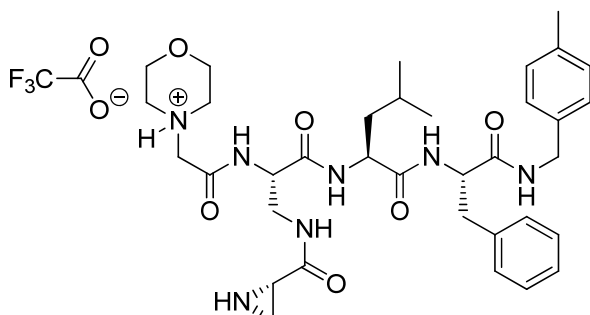
(S)-methyl-1-trityl-aziridine-2-carboxylic acid (1 g, 2.91 mmol) was dissolved in THF (4.61 mL), stirred at 0 °C and aqueous NaOH (1M, 4.66 mL, 4.66 mmol) was added slowly. The mixture was allowed to reach RT and stirred overnight. Afterwards, aqueous HCl (1 M) was added until the mixture had pH 5-6 and

concentrated in vacuo. The mixture was extracted with  $\text{CH}_2\text{Cl}_2$ , dried over  $\text{Na}_2\text{SO}_4$  and filtered. Evaporation of the solvent and purification via flash column chromatography (PE  $\rightarrow$  50% EA/PE, v/v) yielded **1-AZ-a** (936 mg, 2.84 mmol, 98%) as a white solid.  $^1\text{H NMR}$  (300 MHz,  $\text{DMSO-d}_6$ ):  $\delta$  = 12.65 (br s, 1H), 7.46 – 7.40 (m, 6H), 7.36 – 7.24 (m, 9H), 2.18 (dd,  $J$  = 2.8, 1.5 Hz, 1H), 1.62 (dd,  $J$  = 6.2, 2.7 Hz, 1H), 1.26 (dd,  $J$  = 6.2, 1.6 Hz, 1H) ppm.  $^{13}\text{C NMR}$  (75 MHz,  $\text{DMSO-d}_6$ ):  $\delta$  = 172.5, 143.9, 129.3, 128.2, 127.4, 74.2, 31.7, 28.2 ppm.



**(S)-2,5-dioxopyrrolidin-1-yl 1-tritylaziridine-2-carboxylate (1-AZ-b)**

PyBOP (1.48 g, 2.84 mmol) and *N*-hydroxysuccinimide (297 mg, 2.58 mmol) were added to a solution of **1-AZ-a** (850 mg, 2.58 mmol) in  $\text{CH}_2\text{Cl}_2$  (14.4 mL) at 0 °C. The reaction mixture was stirred for 10 min before DIPEA (721  $\mu\text{L}$ , 4.13 mmol) was added dropwise. The reaction was then allowed to reach RT and was stirred overnight. After evaporation of the solvent, the residue was purified by flash column chromatography (PE  $\rightarrow$  50% EA/PE, v/v) yielding **1-AZ-b** (714 mg, 1.74 mmol, 67%) as a white solid.  $^1\text{H NMR}$  (300 MHz,  $\text{DMSO-d}_6$ ):  $\delta$  = 7.45 – 7.28 (m, 15H), 2.85 (s, 4H), 2.02 (dd,  $J$  = 6.0, 2.6 Hz, 1H), 1.55 (dd,  $J$  = 6.0, 1.2 Hz, 1H) ppm.  $^{13}\text{C NMR}$  (75 MHz,  $\text{DMSO-d}_6$ ):  $\delta$  = 170.5, 167.2, 143.2, 129.3, 128.4, 127.7, 74.6, 30.0, 29.6, 26.0 ppm.

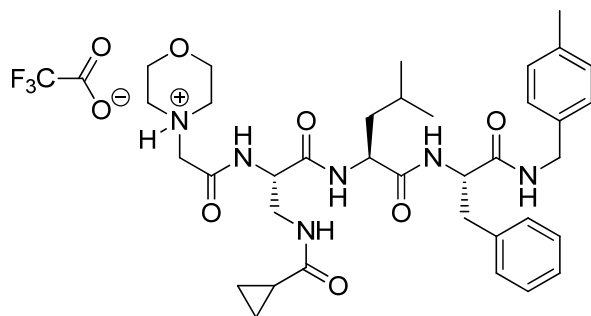


**MorphAc-Dap(*N*- $\beta$ -aziridine-2-carbonyl)-Leu-Phe-4-methylbenzylamine · TFA (1-AZ)**

Succinimide ester **1-AZ-b** (43.2 mg, 0.101 mmol) was added to a solution of capped peptidic backbone **1** (35 mg, 0.051 mmol) in  $\text{CH}_2\text{Cl}_2$  (0.4 mL) at 0 °C. After addition of DIPEA (17.7  $\mu\text{L}$ , 0.101 mmol) the reaction mixture was stirred for 15 min at 0 °C, then allowed to reach RT and was stirred for 30 min. After evaporation of the solvent, the residue was treated with TFA (114  $\mu\text{L}$ , 1.48 mmol) for 30 min and purified by RP-HPLC ( $t_R$  = 25 min, linear gradient 20  $\rightarrow$  90% ACN/ $\text{H}_2\text{O}$  + 0.1% TFA in 80 min). Subsequent lyophilization yielded **1-AZ** (12.4 mg, 0.016 mmol, 32%) as a white powder.  $^1\text{H NMR}$  (500 MHz,  $\text{DMSO-d}_6$ ):  $\delta$  = 8.95 (s, 1H), 8.86 (d,  $J$  = 8.0 Hz, 1H), 8.51 (t,  $J$  = 6.0 Hz, 1H), 8.36 (d,  $J$  = 7.9 Hz, 1H), 8.18 – 8.11 (m, 1H), 7.27 – 7.19 (m, 5H), 7.09 (d,  $J$  = 7.8 Hz, 2H), 7.01 (d,  $J$  = 8.0 Hz, 2H), 4.59 – 4.46 (m, 2H), 4.29 – 4.17 (m, 3H), 3.82 – 3.66 (m, 6H), 3.57 – 3.36 (m, 4H), 3.29 – 3.12 (m, 4H),

### 3. Targeting a non-catalytic cysteine of subunit $\beta 5i$

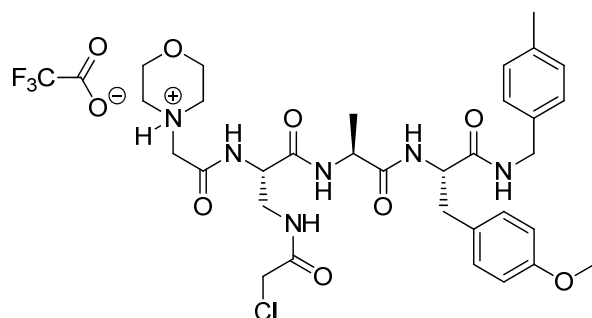
3.00 (dd,  $J = 13.7, 5.5$  Hz, 1H), 2.87 (dd,  $J = 13.7, 8.9$  Hz, 1H), 2.27 (s, 3H), 1.57 – 1.47 (m, 1H), 1.42 – 1.35 (m, 2H), 0.83 (dd,  $J = 21.2, 6.5$  Hz, 6H) ppm.  $^{13}\text{C}$  NMR (126 MHz, DMSO- $d_6$ ):  $\delta = 172.3, 171.3, 169.1, 158.8, 158.5, 138.0, 136.3, 136.2, 63.6, 54.9, 54.4, 52.5, 52.3, 52.0, 42.3, 41.0, 38.1, 32.1, 26.1, 24.6, 23.5, 21.9, 21.1$  ppm. HRMS (ESI):  $m/z$ : calcd. for  $\text{C}_{35}\text{H}_{50}\text{N}_7\text{O}_6$  [ $M+\text{H}^+$ ] 664.3817; found 664.3822.



#### MorphAc-Dap(*N*- $\beta$ -cyclopropane-carbonyl)-Leu-Phe-4-methylbenzyl-amine · TFA (**1-CP**)

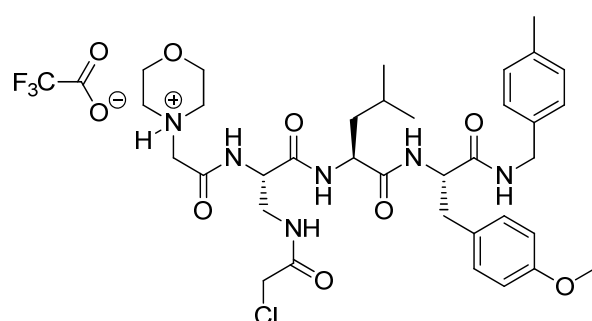
HATU (18.14 mg, 0.048 mmol) was added to a solution of cyclopropanecarboxylic acid (4.11 mg, 0.048 mmol) in  $\text{CH}_2\text{Cl}_2$  (0.3 mL) at 0 °C. The reaction mixture was stirred for 20 min before adding capped peptidic backbone **1** (30 mg, 0.043 mmol). Afterwards, the reaction mixture was stirred for 10 min at 0 °C and DIPEA (16.7  $\mu\text{L}$ , 0.095 mmol) was added dropwise. The reaction was then allowed to reach RT and was stirred overnight. After evaporation of the solvent, the residue was purified by RP-HPLC ( $t_R = 32$  min, linear gradient 20  $\rightarrow$  100% ACN/ $\text{H}_2\text{O}$  + 0.1% TFA in 80 min) and subsequent lyophilization yielded **1-CP** (10.2 mg, 0.013 mmol, 31%) as a white powder.  $^1\text{H}$  NMR (500 MHz, DMSO- $d_6$ ):  $\delta = 10.24$  (br s, 1H), 8.75 (br s, 1H), 8.45 (q,  $J = 4.5, 3.1$  Hz, 1H), 8.27 (d,  $J = 7.6$  Hz, 1H), 8.17 – 8.04 (m, 2H), 7.29 – 7.17 (m, 5H), 7.08 (d,  $J = 7.8$  Hz, 2H), 7.00 (d,  $J = 7.9$  Hz, 2H), 4.62 – 4.51 (m, 1H), 4.43 (q,  $J = 6.6$  Hz, 1H), 4.32 – 4.14 (m, 3H), 4.06 – 3.66 (m, 6H), 3.40 – 3.36 (m, 2H), 3.35 – 3.04 (m, 4H), 3.00 (dd,  $J = 13.7, 5.9$  Hz, 1H), 2.86 (dd,  $J = 13.7, 8.6$  Hz, 1H), 2.26 (s, 3H), 1.61 – 1.49 (m, 2H), 1.44 – 1.34 (m, 2H), 0.82 (dd,  $J = 23.4, 6.6$  Hz, 6H), 0.72 - 0.60 (m, 4H) ppm.  $^{13}\text{C}$  NMR (126 MHz, DMSO- $d_6$ ):  $\delta = 173.8, 172.3, 171.2, 169.6, 158.4, 158.2, 138.0, 136.4, 136.2, 129.6, 129.2, 128.5, 127.4, 126.8, 63.6, 54.4, 53.4, 52.3, 52.0, 42.2, 41.0, 40.9, 38.1, 24.5, 23.5, 21.9, 21.1, 14.1, 7.0, 6.9$  ppm. HRMS (ESI):  $m/z$ : calcd. for  $\text{C}_{36}\text{H}_{51}\text{N}_6\text{O}_6$  [ $M+\text{H}^+$ ] 663.3865; found 663.3875.

## Synthesis of C-terminal capped peptide inhibitors for backbone optimization


**MorphAc-Dap(N- $\beta$ -2-chloroacetyl)-Ala-Tyr(OMe)-4-methylbenzylamine · TFA (2-CA)**

*N*-(chloroacetoxy)succinimide (16.9 mg, 0.088 mmol) was added to a solution of capped peptidic backbone **2-CA-b** (20 mg, 0.029 mmol) in  $\text{CH}_2\text{Cl}_2$  (0.3 mL) at 0 °C. After addition of DIPEA (10.3  $\mu\text{L}$ ,

0.059 mmol) the reaction mixture was stirred for 15 min at 0 °C, then allowed to reach RT and was stirred for 30 min. After evaporation of the solvent, the residue was purified by RP-HPLC ( $t_R = 24$  min, linear gradient 15  $\rightarrow$  60% ACN/ $\text{H}_2\text{O}$  + 0.1% TFA in 80 min). Subsequent lyophilization yielded **2-CA** (6.2 mg, 8.2  $\mu\text{mol}$ , 28%) as a white powder.  $^1\text{H NMR}$  (500 MHz,  $\text{DMSO-d}_6$ ):  $\delta = 10.23$  (br s, 1H), 8.80 (br s, 1H), 8.45 (t,  $J = 6.0$  Hz, 1H), 8.35 (d,  $J = 7.1$  Hz, 1H), 8.21 (t,  $J = 6.0$  Hz, 1H), 8.06 (d,  $J = 8.1$  Hz, 1H), 7.10 (dd,  $J = 18.4, 8.2$  Hz, 4H), 7.00 (d,  $J = 7.8$  Hz, 2H), 6.80 (d,  $J = 8.6$  Hz, 2H), 4.53 – 4.43 (m, 2H), 4.31 – 4.13 (m, 3H), 4.05 (d,  $J = 5.1$  Hz, 2H), 4.02 – 3.73 (m, 5H), 3.72 (s, 3H), 3.16 (s, 6H), 2.91 (dd,  $J = 13.7, 6.1$  Hz, 1H), 2.80 (dd,  $J = 13.7, 8.2$  Hz, 1H), 2.27 (s, 3H), 1.18 (d,  $J = 7.1$  Hz, 3H) ppm.  $^{13}\text{C NMR}$  (126 MHz,  $\text{DMSO-d}_6$ ):  $\delta = 172.5, 171.1, 169.2, 166.9, 158.3, 136.4, 136.2, 130.7, 129.7, 129.2, 127.5, 113.9, 63.5, 55.4, 54.8, 52.6, 52.4, 49.0, 43.1, 42.2, 41.1, 37.4, 21.1, 18.4$  ppm. **HRMS** (ESI):  $m/z$ : calcd. for  $\text{C}_{32}\text{H}_{44}\text{ClN}_6\text{O}_7$  [ $M+H^+$ ] 659.2955; found 659.2963.

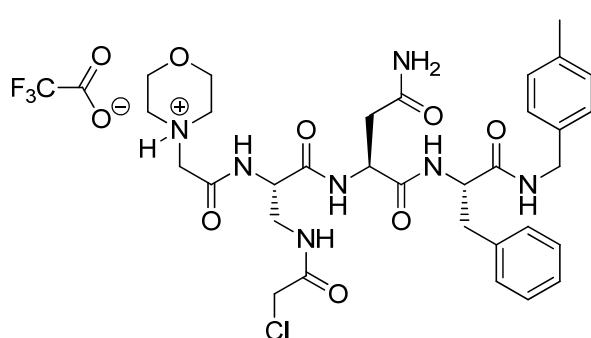

**MorphAc-Dap(N- $\beta$ -2-chloroacetyl)-Leu-Tyr(OMe)-4-methylbenzylamine · TFA (3-CA)**

*N*-(chloroacetoxy)succinimide (23 mg, 0.12 mmol) was added to a solution of capped peptidic backbone **3-CA-b** (25 mg, 0.04 mmol) in  $\text{CH}_2\text{Cl}_2$  (0.3 mL) at 0 °C. After addition of DIPEA (14  $\mu\text{L}$ ,

0.08 mmol) the reaction mixture was stirred for 15 min at 0 °C, then allowed to reach RT and was stirred for 30 min. After evaporation of the solvent, the residue was purified by RP-HPLC ( $t_R = 29$  min, linear gradient 15  $\rightarrow$  90% ACN/ $\text{H}_2\text{O}$  + 0.1% TFA in 80 min). Subsequent lyophilization yielded **3-CA** (15.9 mg, 0.023 mmol, 57%) as a white powder.  $^1\text{H NMR}$  (500 MHz,  $\text{DMSO-d}_6$ ):  $\delta = 10.25$  (br s, 1H), 8.79 (br s, 1H), 8.45 (t,  $J = 5.9$  Hz,

### 3. Targeting a non-catalytic cysteine of subunit $\beta 5i$

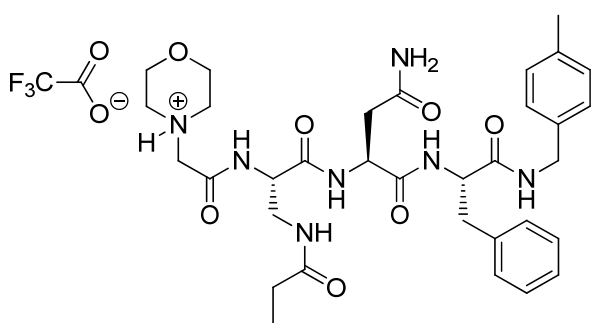
1H), 8.30 (d,  $J = 7.8$  Hz, 1H), 8.20 (t,  $J = 6.1$  Hz, 1H), 8.05 (d,  $J = 8.2$  Hz, 1H), 7.14 – 7.06 (m, 4H), 7.00 (d,  $J = 7.9$  Hz, 2H), 6.80 (d,  $J = 8.7$  Hz, 2H), 4.49 (p,  $J = 7.8, 7.4$  Hz, 2H), 4.30 – 4.13 (m, 3H), 4.06 (d,  $J = 7.2$  Hz, 2H), 3.99 – 3.73 (m, 6H), 3.71 (s, 3H), 3.41 – 3.07 (m, 6H), 2.92 (dd,  $J = 13.7, 6.2$  Hz, 1H), 2.79 (dd,  $J = 13.7, 8.3$  Hz, 1H), 2.27 (s, 3H), 1.59 – 1.47 (m, 1H), 1.45 – 1.35 (m, 2H), 0.83 (dd,  $J = 22.7, 6.6$  Hz, 6H) ppm.  $^{13}\text{C NMR}$  (126 MHz, DMSO- $d_6$ ):  $\delta = 172.2, 171.2, 169.4, 166.9, 158.5, 158.3, 136.4, 136.2, 130.7, 129.7, 129.2, 127.5, 113.9, 63.6, 55.4, 54.6, 52.7, 52.3, 52.0, 37.3, 24.6, 23.5, 21.8, 21.1$  ppm. **HRMS** (ESI):  $m/z$ : calcd. for  $\text{C}_{32}\text{H}_{44}\text{ClN}_6\text{O}_7$  [ $M+\text{H}^+$ ] 701.3424; found 701.3423.



#### **MorphAc-Dap(N- $\beta$ -2-chloroacetyl)-Asn-Phe-4-methylbenzylamine · TFA (4-CA)**

*N*-(chloroacetoxy)succinimide (19.3 mg, 0.101 mmol) was added to a solution of capped peptidic backbone **4-CA-b** (20 mg, 0.034 mmol) in  $\text{CH}_2\text{Cl}_2$  (0.3 mL) at 0 °C. After addition of DIPEA (11.7  $\mu\text{L}$ , 0.067 mmol) the reaction mixture was

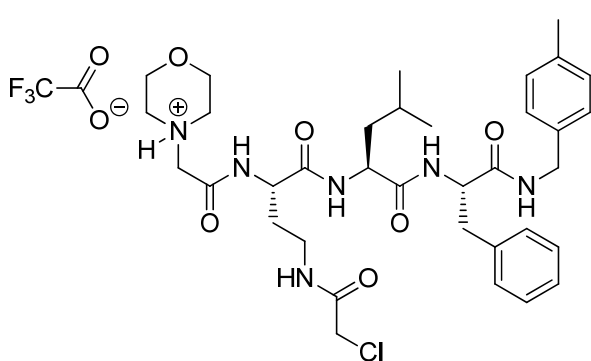
stirred for 15 min at 0 °C, then allowed to reach RT and was stirred for 30 min. After evaporation of the solvent, the residue was purified by RP-HPLC ( $t_R = 25$  min, linear gradient 15  $\rightarrow$  90% ACN/ $\text{H}_2\text{O}$  + 0.1% TFA in 80 min). Subsequent lyophilization yielded **4-CA** (14 mg, 0.021 mmol, 62%) as a white powder.  $^1\text{H NMR}$  (500 MHz, DMSO- $d_6$ ):  $\delta = 10.25$  (br s, 1H), 8.82 (br s, 1H), 8.50 (t,  $J = 6.0$  Hz, 1H), 8.44 (d,  $J = 7.6$  Hz, 1H), 8.23 – 8.13 (m, 2H), 7.47 – 7.42 (m, 1H), 7.30 – 7.18 (m, 5H), 7.09 (d,  $J = 7.8$  Hz, 2H), 7.03 (d,  $J = 7.8$  Hz, 2H), 7.01 – 6.98 (m, 1H), 4.58 – 4.51 (m, 1H), 4.50 – 4.43 (m, 2H), 4.21 (d,  $J = 6.0$  Hz, 2H), 4.06 (d,  $J = 3.7$  Hz, 2H), 4.01 – 3.60 (m, 6H), 3.40 – 3.10 (m, 6H), 3.04 (dd,  $J = 13.8, 5.2$  Hz, 1H), 2.85 (dd,  $J = 13.8, 8.9$  Hz, 1H), 2.56 (dd,  $J = 15.7, 5.7$  Hz, 1H), 2.41 (dd,  $J = 15.7, 7.7$  Hz, 1H), 2.27 (s, 3H).  $^{13}\text{C NMR}$  (126 MHz, DMSO- $d_6$ ):  $\delta = 171.9, 171.3, 171.0, 169.3, 166.9, 158.4, 138.2, 136.4, 136.2, 129.6, 129.2, 128.6, 127.5, 126.8, 63.6, 54.8, 52.6, 52.4, 50.4, 43.1, 42.3, 41.2, 37.8, 37.3$  ppm. **HRMS** (ESI):  $m/z$ : calcd. for  $\text{C}_{32}\text{H}_{43}\text{ClN}_7\text{O}_7$  [ $M+\text{H}^+$ ] 672.2907; found 672.2912.



**MorphAc-Dap(N- $\beta$ -propionyl)-Asn-Phe-4-methylbenzylamine · TFA (4-PA)**

Propionyl chloride (15.1  $\mu$ L, 0.173 mmol) was added to a solution of capped peptidic backbone **4-CA-b** (30 mg, 0.043 mmol) in  $\text{CH}_2\text{Cl}_2$  (0.3 mL) at 0 °C. After addition of DIPEA (22.7  $\mu$ L, 0.0130 mmol) the reaction mixture was stirred for 15 min at

0 °C, then allowed to reach RT and was stirred for 30 min. After evaporation of the solvent, the residue was purified by RP-HPLC ( $t_R$  = 28 min, linear gradient 5  $\rightarrow$  100% ACN/ $\text{H}_2\text{O}$  + 0.1% TFA in 80 min). Subsequent lyophilization yielded **4-PA** (17.8 mg, 0.024 mmol, 55%) as a white powder.  **$^1\text{H NMR}$**  (500 MHz,  $\text{DMSO-d}_6$ ):  $\delta$  = 10.26 (s, 1H), 8.75 (s, 1H), 8.50 (t,  $J$  = 6.1 Hz, 1H), 8.42 (d,  $J$  = 7.5 Hz, 1H), 8.16 (d,  $J$  = 8.0 Hz, 1H), 7.77 (t,  $J$  = 6.1 Hz, 1H), 7.45 (d,  $J$  = 2.4 Hz, 1H), 7.30 – 7.17 (m, 5H), 7.10 (d,  $J$  = 7.8 Hz, 2H), 7.05 (d,  $J$  = 7.9 Hz, 2H), 7.00 (d,  $J$  = 2.3 Hz, 1H), 4.54 (q,  $J$  = 7.2 Hz, 1H), 4.52 – 4.44 (m, 1H), 4.41 (q,  $J$  = 6.8 Hz, 1H), 4.22 (d,  $J$  = 6.1 Hz, 2H), 4.04 – 3.68 (m, 6H), 3.48 – 3.11 (m, 6H), 3.05 (dd,  $J$  = 13.8, 5.2 Hz, 1H), 2.87 (dd,  $J$  = 13.8, 8.9 Hz, 1H), 2.56 (dd,  $J$  = 15.7, 5.7 Hz, 2H), 2.41 (dd,  $J$  = 15.7, 7.6 Hz, 1H), 2.28 (s, 3H), 2.08 (q,  $J$  = 7.5 Hz, 2H), 0.98 (t,  $J$  = 7.6 Hz, 3H) ppm.  **$^{13}\text{C NMR}$**  (126 MHz,  $\text{DMSO-d}_6$ ):  $\delta$  = 174.0, 172.0, 171.3, 171.0, 169.6, 158.2, 138.2, 136.5, 136.2, 129.6, 129.2, 128.6, 127.5, 126.8, 63.6, 54.9, 53.2, 52.4, 50.4, 42.3, 40.7, 37.7, 37.3, 28.9, 21.1, 10.2 ppm. **HRMS** (ESI):  $m/z$ : calcd. for  $\text{C}_{33}\text{H}_{46}\text{N}_7\text{O}_7$  [ $M+\text{H}^+$ ] 652.3453; found 652.3461.



**MorphAc-Dab(N- $\beta$ -2-chloroacetyl)-Leu-Phe-4-methylbenzylamine · TFA (1-Dab-CA)**

*N*-(chloroacetoxy)succinimide (24.4 mg, 0.128 mmol) was added to a solution of capped peptidic backbone **Dab-CA-b** (30 mg, 0.043 mmol) in  $\text{CH}_2\text{Cl}_2$  (0.6 mL) at 0 °C. After addition of DIPEA (14.9  $\mu$ L,

0.085 mmol) the reaction mixture was stirred for 15 min at 0 °C, then allowed to reach RT and was stirred for 30 min. After evaporation of the solvent, the residue was purified by RP-HPLC ( $t_R$  = 28 min, linear gradient 15  $\rightarrow$  100% ACN/ $\text{H}_2\text{O}$  + 0.1% TFA in 80 min). Subsequent lyophilization yielded **1-Dab-CA** (23.8 mg, 0.030 mmol, 72%) as a white powder.  **$^1\text{H NMR}$**  (500 MHz,  $\text{DMSO-d}_6$ ):  $\delta$  = 10.21 (br s, 1H), 8.82 (br s, 1H), 8.40 (t,

### 3. Targeting a non-catalytic cysteine of subunit $\beta 5i$

---

$J = 6.0$  Hz, 1H), 8.22 (t,  $J = 5.6$  Hz, 1H), 8.17 (dd,  $J = 8.1, 3.8$  Hz, 2H), 7.27 – 7.18 (m, 5H), 7.08 (d,  $J = 7.8$  Hz, 2H), 7.00 (d,  $J = 7.9$  Hz, 2H), 4.57 – 4.49 (m, 1H), 4.39 – 4.33 (m, 1H), 4.30 (q,  $J = 7.8$  Hz, 1H), 4.24 – 4.14 (m, 2H), 4.05 (s, 2H), 4.01 – 3.73 (m, 6H), 3.35 (s, 4H), 3.12 (q,  $J = 6.9$  Hz, 2H), 2.97 (dd,  $J = 13.7, 6.0$  Hz, 1H), 2.85 (dd,  $J = 13.7, 8.5$  Hz, 1H), 2.26 (s, 3H), 1.84 – 1.75 (m, 1H), 1.73 – 1.60 (m, 1H), 1.59 – 1.50 (m, 1H), 1.39 (t,  $J = 7.3$  Hz, 2H), 0.83 (dd,  $J = 24.7, 6.6$  Hz, 6H) ppm.  **$^{13}\text{C}$  NMR** (126 MHz, DMSO- $d_6$ ):  $\delta = 172.1, 171.0, 170.7, 166.4, 138.0, 136.4, 136.2, 129.6, 129.2, 128.5, 127.5, 126.7, 63.5, 54.4, 52.3, 51.5, 51.1, 43.1, 42.2, 41.3, 38.0, 36.3, 32.4, 24.6, 23.5, 22.0, 21.1$  ppm. **HRMS** (ESI):  $m/z$ : calcd. for  $\text{C}_{35}\text{H}_{50}\text{ClN}_6\text{O}_6$  [ $M+\text{H}^+$ ] 685.3475; found 685.3479.



### 3.1.7 Supplementary references

- [1] M. Groll, L. Ditzel, J. Löwe, D. Stock, M. Bochtler, H. Bartunik, R. Huber, *Nature* **1997**, *386*, 463–471.
- [2] W. Heinemeyer, A. Cruhler, V. Mohrle, Y. Mahe, D. H. Wolf, *J. Biol. Chem.* **1993**, *268*, 5115–5120.
- [3] W. Heinemeyer, M. Fischer, T. Krimmer, U. Stachon, D. H. Wolf, *J. Biol. Chem.* **1997**, *272*, 25200–25209.
- [4] R. S. B. Sikorski, J. D., *Academic Press Inc., San Diego* **1991**, *194*, 302–318.
- [5] M. Groll, R. Huber, *Methods Enzymol.* **2005**, *398*, 329–336.
- [6] W. Kabsch, *Acta Crystallogr. D. Biol. Crystallogr.* **2010**, *66*, 125–132.
- [7] E. Potterton, P. Briggs, M. Turkenburg, E. Dodson, *Acta Crystallogr. D. Biol. Crystallogr.* **2003**, *59*, 1131–1137.
- [8] D. Turk, *Acta Crystallogr. D. Biol. Crystallogr.* **2013**, *69*, 1342–1357.
- [9] M. L. Stein, H. Cui, P. Beck, C. Dubiella, C. Voss, A. Krüger, M. Groll, *Angew. Chem. Int. Ed.* **2014**, *53*, 1679–1683.
- [10] H. E. Gottlieb, V. Kotlyar, A. Nudelman, *J. Org. Chem.* **1997**, *62*, 7512–7515.



## 4 Ligand-induced active site crosslinking of subunit $\beta 5i$

This chapter contains research which was originally published in *Angewandte Chemie International Edition* **2014**, *53* (44), 11969-11973; *Angewandte Chemie* **2014**, *126* (44), 12163-12167, by Christian Dubiella, Haissi Cui, Malte Gersch, Arwin J. Brouwer, Stephan A. Sieber, Achim Krüger, Rob M. J. Liskamp and Michael Groll.

Copyright © 2014 Wiley-VCH Verlag GmbH & Co. KGaA, Weinheim, Germany.  
Reproduced with permission.

### *Summary*

The concept of proteasome inhibition ranks among the latest achievements in the treatment of blood cancer and represents a promising strategy for modulating autoimmune diseases.

In this publication, we describe peptidic sulfonyl fluoride inhibitors that selectively block the catalytic  $\beta 5i$  subunit of the iCP without inducing cytotoxic effects. Structural and mass spectrometric analyses revealed a novel reaction mechanism involving polarity inversion and irreversible crosslinking of the proteasomal active site. Based on the enhanced isoform selectivity, we characterized the sulfonyl fluoride headgroup for the development and optimization of iCP selective compounds and their possible application in autoimmune disorders.

This summary is based on the above mentioned publication and subject of copyright © 2014 Wiley-VCH Verlag GmbH & Co. KGaA, Weinheim, Germany.

### *Author contributions*

C. Dubiella and M. Groll conceived the project including planning and execution. C. Dubiella performed all experiments unless noted otherwise including organic synthesis, activity assays and crystal soaking experiments. H. Cui performed cell-based activity and cytotoxicity assays under the supervision of A. Krüger. M. Gersch executed mass spectrometric analyses under supervision of S. A. Sieber. A. J. Brouwer provided the first peptido sulfonyl fluoride compound (compound 14)<sup>[14]</sup> for initial tests under the supervision of R. M. J. Liskamp. M. Groll solved crystal structures and supervised the project. C. Dubiella wrote the manuscript with input of M. Groll, H. Cui, M. Gersch and S. A. Sieber.

# Selective Inhibition of the Immunoproteasome by Ligand-Induced Crosslinking of the Active Site \*\*

Christian Dubiella, Haissi Cui, Malte Gersch, Arwin J. Brouwer, Stephan A. Sieber, Achim Krüger, Rob M. J. Liskamp,\* and Michael Groll\*

**Abstract:** The concept of proteasome inhibition ranks among the latest achievements in the treatment of blood cancer and represents a promising strategy for modulating autoimmune diseases. In this study, we describe peptidic sulfonyl fluoride inhibitors that selectively block the catalytic  $\beta 5$  subunit of the immunoproteasome by inducing only marginal cytotoxic effects. Structural and mass spectrometric analyses revealed a novel reaction mechanism involving polarity inversion and irreversible crosslinking of the proteasomal active site. We thus identified the sulfonyl fluoride headgroup for the development and optimization of immunoproteasome selective compounds and their possible application in autoimmune disorders.

The 20S proteasome (core particle; CP) is a sensitive target for the clinically applied inhibitors bortezomib (Velcade) and carfilzomib (CFZ, Kyprolis; Figure 1). Its blockage in malignant cells emerged as an effective approach for the treatment of blood cancers such as multiple myeloma and mantle cell lymphoma.<sup>[1,2]</sup> Moreover, the ongoing evaluation of the anti-inflammatory immunoproteasome (iCP) inhibitor ONX 0914 (former PR-957; Figure 1) in preclinical studies has given rise to a novel therapeutic strategy for modulating autoimmune disorders including rheumatoid arthritis and multiple sclerosis.<sup>[3,4]</sup> A special attribute of ONX 0914 is the reduction of disease-associated immune responses by selectively blocking the  $\beta 5$  subunit of the iCP ( $\beta 5i$  or LMP7).<sup>[3]</sup> However, the therapeutic window of iCP inhibitors like ONX 0914 entirely depends on their selectivity for  $\beta 5i$  over  $\beta 5c$ , in order to prevent cytotoxic effects that arise from undesired co-

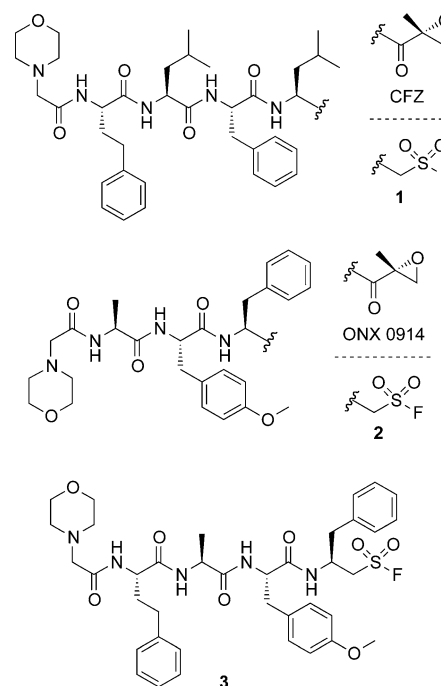


**Figure 1.**  $\alpha',\beta'$ -Epoxyketones carfilzomib (CFZ) and ONX 0914 as well as their peptido sulfonyl fluoride (PSF) counterparts 1, 2, and compound 3.

inhibition of the constitutive proteasome (cCP).<sup>[5,6]</sup> Thus, the decisive element of iCP inhibitor design is the capability to discriminate between the similar chymotrypsin-like (ChTL) activities of  $\beta 5i$  and  $\beta 5c$ .<sup>[7]</sup> CFZ as well as ONX 0914 feature an electrophilic  $\alpha',\beta'$ -epoxyketone warhead that forms a covalent and irreversible adduct with both nucleophiles, Thr1O <sup>$\gamma$</sup>  and Thr1N, of the catalytically active threonine (Thr1) at the  $\beta 5$  subunit (see Scheme S1 in the Supporting Information).<sup>[8–10]</sup> Since CFZ and ONX 0914 have identical warheads, ONX 0914's favorable binding to  $\beta 5i$  solely originates from its backbone architecture, which fulfills the individual binding requirements of  $\beta 5i$  as opposed to  $\beta 5c$ .<sup>[11]</sup> Recently, extensive research on the optimization of peptide backbones by incorporation of unnatural amino acids resulted in  $\beta 5i$ - and  $\beta 5c$ -specific epoxyketones.<sup>[5,12,13]</sup> However, studies on various functional reactive groups and peptido sulfonyl fluoride (PSF) proteasome inhibitors suggest that also warheads have a direct influence on the selectivity for individual active  $\beta$ -subunits.<sup>[14–16]</sup> Notably, PSF compounds block the CP activity in the low nanomolar range,<sup>[16]</sup> albeit they are the only peptidic CP inhibitors known so far whose electrophilic

[\*] C. Dubiella, Dr. M. Gersch, Prof. Dr. S. A. Sieber, Prof. Dr. M. Groll  
Center for Integrated Protein Science Munich (CIPSM)  
Department of Chemistry, Technische Universität München  
Lichtenbergstrasse 4, 85747 Garching (Germany)  
E-mail: michael.groll@tum.de

Prof. Dr. R. M. J. Liskamp  
University of Glasgow  
University Avenue, Glasgow G12 8QQ (UK)  
E-mail: robert.liskamp@glasgow.ac.uk

H. Cui, Prof. Dr. A. Krüger  
Institute for Experimental Oncology and Therapy Research  
Technische Universität München, 81675 München (Germany)

A. J. Brouwer  
Utrecht University, 3508 TB Utrecht (The Netherlands)

[\*\*] This work was funded by SFB 1035A2 and DFG GR 1861/10-1. We thank R. Feicht, R. Baur, and A. Späth for assistance with the experiments and the staff of PXI of Paul Scherrer Institute, Swiss Light Source (Villigen, Switzerland) for help with data collection.



Supporting information for this article is available on the WWW under <http://dx.doi.org/10.1002/anie.201406964>.

headgroup is shifted by a methylene unit, which demands an exceptional binding mode. Therefore, we set out to elucidate the PSF's mode of action, commencing with the synthesis of the CFZ and ONX 0914 PSF counterparts **1** and **2** (Figure 1). Next, we determined crystal structures of yeast CP (yCP):**1** with resolutions up to 2.1 Å by performing crystal soaking experiments with incubation times of 1–6 h prior to data collection (see Table ST1).

Based on the identical headgroups of the PSF and the common serine protease inhibitor phenylmethanesulfonyl fluoride (PMSF), we anticipated a similar inactivation mechanism through the formation of a covalent adduct on Thr1 upon attack of Thr1O<sup>γ</sup> on the sulfur atom. Unexpectedly, after incubation of the crystal for 2 h, the yCP:**1** structure revealed empty substrate binding channels (2.1 Å resolution,  $R_{\text{free}} = 19.7\%$ , PDB ID 4R17). Instead, the  $F_o - F_c$  map displayed negative electron density at the Thr1 side chain of subunit β5, disclosing a chemical modification of the catalytic center (see Figure S1a), whereas β1 and β2 remained identical to the apo state. To identify a short-lived reaction intermediate of **1** at β5 we conducted time-resolved intact protein mass spectrometry using LC-ESI-LTQ-FT-MS analysis on various CP types incubated with **1** and **2** (Figure 2).

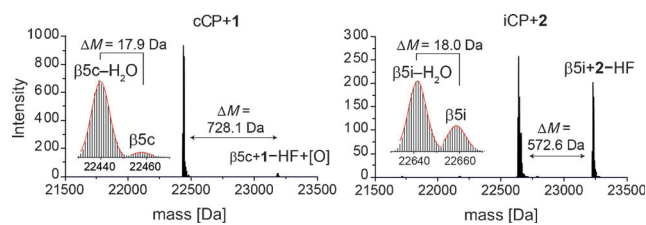


**Figure 2.** Deconvoluted intact-protein mass spectra of the β5c and β5i subunits following treatment of cCP with **1** (left panel) and iCP with **2** (right panel) (25 μM) after incubation for 12 h. The species labeled “–H<sub>2</sub>O” represent either the aziridine or the crosslinked state (expected mass difference: 18.0 Da). The insets feature enlargements of the major species. The species labeled “+2–HF” represents the covalently modified intermediate of the β5 subunits prior to dehydroxylation (expected mass difference: 572.7 Da). See Figure S5 for spectra of β5 of untreated cCP and iCP.

Spectra with incubation times up to 2 h confirmed the formation of a covalent adduct on the β5 subunit of all applied CP types with an observed mass increase corresponding to the ligand upon fluorine release (see Figure 2 and Figure S2). Furthermore, we observed a formal loss of a water molecule (–18 Da) at the β5 subunit which was validated by multiple experiments and different mass spectra deconvolution algorithms (see Figures S3 and S4 and Tables ST2 and ST3).

These findings suggest either an addition–elimination reaction as described for PMSF, which for example converts the active Ser195 of thrombin into dehydroalanine,<sup>[17]</sup> or an addition–displacement mechanism comprising sulfonylation of Thr1O<sup>γ</sup>, followed by an intramolecular substitution by Thr1N to yield an aziridine. While the PMSF-induced elimination reaction requires strong alkaline conditions, our experiments were carried out at pH 6.8–7.5, indicating that

dehydroxylation of Thr1 is rather an integral part of the inhibition mechanism than an artificially base-induced event. Consistently, the  $F_o - F_c$  electron density map clearly depicts the intramolecular displacement product (*S,S*)-aziridine-T1' (Figure 3b), thus excluding the elimination product (*E*)-dehydrobutyryne (Dhb) (Figure S1b, Supporting Information). Moreover, cyclization initiated by Thr1N is confirmed

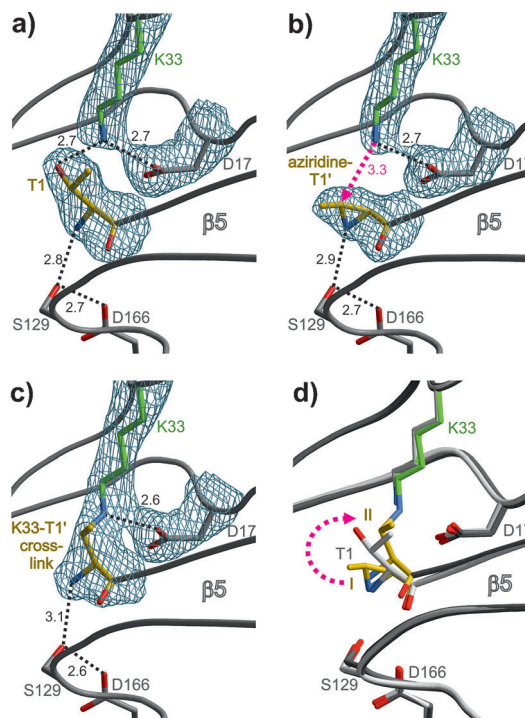
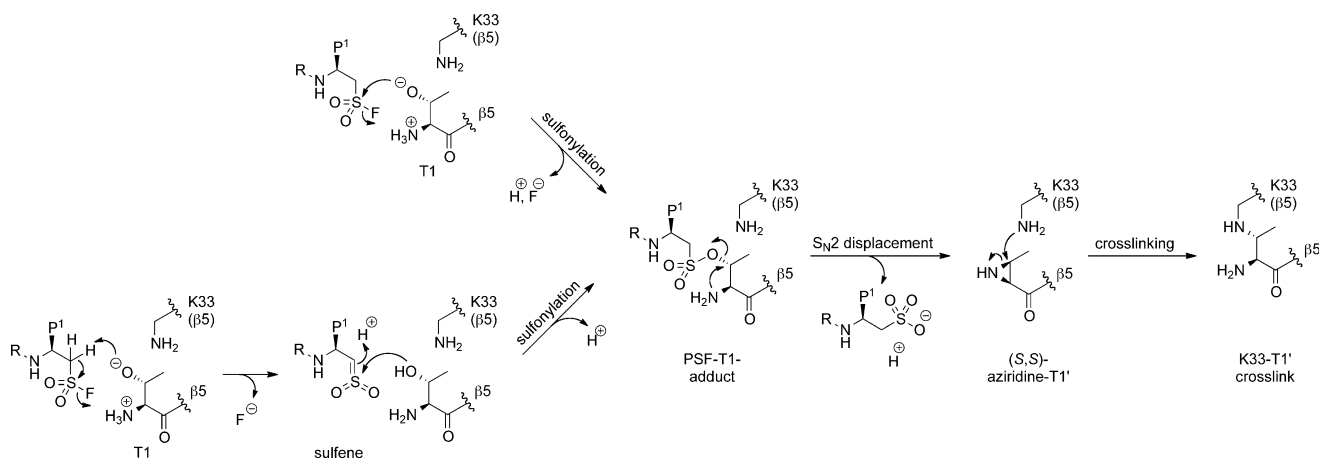


**Figure 3.** Comparative X-ray analysis of the β5 active site after time-dependent soaking experiments of yCP crystals with **1**. The  $2F_o - F_c$  electron density maps (blue mesh, contoured at  $1\sigma$ ) show distances in Å as black dashed lines. The active site triad Thr1 (T1), Asp17 (D17), and Lys33 (K33) has been excluded prior to phasing. Stereoviews of (a)–(d) are depicted in Figure S6. a) Subunit β5 of the apo structure with unmodified T1 (yellow).<sup>[18]</sup> b) Aziridine-T1' (yellow) formation on β5 after 2 h soaking time with **1**. The trajectory of the nucleophilic attack of K33 (green) is shown as a pink dashed arrow (PDB ID 4R17). c) K33-T1'-crosslink (yellow) formation on subunit β5 after 6 h soaking time (PDB ID 4R18). d) Superposition of the apo structure with unmodified T1 (light gray), the aziridine-T1' intermediate (I, yellow), and the K33-T1'-crosslink (II, yellow). The structural rearrangement of T1 upon its conversion into intermediate I and crosslink II is illustrated with a pink dashed arrow.

by the inverted stereoconfiguration of the methyl group in (*S,S*)-aziridine-Thr1', implying an  $S_N2$ -like displacement. To analyze the stability of the aziridine ring we conducted further soaking experiments with extended incubation times up to 6 h at pH 6.8. The  $2F_o - F_c$  electron density map of the yCP:**1** structure revealed a  $S_N2$ -type ring-opening of the aziridine-Thr1' by attack of the amino group of Lys33 (Lys33N<sup>ε</sup>), yielding an intramolecular crosslink in β5 (Figure 3c; 2.4 Å resolution,  $R_{\text{free}} = 19.5\%$ , PDB ID 4R18). This Lys33-Thr1' bond proves the presence of a polarity-inversed Thr1 intermediate and is certainly surprising, since the function of Lys33N<sup>ε</sup> is to maintain the  $pK_a$  of Thr1O<sup>γ</sup>, and hence



**Scheme 1.** Proposed three-step inactivation mechanism of the PSF compounds at the proteasomal active site of subunit  $\beta 5$ . Hypothetically, the sulfenylation of Thr107 is conceivable by two different mechanisms: a direct nucleophilic attack of Thr107 on the electrophilic sulfur center (upper left corner), or by elimination and sulfene formation (lower left corner). The substituent R indicates the rest of the peptidic backbone and P1 refers to the amino acid side chain of the inhibitor protruding into the S1 specificity pocket.

possesses only a moderate intrinsic nucleophilicity.<sup>[19]</sup> From an organic chemical point of view this aziridine ring-opening is also unexpected, since normally the presence of electron-withdrawing groups on the aziridine nitrogen is required.<sup>[20]</sup>

Intriguingly, superposition of the apo and yCP:1 structures illustrates that the flexibility of the aziridine-Thr1'-containing  $\beta 5$  chain solely accounts for closing the 3.3 Å gap between Lys33N<sup>e</sup> and the electrophile, while all remaining residues retain their position (Figure 3d). Consequently, the decline of structural integrity upon dehydroxylation of Thr1 presents a precondition to perform the crosslinkage. Based on these distinct snapshots of the reaction intermediates, we propose a three-step mechanism of the PSF compounds resulting in the crosslinking of the proteasomal active site (Scheme 1).

Our next goal was to investigate whether this complex mechanism could contribute to increased  $\beta 5i$  selectivity and thus reduced cytotoxicity. Therefore, we compared the potency and  $\beta 5$  subunit selectivity of **1** and **2** with that of their  $\alpha',\beta'$ -epoxyketone originals by performing *in vitro* IC<sub>50</sub> assays with purified human iCP, cCP, and yeast CP (yCP) (Table 1, Figure 4). Remarkably, **2** (IC<sub>50</sub>  $\beta 5c/\beta 5i$ : 25) turned out to be roughly three times more selective for  $\beta 5i$  than ONX 0914 (IC<sub>50</sub>  $\beta 5c/\beta 5i$ : 9), despite identical backbone architecture. However, the improved  $\beta 5i$  selectivity of **2** was accompanied by a 20-fold decreased potency (IC<sub>50</sub> ( $\beta 5i$ ): 1134 nm) compared to ONX 0914 (IC<sub>50</sub> ( $\beta 5i$ ): 57 nm), indicat-

**Table 1:** *In vitro* IC<sub>50</sub> values [nm] against the ChTL activity of various purified CP types.

Compound	IC <sub>50</sub> $\gamma\beta 5$	IC <sub>50</sub> $\beta 5c$	IC <sub>50</sub> $\beta 5i$	IC <sub>50</sub> $\beta 5c/\beta 5i$ <sup>[a]</sup>
CFZ	3 ± 1	5 ± 1	21 ± 3	0.2
<b>1</b>	21 ± 2	28 ± 2	54 ± 10	0.5
ONX 0914	145 ± 15	513 ± 30	57 ± 10	9
<b>2</b>	15420 ± 635	28460 ± 1305	1134 ± 146	25
<b>3</b>	1775 ± 476	3927 ± 550	139 ± 34	28

[a] A high IC<sub>50</sub>  $\beta 5c/\beta 5i$  ratio indicates selectivity for  $\beta 5i$ .

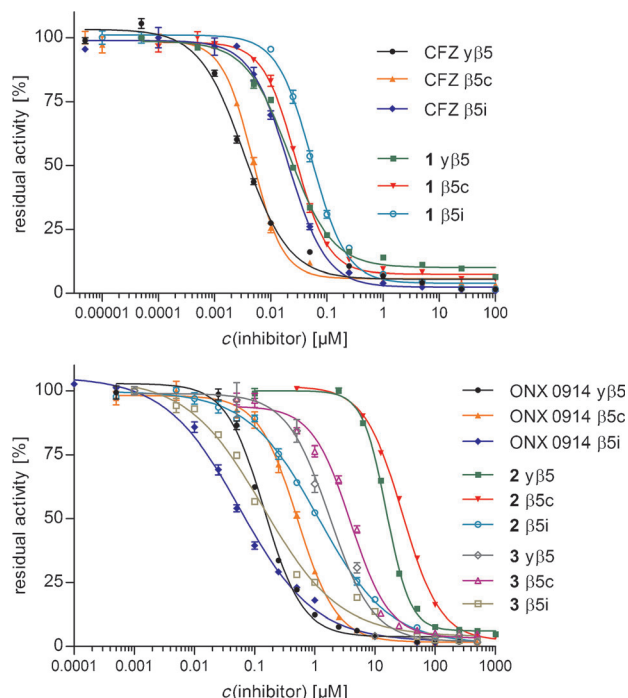


**Figure 4.** *In vitro* IC<sub>50</sub> assays against the ChTL activity of various purified CP types after 1 h incubation at various concentrations of CFZ and **1** (left panel) as well as ONX 0914, **2**, and **3** (right panel) using a fluorogenic substrate assay. Data of three repetitions were normalized to DMSO-treated controls and are presented as relative activity with standard deviation (Table 1).

ing that PSF ligands require at least capped tetrapeptidic backbones for sufficient stabilization during proteasomal binding. Thus, we extended **2** with a homophenylalanine in P4 to generate compound **3** (Figure 1).

Since the S4 specificity pockets of iCP and cCP are identically shaped by the  $\beta 6$  subunit, **3** exhibited up to eightfold improved potency against  $\beta 5i$  (IC<sub>50</sub> ( $\beta 5i$ ): 139 nm) and  $\beta 5c$  (IC<sub>50</sub> ( $\beta 5c$ ): 3927 nm), respectively. Importantly, **3**



**Table 2:** In vivo  $IC_{50}$  values [nM] against the ChTL activity and  $LC_{50}$  values [nM] against HeLa and THP-1 cells.

Compound	$IC_{50}$	$IC_{50}$	$LC_{50}$	$LC_{50}$	$LC_{50}/IC_{50}^{[a]}$	$LC_{50}/IC_{50}^{[a]}$
	HeLa	THP-1	HeLa	THP-1	HeLa	THP-1
CFZ	6 ± 1	7 ± 1	28 ± 6	12 ± 1	5	2
<b>1</b>	29 ± 3	35 ± 4	353 ± 63	156 ± 16	12	4
ONX 0914	78 ± 10	22 ± 2	333 ± 48	110 ± 14	4	5
<b>2</b>	5032 ± 577	1789 ± 378	> 100000	> 100000	> 19	> 56
<b>3</b>	550 ± 59	146 ± 40	> 100000	5746 ± 1436	> 182	39

[a] A high  $LC_{50}/IC_{50}$  ratio indicates low cytotoxicity relative to the corresponding  $IC_{50}$  value.

displayed an even enhanced  $\beta 5i$  selectivity ( $IC_{50} \beta 5c/\beta 5i$ : 28) compared to **2**. By contrast, **1** and CFZ inhibited the  $\beta 5$  subunits of all analyzed CP types in the single- and double-digit nanomolar range without any preference for  $\beta 5i$ . This suggests that the PSF headgroup emphasizes the influence of the peptidic backbone to a greater extent than the  $\alpha',\beta'$ -epoxyketone warhead.

The in vitro findings were confirmed by determining the in vivo  $IC_{50}$  values of **1**, **2**, their  $\alpha',\beta'$ -epoxyketone counterparts as well as **3** in cell culture assays (Table 2, Figure 5a). We used either the THP-1 cell line, which is derived from acute monocytic leukemia and expresses high levels of iCP, or the HeLa cell line, which primarily contains cCP.<sup>[21]</sup> ONX 0914, **2**, and **3** turned out to be three to four times more selective for THP-1 cells over HeLa cells, while **1** and CFZ displayed virtually similar potencies on both cell lines in accordance with the in vitro  $IC_{50}$  assays.

To evaluate the cytotoxic profiles of the compounds we determined the  $LC_{50}$  values against THP-1 and HeLa cells in viability assays (Table 2, Figure 5b). Notably, **2** and **3** hardly affected the viability of either cell line, arguably reflecting their high  $\beta 5i$  selectivity and low off-target binding. The in vivo  $IC_{50}$  values of **1** ( $IC_{50}$  (THP-1): 35 nM,  $IC_{50}$  (HeLa): 29 nM) exclude that the low cytotoxicity is caused by

a rapid hydrolysis of the PSF headgroup.

In summary, the presented comparative study of iCP-selective  $\alpha',\beta'$ -epoxyketone and PSF counterparts highlights the sulfonyl fluoride headgroup as a promising motif for  $\beta 5i$  targeting. In contrast to all analyzed CP inhibitors to date, PSFs manipulate the proteasomal activity by a previously unobserved mode of action through polarity inversion and intramolecular crosslinking of the active site. In contrast to the unspecific serine protease inhibitor PMSF, the additional peptidic backbone accounts for site-selective proteasome inhibition. Thus, target-specific iCP blockage of the PSF in the nanomolar range along with low cytotoxicity broadens the therapeutic window of PSF as potential future anti-inflammatory inhibitors.

Received: July 7, 2014

Published online: September 22, 2014

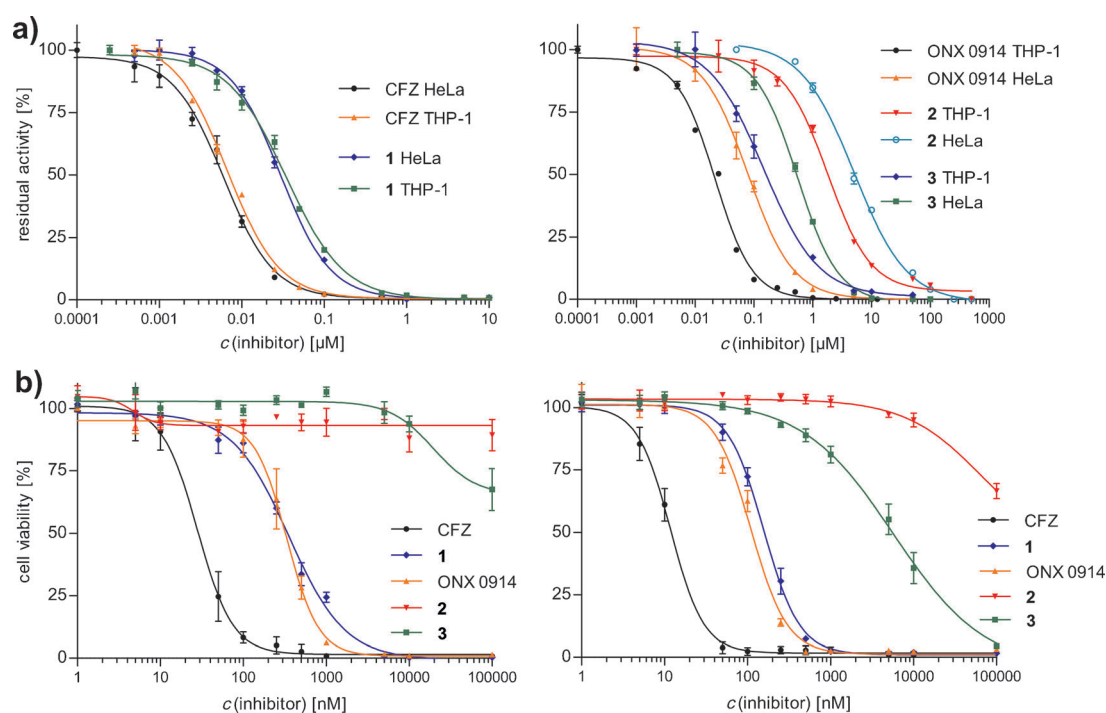


**Figure 5.** a) In vivo  $IC_{50}$  assays against the ChTL activity in HeLa and THP-1 cells after 105 min incubation at various concentrations of CFZ and **1** (left panel) as well as ONX 0914, **2**, and **3** (right panel) using a luminogenic substrate assay. b)  $LC_{50}$  against HeLa (left panel) and THP-1 (right panel) cells after 48 h incubation at concentrations of CFZ, **1**, ONX 0914, **2**, and **3** between 1 nM and 100 μM using an AlamarBlue-based cell viability assay. Data of three repetitions were normalized to DMSO-treated controls and are presented as relative activity with standard deviation (Table 2).

**Keywords:** drug design · inhibitors · immunoproteasome · peptido sulfonyl fluoride · umpolung

- 
- [1] P. G. Richardson, T. Hideshima, K. C. Anderson, *Cancer Control* **2003**, *10*, 361–369.
- [2] S. D. Demo, C. J. Kirk, M. A. Aujay, T. J. Buchholz, M. Dajee, M. N. Ho, J. Jiang, G. J. Laidig, E. R. Lewis, F. Parlati, et al., *Cancer Res.* **2007**, *67*, 6383–6391.
- [3] T. Muchamuel, M. Basler, M. A. Aujay, E. Suzuki, K. W. Kalim, C. Lauer, C. Sylvain, E. R. Ring, J. Shields, J. Jiang, et al., *Nat. Med.* **2009**, *15*, 781–787.
- [4] M. Basler, S. Mundt, T. Muchamuel, C. Moll, J. Jiang, M. Groettrup, C. J. Kirk, *EMBO Mol. Med.* **2014**, *6*, 226–238.
- [5] F. Parlati, S. J. Lee, M. Aujay, E. Suzuki, K. Levitsky, J. B. Lorens, D. R. Micklem, P. Ruurs, C. Sylvain, Y. Lu, et al., *Blood* **2009**, *114*, 3439–3447.
- [6] D. Niewerth, J. van Meerloo, G. Jansen, Y. G. Assaraf, T. C. Hendrickx, C. J. Kirk, J. L. Anderl, S. Zweegman, G. J. L. Kaspers, J. Cloos, *Biochem. Pharmacol.* **2014**, *89*, 43–51.
- [7] E. M. Huber, M. Groll, *Angew. Chem. Int. Ed.* **2012**, *51*, 8708–8720; *Angew. Chem.* **2012**, *124*, 8838–8850.
- [8] M. Groll, K. B. Kim, N. Kairies, R. Huber, C. M. Crews, *J. Am. Chem. Soc.* **2000**, *122*, 1237–1238.
- [9] L. Meng, R. Mohan, B. H. Kwok, M. Elofsson, N. Sin, C. M. Crews, *Proc. Natl. Acad. Sci. USA* **1999**, *96*, 10403–10408.
- [10] A. Rentsch, D. Landsberg, T. Brodmann, L. Bülow, A.-K. Girbig, M. Kalesse, *Angew. Chem. Int. Ed.* **2013**, *52*, 5450–5488; *Angew. Chem.* **2013**, *125*, 5560–5599.
- [11] E. M. Huber, M. Basler, R. Schwab, W. Heinemeyer, C. J. Kirk, M. Groettrup, M. Groll, *Cell* **2012**, *148*, 727–738.
- [12] G. de Bruin, E. M. Huber, B.-T. Xin, E. J. van Rooden, K. Al-Ayed, K.-B. Kim, A. F. Kisselev, C. Driessen, M. van der Stelt, G. A. van der Marel, et al., *J. Med. Chem.* **2014**, *57*, 6197–6209.
- [13] A. V. Singh, M. Bandi, M. A. Aujay, C. J. Kirk, D. E. Hark, N. Raje, D. Chauhan, K. C. Anderson, *Br. J. Haematol.* **2011**, *152*, 155–163.
- [14] M. L. Stein, H. Cui, P. Beck, C. Dubiella, C. Voss, A. Krüger, M. Groll, *Angew. Chem. Int. Ed.* **2014**, *53*, 1679–1683; *Angew. Chem.* **2014**, *126*, 1705–1709.
- [15] M. Screen, M. Britton, S. L. Downey, M. Verdoes, M. J. Voges, A. E. M. Blom, P. P. Geurink, M. D. P. Risseeuw, B. I. Florea, W. A. van der Linden, et al., *J. Biol. Chem.* **2010**, *285*, 40125–40134.
- [16] A. J. Brouwer, A. Jonker, P. Werkhoven, E. Kuo, N. Li, N. Gallastegui, J. Kemmink, B. I. Florea, M. Groll, H. S. Overkleeft, et al., *J. Med. Chem.* **2012**, *55*, 10995–11003.
- [17] R. W. Ashton, H. A. Scheraga, *Biochemistry* **1995**, *34*, 6454–6463.
- [18] M. Groll, L. Ditzel, J. Löwe, D. Stock, M. Bochtler, H. Bartunik, R. Huber, *Nature* **1997**, *386*, 463–471.
- [19] M. Groll, T. Clausen, *Curr. Opin. Struct. Biol.* **2003**, *13*, 665–673.
- [20] X. E. Hu, *Tetrahedron* **2004**, *60*, 2701–2743.
- [21] D. Niewerth, G. J. L. Kaspers, Y. G. Assaraf, J. van Meerloo, C. J. Kirk, J. Anderl, J. L. Blank, P. M. van de Ven, S. Zweegman, G. Jansen, et al., *J. Hematol. Oncol.* **2014**, *7*, 7.
-



## 4.1 Supporting information

### Selective Inhibition of the Immunoproteasome by Ligand-Induced Crosslinking of the Active Site

C. Dubiella, H. Cui, M. Gersch, A. J. Brouwer, S. A. Sieber, A. Krüger, R. M. J. Liskamp & M. Groll

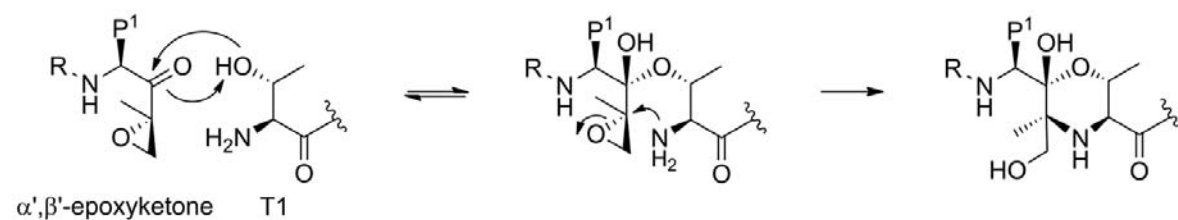
*Angewandte Chemie International Edition* **2014**, 53 (44), 11969-11973;

*Angewandte Chemie* **2014**, 126 (44), 12163-12167.

### Supporting Information Table of Contents

4.1.1	Supplementary schemes .....	70
4.1.2	Supplementary figures .....	70
4.1.3	Supplementary tables .....	75
4.1.4	Supplementary in vitro methods .....	77
	Protein purification .....	77
	IC <sub>50</sub> value determination.....	77
	Intact protein mass spectrometry .....	77
	Crystallization and structure elucidation.....	78
4.1.5	Supplementary cell culture methods.....	78
	IC <sub>50</sub> determination with Proteasome-Glo™ chymotrypsin-like cell-based assay .....	78
	LC <sub>50</sub> determination via AlamarBlue-based viability assay .....	79
4.1.6	Supplementary chemical synthesis.....	79
	General remarks .....	79
	General procedure for the synthesis of peptidic backbones.....	80
	Synthesis of sulfonyl fluoride headgroups.....	81
	Final coupling of peptidic backbones and sulfonyl fluoride headgroups.....	86
4.1.7	Supplementary references.....	88

### 4.1.1 Supplementary schemes



**Scheme S1** Binding of  $\alpha',\beta'$ -epoxyketones to Thr1 (T1) at the proteasomal active site.

### 4.1.2 Supplementary figures

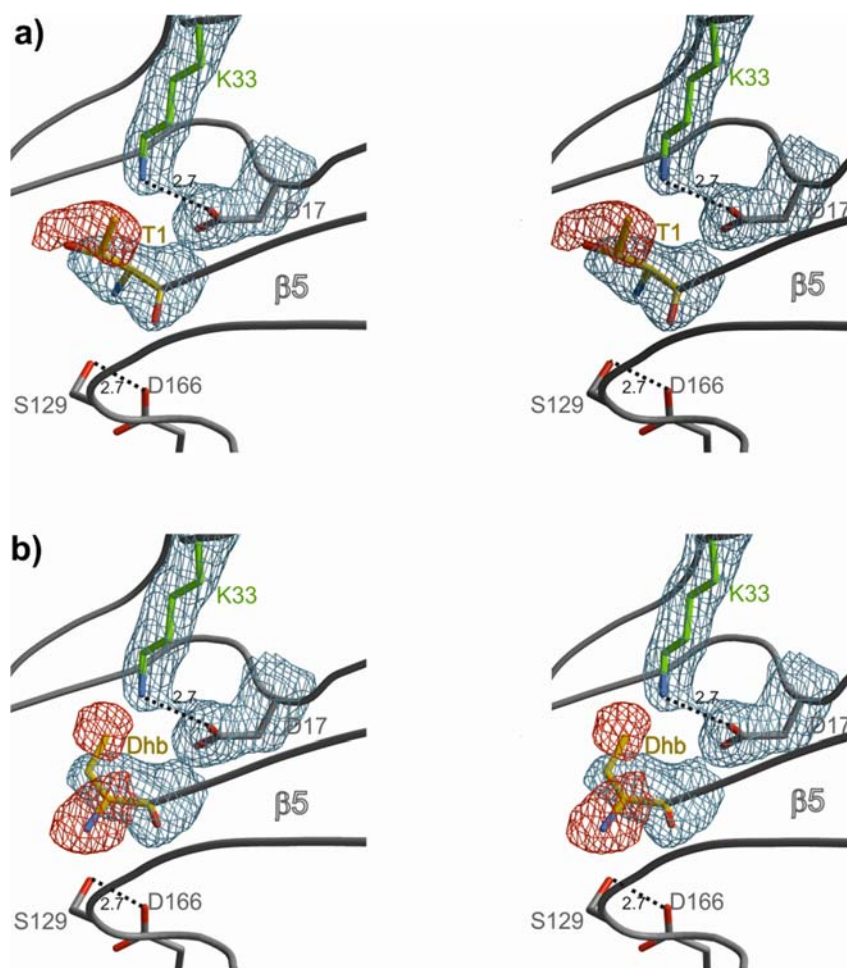


**Figure S1** Stereo view of the  $2F_o-F_c$  (gray mesh, contoured at  $1\sigma$ ) and the  $1F_o-F_c$  electron density (red mesh, contoured at  $-3\sigma$ ) maps of the chymotrypsin-like  $y\beta 5$  active site displaying the active site nucleophile Thr1 (T1), Lys 33 (K33) (green), Asp17 (D17), Ser129 (S129) and Asp166 (D166) (gray) with distances in Å (black dashed lines). a)  $yCP:1(2\text{ h})$  structure refined with Thr1. b)  $yCP:1(2\text{ h})$  structure refined with (*E*)-dehydrobutyryne (Dhb) instead of Thr1.

#### 4. Ligand-induced active site crosslinking of subunit $\beta 5i$

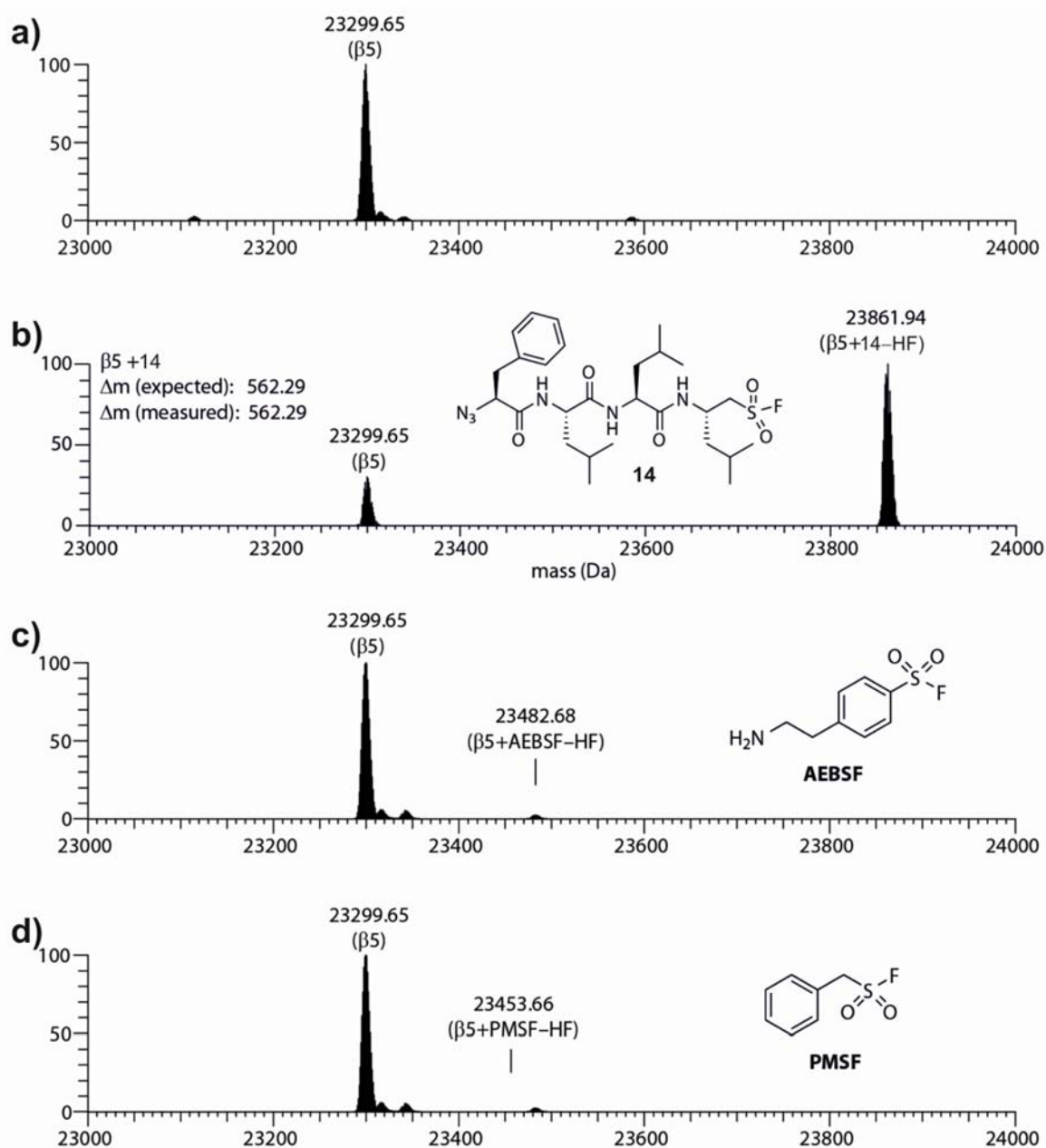


**Figure S2** a+b) Treatment of yCP with compound 14 ( $N_3$ Phe-Leu-Leu-Leu- $\psi$ -[CH<sub>2</sub>SO<sub>2</sub>]-F)<sup>[1]</sup> (1  $\mu$ M, 30 min, 25°C) as PSF model compound resulted in the formation of a species with increased mass matching the addition of one equivalent of compound 14<sup>[1]</sup> to the catalytic subunit y $\beta 5$  and subsequent elimination of hydrogen fluoride. c+d) Treatment of yCP with sulfonyl fluorides PMSF and AEBSF (100  $\mu$ M, 24 h, 25°C) did not alter the mass of the subunit  $\beta 5$ . For detailed information of the mass analysis see the following Tables ST2-3 and Figures S4-5.

#### 4. Ligand-induced active site crosslinking of subunit $\beta 5$

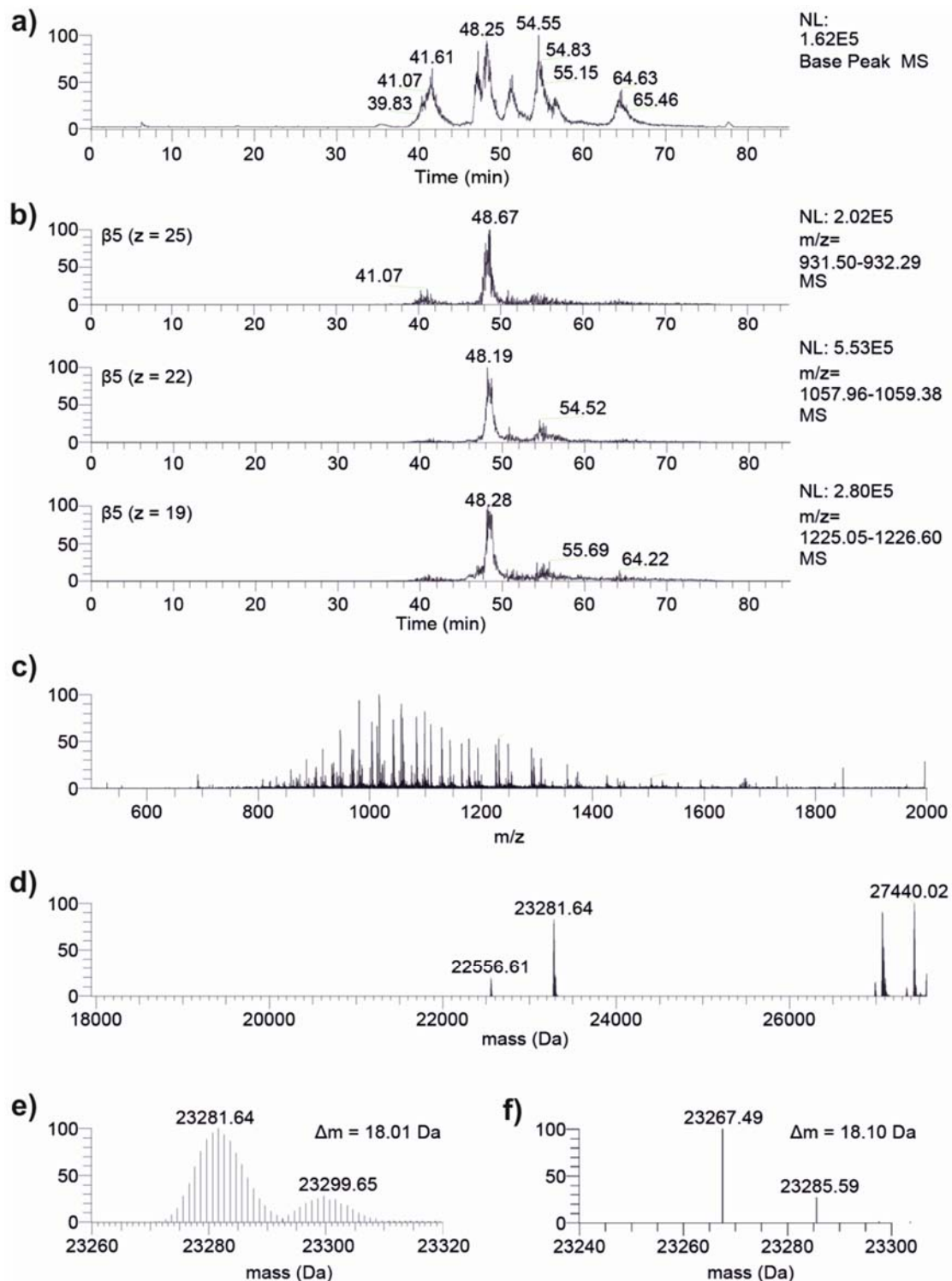


**Figure S3** a) Base peak chromatogram of yCP treated with substoichiometric amounts of compound 14<sup>[1]</sup> (1  $\mu$ M). b) Extracted ion chromatograms of masses corresponding to the  $z = 25$ ,  $z = 22$  and  $z = 19$  charged states of the  $\beta 5$  subunit displaying a retention time of 47.8-49.0 min. c) Mass spectrum averaged from the full scans in this time frame. d) Deconvolution of the spectrum shown in C with Xtract. e) Close-up view on the  $\beta 5$  subunit mass displaying the presence of two species. f) Monoisotopic masses of these species calculated by Xtract.

#### 4. Ligand-induced active site crosslinking of subunit $\beta 5i$

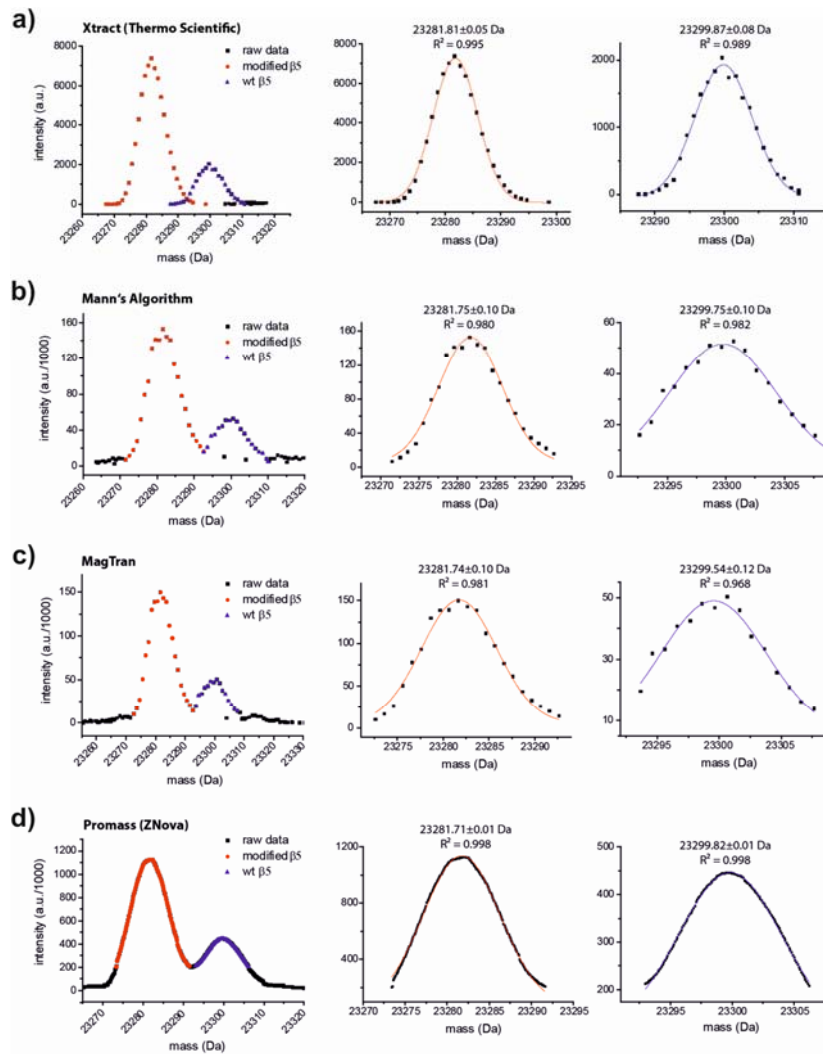


**Figure S4** Comparison of different deconvolution algorithms on the data shown in Figure S4 ( $R = 200000$ ). Gaussian curves were fitted to determine the maxima. a) Xtract (Thermo Scientific) (S/N-threshold: 2; Fit factor: 44; Remainder: 25%; low-high: 600–2000  $m/z$ ). b) Mann's Algorithm as implemented in MagTran. c) MagTran algorithm (Modus: Isotope, then Charge; Isotope envelope: 1-15 Da; Mass range: 10000-30000 Da; Charge range: 1-100; S/N-threshold: 1; Mass accuracy: 0.05 Da; maxima are plotted). d) Promass (ZNova) (Input: 800-1350  $m/z$ ; Output: 23000-24000; 0.1 Da mass step size; Peak width: 4; Merge width: 0.4; S/N-Threshold: 2; Smooth width: 5; Num of smooths: 2).

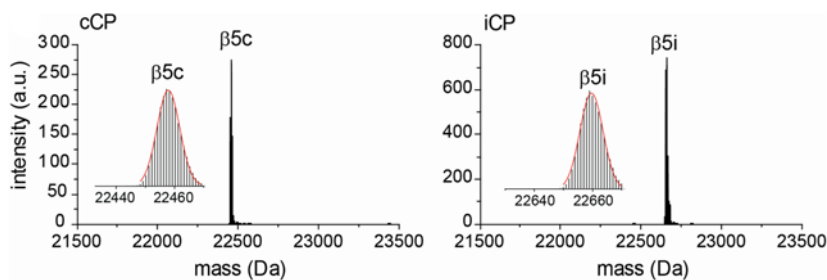


**Figure S5** Deconvoluted intact-protein mass spectra of the  $\beta 5c$  and  $\beta 5i$  subunits of untreated, human cCP and iCP, respectively. The insets feature zooms on the major species.

#### 4. Ligand-induced active site crosslinking of subunit $\beta 5i$

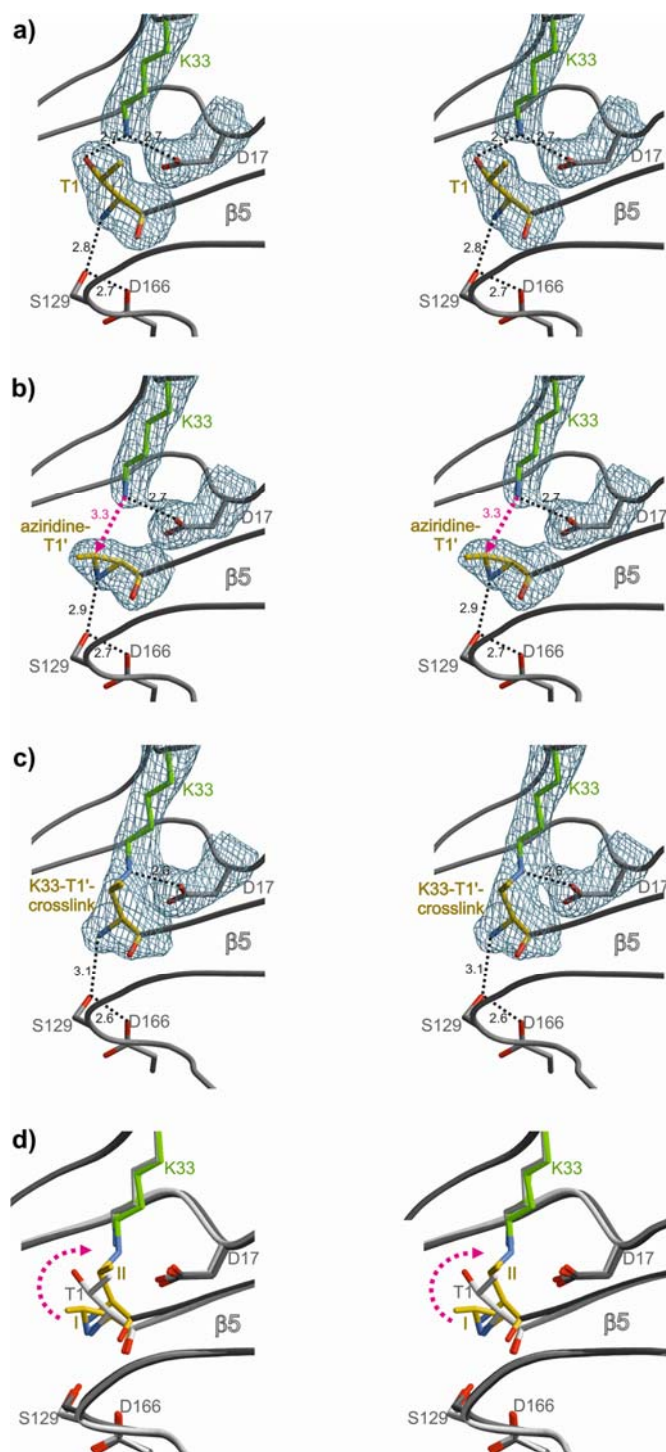


**Figure S6** Stereo views of the  $2F_o - F_c$  electron density maps (gray mesh, contoured at  $1\sigma$ ) with  $y\beta 5$  active site residues according to Figure S1. a)  $yCP$  apo structure with unmodified T1 (yellow). b)  $yCP:1(2\text{ h})$  structure with (*S,S*)-aziridine-T1' (yellow). The trajectory of the nucleophilic attack of  $K33N^{\epsilon}$  on aziridine-T1' is shown as a dashed arrow in pink (PDB ID 4R17). c)  $yCP:1(6\text{ h})$  structure with K33-T1'-crosslink (yellow) (PDB ID 4R18). d) Stereo view of the structural superposition of  $yCP$  apo (T1 in light gray),  $yCP:1(2\text{ h})$  (aziridine-T1' (I) in yellow) and  $yCP:1(6\text{ h})$  K33-T1'-crosslink (II) in yellow). Conformational changes between intermediate I and crosslink II are illustrated by a dashed arrow in pink.

### 4.1.3 Supplementary tables

**Table ST1** Crystallographic data collection and refinement statistics of the yCP incubated with **1**, soaking times 2 h and 6 h.

Crystallographic data	yCP:1(2 h)*	yCP:1(6 h)*
<b>Crystal parameters</b>		
Space group	P2 <sub>1</sub>	P2 <sub>1</sub>
Cell constants	a = 134.72 Å	136.58 Å
(dataset was collected from 1 crystal / 1 CP per AU)	b = 301.36 Å	300.82 Å
	c = 144.74 Å	146.29 Å
	$\beta = 112.807^\circ$	113.202°
<b>Data collection</b>		
Beamline	X06SA, SLS	X06SA, SLS
Wavelength, (Å)	1.0	1.0
Resolution range, (Å) <sup>†</sup>	30-2.1 (2.2-2.1)	30-2.4 (2.5-2.4)
No. observations	1,888,610	1,281,847
No. unique reflections <sup>‡</sup>	608,720	408,278
Completeness, (%) <sup>†</sup>	98.8 (99.4)	96.9 (97.8)
R <sub>merge</sub> , (%) <sup>†,§</sup>	4.4 (56.8)	4.4 (41.7)
I/ $\sigma$ (I) <sup>†</sup>	18.3 (2.9)	17.3 (4.0)
<b>Refinement (REFMAC5)</b>		
Resolution range, (Å)	15-2.1	15-2.4
No. reflections working set	578,284	387,863
No. reflections test set	30,436	20,414
No. non-hydrogen	49,374	49,374
Water, Mg <sup>2+</sup>	3484	1751
R <sub>work</sub> /R <sub>free</sub> (%) <sup>¶</sup>	18.5/19.7	17.7/19.5
RMSD bond (Å)/(°) <sup>**</sup>	0.005/1.09	0.004/0.98
Average B-factor (Å <sup>2</sup> )	46.4	56.7
Ramachandran plot, % <sup>***</sup>	97.3/2.5/0.2	97.5/2.2/0.3
PDB accession code	4R17	4R18

\*Dataset has been collected on a single crystal.

<sup>†</sup>Values in parentheses of resolution range, completeness, R<sub>merge</sub>, and I/ $\sigma$  (I) correspond to the last resolution shell.

<sup>‡</sup>Friedel pairs were treated as identical reflections.

<sup>§</sup>R<sub>merge</sub> (I) =  $\sum_{hkl} \sum_j [|I(hkl)_j - \langle I(hkl) \rangle|] / \sum_{hkl} I_{hkl}$ , where  $I(hkl)_j$  is the measurement of the intensity of reflection hkl and  $\langle I(hkl) \rangle$  is the average intensity.

<sup>¶</sup>R =  $\sum_{hkl} [|F_{obs}| - |F_{calc}|] / \sum_{hkl} |F_{obs}|$ , where R<sub>free</sub> is calculated without a sigma cut off for a randomly chosen 5% of reflections, which were not used for structure refinement, and R<sub>work</sub> is calculated for the remaining reflections.

<sup>\*\*</sup>Deviations from ideal bond lengths/angles.

<sup>\*\*\*</sup>Number of residues in favored region/allowed region/outlier region.



#### 4. Ligand-induced active site crosslinking of subunit $\beta 5$

**Table ST2** Masses of  $\gamma\beta 5$  after treatment of  $\gamma\text{CP}$  with substoichiometric amounts of compound 14<sup>[1]</sup> determined by different algorithms (all values are listed in Da). The results support the crystallographic achievements in which Thr10 $\gamma$  of subunit  $\beta 5$  is converted to an aziridine ( $\Delta m(-\text{H}_2\text{O}, \text{expected}) = 18.02$  Da).

Algorithm	Mass $\gamma\beta 5$ modified	Mass $\gamma\beta 5$	Mass difference
Xtract highest peak	23281.64	23299.65	18.01
Xtract Monoisotopic	23267.49	23285.59	18.10
Xtract Gaussian	23281.81 $\pm$ 0.05	23299.87 $\pm$ 0.08	18.06 $\pm$ 0.09
Mann's algorithm	23281.75 $\pm$ 0.10	23299.75 $\pm$ 0.10	18.00 $\pm$ 0.14
MagTran	23281.74 $\pm$ 0.10	23299.54 $\pm$ 0.12	17.80 $\pm$ 0.16
Promass (ZNova)	23281.71 $\pm$ 0.10	23299.82 $\pm$ 0.10	18.09 $\pm$ 0.14
Average			18.01 $\pm$ 0.10

**Table ST3** Masses of subunit  $\beta 5$  after treatment of  $\gamma\text{CP}$  with substoichiometric amounts of compound 14<sup>[1]</sup> (5 independent samples, Xtract highest peaks are given in Da).

Sample number	Mass $\gamma\beta 5$ modified	Mass $\gamma\beta 5$	Mass difference
Sample 1	23281.64	23299.65	18.01
Sample 2	23281.63	23299.65	18.02
Sample 3	23281.64	23299.65	18.01
Sample 4	23281.66	23281.68	18.02
Sample 5	23281.65	23281.65	18.00
Average			18.01 $\pm$ 0.01



#### 4.1.4 Supplementary in vitro methods

##### *Protein purification*

20S proteasome from *Saccharomyces cerevisiae* (yCP) was purified as previously described.<sup>[2]</sup> Yeast cells were lysed in a continuous cell disruption system and centrifuged at 40,000 g. After precipitation in aqueous 40%  $(\text{NH}_4)_2\text{SO}_4$ , the suspension was applied to a phenyl sepharose HIC column. Eluted fractions displaying 20S proteasome activity were pooled and purified using FPLC with a hydroxyapatite column. Polishing was performed via a Resource-Q anion exchange column and a Superose 6 size exclusion chromatography. The pooled fractions were concentrated to 40 mg/mL in 20 mM Tris (pH 7.5) and used for further crystallization trials and in vitro assays.

##### *IC<sub>50</sub> value determination*

In vitro proteasome inhibition assays were performed by fluorescence assays in 96-well plates. Assay mixtures contained 10  $\mu\text{g/mL}$  of freshly purified yCP or commercially available purified human cCP (Boston Biochem) and human iCP (Boston Biochem) in 100 mM Tris/HCl (pH 7.5) buffer. Inhibitors were dissolved in DMSO and added at various concentrations with three repetitions each, thereby not surpassing a final concentration of 10% (w/v) DMSO. After an incubation time of 60 min at RT, the fluorogenic substrate Suc-Leu-Leu-Val-Tyr-AMC (Bachem) was added to measure the residual activity of the chymotrypsin-like site. The assay mixture was incubated for another hour at RT, afterwards fluorescence was determined on a Varian Cary Eclipse photofluorometer with excitation and emission wavelengths of  $\lambda_{\text{exc}} = 360 \text{ nm}$  and  $\lambda_{\text{em}} = 460 \text{ nm}$ , respectively.

##### *Intact protein mass spectrometry*

Analyses were carried out on a Dionex UltiMate 3000 HPLC system coupled to a Thermo Scientific LTQ-FT Ultra mass spectrometer with an ESI source (RT; ionization voltage: 3.9 kV, Tube lens: 110 V, capillary voltage: 20 V, sheath gas, aux gas and sweep gas: off). Eluent A consisted of  $\text{H}_2\text{O}$  with 0.1% formic acid, eluent B consisted of 90% acetonitrile and 10%  $\text{H}_2\text{O}$  with 0.1% formic acid. All solvents were of LC/MS grade (Sigma Aldrich). Buffered CP samples (6  $\mu\text{g}$  per run, treated with inhibitor where appropriate) were brought to 30% (v/v) acetonitrile and separated on a C4 column (BioBasic-4, Thermo Scientific, 150 mm x 1 mm, 5  $\mu\text{m}$ ; flow: 0.050 mL/min) with a gradient from 30% to 60% B over 60 min preceded by a 15 min equilibration step at 30% B and followed by a washing step at 100% B for 5 min. The mass spectrometer was run in positive mode, collecting full scans at high resolution ( $R = 200,000$ ) from  $m/z$  500 to  $m/z$  2,000. Spectra containing data

on  $\beta 5$  subunits were selected and averaged using customized software (M. Gersch, S.A. Sieber, to be published elsewhere) and data were analyzed by Thermo Scientific Xtract<sup>[3]</sup> and Thermo Scientific Xcalibur software for deconvolution and quantification unless noted otherwise. Promass<sup>[4]</sup> (Enovatia, as implemented in Bioworks, with customized settings), MagTran<sup>[4]</sup> and Mann's Algorithm<sup>[5]</sup> (as implemented in MagTran) were used to confirm the deconvolution results. For details and parameter values, see Tables ST2-3 and Figures S4-5. Gaussian fits were carried out with OriginPro.

##### *Crystallization and structure elucidation*

Crystals of yCP were grown in hanging drop plates at 20 °C as previously described,<sup>[2,6]</sup> using a protein concentration of 40 mg/mL in Tris/HCl (20 mM, pH 7.5) and EDTA (1 mM). The drops contained 1  $\mu$ L of protein and 1  $\mu$ L of the reservoir solution consisting of 30 mM MgAc<sub>2</sub>, 100 mM morpholino-ethane-sulfonic acid (MES) (pH 7.2) and 10% (v/v) 2-methyl-2,4-pentanediol. Crystals appeared after two days and were then soaked with inhibitor in DMSO at final concentrations of 10 mM between 1 h and 6 h following complementation of the droplets with cryoprotecting buffer consisting of 30% (w/v) 2-methyl-2,4-pentanediol, 20 mM MgAc<sub>2</sub>, 100 mM MES (pH 6.9). Crystals were supercooled in a stream of liquid nitrogen gas at 100 K (Oxford Cryo Systems). Datasets of CP:inhibitor structures were collected up to 2.1 Å resolution using synchrotron radiation ( $\lambda = 1.0$  Å) at the X06SA-beamline (Swiss Light Source, Villigen, Switzerland, Table ST1). X-ray intensities were assessed with the program XDS<sup>[7]</sup> and data reduction was carried out using XSCALE<sup>[7]</sup>. Molecular replacement started with the coordinates of yCP (pdb entry code: 1RYP) and Translation/Libration/Screw (TLS) refinements were performed with REFMAC5 in the CCP4i suite<sup>[8]</sup>. Model building was carried out with the program package MAIN<sup>[9]</sup>.

#### **4.1.5 Supplementary cell culture methods**

##### *IC<sub>50</sub> determination with Proteasome-Glo™ chymotrypsin-like cell-based assay*

In vivo proteasome inhibition assays were performed with bioluminescence assays (Promega) in 96-well plates (Thermo Scientific). HeLa and THP-1 cells were plated at 5,000 cells per well and incubated with various inhibitor concentrations for 105 min with three repetitions each, thereby not surpassing a final concentration of 1% (w/v) of DMSO. The residual chymotrypsin-like activity was determined by the hydrolysis of the  $\beta 5$  specific substrate Suc-LLVY-aminoluciferin in the presence of luciferase using the Proteasome-Glo™ reagents according to the manufacturer's instructions. The resulting luminescence was detected with a PHERAstar Plus (BMG Labtech) plate-reading luminometer.

#### *LC<sub>50</sub> determination via AlamarBlue-based viability assay*

Viability of HeLa and THP-1 cells was monitored in dependency of different CP inhibitor concentrations using an AlamarBlue-based assay.<sup>[10]</sup> 5,000 HeLa cells were seeded in a 96-well plate for 48 h, to allow complete attachment of the cells, prior to inhibitor exposure. The same number of non-adherent THP-1 cells was seeded directly in the presence of inhibitor. All inhibitors were dissolved in DMSO and 0.1% DMSO was used as a control. After 48 h, HeLa cells were washed with PBS (137 mM NaCl, 2.7 mM KCl and 10 mM phosphate buffer) to remove dead cells and AlamarBlue (resazurin) was added in a 1:10 dilution to both cell lines for 2 h. Cell viability was monitored by measuring the reduction of resazurin to resorufin by metabolically active cells using fluorescence at 590 nm ( $\lambda_{\text{exc}} = 530$  nm) in a Wallac 1420 Victor<sup>2</sup>. HeLa cells were cultured in Dulbecco's Modified Eagle Medium (DMEM) supplemented with 10% FCS, 2 mM L-glutamine, 1 mM sodium pyruvate, and MEM non-essential amino acids. THP-1 cells were cultured in RPMI medium supplemented with 10% FCS and 2 mM L-glutamine. Cells were regularly tested for mycoplasma contamination and were identified to be negative.

#### **4.1.6 Supplementary chemical synthesis**

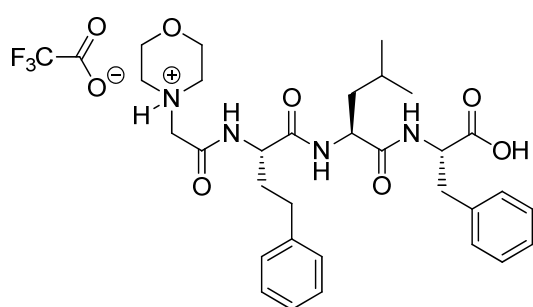
##### *General remarks*

All chemicals and reagents were purchased in quality reagent grade or higher from commercial sources (Johnson Matthey Plc. (Alfa Aesar), Sigma-Aldrich Co. LLC, Merck KGaA, Iris Biotech GmbH, Protein Technologies Inc.) and used as received. Anhydrous solvents were purchased from commercial sources (VWR International GmbH, Merck KGaA). Analytical thin-layer chromatography (TLC) was carried out on Merck silica gel 60 F<sub>254</sub> plates and compounds visualized by UV light absorption ( $\lambda = 254$  nm) or common TLC stains (ninhydrin; KMnO<sub>4</sub>). Flash column chromatography was performed on a Reveleris<sup>®</sup> X1 Flash Chromatography System (W. R. Grace & Co.) using pre packed GraceResolv<sup>™</sup> silica cartridges 4-80 g (W. R. Grace & Co.). <sup>1</sup>H- and <sup>13</sup>C-NMR spectra were recorded on a Bruker Avance I (360 MHz) NMR system or Bruker AV-500 (500 MHz) NMR spectrometer and referenced to the residual proton or carbon signal of the deuterated solvent.<sup>[11]</sup> Chemical shifts are reported in parts per million (ppm) and coupling constants (*J*) are given in hertz (Hz). High resolution mass spectra (HR-ESI-MS and HR-HPLC-ESI-MS) were recorded with a Dionex UltiMate 3000 HPLC system eluting on a Waters XBridge C18 column (3.5  $\mu$ m, 4.6 x 100 mm; flow = 1.1 mL/min; column temperature = 30 °C), coupled with a Thermo Scientific LTQ-FT Ultra mass spectrometer and an ESI source. The applied buffers consisted of a gradient mixture of 0.1% (v/v)

formic acid in H<sub>2</sub>O (buffer A) and 0.1% (v/v) formic acid in ACN:H<sub>2</sub>O 90:10 (v/v) (buffer B). ESI-MS and LC-ESI-MS mass spectra were recorded with a Dionex UltiMate 3000 HPLC system coupled with a Thermo LCQ fleet. Reversed-phase HPLC purification was accomplished with a system consisting of a Waters 1525 binary HPLC pump, X-Bridge™ Prep C18 column (5  $\mu$ m, 10 x 250 mm), Waters 2998 PDA detector and Waters Fraction Collector III (Waters Corp.). The applied buffers were H<sub>2</sub>O with 0.1% TFA (v/v) (buffer A) and ACN with 0.1% TFA (v/v) (buffer B). Lyophilization was performed on a Christ Alpha 2-4 LD plus.

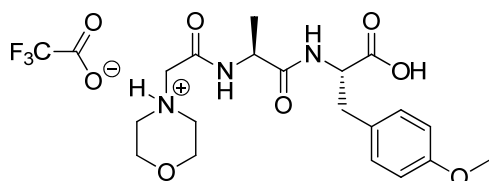
#### *General procedure for the synthesis of peptidic backbones*

Peptidic backbones were prepared via solid-phase peptide synthesis using Fmoc-protected amino acids and a PS3 Peptide Synthesizer (Protein Technologies, Inc.). Trityl-Cl resin (1.40 mmol Cl<sup>-</sup>/g loading) was used in a 0.2 mmol scale and Fmoc-protected amino acids (0.4 mmol, 2 eq.) were deprotected with 20% (v/v) piperidine in DMF. Activation of amino acids (0.4 mmol, 2 eq.) for coupling was performed using HCTU (0.4 mmol, 2 eq.) and 0.4 M DIPEA in DMF. Cleavage from the resin was performed with 25% TFA (v/v) in CH<sub>2</sub>Cl<sub>2</sub> following evaporation and treatment with Amberlyst A-21 to remove excess of TFA. The residual solution was lyophilized to yield the peptidic backbone as white powdery TFA-salt of the free acid. The backbones were used in the next coupling step without further purification.

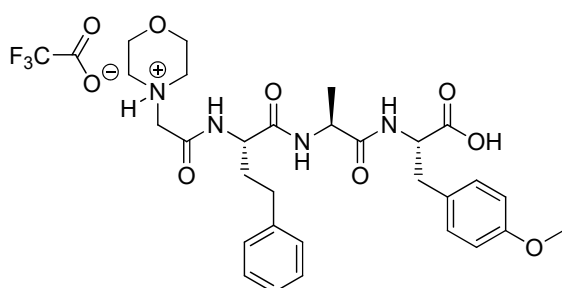


#### **MorphAc-hPhe-Leu-Phe-OH · TFA (4)**

**<sup>1</sup>H NMR** (500 MHz, DMSO-d<sub>6</sub>):  $\delta$  = 12.75 (s, 1H), 10.25 (s, 1H), 8.85 (s, 1H), 8.22 (d,  $J$  = 7.8 Hz, 1H), 8.16 (d,  $J$  = 8.4 Hz, 1H), 7.33 – 7.27 (m, 2H), 7.23 – 7.04 (m, 8H), 4.48 – 4.32 (m, 3H), 4.11 – 3.64 (m, 6H), 3.47 – 3.10 (m, 4H), 3.04 (dd,  $J$  = 14.0, 5.1 Hz, 1H), 2.89 (dd, 1H), 2.67 – 2.52 (m, 2H), 1.92 – 1.83 (m, 1H), 1.83 – 1.73 (m, 1H), 1.63 – 1.52 (m, 1H), 1.41 (t,  $J$  = 7.3 Hz, 2H), 0.85 (dd,  $J$  = 24.0, 6.6 Hz, 6H) ppm. **<sup>13</sup>C NMR** (126 MHz, DMSO-d<sub>6</sub>):  $\delta$  = 173.2, 172.3, 170.9, 141.8, 137.9, 129.4, 128.8, 128.7, 128.5, 126.8, 126.4, 63.6, 53.6, 53.0, 52.3, 51.2, 41.4, 36.9, 34.7, 31.9, 24.5, 23.5, 22.1 ppm. **MS** (ESI):  $m/z$ : calcd. for C<sub>31</sub>H<sub>43</sub>N<sub>4</sub>O<sub>6</sub> [ $M+H^+$ ] 567.32; found 567.21.

**MorphAc-Ala-Tyr(OMe)-OH · TFA (5)**

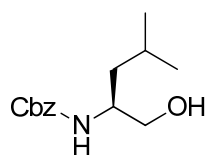
**$^1\text{H NMR}$**  (360 MHz, DMSO- $d_6$ ):  $\delta$  = 12.79 (s, 1H), 10.28 (s, 1H), 8.70 (s, 1H), 8.30 (d,  $J$  = 7.9 Hz, 1H), 7.15 (d,  $J$  = 8.5 Hz, 2H), 6.83 (d,  $J$  = 8.6 Hz, 2H), 4.47 – 4.28 (m, 2H), 3.81 (s, 6H), 3.71 (s, 3H), 3.18 (s, 4H), 3.05 – 2.77 (m, 2H), 1.22 (d,  $J$  = 7.1 Hz, 3H) ppm.  **$^{13}\text{C NMR}$**  (91 MHz, DMSO- $d_6$ ):  $\delta$  = 173.2, 172.0, 158.4, 130.6, 129.8, 114.1, 63.8, 55.4, 54.2, 52.4, 48.6, 36.2, 18.8 ppm. **MS** (ESI):  $m/z$ : calcd. for  $\text{C}_{19}\text{H}_{28}\text{N}_3\text{O}_6$  [ $M+\text{H}^+$ ] 394.20; found 394.16.

**MorphAc-hPhe-Ala-Tyr(OMe)-OH · TFA (6)**

**$^1\text{H NMR}$**  (500 MHz, DMSO- $d_6$ ):  $\delta$  = 12.77 (s, 1H), 10.26 (s, 1H), 8.88 (s, 1H), 8.24 (d,  $J$  = 7.5 Hz, 1H), 8.12 (d,  $J$  = 7.8 Hz, 1H), 7.32 – 7.10 (m, 7H), 6.81 – 6.75 (m, 2H), 4.46 – 4.28 (m, 3H), 4.11 – 3.68 (m, 6H), 3.66 (s, 3H), 3.47 – 3.10 (m, 4H), 2.96 (dd,  $J$  = 14.0, 5.2 Hz, 1H), 2.83 (dd,  $J$  = 14.0, 8.4 Hz, 1H), 2.64 – 2.52 (m, 2H), 1.97 – 1.86 (m, 1H), 1.86 – 1.74 (m, 1H), 1.20 (d,  $J$  = 7.1 Hz, 3H) ppm.  **$^{13}\text{C NMR}$**  (126 MHz, DMSO- $d_6$ ):  $\delta$  = 173.2, 172.5, 170.7, 158.3, 141.7, 130.6, 129.6, 128.8, 128.7, 126.4, 114.0, 63.6, 55.3, 54.1, 52.9, 52.3, 48.4, 36.2, 34.6, 31.8, 18.7 ppm. **MS** (ESI):  $m/z$ : calcd. for  $\text{C}_{29}\text{H}_{39}\text{N}_4\text{O}_7$  [ $M+\text{H}^+$ ] 555.28; found 555.22.

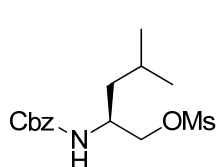
*Synthesis of sulfonyl fluoride headgroups*

The sulfonyl fluoride headgroups & precursors were previously described in literature.<sup>[12-14]</sup>

**Cbz-L-leucinol (7)**

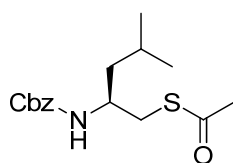
L-leucinol (5 g, 42.7 mmol) and  $\text{Na}_2\text{CO}_3$  (9.04 g, 85 mmol) were dissolved in a mixture of  $\text{H}_2\text{O}$  (40 mL) and dioxane (40 mL). The suspension was cooled to 0 °C and Cbz-Cl (9.14 mL, 64 mmol) was added dropwise. The reaction was stirred overnight at RT. After concentration under reduced pressure, the mixture was extracted with  $\text{CH}_2\text{Cl}_2$  (2 x 50 mL) and the combined organic layers were washed with 5% citric acid (30 mL), sat.  $\text{NaHCO}_3$  (30 mL) and brine (30 mL), dried over  $\text{Na}_2\text{SO}_4$  and filtered. Evaporation of the solvent and purification by flash column chromatography (PE  $\rightarrow$  20% EA/PE, v/v) yielded **7** (10.71 g, 42.6 mmol, 100%) as a viscous colorless oil.  **$^1\text{H NMR}$**  (360 MHz,  $\text{CDCl}_3$ ):  $\delta$  = 7.41 – 7.36 (m, 5H),

5.12 (s, 2H), 4.84 (br s, 1H), 3.88 – 3.75 (m, 1H), 3.75 – 3.66 (m, 1H), 3.63 – 3.49 (m, 1H), 1.85 (br s, 1H), 1.76 – 1.59 (m, 1H), 1.45 – 1.26 (m, 2H), 0.95 (d,  $J = 6.6$  Hz, 6H) ppm.  $^{13}\text{C}$  NMR (91 MHz,  $\text{CDCl}_3$ ):  $\delta = 156.8, 136.4, 128.5, 128.2, 128.1, 127.0, 66.9, 65.4, 51.5, 40.5, 24.8, 23.1, 22.2$  ppm. **MS** (ESI):  $m/z$ : calcd. for  $\text{C}_{14}\text{H}_{22}\text{NO}_3$  [ $M+\text{H}^+$ ] 252.16; found 251.83.



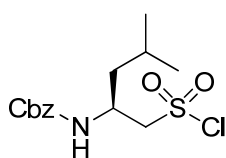
#### **Cbz-L-Leu-[CH<sub>2</sub>O]-Ms (8)**

$\text{NEt}_3$  (7.13 mL, 51.2 mmol) was added to a solution of **7** (10.71 g, 42.6 mmol) in  $\text{CH}_2\text{Cl}_2$  (142 mL). After cooling the mixture to  $0^\circ\text{C}$  Ms-Cl (3.99 mL, 51.2 mmol) was added dropwise and the reaction mixture was stirred at RT overnight. The solution was washed with 5% citric acid (40 mL),  $\text{H}_2\text{O}$  (40 mL) and brine (30 mL). The organic layer was dried over  $\text{Na}_2\text{SO}_4$  and filtered. Concentration under reduced pressure and purification by flash column chromatography (PE  $\rightarrow$  10% EA/PE, v/v) yielded **8** (11.87 g, 36 mmol, 84%) as a white solid.  $^1\text{H}$  NMR (360 MHz,  $\text{CDCl}_3$ ):  $\delta = 7.41 - 7.36$  (m, 5H), 5.13 (s, 2H), 4.82 (br s, 1H), 4.30 (dd,  $J = 10.1, 3.8$  Hz, 1H), 4.18 (dd,  $J = 10.2, 4.2$  Hz, 1H), 4.10 – 3.95 (m, 1H), 2.97 (s, 3H), 1.79 – 1.66 (m, 1H), 1.55 – 1.31 (m, 2H), 0.96 (d,  $J = 6.6$  Hz, 6H) ppm.  $^{13}\text{C}$  NMR (91 MHz,  $\text{CDCl}_3$ ):  $\delta = 155.8, 136.3, 128.7, 128.6, 128.2, 128.1, 71.3, 67.0, 48.6, 46.3, 37.3, 24.6, 22.9, 22.0$  ppm. **MS** (ESI):  $m/z$ : calcd. for  $\text{C}_{15}\text{H}_{24}\text{NO}_5\text{S}$  [ $M+\text{H}^+$ ] 330.14; found 329.78.

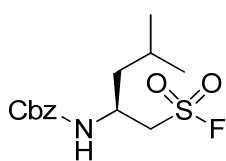


#### **Cbz-L-Leu-[CH<sub>2</sub>S]-Ac (9)**

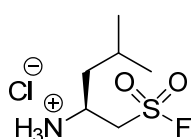
Under an argon atmosphere, thioacetic acid (1.22 mL, 17 mmol) was added to a suspension of  $\text{Cs}_2\text{CO}_3$  (2.88 g, 8.85 mmol) in DMF (68.1 mL). After stirring for 30 min at RT, mesylate **8** (4.48 g, 13.60 mmol) was added at once and the mixture was stirred in an aluminium foil-covered flask at  $50^\circ\text{C}$  overnight. After evaporation of the solvent the residue was resolved in EA (50 mL) and washed with 5%  $\text{NaHCO}_3$  (30 mL) and  $\text{H}_2\text{O}$  (15 mL). The organic layer was separated, dried over  $\text{Na}_2\text{SO}_4$ , filtered and evaporated. After purification via flash column chromatography (PE  $\rightarrow$  10% EA/PE, v/v) **9** was obtained as brown oil that crystallized overnight (2.88 g, 9.31 mmol, 68%).  $^1\text{H}$  NMR (500 MHz,  $\text{CDCl}_3$ ):  $\delta = 7.40 - 7.31$  (m, 5H), 5.14 (d,  $J = 12.3$  Hz, 1H), 5.08 (d,  $J = 12.3$  Hz, 1H), 4.68 (d,  $J = 9.0$  Hz, 1H), 3.99 – 3.87 (m, 1H), 3.13 (dd,  $J = 13.9, 4.7$  Hz, 1H), 3.01 (dd,  $J = 13.9, 7.2$  Hz, 1H), 2.32 (s, 3H), 1.73 - 1.66 (m, 1H), 1.45 – 1.29 (m, 2H), 0.93 (d,  $J = 6.7$  Hz, 6H) ppm.  $^{13}\text{C}$  NMR (126 MHz,  $\text{CDCl}_3$ ):  $\delta = 195.7, 156.0, 136.6, 128.5, 128.1, 128.1, 66.7, 49.3, 43.6, 34.3, 30.6, 24.9, 23.0, 22.2$  ppm. **MS** (ESI):  $m/z$ : calcd. for  $\text{C}_{16}\text{H}_{24}\text{NO}_3\text{S}$  [ $M+\text{H}^+$ ] 310.15; found 309.73.

**Cbz-L-Leu-[CH<sub>2</sub>SO<sub>2</sub>]-Cl (10)**

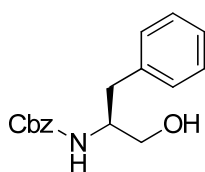
NCS (394 mg, 2.95 mmol) was dissolved in a cooled (0 °C - 10 °C) mixture of HCl (2 M, 197  $\mu$ L, 0.394 mmol) and ACN (985  $\mu$ L) and stirred for 15 min. The thioacetate **9** (228.5 mg, 0.738 mmol) was dissolved in ACN (197  $\mu$ L) and added to the mixture. After stirring for 15 min at RT the solution was diluted with isopropyl ether (4 mL), washed with brine (3 x 2 mL), dried over MgSO<sub>4</sub>, filtered and concentrated to yield **10** (236 mg, 0.707 mmol, 96%(crude product)) as a colorless oil which was used without further purification in the next step.

**Cbz-L-Leu-[CH<sub>2</sub>SO<sub>2</sub>]-F (11)**

KF (82 mg, 1.41 mmol) and 18-c-6 ether (9.34 mg, 0.035 mmol) were added to a solution of sulfonyl chloride **10** (236 mg, 0.707 mmol) in ACN (3.5 mL) under an argon atmosphere. The reaction mixture was stirred at RT overnight. After evaporation of the solvent the residue was purified by flash column chromatography (PE  $\rightarrow$  10% EA/PE, v/v) yielding **11** (174 mg, 0.548 mmol, 78%) as colorless oil which crystallized overnight. <sup>1</sup>H NMR (360 MHz, , CDCl<sub>3</sub>):  $\delta$  = 7.45 – 7.26 (m, 5H), 5.13 (s, 3H), 4.29 – 4.15 (m, 1H), 3.80 – 3.56 (m, 2H), 1.80 – 1.61 (m, 2H), 1.60 - 1.43 (m, 1H), 0.96 (d,  $J$  = 4.7 Hz, 6H) ppm. <sup>13</sup>C NMR (91 MHz, CDCl<sub>3</sub>):  $\delta$  = 155.5, 136.0, 128.7, 128.6, 128.3, 128.0, 67.1, 54.8, 54.7, 45.9, 42.0, 24.8, 22.8, 21.6 ppm. MS (ESI):  $m/z$ : calcd. for C<sub>14</sub>H<sub>21</sub>FNO<sub>4</sub>S [ $M+H^+$ ] 318.12; found 317.71.

**L-Leu-[CH<sub>2</sub>SO<sub>2</sub>]-F · HCl (12)**

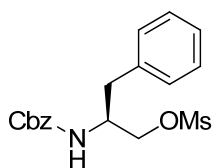
HBr in acetic acid (33%, 2.25 mL, 13.70 mmol) was added dropwise to a solution of sulfonyl fluoride **11** (174 mg, 0.548 mmol) in CH<sub>2</sub>Cl<sub>2</sub> and stirred at RT for 45 min. After concentration in vacuo the residue was dissolved in H<sub>2</sub>O (3.9 mL) and DOWEX 1 x 8 (Cl-form, 300 mg) were pured into the solution. After stirring for 15 min the solution was filtered and the filter residue was washed with H<sub>2</sub>O. After lyophilization **12** (118 mg, 0.537 mmol, 98%(crude product)) was obtained as a white powder which was used without further purification in the next step.

**Cbz-L-phenylalaninol (13)**

L-phenylalaninol (5 g, 33.1 mmol) and Na<sub>2</sub>CO<sub>3</sub> (7.01 g, 66.1 mmol) were dissolved in a mixture of H<sub>2</sub>O (31 mL) and dioxane (31 mL). The suspension was cooled to 0 °C and Cbz-Cl (7.08 mL, 49.6 mmol) was added dropwise. The reaction was stirred overnight at RT. After concentration under reduced pressure, the mixture was extracted with CH<sub>2</sub>Cl<sub>2</sub> (2 x 40 mL) and the combined

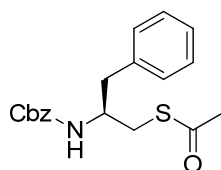
#### 4. Ligand-induced active site crosslinking of subunit $\beta 5i$

organic layers were washed with 5% citric acid (30 mL), sat.  $\text{NaHCO}_3$  (20 mL) and brine (20 mL), dried over  $\text{Na}_2\text{SO}_4$  and filtered. Evaporation of the solvent and purification by flash column chromatography (PE  $\rightarrow$  60% EA/PE, v/v) yielded **13** (8.54 g, 29.9 mmol, 91%) as a white solid.  $^1\text{H NMR}$  (360 MHz,  $\text{CDCl}_3$ ):  $\delta$  = 7.42 – 7.28 (m, 7H), 7.27 – 7.18 (m, 3H), 5.10 (s, 2H), 5.01 (s, 1H), 4.05 – 3.90 (m, 1H), 3.75 – 3.55 (m, 2H), 2.89 (d,  $J$  = 7.2 Hz, 2H) ppm.  $^{13}\text{C NMR}$  (91 MHz,  $\text{CDCl}_3$ ):  $\delta$  = 137.5, 136.3, 129.3, 128.6, 128.5, 128.2, 128.1, 126.7, 66.9, 64.1, 54.1, 37.4 ppm. **MS** (ESI):  $m/z$ : calcd. for  $\text{C}_{17}\text{H}_{20}\text{NO}_3$  [ $M+\text{H}^+$ ] 286.14; found 285.85.



#### **Cbz-L-Phe-[CH<sub>2</sub>O]-Ms (14)**

$\text{NEt}_3$  (5.01 mL, 35.9 mmol) was added to a solution of **13** (8.54 g, 29.9 mmol) in  $\text{CH}_2\text{Cl}_2$  (100 mL). After cooling to 0 °C  $\text{Ms-Cl}$  (2.8 mL, 35.9 mmol) was added dropwise and the reaction mixture was stirred at RT overnight. After the addition of  $\text{CH}_2\text{Cl}_2$  (25 mL) the organic layer was washed with  $\text{H}_2\text{O}$  (2 x 20 mL) and brine (2 x 20 mL). The organic layer was separated, dried over  $\text{Na}_2\text{SO}_4$  and filtered. Concentration under reduced pressure and purification by flash column chromatography (PE  $\rightarrow$  10% EA/PE, v/v) yielded **14** (10.22 g, 28.1 mmol, 94%) as a white solid.  $^1\text{H NMR}$  (360 MHz,  $\text{CDCl}_3$ ):  $\delta$  = 7.43 – 7.28 (m, 8H), 7.27 – 7.20 (m, 2H), 5.11 (s, 2H), 5.02 (d,  $J$  = 8.1 Hz, 1H), 4.33 – 4.10 (m, 3H), 2.98 (s, 3H), 2.96 – 2.85 (m, 2H) ppm.  $^{13}\text{C NMR}$  (91 MHz,  $\text{CDCl}_3$ ):  $\delta$  = 155.6, 136.3, 136.2, 129.2, 128.8, 128.6, 128.3, 128.1, 127.1, 69.5, 67.0, 51.4, 37.3, 37.1 ppm. **MS** (ESI):  $m/z$ : calcd. for  $\text{C}_{18}\text{H}_{22}\text{NO}_5\text{S}$  [ $M+\text{H}^+$ ] 364.12; found 363.75.

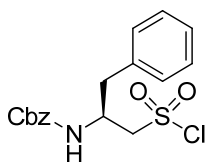


#### **Cbz-L-Phe-[CH<sub>2</sub>S]-Ac (15)**

Under an argon atmosphere, thioacetic acid (0.988 mL, 13.76 mmol) was added to a suspension of  $\text{Cs}_2\text{CO}_3$  (2.33 g, 7.15 mmol) in DMF (55 mL). After stirring for 30 min at RT mesylate **14** (4 g, 11 mmol) was added at once and the mixture was stirred in an aluminium foil-covered flask at 50 °C overnight. After evaporation of the solvent the residue was resolved in EA (50 mL) and washed with 5% aqueous  $\text{NaHCO}_3$  (30 mL) and  $\text{H}_2\text{O}$  (20 mL). The organic layer was separated, dried over  $\text{Na}_2\text{SO}_4$ , filtered and evaporated. After purification by flash column chromatography (PE  $\rightarrow$  10% EA/PE, v/v) **15** was obtained as a brown solid (2.93 g, 8.53 mmol, 78%).  $^1\text{H NMR}$  (360 MHz,  $\text{CDCl}_3$ ):  $\delta$  = 7.43 – 7.16 (m, 10H), 5.09 (s, 2H), 4.90 (d,  $J$  = 8.7 Hz, 1H), 4.13 – 4.03 (m, 1H), 3.11 (dd,  $J$  = 14.0, 4.6 Hz, 1H), 3.05 – 2.89 (m, 2H), 2.82 (dd,  $J$  = 13.6, 7.1 Hz, 1H), 2.35 (s, 3H) ppm.  $^{13}\text{C NMR}$  (91 MHz,  $\text{CDCl}_3$ ):  $\delta$  = 195.9,

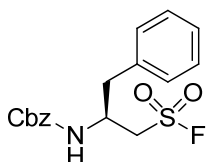


155.8, 137.0, 136.5, 129.3, 128.6, 128.5, 128.1, 128.0, 126.8, 66.6, 52.6, 40.4, 32.7, 30.6 ppm. **MS** (ESI):  $m/z$ : calcd. for  $C_{19}H_{22}NO_3S$  [ $M+H^+$ ] 344.13; found 343.75.



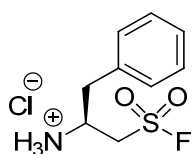
#### **Cbz-L-Phe-[CH<sub>2</sub>SO<sub>2</sub>]-Cl (16)**

NCS (467 mg, 3.49 mmol) was dissolved in a cooled (10 °C) 0 °C mixture of HCl (2 M, 233  $\mu$ L, 0.466 mmol) and ACN (1.39 mL) and stirred for 15 min. The thioacetate ester **15** (300 mg, 0.874 mmol) was added at once to the mixture. After stirring for 15 min at RT the reaction mixture was diluted with  $CH_2Cl_2$  (4 mL), washed with brine (3 x 2 mL), dried over  $MgSO_4$  and concentrated to give **16** (341 mg, 0.926 mmol, 106% (crude product)) as a light yellow solid which was used without further purification in the next step.



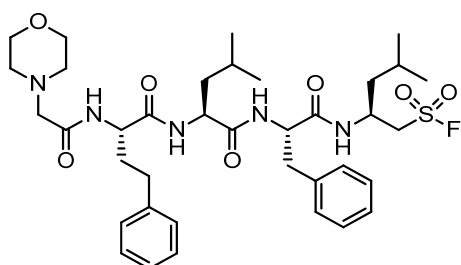
#### **Cbz-L-Phe-[CH<sub>2</sub>SO<sub>2</sub>]-F (17)**

KF (108 mg, 1.854 mmol) and 18-c-6 ether (12.25 mg, 0.046 mmol) were added to a solution of sulfonyl chloride **16** (341 mg, 0.926 mmol) in ACN (4.64 mL) under an argon atmosphere. The reaction mixture was stirred at RT overnight. After evaporation of the solvent the residue was purified by flash column chromatography (PE  $\rightarrow$  35% EA/PE, v/v) yielding **17** (207 mg, 0.589 mmol, 63%) as a white solid. **<sup>1</sup>H NMR** (360 MHz,  $DMSO-d_6$ ):  $\delta$  = 7.61 (d,  $J$  = 8.7 Hz, 1H), 7.36 – 7.17 (m, 10H), 4.96 (s, 2H), 4.33 – 4.12 (m, 2H), 4.05 – 3.92 (m, 1H), 2.93 (dd,  $J$  = 13.6, 4.8 Hz, 1H), 2.81 (dd,  $J$  = 13.6, 9.6 Hz, 1H) ppm. **<sup>13</sup>C NMR** (91 MHz,  $DMSO-d_6$ ):  $\delta$  = 155.7, 137.7, 137.5, 129.7, 128.7, 128.1, 127.8, 127.0, 65.6, 54.5, 54.4, 48.8 ppm. **MS** (ESI):  $m/z$ : calcd. for  $C_{17}H_{19}FNO_4S$  [ $M+H^+$ ] 352.10; found 351.81.

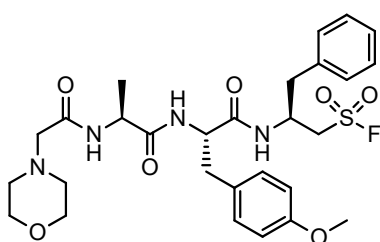


#### **L-Phe-[CH<sub>2</sub>SO<sub>2</sub>]-F · HCl (18)**

HBr in acetic acid (33%, 2.34 mL, 14.23 mmol) was added dropwise to a solution of sulfonyl fluoride **17** (200 mg, 0.569 mmol) in  $CH_2Cl_2$ . After stirring at RT for 45 min and subsequent concentration in vacuo the residue was dissolved in  $H_2O$  (4 mL) and DOWEX (400 mg) were poured into the solution. After stirring for 15 min the solution was filtered and the filter residue was washed with  $H_2O$ . After lyophilization **18** (132.8 mg, 0.523 mmol, 92% (crude product)) was obtained as a white powder which was used without further purification in the next step.

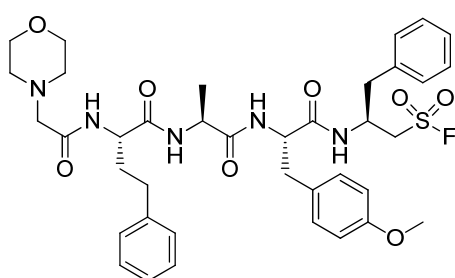
*Final coupling of peptidic backbones and sulfonyl fluoride headgroups***MorphAc-hPhe-Leu-Phe-Leu- $\psi$ -[CH<sub>2</sub>SO<sub>2</sub>]-F (1)**

HATU (70.5 mg, 0.185 mmol) was added to a cooled (0 °C) solution of peptidic backbone **4** (126 mg, 0.185 mmol) in CH<sub>2</sub>Cl<sub>2</sub> (0.99 mL) and stirred for 20 min, under an argon atmosphere, prior adding sulfonyl fluoride headgroup **12** (37.0 mg, 0.168 mmol). The reaction mixture was stirred at 0 °C for 30 min. Afterwards, DIPEA (85  $\mu$ L, 0.488 mmol) was added dropwise and the reaction was allowed to reach RT and was stirred overnight. After evaporation of the solvent the residue was dissolved in DMF (0.25 mL). Purification by RP-HPLC ( $t_R$  = 24 min, linear gradient 20  $\rightarrow$  100% ACN/H<sub>2</sub>O + 0.1% TFA in 120 min), treatment with Amberlyst A-21 and lyophilization yielded **1** (49.8 mg, 0.068 mmol, 40%) as white powder. **<sup>1</sup>H NMR** (500 MHz, DMSO-*d*<sub>6</sub>):  $\delta$  = 8.23 (d,  $J$  = 8.4 Hz, 1H), 8.13 (d,  $J$  = 8.8 Hz, 1H), 8.05 (d,  $J$  = 8.2 Hz, 1H), 7.30 – 7.06 (m, 10H), 4.42 (dd,  $J$  = 9.5, 5.0 Hz, 1H), 4.38 – 4.27 (m, 3H), 4.09 – 4.02 (m, 1H), 3.74 (dd,  $J$  = 14.6, 8.4 Hz, 1H), 3.65 – 3.55 (m, 4H), 3.02 – 2.88 (m, 3H), 2.79 (dd,  $J$  = 14.2, 9.6 Hz, 1H), 2.46 – 2.41 (m, 4H), 1.94 – 1.73 (m, 2H), 1.57 - 1.41 (m, 3H), 1.39 – 1.27 (m, 3H), 0.88 – 0.76 (m, 12H) ppm. **<sup>13</sup>C NMR** (126 MHz, DMSO-*d*<sub>6</sub>):  $\delta$  = 172.1, 171.0, 170.8, 141.8, 138.1, 129.4, 128.8, 128.7, 128.4, 126.6, 126.4, 66.6, 61.8, 54.8, 54.7, 54.1, 53.6, 53.5, 53.0, 51.3, 43.1, 42.8, 41.4, 37.5, 34.7, 31.9, 24.5, 24.1, 23.7, 23.5, 22.2, 21.6 ppm. RP-HPLC:  $t_R$  = 12 min (linear gradient 0  $\rightarrow$  90% in 25 min). **HRMS** (ESI):  $m/z$ : calcd. for C<sub>37</sub>H<sub>55</sub>FN<sub>5</sub>O<sub>7</sub>S [ $M+H^+$ ] 732.3801; found 732.3803.

**MorphAc-Ala-Tyr(OMe)-Phe- $\psi$ -[CH<sub>2</sub>SO<sub>2</sub>]-F (2)**

HATU (82 mg, 0.217 mmol) was added to a cooled (0 °C) solution of acid **5** (110 mg, 0.217 mmol) in CH<sub>2</sub>Cl<sub>2</sub> (1.16 mL) stirred for 20 min, under an argon atmosphere, prior adding sulfonyl fluoride headgroup **18** (50 mg, 0.197 mmol). The reaction mixture was stirred at 0 °C for 30 min. Afterwards, DIPEA (100  $\mu$ L, 0.571 mmol) was added dropwise and the reaction was allowed to reach RT and was stirred overnight. After evaporation of the solvent, the residue was dissolved in DMF (0.25 mL). Purification by RP-HPLC ( $t_R$  = 40 min, linear gradient 10  $\rightarrow$  100% ACN/H<sub>2</sub>O + 0.1% TFA in 100 min), treatment with Amberlyst A-21 and lyophilization yielded **2** (48.4 mg, 0.082 mmol, 41%) as white powder. **<sup>1</sup>H NMR** (500 MHz, DMSO-*d*<sub>6</sub>):  $\delta$  = 8.39 (d,  $J$  = 8.5 Hz, 1H), 8.12 (d,  $J$  = 8.5 Hz, 1H), 7.76 (d,

$J = 7.9$  Hz, 1H), 7.32 – 7.17 (m, 5H), 7.08 (d,  $J = 8.6$  Hz, 2H), 6.77 (d,  $J = 8.6$  Hz, 2H), 4.49 – 4.40 (m, 1H), 4.37 – 4.30 (m, 1H), 4.27 – 4.19 (m, 1H), 4.15 – 4.07 (m, 1H), 3.89 (dd,  $J = 14.4, 9.6$  Hz, 2H), 3.68 (s, 3H), 2.96 – 2.75 (m, 4H), 2.67 – 2.56 (m, 1H), 2.42 – 2.29 (m, 4H), 1.11 (d,  $J = 6.9$  Hz, 3H) ppm.  $^{13}\text{C}$  NMR (126 MHz, DMSO- $d_6$ ):  $\delta = 172.6, 172.1, 171.2, 158.2, 137.3, 130.6, 129.9, 129.7, 128.8, 127.1, 113.8, 66.5, 61.5, 55.3, 54.7, 53.9, 53.8, 53.5, 47.9, 46.6, 36.9, 19.2$  ppm. RP-HPLC:  $t_R = 7.6$  min (linear gradient 0  $\rightarrow$  90% in 25 min). HRMS (ESI):  $m/z$ : calcd. for  $\text{C}_{28}\text{H}_{38}\text{FN}_4\text{O}_7\text{S}$  [ $M+\text{H}^+$ ] 593.2440; found 593.2446.



**MorphAc-hPhe-Ala-Tyr(OMe)-Phe- $\psi$ -[CH<sub>2</sub>SO<sub>2</sub>]-F  
(3)**

HATU (41.5 mg, 0.109 mmol) was added to a cooled (0 °C) solution of peptidic backbone **4** (73 mg, 0.109 mmol) in  $\text{CH}_2\text{Cl}_2$  (0.58 mL) and stirred for 20 min, under an argon atmosphere, prior adding sulfonyl fluoride headgroup **12** (25.2 mg, 0.099 mmol). The reaction mixture was stirred at 0 °C for 30 min. Afterwards, DIPEA (50  $\mu\text{L}$ , 0.288 mmol) was added dropwise and the reaction was allowed to reach RT and was stirred overnight. After evaporation of the solvent the residue was dissolved in DMF (0.25 mL). Purification by RP-HPLC ( $t_R = 34$  min, linear gradient 20  $\rightarrow$  100% ACN/ $\text{H}_2\text{O}$  + 0.1% TFA in 120 min), treatment with Amberlyst A-21 and lyophilization yielded **1** (18.7 mg, 0.025 mmol, 25%) as white powder.  $^1\text{H}$  NMR (500 MHz, DMSO- $d_6$ ):  $\delta = 8.33$  (d,  $J = 8.5$  Hz, 1H), 8.13 (d,  $J = 6.8$  Hz, 1H), 8.00 (d,  $J = 8.3$  Hz, 1H), 7.26 – 7.14 (m, 10H), 7.08 (d,  $J = 8.6$  Hz, 2H), 6.73 (d,  $J = 8.7$  Hz, 2H), 4.48 – 4.38 (m, 1H), 4.38 – 4.18 (m, 3H), 4.13 (ddd,  $J = 14.8, 7.2, 3.5$  Hz, 1H), 3.85 (dd,  $J = 14.9, 9.1$  Hz, 1H), 3.63 (s, 3H), 3.62 – 3.56 (m, 4H), 3.00 – 2.75 (m, 4H), 2.45 – 2.39 (m, 4H), 1.95 – 1.76 (m, 2H), 1.13 (d,  $J = 7.1$  Hz, 3H) ppm.  $^{13}\text{C}$  NMR (126 MHz, DMSO- $d_6$ ):  $\delta = 172.2, 171.2, 170.7, 158.2, 141.7, 137.3, 130.5, 130.0, 129.7, 128.8, 128.7, 127.0, 126.3, 113.8, 66.6, 61.6, 55.3, 54.6, 54.2, 53.8, 53.7, 53.5, 52.9, 48.5, 46.6, 37.0, 34.6, 31.8, 18.7$  ppm. RP-HPLC:  $t_R = 10.5$  min (linear gradient 0  $\rightarrow$  90% in 25 min). HRMS (ESI):  $m/z$ : calcd. for  $\text{C}_{38}\text{H}_{49}\text{FN}_5\text{O}_8\text{S}$  [ $M+\text{H}^+$ ] 754.3280; found 754.3280.

#### 4.1.7 Supplementary references

- [1] A. J. Brouwer, A. Jonker, P. Werkhoven, E. Kuo, N. Li, N. Gallastegui, J. Kemmink, B. I. Florea, M. Groll, H. S. Overkleeft, et al., *J. Med. Chem.* **2012**, *55*, 10995-11003.
- [2] M. Groll, L. Ditzel, J. Löwe, D. Stock, M. Bochtler, H. Bartunik, R. Huber, *Nature* **1997**, *386*, 463–471.
- [3] M. W. Senko, S. C. Beu, F. W. McLafferty, *J. Am. Soc. Mass Spectrom.* **1995**, *6*, 52–56.
- [4] Z. Zhang, a G. Marshall, *J. Am. Soc. Mass Spectrom.* **1998**, *9*, 225–233.
- [5] M. Mann, C. K. Meng, J. B. Fenn, *Anal. Chem.* **1989**, *61*, 1702–1708.
- [6] M. Groll, R. Huber, *Methods Enzymol.* **2005**, *398*, 329–336.
- [7] W. Kabsch, *Acta Crystallogr. D. Biol. Crystallogr.* **2010**, *66*, 125–132.
- [8] E. Potterton, P. Briggs, M. Turkenburg, E. Dodson, *Acta Crystallogr. D. Biol. Crystallogr.* **2003**, *59*, 1131–1137.
- [9] D. Turk, *Acta Crystallogr. D. Biol. Crystallogr.* **2013**, *69*, 1342–1357.
- [10] M. L. Stein, H. Cui, P. Beck, C. Dubiella, C. Voss, A. Krüger, M. Groll, *Angew. Chem. Int. Ed.* **2014**, *53*, 1679–1683; *Angew. Chem.* **2014**, *126*, 1705-1709.
- [11] H. E. Gottlieb, V. Kotlyar, A. Nudelman, *J. Org. Chem.* **1997**, *62*, 7512–7515.
- [12] A. J. Brouwer, T. Ceylan, T. Van Der Linden, R. M. J. Liskamp, *Tetrahedron Lett.* **2009**, *50*, 3391–3393.
- [13] A. J. Brouwer, T. Ceylan, A. M. Jonker, T. van der Linden, R. M. J. Liskamp, *Bioorg. Med. Chem.* **2011**, *19*, 2397–2406.
- [14] M. FanHua, C. Ning, X. JiaXi, *Sci. China Chem.* **2012**, *55*, 2548–2553.

## 5 20S Proteasome inhibitors with fluorescent feedback

This chapter contains unpublished research and results which were partially published in a patent application: “Proteasome inhibitor comprising a signal-emitting moiety” by Christian Dubiella & Michael Groll, European Patent Application, **2015**, EP15182683.1 - 1453.

### 5.1 Introduction

A plethora of proteolytic mechanisms have been discovered. They all follow a common principle of catalysis: direct or indirect increase of the nucleophilicity of a water molecule for the hydrolysis of peptide bonds. In particular, the cCP and iCP present the major intracellular proteolytic machineries which exploit the basicity of an N-terminal threonine (Thr1) at their catalytically active subunits.<sup>[1]</sup> In contrast to moderately nucleophilic water ( $pK_a = 15$ ),<sup>[2]</sup> the alkoxide of Thr1 as active site nucleophile ( $pK_a \approx 9$ )<sup>[3]</sup> readily reacts with electrophilic warheads. However, the generally high reactivity of these pharmacophores such as borates, epoxyketones, vinyl sulfones, lactones and Michael systems cannot be adjusted to match the individual basicity of Thr1.<sup>[4]</sup> In consequence, certain amounts of inhibitor are sacrificed to hydrolysis and off-target activity. Recently, peptido sulfonyl fluorides were discovered as potent and selective inhibitors of the active subunits  $\beta 5c$  and  $\beta 5i$ .<sup>[5,6]</sup> For the first time, this class of CP inhibitors employs a pharmacophore whose reactivity depends on the leaving group (LG) ability. This offers the possibility to tune its reactivity by exchanging the fluoride LG with deactivated phenols or fluorogenic LGs. In general, phenyl sulfonic esters have a reduced reactivity compared to sulfonyl halides, but can still act as electrophiles depending on the nature of the deactivating electron-withdrawing groups on the LG.<sup>[7,8]</sup> In fact, pentafluorophenol (PFP) esters emerged as substitutes for acid halides and succinimidyl esters as activated esters in conjugation reactions due to their high water stability and long shelf life.<sup>[9,10]</sup> Although the LG ability is based on reaction rates,<sup>[11]</sup> it can be roughly correlated with the  $pK_a$  value of its conjugated acid. In particular, the use of LGs that are easily detectable are of interest. They allow a direct quantification of active CPs because their release is an integral part of the inhibitory mechanism.<sup>[5]</sup> This is in contrast to currently existing activity-based probes and antibodies assays (ProCISE)<sup>[12]</sup> which only permit a rough estimation of CP concentrations in-gel or require many working steps for an accurate quantification.<sup>[13-15]</sup>

## 5.2 Results and discussion

The initial aim of this project was to identify the  $pK_a$  range of the LG which enables substantial cCP inhibition. Therefore, a sulfonyl chloride precursor of L-leucine was derivatized with phenol ( $pK_a = 9.9$ ),<sup>[16]</sup> 2,4,6-trifluorophenol (TFP;  $pK_a \approx 7.6$ ) and pentafluorophenol (PFP;  $pK_a = 5.5$ ).<sup>[16]</sup> The phenyl sulfonic ester precursors were coupled via HATU-mediated amide coupling to a carfilzomib peptide backbone which was prepared by solid phase peptide synthesis using the Fmoc strategy. This convergent synthesis strategy allowed the facile preparation of the peptide sulfonate esters (PSE) **1**, **2** and **3** (Figure 5.1).

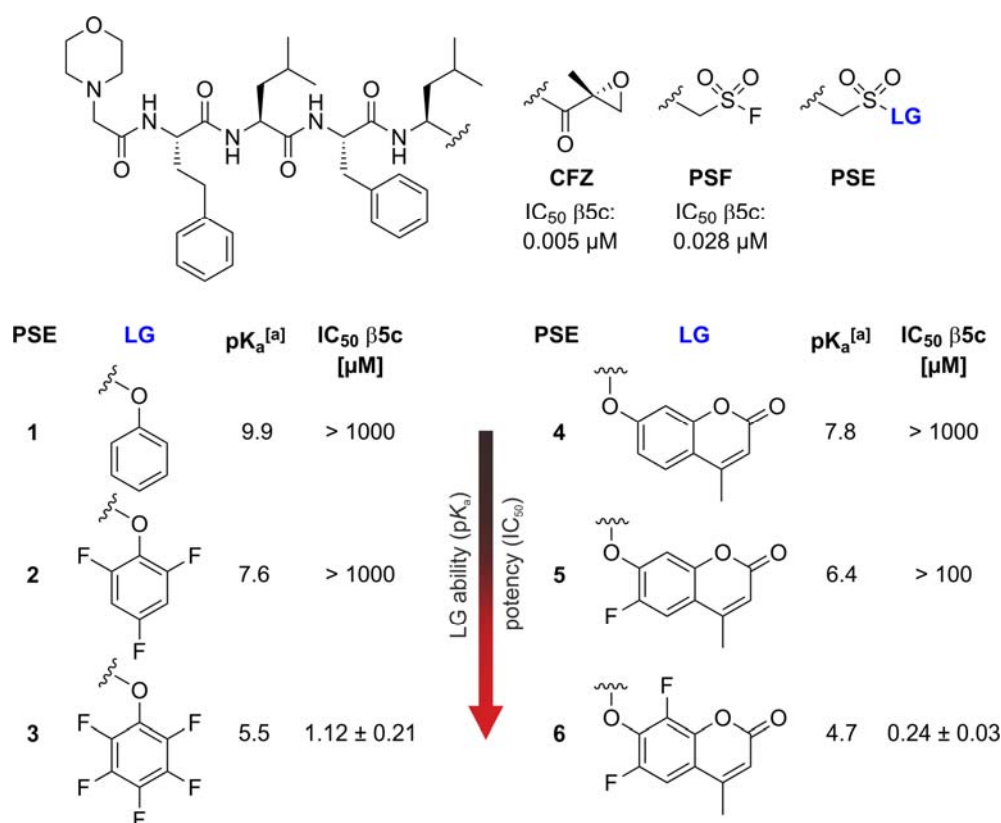


**Figure 5.1** Carfilzomib (CFZ) and its peptidic sulfonyl fluoride (PSF) as well as sulfonic ester (PSE) counterparts with their corresponding leaving groups (LG) and  $pK_a$  values. Their  $IC_{50}$  values were determined on purified human cCP in fluorogenic and luminogenic substrate assays. [a]: the  $pK_a$  values of the conjugate acids of the LG are given.<sup>[16,17]</sup>

To evaluate the potency of the PSEs against the ChTL activity of subunit  $\beta 5c$ , the  $IC_{50}$  values on purified human cCP were determined using a fluorogenic 7-amino-4-methylcoumarin (AMC) substrate assay. Indeed, **3** substantially inhibited subunit  $\beta 5c$  ( $IC_{50} = 1.12 \mu M$ , Figure 5.1), however with 40-fold decreased potency compared to its sulfonyl fluoride counterpart ( $IC_{50} = 0.028 \mu M$ ). In contrast, the less fluorinated PSE **2** was

at least 1000-fold less potent than **3** and had hardly no effects on  $\beta$ 5c-activity ( $IC_{50} > 1$  mM). Notably, the non-fluorinated PSE **1** did not have any effect on the ChTL activity ( $IC_{50} > 1$  mM). To exclude the possibility of reversible binding of the PSE **3** to the active site, yCP crystals were soaked with PSE **3** for X-ray crystallographic analysis. Subsequent structure elucidation revealed an irreversible crosslink in the  $\beta$ 5 subunit, analogous to the PSFs.<sup>[5]</sup> This mode of action requires PFP to be released as a LG, thereby excluding enhanced reversible binding of **3** due to protein interactions of the perfluorinated phenol with the primed site as observed with  $\alpha$ -ketoamide CP inhibitors.<sup>[18]</sup>

Next, the  $\beta$ 5c binding affinity was improved by employing a highly deactivated fluorogenic LG with a  $pK_a$  value ranging from 4 to 6. Based on the limited space at the proteasomal active site, 6,8-difluoro-4-methylumbelliferone (DiFMU;  $pK_a = 4.7$ )<sup>[17]</sup> was chosen as a small reporter LG with excellent photophysical properties including a high quantum yield ( $\Phi_F = 0.89$ ) and high resistance to photobleaching.<sup>[17]</sup> Furthermore, DiFMU bound to sulfonic ester groups is non-fluorescent and is widely used in substrate assays for several enzyme classes.<sup>[19-21]</sup> In addition, the less fluorinated PSE **4** and **5**, with 4-methylumbelliferone (MU;  $pK_a = 7.8$ )<sup>[17]</sup> and 6-fluoro-4-methylumbelliferone (FMU;  $pK_a = 6.4$ )<sup>[17]</sup> respectively, were prepared as controls (Figure 5.1). Their potency against  $\beta$ 5c of purified human cCP was evaluated by determining their  $IC_{50}$  values in luminogenic aminoluciferin substrate assays which are orthogonal to the released MU fluorophores (Figure 5.2).

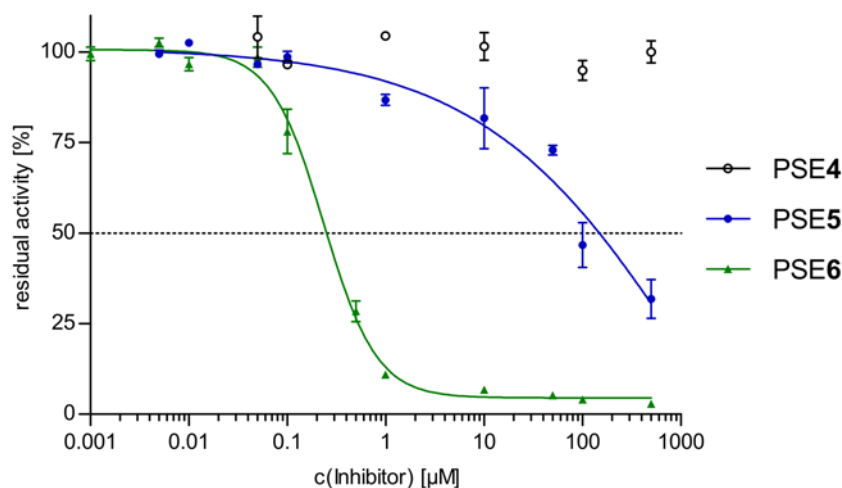


**Figure 5.2** In vitro  $IC_{50}$  assays against the ChTL activity of purified human cCP after 1 h incubation with various concentrations of PSE **4**, **5** and **6** using the luminogenic Suc-LLVY-aminoluciferin substrate assay. Data of three repetitions were normalized to DMSO-treated controls and are presented as relative activity with standard deviation.

PSE **6** containing DiFMU ( $IC_{50} = 0.236$   $\mu$ M, Figure 1, Figure S2) was over 400-fold more active than the mono-fluorinated PSE **5** ( $IC_{50} > 100$   $\mu$ M) and non-fluorinated **4**

## 5. 20S proteasome inhibitors with fluorescent feedback

( $IC_{50} > 1000 \mu\text{M}$ ), confirming once again that the PSEs require LGs with a  $pK_a < 6$  for inhibition in the nanomolar range. Based on the hypothesis that each of the released fluorophores correlates with a blocked active site, it was investigated if the fluorescence signal was proportional to the amount of CPs inhibited (Figure 5.3). This would allow a quantification of active CP, provided that non-stoichiometric hydrolysis is negligible, which is in contrast to fluorogenic substrates that are constantly turned over by the CP. In consequence, common substrate assays are only useful to determine the mere presence of proteolytic activity rather than the total quantity of CP in the sample.

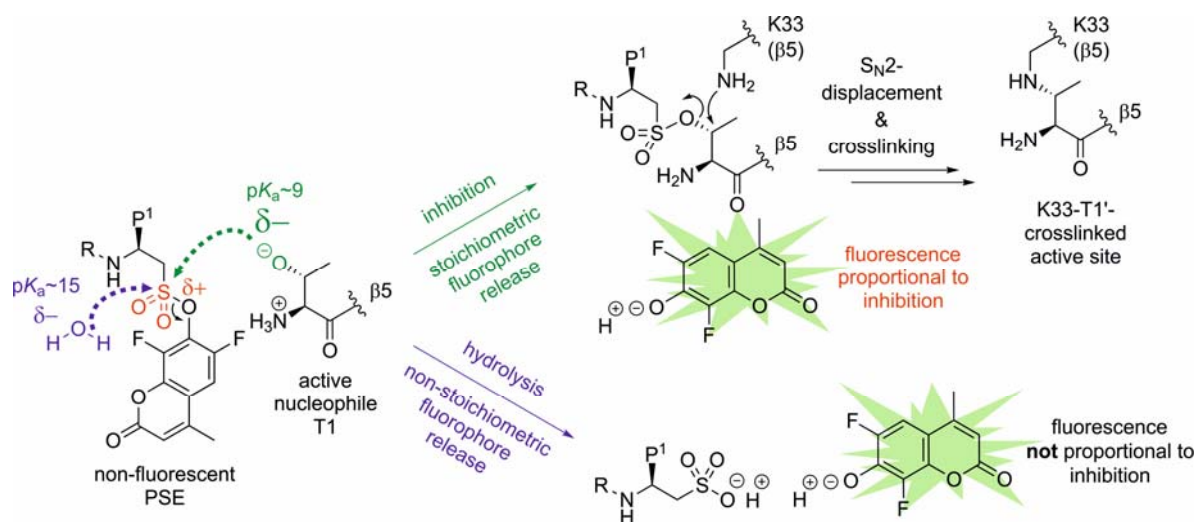


**Figure 5.3** Proposed inactivation mechanism of the PSEs which react with the proteasomal active site of subunit  $\beta 5$  similar to the PSFs. A stoichiometric release of DiFMU during inhibition without unspecific hydrolysis allows an accurate quantification of inhibition. The substituent R indicates the remaining part of the inhibitor backbone; P1 refers to the amino acid side chain protruding into the S1 specificity pocket.

For this purpose, the fluorescence emission in assays with varying cCP concentrations (1 - 0.001 mg/mL; 1.4  $\mu\text{M}$  – 0.0014  $\mu\text{M}$ ) was determined while the concentration of PSE **6** was kept constant (1  $\mu\text{M}$ ). After an incubation time of 1 h, the fluorescence signal was indeed found to be proportional to the amount of cCP in the sample (Figure 5.4b). Even concentrations as low as 0.001 mg/mL (0.0014  $\mu\text{M}$ ) of cCP (cCP:**6** (1  $\mu\text{M}$ ) ratio  $\approx$  1:716) exhibited detectable signals, indicating a slow hydrolysis rate of **6**. Subsequent kinetic studies without cCP at different pH values (6.5 – 8.5) confirmed that after 3 h incubation time at pH 8.5 only 7% of PSE **6** were converted by hydrolysis, thereby highlighting the assay's high sensitivity (Figure 5.4a).



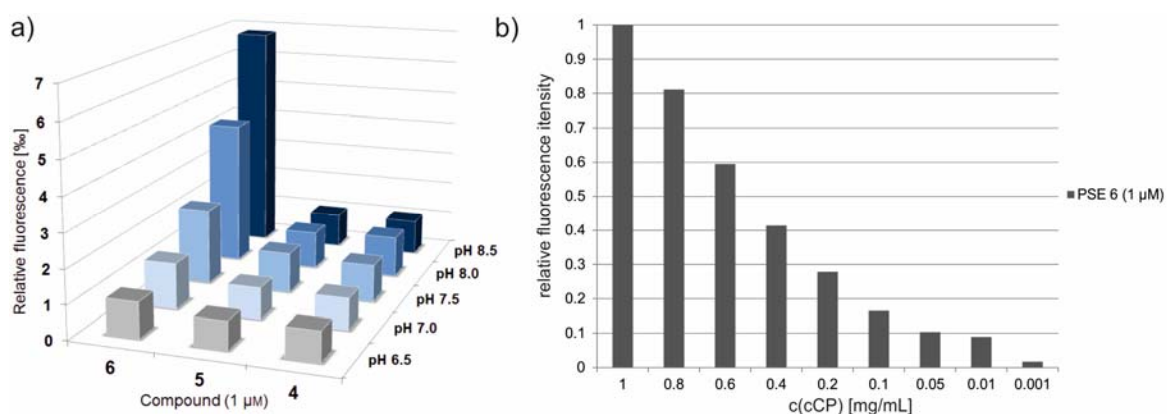


**Figure 5.4** a) Comparative analysis of the hydrolysis rates of PSE **4**, **5** and **6** at different pH values (6.5 - 8.5) after 3 h incubation at 37 °C. The fluorescence (excitation:  $\lambda = 380$  nm; emission:  $\lambda = 430$  nm) was related to a 1  $\mu$ M DiFMU standard and is given in permille [‰]. b) Fluorescence intensity of samples (total volume 40  $\mu$ L) with varying concentrations (1 - 0.001 mg per mL) of human purified cCP treated with PSE **6** for 1 h at pH 7.5.

Further kinetics with cCP confirmed that a concentration of 1  $\mu$ M of PSE **6** (cCP:**6** ratio  $\approx$  1:1) and an incubation time of 15 minutes are already sufficient to obtain a constant and reproducible read-out. After 15 min, the fluorescence signal increased at the same rate in all samples which kept the results constant (Figure 5.5).

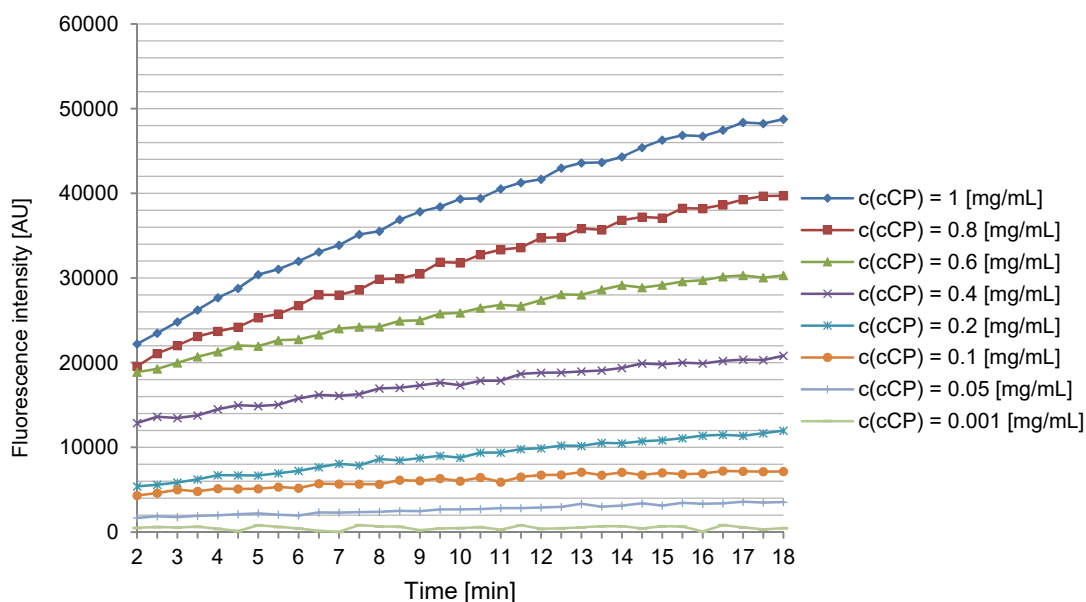


**Figure 5.5** Kinetic experiment with varying concentrations of human cCP (1 – 0.001 mg/mL; 1.4  $\mu$ M – 0.0014  $\mu$ M) treated with 1  $\mu$ M of PSE **6** at pH 7.5 and 37 °C. The start of the measurement was delayed for 2 min due to technical reasons. Data of three repetitions were averaged.

To prove that the observed fluorescence is caused solely by the active site nucleophile of the CP, the latter was inactivated by adding 10  $\mu$ M of carfilzomib prior to the measurement

with the PSE **6**. These pre-inactivated CP samples exhibited only background fluorescence caused by hydrolysis.

These results inspired the design of fluorescent PSEs that selectively inhibit  $\beta 5i$  in order to determine active iCP concentrations beside cCP in solution. The current state-of-the-art  $\beta 5i$ -specific tripeptide of LU-035i (see Figure 2.4) and a tetrapeptide derived from ONX 0914 (Figure 1.5) served as blueprints for peptide backbone design. The backbones were coupled to L-phenylalanine and 3-cyclohexyl-L-alanine DiFMU precursors which generated the PSE **7**, **8** and the hybrid compound PSE **9** (Figure 5.6).

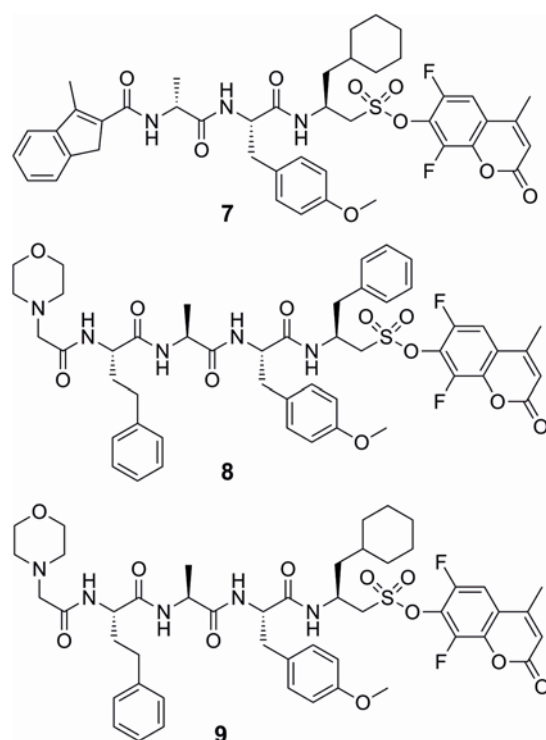


**Figure 5.6** ICP selective PSEs **7**, **8** and **9** which are currently being assessed in vitro and in cell culture.

Currently, the evaluations of PSE **7**, **8** and **9** in assays with purified human iCP and in cell culture are ongoing. Preliminary results suggest their ability to selectively detect active iCPs in solution. This concept might be further improved by using fluorinated luciferin derivatives as leaving groups to generate luminogenic CP inhibitors. Bioluminescent assays have improved sensitivity and superior applicability in cell lysates and biological samples compared to fluorogenic assays. In conclusion, the presented concept might represent the simplest procedure to detect and quantify proteasomal activity. It could be potentially useful as research tool or even in medical diagnostics according to the involvement of 20S proteasomes in a multitude of disease-associated processes.

### 5.3 Methods

#### *IC<sub>50</sub> value determination with the Proteasome-Glo™ chymotrypsin-like luminescent substrate assay*

Luminescent in vitro proteasome inhibition assays were performed with bioluminescence assays (Promega) in 96-well plates (Sigma Aldrich). Assay mixtures contained 10 µg/mL commercially available purified human cCP (Boston Biochem) or human iCP (Boston Biochem) in 100 mM Tris/HCl (pH 7.5) buffer. Inhibitors were dissolved in DMSO and added at various concentrations with three repetitions each, thereby not surpassing a final concentration of 10% (v/v) DMSO. After an incubation time of 60 min at RT, the chymotrypsin-like activity was determined by the hydrolysis of the β5 specific substrate Suc-Leu-Leu-Val-Tyr-aminoluciferin in the presence of luciferase using the Proteasome-Glo™ reagents according to the manufacturer's instructions. The resulting luminescence was detected with a PHERAstar Plus (BMG Labtech) plate-reader.

#### *Fluorescent inhibitor assay with various proteasome concentrations*

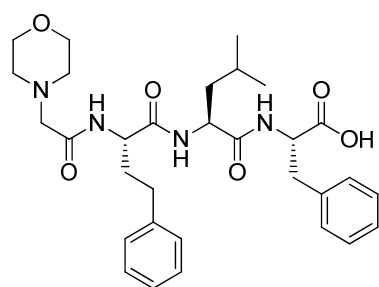
Fluorescent inhibitor assays were performed in 96-well plates (Sigma Aldrich). Samples with a total volume of 39 µL contained 1 – 0.001 mg/mL (1.4 µM – 0.0014 µM) commercially available purified human cCP (Boston Biochem) or human iCP (Boston Biochem) in 100 mM NaCl, 1 mM DTT, 100 mM Tris/HCl (pH 7.5) buffer. Fluorogenic inhibitors were dissolved in DMSO and added resulting in constant concentrations (1, 5, 25 µM) with three repetitions each, thereby not surpassing a final concentration of 10% (v/v) DMSO. The resulting fluorescence intensity was measured on a Tecan infinite M200 or F200 multiplate reader with excitation and emission wavelengths of  $\lambda_{\text{excitation}} = 380$  and  $\lambda_{\text{emission}} = 430$  nm, respectively.

#### *Fluorescent inhibitor assay for determination of hydrolytic stability*

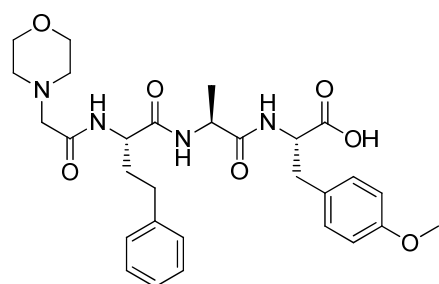
Fluorescent inhibitor assays were performed analogously to the described fluorescent inhibitor assay without the addition of proteasome. Buffer solutions with a total volume of 39 µL containing 100 mM NaCl, 1 mM DTT, 100 mM Tris/HCl in aqueous solution with different pH (6.5 – 8.5) were incubated with 1 µL fluorogenic inhibitor to yield a final concentration of 1 µM at 37 °C. The resulting fluorescence intensity was measured on a Tecan infinite M200 pro or F200 multiplate reader with excitation and emission wavelengths of  $\lambda_{\text{excitation}} = 380$  and  $\lambda_{\text{emission}} = 430$  nm, respectively. The measured fluorescence intensity was related to a 1 µM standard sample of DiFMU (Life Technologies) in the buffer solution described above.

*General procedure for the synthesis of peptidic backbones*

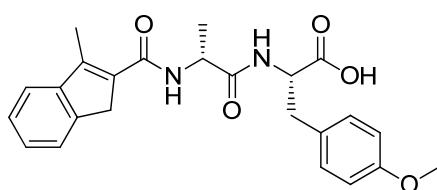
Peptidic backbones were prepared via solid-phase peptide synthesis using Fmoc-protected amino acids and a PS3 Peptide Synthesizer (Protein Technologies, Inc.). Preloaded L-Tyr(OMe)-2-Chlorotrityl-Cl resin (0.63 mmol/g loading) and L-Phe-2-Chlorotrityl-Cl resin (0.74 mmol/g loading) were used in a 0.2 mmol scale. Fmoc-protected amino acids (0.4 mmol, 2 eq.) were deprotected with 20% (v/v) piperidine in DMF. Activation of amino acids (0.4 mmol, 2 eq.) for coupling was performed using HCTU (0.4 mmol, 2 eq.) and 0.4 M DIPEA in DMF. Cleavage from the resin was performed with 20% 1,1,1,3,3,3-hexafluoro-2-propanol (v/v) in CH<sub>2</sub>Cl<sub>2</sub> following evaporation. The residual solid was dissolved in H<sub>2</sub>O and lyophilized to yield the peptidic backbone quantitatively as white powdery TFA salts of the free acid.

**MorphAc-hPhe-Leu-Phe-OH (A)**

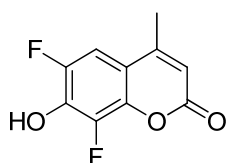
**<sup>1</sup>H NMR** (300 MHz, DMSO-d<sub>6</sub>): δ = 8.18 (d, *J* = 7.8 Hz, 1H), 8.06 (d, *J* = 8.3 Hz, 1H), 7.90 (d, *J* = 8.3 Hz, 1H), 7.33 - 7.24 (m, 2H), 7.23 - 7.07 (m, 8H), 4.51 - 4.30 (m, 3H), 3.61 (t, *J* = 4.7 Hz, 4H), 3.48 - 3.19 (m, 6H), 3.07 - 2.85 (m, 4H), 1.99 - 1.71 (m, 2H), 1.67 - 1.50 (m, 1H), 1.42 (t, *J* = 7.3 Hz, 2H), 0.85 (dd, *J* = 14.2, 6.5 Hz, 6H) ppm. **<sup>13</sup>C NMR** (75 MHz, DMSO-d<sub>6</sub>): δ = 173.2, 172.3, 171.3, 169.1, 142.0, 137.9, 129.4, 128.8, 128.7, 128.5, 126.8, 126.2, 66.6, 53.6, 52.2, 51.2, 37.0, 34.9, 31.8, 24.5, 23.5, 22.1 ppm. **MS** (ESI): *m/z*: calcd. for C<sub>31</sub>H<sub>43</sub>N<sub>4</sub>O<sub>6</sub> [*M*+H<sup>+</sup>] 567.32; found 567.21.

**MorphAc-hPhe-Ala-Tyr(OMe)-OH (B)**

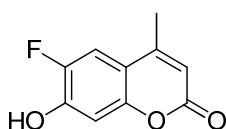
**<sup>1</sup>H NMR** (360 MHz, DMSO-d<sub>6</sub>): δ = 8.11 (dd, *J* = 13.1, 7.6 Hz, 2H), 7.90 (d, *J* = 8.2 Hz, 1H), 7.26 (t, *J* = 7.4 Hz, 2H), 7.21 - 7.09 (m, 5H), 6.78 (d, *J* = 8.1 Hz, 2H), 4.45 - 4.28 (m, 3H), 3.67 (s, 3H), 3.61 (t, *J* = 4.6 Hz, 4H), 3.05 - 2.79 (m, 4H), 2.48 - 2.37 (m, 4H), 2.01 - 1.76 (m, 2H), 1.20 (d, *J* = 7.0 Hz, 3H) ppm. **<sup>13</sup>C NMR** (126 MHz, DMSO-d<sub>6</sub>): δ = 173.3, 172.6, 171.2, 169.2, 158.3, 142.0, 130.6, 129.6, 128.7, 128.7, 126.2, 114.0, 66.6, 61.8, 55.3, 54.2, 53.7, 52.1, 48.3, 36.2, 34.9, 31.8, 18.6 ppm. **MS** (ESI): *m/z*: calcd. for C<sub>29</sub>H<sub>39</sub>N<sub>4</sub>O<sub>7</sub> [*M*+H<sup>+</sup>] 555.28; found 555.22.

**3-MeIndAc-D-Ala-Tyr(OMe)-OH (C)**

**<sup>1</sup>H NMR** (500 MHz, DMSO-*d*<sub>6</sub>): δ = 7.44 – 7.38 (m, 2H), 7.36 – 7.28 (m, 2H), 7.09 (d, *J* = 8.6 Hz, 2H), 6.78 (d, *J* = 8.6 Hz, 2H), 4.90 (p, *J* = 7.1 Hz, 1H), 4.75 (q, *J* = 6.4 Hz, 1H), 3.70 (s, 3H), 3.50 (s, 2H), 3.18 (dd, *J* = 14.0, 5.4 Hz, 1H), 3.00 (dd, *J* = 14.0, 6.5 Hz, 1H), 2.45 (t, *J* = 2.2 Hz, 3H), 1.33 (d, *J* = 6.9 Hz, 3H) ppm. **<sup>13</sup>C NMR** (126 MHz, DMSO-*d*<sub>6</sub>): δ = 173.8, 172.6, 166.2, 158.6, 149.0, 145.3, 142.2, 130.9, 130.5, 128.0, 127.5, 126.8, 123.8, 120.9, 113.9, 55.1, 53.6, 48.4, 38.0, 36.7, 19.0, 12.3 ppm. **MS** (ESI): *m/z*: calcd. for C<sub>24</sub>H<sub>27</sub>N<sub>2</sub>O<sub>5</sub> [*M*+*H*<sup>+</sup>] 423.19; found 422.90.

*Synthesis of fluorinated 4-methylumbelliferones***6,8-Difluoro-4-methylumbelliferone (DiFMU)**

Ethyl acetoacetate (432 μL, 445 mg, 3.42 mmol) and 2,4-difluorobenzene-1,3-diol (500 mg, 3.42 mmol) were cooled down to 0 °C, and methanesulfonic acid (5.56 mL, 8.22 g, 85.6 mmol, 25.0 eq) was added slowly to the mixture. The mixture was allowed to reach room temperature and stirred overnight. Afterwards, the mixture was cooled down to 0 °C and H<sub>2</sub>O (10 mL) was added slowly. The formed precipitate was filtered, washed with H<sub>2</sub>O and solubilized with 1 M NaOH. After reprecipitation with 10% sulfuric acid (approx. pH 1), the precipitate was filtered again, washed with H<sub>2</sub>O and dissolved in acetone. The solvent was evaporated to yield DiFMU (577 mg, 2.72 mmol, 79%) as a yellow powder. **<sup>1</sup>H NMR** (360 MHz, DMSO-*d*<sub>6</sub>): δ = 11.49 (s, 1H), 7.48 (dd, *J* = 11.4, 2.2 Hz, 1H), 6.31 (d, *J* = 1.5 Hz, 1H), 2.36 (d, *J* = 1.3 Hz, 3H) ppm. **<sup>13</sup>C NMR** (91 MHz, DMSO-*d*<sub>6</sub>) δ = 159.2 (s), 153.6 (t, *J* = 2.8 Hz), 148.9 (dd, *J* = 239.3, 5.2 Hz), 139.8 (dd, *J* = 9.4, 2.1 Hz), 139.8 (dd, *J* = 244.0, 6.7 Hz), 138.0 (dd, *J* = 18.1, 12.8 Hz), 112.8 (s), 111.4 (d, *J* = 9.2 Hz), 106.8 (dd, *J* = 21.6, 3.2 Hz), 18.67 (s) ppm. **<sup>19</sup>F NMR** (471 MHz, DMSO-*d*<sub>6</sub>): δ = -136.17 (t, *J* = 10.3 Hz), -153.83 (dd, *J* = 9.1, 2.2 Hz) ppm. **MS** (ESI): *m/z*: calcd. for C<sub>10</sub>H<sub>7</sub>F<sub>2</sub>O<sub>3</sub> [*M*+*H*<sup>+</sup>] 213.04; found 213.04.

**6-Fluoro-4-methylumbelliferone (FMU)**

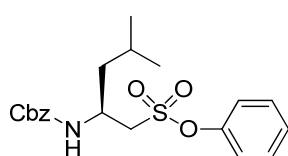
Methanesulfonic acid (6.34 mL, 9.34 g, 97.6 mmol) was added slowly to a mixture of ethyl acetoacetate (493 mL, 508 mg, 3.90 mmol) and 4-difluorobenzene-1,3-diol (500 mg, 3.90 mmol) at 0 °C. The mixture was allowed to reach room temperature and stirred overnight. Afterwards, the mixture was cooled down to 0 °C and H<sub>2</sub>O (10 mL) was added slowly. The formed precipitate was

## 5. 20S proteasome inhibitors with fluorescent feedback

filtered, washed with H<sub>2</sub>O and solubilized with 1 M NaOH. After reprecipitation with 10% sulfuric acid (approx. pH 1), the precipitate was filtered again, washed with H<sub>2</sub>O and dissolved in acetone. The solvent was evaporated to yield FMU (684 mg, 3.52 mmol, 90%) as a rose-colored powder. **<sup>1</sup>H NMR** (360 MHz, DMSO-d<sub>6</sub>): δ = 11.10 (s, 1H), 7.59 (d, *J* = 11.6 Hz, 1H), 6.90 (d, *J* = 7.5 Hz, 1H), 6.21 (d, *J* = 1.5 Hz, 1H), 2.36 (d, *J* = 1.2 Hz, 3H) ppm. **<sup>13</sup>C NMR** (91 MHz, DMSO-d<sub>6</sub>) δ = 160.5, 152.2 (dd, *J* = 255.4, 2.0 Hz), 149.5, 149.3, 147.2, 112.3, 112.0, 111.9, 111.8, 105.0 (d, *J* = 3.1 Hz), 18.6 ppm. **<sup>19</sup>F NMR** (471 MHz, DMSO-d<sub>6</sub>): δ = -139.56 (dd, *J* = 11.7, 7.5 Hz) ppm. **MS** (ESI): *m/z*: calcd. for C<sub>10</sub>H<sub>8</sub>FO<sub>3</sub> [*M*+H<sup>+</sup>] 195.05; found 195.08.

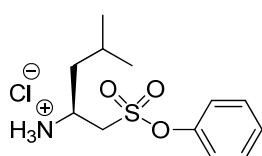
### Synthesis of sulfonate ester headgroups

The sulfonyl chloride headgroup precursors derived from L-leucinol and L-phenylalaninol were synthesized according to our previously published protocol.<sup>[5]</sup>



#### Cbz-L-Leu-[CH<sub>2</sub>SO<sub>2</sub>]-Phenol (Phe-A)

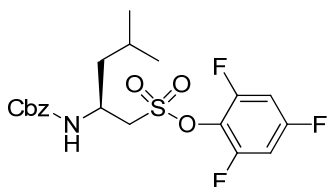
A solution of Cbz-L-Leu-[CH<sub>2</sub>SO<sub>2</sub>]-Cl (143 mg, 0.428 mmol) in CH<sub>2</sub>Cl<sub>2</sub> (1.5 mL) was cooled down to 0 °C before phenol (40.3 mg, 0.428 mmol) was added and the mixture was stirred for 15 min. Afterwards, NEt<sub>3</sub> (119 μL, 87 mg, 0.857 mmol) was added and the mixture was stirred overnight at RT. Evaporation of the solvent and purification via flash column chromatography (PE → 20% EA/PE, v/v) yielded sulfonate **Phe-A** (96 mg, 0.245 mmol, 57%) as a white solid. **<sup>1</sup>H NMR** (300 MHz, CDCl<sub>3</sub>): δ = 7.50 – 7.29 (m, 10H), 5.03 (d, *J* = 2.1 Hz, 2H), 4.15 (dd, *J* = 12.7, 6.9 Hz, 1H), 3.72 – 3.56 (m, 2H), 1.65 – 1.33 (m, 3H), 0.87 (dd, *J* = 6.5, 1.8 Hz, 6H) ppm. **<sup>13</sup>C NMR** (75 MHz, CDCl<sub>3</sub>): δ = 155.9, 137.5, 130.6, 129.8, 128.7, 128.2, 128.0, 127.8, 122.7, 115.7, 65.7, 54.9, 45.6, 43.4, 24.5, 23.5, 21.8 ppm. **MS** (ESI): *m/z*: calcd. for C<sub>20</sub>H<sub>26</sub>NO<sub>5</sub>S [*M*+H<sup>+</sup>] 392.15; found 391.91.



#### Cbz-L-Leu-[CH<sub>2</sub>SO<sub>2</sub>]-Phenol · HCl (Phe-B)

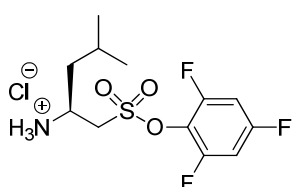
HBr in acetic acid (33%, 0.84 mL, 5.11 mmol) was added dropwise to a solution of sulfonate **Phe-A** (80 mg, 0.204 mmol) in CH<sub>2</sub>Cl<sub>2</sub> (1.5 mL) and stirred at RT for 45 min. After concentration *in vacuo* the residue was dissolved in H<sub>2</sub>O (1.5 mL) and DOWEX<sup>®</sup> 1X8 (Cl-form, 90 mg) was added to solution. The mixture was stirred for 15 min, the solution was filtered and the residue was washed with H<sub>2</sub>O. After lyophilization hydrochloride **Phe-B** (50 mg, 0.170 mmol, 83%

(crude product)) was obtained as a light yellow powder which was used without further purification in the next step.



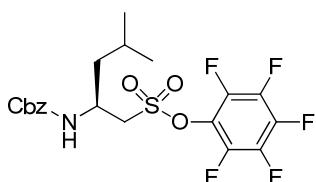
#### Cbz-L-Leu-[CH<sub>2</sub>SO<sub>2</sub>]-2,4,6-TFP (TFP-A)

A solution of Cbz-L-Leu-[CH<sub>2</sub>SO<sub>2</sub>]-Cl (216 mg, 0.647 mmol) in CH<sub>2</sub>Cl<sub>2</sub> (2.2 mL) was cooled down to 0 °C before 2,4,6-trifluorophenol (96 mg, 0.647 mmol) was added and the mixture was stirred for 15 min. Afterwards, NEt<sub>3</sub> (180 μL, 1.294 mmol) was added and the mixture was stirred overnight at RT. Evaporation of the solvent and purification via flash column chromatography (PE → 20% EA/PE, v/v) yielded sulfonate **TFP-A** (157 mg, 0.353 mmol, 55%) as a yellow oil. <sup>1</sup>H NMR (300 MHz, CDCl<sub>3</sub>): δ = 7.55 – 7.41 (m, 3H), 7.36 – 7.27 (m, 5H), 5.03 (d, *J* = 1.3 Hz, 2H), 4.28 – 4.12 (m, 1H), 3.87 (dd, *J* = 14.4, 4.1 Hz, 1H), 3.75 (dd, *J* = 14.4, 8.4 Hz, 1H), 1.71 – 1.47 (m, 2H), 1.45 – 1.28 (m, 1H), 0.88 (dd, *J* = 6.5, 2.2 Hz, 6H). <sup>13</sup>C NMR (75 MHz, CDCl<sub>3</sub>): δ = 155.9, 137.5, 128.7, 128.2, 127.9, 102.6, 65.7, 56.3, 45.6, 43.4, 24.5, 23.6, 21.7 ppm. <sup>19</sup>F NMR (471 MHz, DMSO-d<sub>6</sub>): δ = -107.15 (t, *J* = 5.3 Hz), -121.52 (d, *J* = 5.2 Hz) ppm. MS (ESI): *m/z*: calcd. for C<sub>20</sub>H<sub>23</sub>F<sub>3</sub>NO<sub>5</sub>S [*M*+H<sup>+</sup>] 446.12; found 445.90.



#### Cbz-L-Leu-[CH<sub>2</sub>SO<sub>2</sub>]-2,4,6-TFP · HCl (TFP-B)

HBr in acetic acid (33%, 1.31 mL, 7.97 mmol) was added dropwise to a solution of sulfonate **TFP-A** (142 mg, 0.319 mmol) in CH<sub>2</sub>Cl<sub>2</sub> (2.3 mL) and stirred at RT for 45 min. After concentration *in vacuo* the residue was dissolved in H<sub>2</sub>O (2.3 mL) and DOWEX® 1X8 (Cl-form, 160 mg) was added to solution. The mixture was stirred for 15 min, the solution was filtered and the residue was washed with H<sub>2</sub>O. After lyophilization hydrochloride **TFP-B** (97 mg, 0.279 mmol, 87% (crude product)) was obtained as a white powder which was used without further purification in the next step.

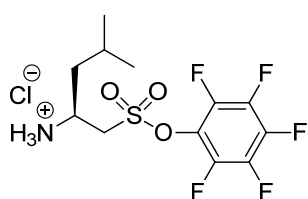


#### Cbz-L-Leu-[CH<sub>2</sub>SO<sub>2</sub>]-PFP (PFP-A)

A solution of Cbz-L-Leu-[CH<sub>2</sub>SO<sub>2</sub>]-Cl (143 mg, 0.428 mmol) in CH<sub>2</sub>Cl<sub>2</sub> (1.5 mL) was cooled down to 0 °C before pentafluorophenol (79 mg, 0.428 mmol) was added and the mixture was stirred for 15 min. Afterwards, NEt<sub>3</sub> (119 μL, 87 mg, 0.857 mmol) was added and the mixture was stirred overnight at RT. Evaporation of the solvent and purification via flash column chromatography (PE → 25% EA/PE, v/v) yielded

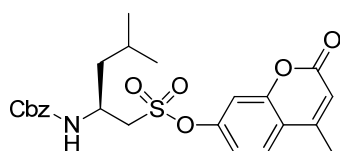
## 5. 20S proteasome inhibitors with fluorescent feedback

sulfonate **PFP-A** (120 mg, 0.249 mmol, 58%) as a light yellow solid. **<sup>1</sup>H NMR** (300 MHz, CDCl<sub>3</sub>): δ = 7.45 (d, *J* = 8.8 Hz, 1H), 7.39 – 7.26 (m, 5H), 5.03 (d, *J* = 2.2 Hz, 2H), 4.29 – 4.13 (m, 1H), 4.09 – 3.95 (m, 1H), 3.83 (dd, *J* = 14.4, 8.6 Hz, 1H), 1.71 – 1.48 (m, 2H), 1.43 – 1.29 (m, 1H), 0.88 (dd, *J* = 6.4, 1.5 Hz, 6H) ppm. **<sup>13</sup>C NMR** (75 MHz, CDCl<sub>3</sub>): δ = 155.9, 137.5, 128.7, 128.2, 128.0, 65.7, 56.5, 45.6, 43.3, 24.4, 23.6, 21.6 ppm. **<sup>19</sup>F NMR** (471 MHz, DMSO-*d*<sub>6</sub>): δ = -151.55 (d, *J* = 20.0 Hz), -156.32 (t, *J* = 23.3 Hz), -161.79 – -161.98 (m), -165.44 (dd, *J* = 23.5, 19.8 Hz) ppm. **MS** (ESI): *m/z*: calcd. for C<sub>20</sub>H<sub>21</sub>F<sub>5</sub>NO<sub>5</sub>S [*M*+*H*<sup>+</sup>] 482.11; found 481.65.



### **Cbz-L-Leu-[CH<sub>2</sub>SO<sub>2</sub>]-PFP · HCl (PFP-B)**

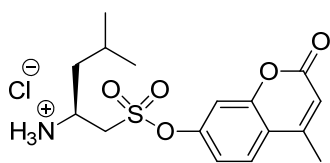
HBr in acetic acid (33%, 0.9 mL, 5.45 mmol) was added dropwise to a solution of sulfonate **PFP-A** (105 mg, 0.218 mmol) in CH<sub>2</sub>Cl<sub>2</sub> (1.6 mL) and stirred at RT for 45 min. After concentration *in vacuo* the residue was dissolved in H<sub>2</sub>O (1.6 mL) and DOWEX<sup>®</sup> 1X8 (Cl-form, 120 mg) was added to solution. The mixture was stirred for 15 min, the solution was filtered and the residue was washed with H<sub>2</sub>O. After lyophilization hydrochloride **PFP-B** (64 mg, 0.167 mmol, 76% (crude product)) was obtained as a light yellow powder which was used without further purification in the next step.



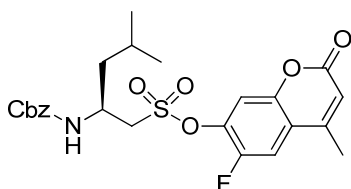
### **Cbz-L-Leu-[CH<sub>2</sub>SO<sub>2</sub>]-MU (MU-A)**

A solution of Cbz-L-Leu-[CH<sub>2</sub>SO<sub>2</sub>]-Cl (187 mg, 0.560 mmol) in CH<sub>2</sub>Cl<sub>2</sub> (1.9 mL) was cooled down to 0 °C before MU (118 mg, 0.672 mmol) was added and the mixture was stirred for 15 min. Afterwards, NEt<sub>3</sub> (133 μL, 96 mg, 0.952 mmol) was added and the mixture was stirred overnight at RT. Evaporation of the solvent and purification via flash column chromatography (PE → 50% EA/PE, v/v) yielded sulfonate **MU-A** (225 mg, 0.476 mmol, 85%) as a light yellow solid. **<sup>1</sup>H NMR** (300 MHz, CDCl<sub>3</sub>): δ = 7.62 (d, *J* = 8.5 Hz, 1H), 7.39 – 7.31 (m, 5H), 6.94 (d, *J* = 2.4 Hz, 1H), 6.33 (d, *J* = 1.3 Hz, 1H), 5.21 (d, *J* = 8.8 Hz, 1H), 5.14 (s, 2H), 4.39 – 4.25 (m, 1H), 3.71 (dd, *J* = 14.6, 5.8 Hz, 1H), 3.56 (dd, *J* = 14.6, 5.0 Hz, 1H), 2.45 (d, *J* = 1.3 Hz, 3H), 1.78 – 1.62 (m, 3H), 0.97 (d, *J* = 6.1 Hz, 6H) ppm. **MS** (ESI): *m/z*: calcd. for C<sub>24</sub>H<sub>28</sub>NO<sub>7</sub>S [*M*+*H*<sup>+</sup>] 474.16; found 473.88.

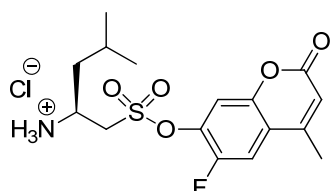


**L-Leu-[CH<sub>2</sub>SO<sub>2</sub>]-MU · HCl (MU-B)**

HBr in acetic acid (33%, 1.8 mL, 10.93 mmol) was added dropwise to a solution of sulfonate **MU-A** (207 mg, 0.437 mmol) in CH<sub>2</sub>Cl<sub>2</sub> (3.2 mL) and stirred at RT for 45 min. After concentration *in vacuo* the residue was dissolved in H<sub>2</sub>O (3.2 mL) and DOWEX® 1X8 (Cl-form, 230 mg) was added to solution. The mixture was stirred for 15 min, the solution was filtered and the residue was washed with H<sub>2</sub>O. After lyophilization hydrochloride **MU-B** (114 mg, 0.303 mmol, 69% (crude product)) was obtained as a white powder which was used without further purification in the next step.

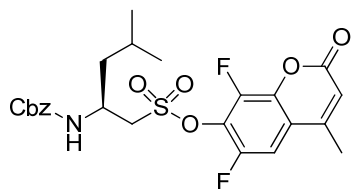
**Cbz-L-Leu-[CH<sub>2</sub>SO<sub>2</sub>]-FMU (FMU-A)**

A solution of Cbz-L-Leu-[CH<sub>2</sub>SO<sub>2</sub>]-Cl (187 mg, 0.560 mmol) in CH<sub>2</sub>Cl<sub>2</sub> (1.9 mL) was cooled down to 0 °C before FMU (131 mg, 0.672 mmol) was added and the mixture was stirred for 15 min. Afterwards, NEt<sub>3</sub> (133 µL, 96 mg, 0.952 mmol) was added and the mixture was stirred overnight at RT. Evaporation of the solvent and purification via flash column chromatography (PE → 60% EA/PE, v/v) yielded sulfonate **FMU-A** (234 mg, 0.476 mmol, 85%) as a light yellow oil. <sup>1</sup>H NMR (300 MHz, CDCl<sub>3</sub>): δ = 7.91 (d, *J* = 10.6 Hz, 1H), 7.68 (d, *J* = 6.6 Hz, 1H), 7.50 (d, *J* = 8.8 Hz, 1H), 7.36 – 7.21 (m, 5H), 6.51 (d, *J* = 1.5 Hz, 1H), 5.03 (d, *J* = 3.6 Hz, 2H), 4.27 – 4.11 (m, 1H), 3.95 – 3.71 (m, 2H), 2.43 (d, *J* = 1.4 Hz, 3H), 1.75 – 1.48 (m, 2H), 1.40 (s, 1H), 0.89 (d, *J* = 6.4 Hz, 6H). <sup>13</sup>C NMR (75 MHz, CDCl<sub>3</sub>): δ = 159.6, 156.0, 151.2 (dd, *J* = 238.5, 1.9 Hz), 128.7, 128.1, 127.9, 119.9 (d, *J* = 7.8 Hz), 115.8, 113.7, 113.4, 113.3, 105.0 (d, *J* = 3.0 Hz), 65.7, 55.9, 45.7, 43.3, 30.0, 24.5, 23.5, 21.7, 18.7 ppm. <sup>19</sup>F NMR (471 MHz, DMSO-*d*<sub>6</sub>): δ = -132.11 (dd, *J* = 10.6, 6.8 Hz) ppm. MS (ESI): *m/z*: calcd. for C<sub>24</sub>H<sub>27</sub>FNO<sub>7</sub>S [M+H<sup>+</sup>] 492.15; found 491.88.

**L-Leu-[CH<sub>2</sub>SO<sub>2</sub>]-FMU · HCl (FMU-B)**

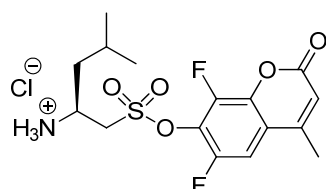
HBr in acetic acid (33%, 1.8 mL, 10.94 mmol) was added dropwise to a solution of sulfonate **FMU-A** (215 mg, 0.437 mmol) in CH<sub>2</sub>Cl<sub>2</sub> (3.2 mL) and stirred at RT for 45 min. After concentration *in vacuo* the residue was dissolved in H<sub>2</sub>O (3.2 mL) and DOWEX® 1X8 (Cl-form, 230 mg) was added to solution. The mixture was stirred for 15 min, the solution was filtered and the residue was washed with H<sub>2</sub>O. After

lyophilization hydrochloride **FMU-B** (133 mg, 0.338 mmol, 77% (crude product)) was obtained as a white powder which was used without further purification in the next step.



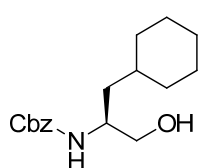
#### Cbz-L-Leu-[CH<sub>2</sub>SO<sub>2</sub>]-DiFMU (DiFMU-A)

A solution of Cbz-L-Leu-[CH<sub>2</sub>SO<sub>2</sub>]-Cl (93 mg, 0.279 mmol) in CH<sub>2</sub>Cl<sub>2</sub> (1 mL) was cooled down to 0 °C before DiFMU (71 mg, 0.334 mmol) was added and the mixture was stirred for 15 min. Afterwards, NEt<sub>3</sub> (66 μL, 48 mg, 0.474 mmol) was added and the mixture was stirred overnight at RT. Evaporation of the solvent and purification via flash column chromatography (PE → 40% EA/PE, v/v) yielded sulfonate **DiFMU-A** (95 mg, 0.186 mmol, 67%) as a light brown solid. **<sup>1</sup>H NMR** (300 MHz, CDCl<sub>3</sub>): δ = 7.41 – 7.29 (m, 5H), 7.25 (dd, *J* = 9.6, 2.3 Hz, 1H), 6.46 – 6.39 (m, 1H), 5.21 (d, *J* = 8.6 Hz, 1H), 5.13 (s, 2H), 4.45 – 4.27 (m, 1H), 3.87 (dd, *J* = 14.5, 5.9 Hz, 1H), 3.76 (dd, *J* = 14.5, 4.7 Hz, 1H), 2.43 (d, *J* = 1.4 Hz, 3H), 1.84 – 1.58 (m, 3H), 0.98 (d, *J* = 6.3 Hz, 6H) ppm. **<sup>13</sup>C NMR** (75 MHz, CDCl<sub>3</sub>): δ = 158.1, 155.6, 151.5 (dd, *J* = 250.7, 2.0 Hz), 150.7 (t, *J* = 2.7 Hz), 128.5, 128.2, 128.0, 119.4 (dd, *J* = 8.6, 1.7 Hz), 117.1, 113.8, 106.2 (dd, *J* = 21.6, 4.0 Hz), 67.0, 56.8, 46.3, 42.4, 24.8, 22.9, 21.6, 18.8 ppm. **<sup>19</sup>F NMR** (471 MHz, DMSO-*d*<sub>6</sub>): δ = -128.00 (d, *J* = 9.6 Hz), -140.63 ppm. **MS** (ESI): *m/z*: calcd. for C<sub>24</sub>H<sub>26</sub>F<sub>2</sub>NO<sub>7</sub>S [*M*+*H*<sup>+</sup>] 510.14; found 509.88.



#### L-Leu-[CH<sub>2</sub>SO<sub>2</sub>]-DiFMU · HCl (DiFMU-B)

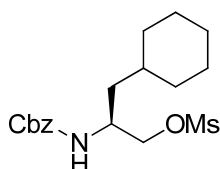
HBr in acetic acid (33%, 0.7 mL, 4.27 mmol) was added dropwise to a solution of sulfonate **DiFMU-A** (87 mg, 0.171 mmol) in CH<sub>2</sub>Cl<sub>2</sub> (1.2 mL) and stirred at RT for 45 min. After concentration *in vacuo* the residue was dissolved in H<sub>2</sub>O (1.2 mL) and DOWEX® 1X8 (Cl-form, 100 mg) was added to solution. The mixture was stirred for 15 min, the solution was filtered and the residue was washed with H<sub>2</sub>O. After lyophilization hydrochloride **DiFMU-B** (59 mg, 0.143 mmol, 84% (crude product)) was obtained as a white powder which was used without further purification in the next step.



#### Cbz-3-cyclohexyl-L-alaninol (CyA-A)

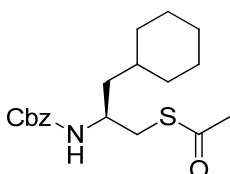
Cyclohexyl-L-alaninol hydrochloride (5 g, 25.8 mmol) and Na<sub>2</sub>CO<sub>3</sub> (5.47 g, 51.62 mmol) were dissolved in a mixture of H<sub>2</sub>O (30 mL) and dioxane (30 mL). The suspension was cooled to 0 °C and Cbz-Cl (5.83 mL, 6.60 g, 38.7 mmol) was added dropwise. The reaction was stirred overnight at

RT. After concentration under reduced pressure, the mixture was extracted with  $\text{CH}_2\text{Cl}_2$  (3  $\times$  50 mL) and the combined organic layers were washed with 5% citric acid (30 mL), sat.  $\text{NaHCO}_3$  (30 mL), brine (30 mL), dried over  $\text{MgSO}_4$  and filtered. Evaporation of the solvent and purification by flash column chromatography (PE  $\rightarrow$  50% EA/PE, v/v) yielded **CyA-A** (7.51 g, 25.8 mmol, 100%) as a viscous colorless oil.  **$^1\text{H NMR}$**  (360 MHz,  $\text{CDCl}_3$ ):  $\delta$  = 7.41 - 7.36 (m, 5H), 5.13 (s, 2H), 4.87 - 4.79 (m, 1H), 4.72 (d,  $J$  = 5.8 Hz, 1H), 3.92 - 3.78 (m, 1H), 3.76 - 3.64 (m, 1H), 3.62 - 3.48 (m, 1H), 1.85 - 1.64 (m, 5H), 1.39 - 1.13 (m, 6H), 1.03 - 0.80 (m, 2H) ppm.  **$^{13}\text{C NMR}$**  (91 MHz,  $\text{CDCl}_3$ ):  $\delta$  = 156.8, 136.4, 128.5, 128.1, 128.0, 71.4, 66.9, 50.9, 39.1, 34.2, 33.8, 32.9, 26.5, 26.2, 26.1 ppm. **MS** (ESI):  $m/z$ : calcd. for  $\text{C}_{17}\text{H}_{26}\text{NO}_3$  [ $M+\text{H}^+$ ] 292.19; found 291.86.



#### **Cbz-3-cyclohexyl-L-Ala-[CH<sub>2</sub>O]-Ms (CyA-B)**

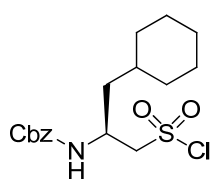
$\text{NEt}_3$  (1.76 mL, 1.21 g, 12.0 mmol) was added to a solution of **CyA-A** (2.91 g, 10.0 mmol) in  $\text{CH}_2\text{Cl}_2$  (30 mL). After cooling the mixture to 0 °C methanesulfonyl chloride (929  $\mu\text{L}$ , 1.37 g, 12 mmol) was added dropwise and the reaction mixture was stirred overnight at RT. Then  $\text{H}_2\text{O}$  (10 mL) was added and the mixture was extracted with  $\text{CH}_2\text{Cl}_2$  (3  $\times$  20 mL). The combined organic layers were washed with 5% citric acid (10 mL),  $\text{H}_2\text{O}$  (10 mL) and brine (10 mL), dried over  $\text{MgSO}_4$  and filtered. Concentration under reduced pressure and purification by flash column chromatography (PE  $\rightarrow$  40% EA/PE, v/v) yielded **CyA-B** (2.79 g, 7.55 mmol, 76%) as a white solid.  **$^1\text{H NMR}$**  (360 MHz,  $\text{CDCl}_3$ ):  $\delta$  = 7.40 - 7.31 (m, 5H), 5.11 (s, 2H), 4.77 (d,  $J$  = 8.7 Hz, 1H), 4.28 (dd,  $J$  = 10.1, 3.9 Hz, 1H), 4.15 (dd,  $J$  = 6.9, 3.5 Hz, 1H), 4.07 - 3.97 (m, 1H), 2.95 (s, 3H), 1.84 - 1.60 (m, 5H), 1.47 - 1.08 (m, 6H), 1.04 - 0.78 (m, 2H) ppm.  **$^{13}\text{C NMR}$**  (91 MHz,  $\text{CDCl}_3$ ):  $\delta$  = 155.8, 136.3, 128.5, 128.2, 128.1, 71.3, 66.9, 47.9, 38.7, 37.3, 34.0, 33.7, 32.7, 26.4, 26.1, 26.0 ppm. **MS** (ESI):  $m/z$ : calcd. for  $\text{C}_{18}\text{H}_{28}\text{NO}_5\text{S}$  [ $M+\text{H}^+$ ] 370.17; found 369.86.



#### **Cbz-3-cyclohexyl-L-Ala-[CH<sub>2</sub>S]-Ac (CyA-C)**

Under an argon atmosphere, thioacetic acid (885  $\mu\text{L}$ , 955 mg, 12.6 mmol) was added to a suspension of  $\text{Cs}_2\text{CO}_3$  (2.13 g, 6.53 mmol) in DMF (35 mL). After stirring for 10 min at RT, a solution of mesylate **CyA-B** (3.71 g, 10.0 mmol) in DMF (15 mL) was added at once and the mixture was stirred in an aluminium foil-covered flask at 50 °C overnight. After evaporation of the solvent the crude product was purified via flash column chromatography (PE  $\rightarrow$  40% EA/PE, v/v) to yield thioacetate **CyA-C** (2.98 g, 8.53 mmol, 85%) as a red-brownish oil

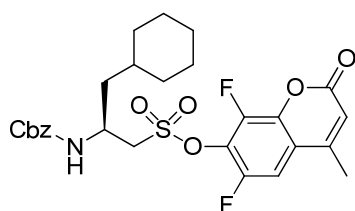
that crystallized overnight.  $^1\text{H NMR}$  (360 MHz,  $\text{CDCl}_3$ ):  $\delta = 7.39 - 7.30$  (m, 5H), 5.09 (s, 2H), 4.64 (d,  $J = 9.1$  Hz, 1H), 3.99 – 3.87 (m, 1H), 3.11 (dd,  $J = 13.8, 4.7$  Hz, 1H), 2.98 (dd,  $J = 13.9, 7.1$  Hz, 1H), 2.30 (s, 3H), 1.84 – 1.60 (m, 5H), 1.41 – 1.07 (m, 6H), 0.99 - 0.78 (m, 2H) ppm.  $^{13}\text{C NMR}$  (91 MHz,  $\text{CDCl}_3$ ):  $\delta = 195.5, 155.9, 136.6, 128.5, 128.0, 128.0, 66.6, 48.7, 42.2, 34.4, 34.3, 33.7, 32.8, 30.5, 26.4, 26.2, 26.1$  ppm. **MS** (ESI):  $m/z$ : calcd. for  $\text{C}_{19}\text{H}_{27}\text{NO}_3\text{S}$  [ $M+\text{H}^+$ ] 350.18; found 349.89.



### Cbz-3-cyclohexyl-L-Ala-[CH<sub>2</sub>SO<sub>2</sub>]-Cl (CyA-D)

NCS (306.0 mg, 2.29 mmol) was dissolved in a mixture of HCl (143  $\mu\text{L}$ , 2 M, 286 mmol) and acetonitrile (985  $\mu\text{L}$ ) at 0 °C and stirred for 15 min.

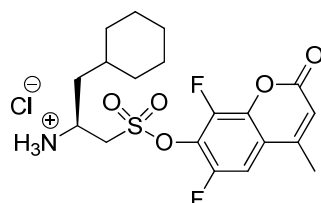
Following addition of thioacetate **CyA-C** (200 mg, 572  $\mu\text{mol}$ ) to the mixture and stirring for 15 min at RT, the solution was diluted with  $\text{CH}_2\text{Cl}_2$  (4 mL), washed with brine (3  $\times$  4 mL), dried over  $\text{MgSO}_4$  and filtered. After evaporation of the solvent, sulfonyl chloride **CyA-D** (278 mg, 744  $\mu\text{mol}$ , *quant.* crude) was obtained as an orange colored oil which was used without further purification in the next step.



### Cbz-3-cyclohexyl-L-Ala-[CH<sub>2</sub>SO<sub>2</sub>]-DiFMU (DiFMU-CyA-A)

A solution of sulfonyl chloride **CyA-D** (214.0 mg, 572  $\mu\text{mol}$ ) in  $\text{CH}_2\text{Cl}_2$  (1.90 mL) was cooled down to 0 °C before DiFMU (127 mg, 601  $\mu\text{mol}$ ) was added and the mixture was stirred for 15 min. Afterwards,  $\text{NEt}_3$  (160  $\mu\text{L}$ , 116 mg, 1.14 mmol)

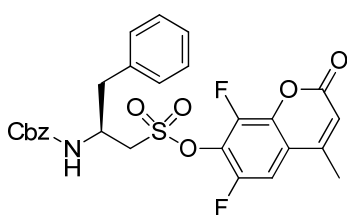
was added and the mixture was stirred overnight at RT. Evaporation of the solvent and purification via flash column chromatography (PE  $\rightarrow$  35% EA/PE, v/v) yielded sulfonate **DiFMU-CyA-A** (214 mg, 389  $\mu\text{mol}$ , 68%, 2 steps) as a light brown solid.  $^1\text{H NMR}$  (360 MHz,  $\text{CDCl}_3$ ):  $\delta = 7.38 - 7.27$  (m, 5H), 7.22 (dd,  $J = 9.7, 2.3$  Hz, 1H), 6.40 (s, 1H), 5.30 (s, 1H), 5.12 (d,  $J = 3.0$  Hz, 2H), 4.41 – 4.29 (m, 1H), 3.85 (dd,  $J = 14.5, 6.0$  Hz, 1H), 3.74 (dd,  $J = 15.1, 4.2$  Hz, 1H), 2.41 (d,  $J = 1.3$  Hz, 3H), 1.83 – 1.60 (m, 5H), 1.43 – 1.11 (m, 6H), 1.04 – 0.86 (m, 2H) ppm.  $^{19}\text{F NMR}$  (471 MHz,  $\text{DMSO-d}_6$ ):  $\delta = -129.84$  (d,  $J = 10.6$  Hz), -143.26 ppm. **MS** (ESI):  $m/z$ : calcd. for  $\text{C}_{27}\text{H}_{30}\text{F}_2\text{NO}_7\text{S}$  [ $M+\text{H}^+$ ] 550.17; found 549.73.



### 3-Cyclohexyl-L-Ala-[CH<sub>2</sub>SO<sub>2</sub>]-DiFMU · HCl (DiFMU-CyA-B)

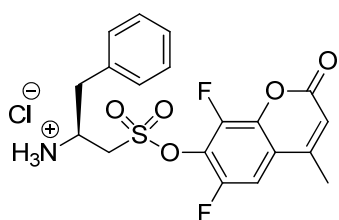
HBr in acetic acid (33%, 1.64 mL, 9.37 mmol) was added dropwise to a solution of sulfonate **DiFMU-CyA-A** (206.0 mg,

375  $\mu\text{mol}$ ) in  $\text{CH}_2\text{Cl}_2$  (4.0 mL) and stirred at RT for 45 min. After concentration *in vacuo* the residue was dissolved in  $\text{H}_2\text{O}$  (4.0 mL) and DOWEX<sup>®</sup> 1X8 (Cl-form, 300 mg) was added to solution. The mixture was stirred for 15 min, the solution was filtered and the residue was washed with  $\text{H}_2\text{O}$ . After lyophilization hydrochloride **DiFMU-CyA-B** (123.0 mg, 272  $\mu\text{mol}$ , 73% (crude product)) was obtained as a white powder which was used without further purification in the next step.



#### Cbz-L-Phe-[CH<sub>2</sub>SO<sub>2</sub>]-DiFMU (DiFMU-F-A)

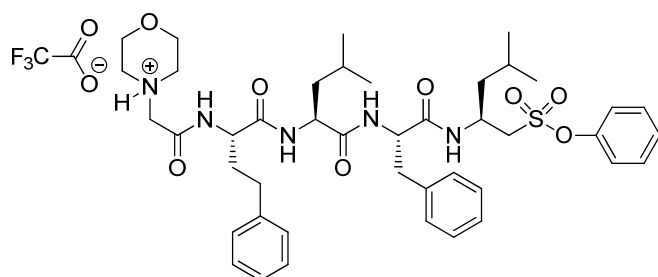
A solution of sulfonyl chloride precursor<sup>[5]</sup> (214.0 mg, 582  $\mu\text{mol}$ ) in  $\text{CH}_2\text{Cl}_2$  (1.90 mL) was cooled down to 0 °C before DiFMU (130 mg, 611  $\mu\text{mol}$ ) was added and the mixture was stirred for 15 min. Afterwards,  $\text{NEt}_3$  (162  $\mu\text{L}$ , 118 mg, 1.16 mmol) was added and the mixture was stirred overnight at RT. Evaporation of the solvent and purification via flash column chromatography (PE  $\rightarrow$  55% EA/PE, v/v) yielded sulfonate **DiFMU-F-A** (208 mg, 383  $\mu\text{mol}$ , 66%) as a light brown solid. **<sup>1</sup>H NMR** (250 MHz,  $\text{CDCl}_3$ ):  $\delta$  = 7.36 - 7.17 (m, 11H), 6.36 (d,  $J$  = 1.4 Hz, 1H), 5.55 (d,  $J$  = 8.2 Hz, 1H), 5.06 (s, 2H), 4.60 – 4.40 (m, 1H), 3.89 (dd,  $J$  = 14.6, 7.1 Hz, 1H), 3.73 (dd,  $J$  = 14.5, 4.8 Hz, 1H), 3.19 - 3.03 (m, 2H), 2.37 (s, 3H) ppm. **<sup>13</sup>C NMR** (63 MHz,  $\text{CDCl}_3$ ):  $\delta$  = 158.1, 155.5, 151.4 (dd,  $J$  = 250.5, 1.9 Hz), 150.9 (t,  $J$  = 2.6 Hz), 143.6 (dd,  $J$  = 258.8, 3.7 Hz), 139.2 (dd,  $J$  = 10.1, 3.0 Hz), 136.2, 129.3, 128.8, 128.4, 128.0, 127.9, 127.2, 119.4 (dd,  $J$  = 8.5, 1.8 Hz), 116.9, 106.3 (dd,  $J$  = 21.6, 4.0 Hz), 66.9, 55.1, 49.2, 39.4, 18.7 ppm. **<sup>19</sup>F NMR** (471 MHz,  $\text{DMSO-d}_6$ ):  $\delta$  = -130.08 (d,  $J$  = 10.6 Hz), -143.47 ppm. **MS** (ESI):  $m/z$ : calcd. for  $\text{C}_{27}\text{H}_{24}\text{F}_2\text{NO}_7\text{S}$  [ $M+\text{H}^+$ ] 544.12; found 543.69.



#### L-Phe-[CH<sub>2</sub>SO<sub>2</sub>]-DiFMU · HCl (DiFMU-F-B)

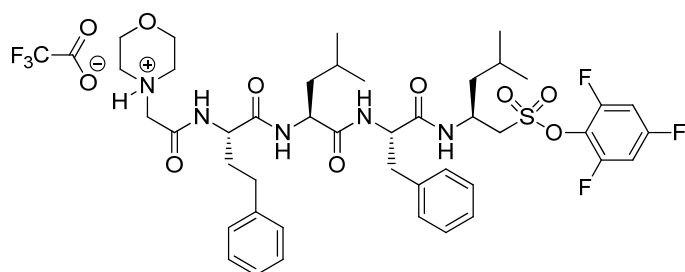
HBr in acetic acid (33%, 1.69 mL, 9.66 mmol, 25.0 eq) was added dropwise to a solution of sulfonate **DiFMU-F-A** (210.0 mg, 386  $\mu\text{mol}$ ) in  $\text{CH}_2\text{Cl}_2$  (4.0 mL) and stirred at RT for 45 min. After concentration *in vacuo* the residue was dissolved in  $\text{H}_2\text{O}$  (4.0 mL) and DOWEX<sup>®</sup> 1X8 (Cl-form, 300 mg) was added to solution. The mixture was stirred for 15 min, the solution was filtered and the residue was washed with  $\text{H}_2\text{O}$ . After lyophilization hydrochloride **DiFMU-F-B** (126 mg, 282  $\mu\text{mol}$ , 73% (crude product)) was obtained as a white powder which was used without further purification in the next step.

## Final coupling of peptidic backbones and sulfonate ester headgroups

**MorphAc-hPhe-Leu-Phe-Leu-ψ-  
[CH<sub>2</sub>SO<sub>2</sub>]-Phenol · TFA (1)**

HATU (20.1 mg, 0.053 mmol) was added to a solution of peptidic backbone **1-b** (30.0 mg, 0.053 mmol) in CH<sub>2</sub>Cl<sub>2</sub> (290 μL) at 0 °C. The reaction mixture was stirred for 20

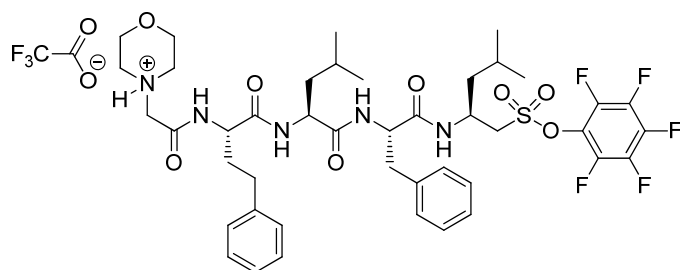
min before adding sulfonate headgroup **Phe-B** (14.1 mg, 0.048 mmol). Afterwards, the reaction mixture was stirred for 10 min at 0 °C and DIPEA (24.4 μL, 0.140 mmol) was added dropwise. The reaction was then allowed to reach RT and was stirred overnight. After evaporation of the solvent the residue was dissolved in DMF (300 μL). Purification by RP HPLC (*t<sub>R</sub>* = 38 min, linear gradient 10 → 100% ACN/H<sub>2</sub>O + 0.1% TFA in 100 min) and subsequent lyophilization yielded **1** (23.0 mg, 0.025 mmol, 53%) as a white powder. **<sup>1</sup>H NMR** (500 MHz, DMSO-*d*<sub>6</sub>): δ = 8.86 (s, 1H), 8.23 – 8.12 (m, 3H), 7.52 – 7.46 (m, 2H), 7.42 – 7.37 (m, 1H), 7.36 – 7.32 (m, 2H), 7.28 (td, *J* = 7.0, 6.6, 5.2 Hz, 2H), 7.22 – 7.07 (m, 8H), 7.06 – 7.01 (m, 1H), 4.39 (dddd, *J* = 39.3, 23.4, 12.2, 6.5 Hz, 5H), 4.14 – 3.68 (m, 10H), 3.57 (dd, *J* = 14.6, 5.5 Hz, 1H), 3.37 (dd, *J* = 14.5, 6.8 Hz, 1H), 3.30 – 3.17 (m, 2H), 2.92 (dd, *J* = 14.1, 5.1 Hz, 1H), 2.77 (dd, *J* = 14.1, 9.3 Hz, 1H), 1.88 (ddt, *J* = 13.2, 10.9, 5.4 Hz, 1H), 1.77 (dddd, *J* = 13.7, 11.0, 8.9, 5.3 Hz, 1H), 1.60 – 1.45 (m, 3H), 1.44 – 1.33 (m, 3H), 0.89 – 0.78 (m, 12H) ppm. **<sup>13</sup>C NMR** (126 MHz, DMSO-*d*<sub>6</sub>): δ = 172.1, 170.8, 158.2, 149.2, 141.8, 138.1, 130.6, 129.4, 128.8, 128.7, 128.4, 127.9, 126.6, 126.4, 122.8, 63.5, 54.7, 54.1, 53.0, 52.2, 51.3, 43.1, 42.9, 41.4, 37.6, 34.7, 31.9, 24.5, 24.2, 23.7, 23.5, 22.2, 21.6 ppm. **HRMS** (ESI): *m/z*: calcd. for C<sub>43</sub>H<sub>60</sub>N<sub>5</sub>O<sub>8</sub>S [*M*+*H*<sup>+</sup>] 806.4157; found 806.4182.

**MorphAc-hPhe-Leu-Phe-Leu-ψ-  
[CH<sub>2</sub>SO<sub>2</sub>]-2,4,6-TFP · TFA (2)**

HATU (20.1 mg, 0.053 mmol) was added to a solution of peptidic backbone **1-b** (30.0 mg, 0.053 mmol) in CH<sub>2</sub>Cl<sub>2</sub> (300 μL) at 0 °C. The reaction mixture was

stirred for 20 min before adding sulfonate headgroup **TFP-B** (16.7 mg, 0.048 mmol). Afterwards, the reaction mixture was stirred for 10 min at 0 °C and DIPEA (24.4 μL, 0.140 mmol) was added dropwise. The reaction was then allowed to reach RT and was

stirred overnight. After evaporation of the solvent the residue was dissolved in DMF (300  $\mu$ L). Purification by RP-HPLC ( $t_R$  = 42 min, linear gradient 10  $\rightarrow$  100% ACN/H<sub>2</sub>O + 0.1% TFA in 100 min) and subsequent lyophilization yielded **2** (9.5 mg, 0.011 mmol, 23%) as a white powder. **<sup>1</sup>H NMR** (500 MHz, DMSO-*d*<sub>6</sub>):  $\delta$  = 8.84 (s, 1H), 8.22 - 8.10 (m, 3H), 7.53 (t, *J* = 8.6 Hz, 2H), 7.29 (t, *J* = 7.6 Hz, 2H), 7.23 - 7.10 (m, 8H), 7.08 - 7.01 (m, 1H), 4.49 - 4.36 (m, 3H), 4.35 - 4.29 (m, 1H), 3.92 - 3.54 (m, 12H), 3.38 - 3.27 (m, 2H), 2.94 (dd, *J* = 14.2, 4.9 Hz, 1H), 2.77 (dd, *J* = 14.2, 9.4 Hz, 1H), 1.93 - 1.83 (m, 1H), 1.82 - 1.73 (m, 1H), 1.60 - 1.48 (m, 3H), 1.42 - 1.33 (m, 3H), 0.89 - 0.76 (m, 12H) ppm. **<sup>13</sup>C NMR** (126 MHz, DMSO-*d*<sub>6</sub>):  $\delta$  = 172.1, 170.8, 170.8, 158.4, 158.2, 156.8, 156.8, 156.7, 156.7, 156.7 (dd, *J* = 16.3, 5.7 Hz), 154.8 (dd, *J* = 16.4, 5.4 Hz), 154.8, 154.8, 154.7, 154.7, 141.8, 138.2, 129.4, 128.8, 128.7, 128.4, 126.6, 126.4, 102.60 (t, *J* = 26.4 Hz), 63.5, 56.2, 54.0, 53.0, 52.3, 51.3, 43.2, 42.9, 41.4, 37.5, 34.7, 31.9, 24.5, 24.2, 23.8, 23.5, 22.2, 21.5 ppm. **<sup>19</sup>F NMR** (471 MHz, DMSO-*d*<sub>6</sub>):  $\delta$  = -110.65 (t, *J* = 4.6 Hz), -124.41 (d, *J* = 5.0 Hz) ppm. **HRMS** (ESI): *m/z*: calcd. for C<sub>43</sub>H<sub>57</sub>F<sub>3</sub>N<sub>5</sub>O<sub>8</sub>S [*M*+*H*<sup>+</sup>] 860.3874; found 860.3903.

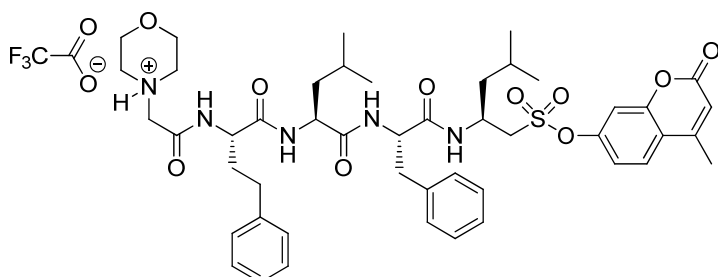


**MorphAc-hPhe-Leu-Phe-Leu- $\psi$ -  
[CH<sub>2</sub>SO<sub>2</sub>]-PFP · TFA (**3**)**

HATU (20.1 mg, 0.053 mmol) was added to a solution of peptidic backbone **1-b** (30.0 mg, 0.053 mmol) in CH<sub>2</sub>Cl<sub>2</sub> (300  $\mu$ L) at 0 °C. The reaction mixture was

stirred for 20 min before adding sulfonate headgroup **PFP-B** (18.5 mg, 0.048 mmol). Afterwards, the reaction mixture was stirred for 10 min at 0 °C and DIPEA (24.4  $\mu$ L, 0.140 mmol) was added dropwise. The reaction was then allowed to reach RT and was stirred overnight. After evaporation of the solvent the residue was dissolved in DMF (300  $\mu$ L). Purification by RP-HPLC ( $t_R$  = 45 min, linear gradient 20  $\rightarrow$  100% ACN/H<sub>2</sub>O + 0.1% TFA in 90 min) and subsequent lyophilization yielded **3** (17.1 mg, 0.017 mmol, 36%) as a white powder. **<sup>1</sup>H NMR** (500 MHz, DMSO-*d*<sub>6</sub>):  $\delta$  = 8.85 (s, 1H), 8.24 - 8.11 (m, 3H), 7.32 - 7.26 (m, 2H), 7.23 - 7.10 (m, 8H), 7.07 - 7.02 (m, 1H), 4.50 - 4.36 (m, 3H), 4.32 (q, *J* = 7.8 Hz, 1H), 4.04 - 3.64 (m, 12H), 3.37 - 3.22 (m, 2H), 2.94 (dd, *J* = 14.2, 4.8 Hz, 1H), 2.77 (dd, *J* = 14.2, 9.5 Hz, 1H), 1.93 - 1.83 (m, 1H), 1.82 - 1.73 (m, 1H), 1.59 - 1.48 (m, 3H), 1.41 - 1.32 (m, 3H), 0.88 - 0.79 (m, 12H) ppm. **<sup>13</sup>C NMR** (126 MHz, DMSO-*d*<sub>6</sub>):  $\delta$  = 172.1, 170.9, 170.8, 158.5, 158.2, 141.8, 138.2, 129.4, 128.8, 128.7, 128.4, 126.6, 126.3, 63.6, 56.3, 54.1, 53.0, 52.3, 51.3, 43.2, 43.0,

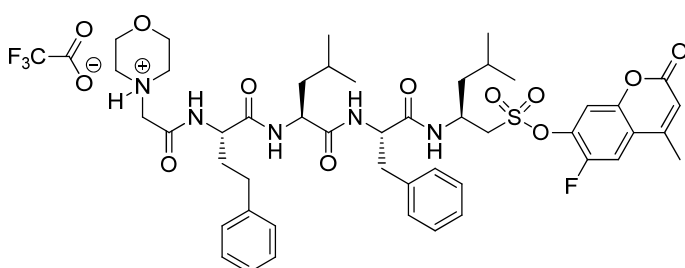
41.4, 37.5, 34.7, 31.9, 24.5, 24.2, 23.8, 23.5, 22.1, 21.5 ppm.  $^{19}\text{F}$  NMR (471 MHz, DMSO- $d_6$ ):  $\delta$  = -154.31 (d,  $J$  = 20.3 Hz), -158.98 (t,  $J$  = 23.3 Hz), -164.61 (t,  $J$  = 21.7 Hz) ppm. HRMS (ESI):  $m/z$ : calcd. for  $\text{C}_{43}\text{H}_{55}\text{F}_5\text{N}_5\text{O}_8\text{S}$  [ $M+\text{H}^+$ ] 896.3686; found 896.3719.



**MorphAc-hPhe-Leu-Phe-Leu- $\psi$ -[CH<sub>2</sub>SO<sub>2</sub>]-MU · TFA (4)**

HATU (33.4 mg, 0.088 mmol) was added to a solution of peptidic backbone **1-b** (49.8 mg, 0.088 mmol) in  $\text{CH}_2\text{Cl}_2$  (470  $\mu\text{L}$ ) at 0 °C. The reaction mixture

was stirred for 20 min before adding sulfonate headgroup **MU-B** (30 mg, 0.080 mmol). Afterwards, the reaction mixture was stirred for 10 min at 0 °C and DIPEA (40.4  $\mu\text{L}$ , 0.231 mmol) was added dropwise. The reaction was then allowed to reach RT and was stirred overnight. After evaporation of the solvent the residue was dissolved in DMF (300  $\mu\text{L}$ ). Purification by RP-HPLC ( $t_{\text{R}}$  = 46 min, linear gradient 10  $\rightarrow$  100% ACN/ $\text{H}_2\text{O}$  + 0.1% TFA in 100 min) and subsequent lyophilization yielded **4** (46.9 mg, 0.048 mmol, 60%) as a white powder.  $^1\text{H}$  NMR (500 MHz, DMSO- $d_6$ ):  $\delta$  = 10.26 (br s, 1H), 8.85 (s, 1H), 8.21 (dd,  $J$  = 13.3, 8.6 Hz, 2H), 8.14 (d,  $J$  = 8.3 Hz, 1H), 7.88 (d,  $J$  = 8.8 Hz, 1H), 7.48 (d,  $J$  = 2.4 Hz, 1H), 7.35 (dd,  $J$  = 8.7, 2.4 Hz, 1H), 7.28 (t,  $J$  = 7.5 Hz, 2H), 7.22 - 7.11 (m, 6H), 7.08 (t,  $J$  = 7.5 Hz, 2H), 7.03 - 6.98 (m, 1H), 6.46 (d,  $J$  = 1.5 Hz, 1H), 4.48 - 4.30 (m, 4H), 4.04 - 3.77 (m, 6H), 3.71 (dd,  $J$  = 14.7, 5.0 Hz, 1H), 3.48 (dd,  $J$  = 14.7, 7.3 Hz, 1H), 3.40 - 3.14 (m, 4H), 2.90 (dd,  $J$  = 14.1, 5.0 Hz, 1H), 2.77 (dd,  $J$  = 14.1, 9.4 Hz, 1H), 2.62 - 2.52 (m, 2H), 2.45 (d,  $J$  = 1.3 Hz, 3H), 1.93 - 1.83 (m, 1H), 1.82 - 1.72 (m, 1H), 1.61 - 1.45 (m, 3H), 1.43 - 1.32 (m, 3H), 0.84 (t,  $J$  = 6.9 Hz, 6H), 0.80 (dd,  $J$  = 6.5, 2.8 Hz, 6H) ppm.  $^{13}\text{C}$  NMR (126 MHz, DMSO- $d_6$ ):  $\delta$  = 172.1, 170.9, 170.8, 159.8, 154.0, 153.2, 151.0, 141.8, 138.1, 129.4, 128.8, 128.7, 128.3, 127.5, 126.6, 126.3, 119.2, 119.2, 114.9, 111.0, 63.5, 55.1, 54.1, 53.0, 52.2, 51.3, 43.2, 43.0, 41.4, 37.5, 34.7, 31.9, 24.5, 24.2, 23.7, 23.5, 22.2, 21.6, 18.7 ppm. HRMS (ESI):  $m/z$ : calcd. for  $\text{C}_{47}\text{H}_{62}\text{N}_5\text{O}_{10}\text{S}$  [ $M+\text{H}^+$ ] 888.4212; found 888.4237.

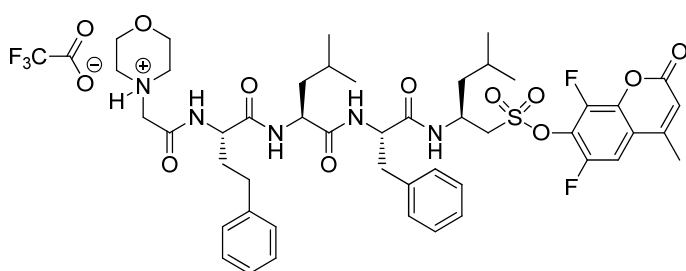


**MorphAc-hPhe-Leu-Phe-Leu- $\psi$ -[CH<sub>2</sub>SO<sub>2</sub>]-FMU · TFA (5)**

HATU (20.13 mg, 0.053 mmol) was added to a solution of peptidic backbone **1-b** (30 mg, 0.045 mmol)



in CH<sub>2</sub>Cl<sub>2</sub> (280 μL) at 0 °C. The reaction mixture was stirred for 20 min before adding sulfonate headgroup **FMU-B** (16.18 mg, 0.041 mmol). Afterwards, the reaction mixture was stirred for 10 min at 0 °C and DIPEA (20.8 μL, 0.119 mmol) was added dropwise. The reaction was then allowed to reach RT and was stirred overnight. After evaporation of the solvent the residue was dissolved in DMF (250 μL). Purification by RP-HPLC (*t<sub>R</sub>* = 31 min, linear gradient 20 → 100% ACN/H<sub>2</sub>O + 0.1% TFA in 90 min) and subsequent lyophilization yielded **5** (12.6 mg, 0.013 mmol, 31%) as a white powder. **<sup>1</sup>H NMR** (500 MHz, DMSO-*d*<sub>6</sub>): δ = 10.24 (br s, 1H), 8.85 (d, *J* = 7.6 Hz, 1H), 8.23 (dd, *J* = 11.5, 8.6 Hz, 2H), 8.14 (d, *J* = 8.2 Hz, 1H), 7.92 (d, *J* = 10.5 Hz, 1H), 7.73 (d, *J* = 6.4 Hz, 1H), 7.33 - 7.26 (m, 2H), 7.21 - 7.12 (m, 6H), 7.11 - 7.04 (m, 2H), 7.02 - 6.96 (m, 1H), 6.52 (d, *J* = 1.4 Hz, 1H), 4.52 - 4.28 (m, 4H), 4.09 - 3.70 (m, 8H), 3.38 - 3.16 (m, 5H), 2.91 (dd, *J* = 14.2, 5.1 Hz, 1H), 2.77 (dd, *J* = 14.1, 9.3 Hz, 1H), 2.67 - 2.52 (m, 2H), 2.43 (d, *J* = 1.3 Hz, 3H), 1.94 - 1.83 (m, 1H), 1.82 - 1.72 (m, 1H), 1.62 - 1.47 (m, 3H), 1.44 - 1.32 (m, 3H), 0.84 (dd, *J* = 6.6, 2.6 Hz, 6H), 0.80 (dd, *J* = 6.5, 1.8 Hz, 6H) ppm. **<sup>13</sup>C NMR** (126 MHz, DMSO-*d*<sub>6</sub>): δ = 172.1, 170.9, 170.8, 159.7, 158.5, 158.3, 152.8, 152.1, 150.2, 149.6, 141.8, 138.5 (d, *J* = 15.1 Hz), 138.1, 129.3, 128.8, 128.7, 128.3, 126.6, 126.4, 120.0, 115.9, 113.6 (d, *J* = 21.7 Hz), 113.3, 63.5, 55.7, 54.1, 53.0, 52.2, 51.3, 43.2, 42.9, 41.4, 37.5, 34.7, 31.9, 24.5, 24.2, 23.7, 23.5, 22.1, 21.6, 18.7 ppm. **<sup>19</sup>F NMR** (471 MHz, DMSO-*d*<sub>6</sub>): δ = -134.64 (dd, *J* = 10.5, 6.6 Hz) ppm. **HRMS** (ESI): *m/z*: calcd. for C<sub>47</sub>H<sub>61</sub>FN<sub>5</sub>O<sub>10</sub>S [*M*+H<sup>+</sup>] 906.4118; found 906.4139.



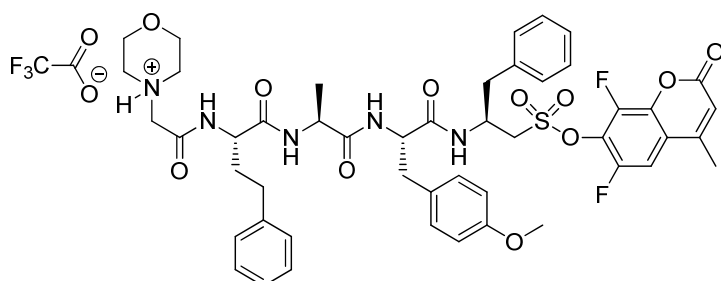
**MorphAc-hPhe-Leu-Phe-Leu-ψ-  
[CH<sub>2</sub>SO<sub>2</sub>]-DiFMU · TFA (6)**

HATU (30.5 mg, 0.080 mmol) was added to a solution of peptidic backbone **1-b** (53.2 mg, 0.080 mmol) in CH<sub>2</sub>Cl<sub>2</sub> (430 μL) at

0 °C. The reaction mixture was stirred for 20 min before adding sulfonate headgroup **DiFMU-B** (30 mg, 0.073 mmol). Afterwards, the reaction mixture was stirred for 10 min at 0 °C and DIPEA (37 μL, 0.211 mmol) was added dropwise. The reaction was then allowed to reach RT and was stirred overnight. After evaporation of the solvent the residue was dissolved in DMF (250 μL). Purification by RP-HPLC (*t<sub>R</sub>* = 39 min, linear gradient 10 → 100% ACN/H<sub>2</sub>O + 0.1% TFA in 100 min) and subsequent lyophilization yielded **6** (35.2 mg, 0.034 mmol, 47%) as a white powder. **<sup>1</sup>H NMR** (500 MHz, DMSO-*d*<sub>6</sub>): δ = 10.22 (s, 1H), 8.84 (s, 1H), 8.24 - 8.10 (m, 3H), 7.83 (dd, *J* = 10.5, 2.0 Hz, 1H), 7.31 - 7.26 (m,

## 5. 20S proteasome inhibitors with fluorescent feedback

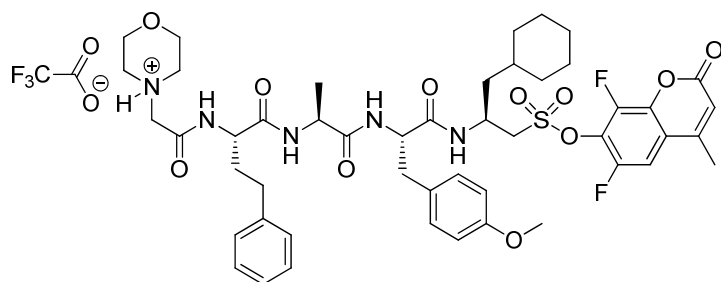
2H), 7.21 – 7.14 (m, 6H), 7.14 – 7.09 (m, 2H), 7.07 – 6.99 (m, 1H), 6.61 (d,  $J = 1.5$  Hz, 1H), 4.52 – 4.42 (m, 2H), 4.41 – 4.35 (m, 1H), 4.32 (q,  $J = 7.9$  Hz, 1H), 4.07 – 3.66 (m, 8H), 3.36 – 3.13 (m, 4H), 2.98 – 2.88 (m, 1H), 2.81 – 2.70 (m, 1H), 2.64 – 2.52 (m, 2H), 2.43 (d,  $J = 1.4$  Hz, 3H), 1.93 – 1.83 (m, 1H), 1.82 – 1.72 (m, 1H), 1.62 – 1.48 (m, 3H), 1.44 – 1.32 (m, 3H), 0.87 – 0.78 (m, 12H) ppm.  $^{13}\text{C}$  NMR (126 MHz, DMSO- $d_6$ ):  $\delta = 172.1$ , 170.9, 170.8, 158.5, 158.3, 158.2, 152.7, 152.1, 150.1, 144.1, 141.7, 139.2, 138.2, 129.4, 128.8, 128.7, 128.4, 126.6, 126.4, 120.0 (d,  $J = 8.9$  Hz), 116.7, 63.5, 56.6, 54.1, 53.0, 52.3, 51.3, 43.3, 42.9, 41.4, 37.5, 34.7, 31.9, 24.5, 24.2, 23.8, 23.5, 22.2, 21.5, 18.8 ppm.  $^{19}\text{F}$  NMR (471 MHz, DMSO- $d_6$ ):  $\delta = -132.51$  (d,  $J = 10.6$  Hz),  $-146.13$  ppm. HRMS (ESI):  $m/z$ : calcd. for  $\text{C}_{47}\text{H}_{60}\text{F}_2\text{N}_5\text{O}_{10}\text{S}$  [ $M+\text{H}^+$ ] 924.4023; found 924.4044.



### MorphAc-hPhe-Ala-Tyr(OMe)- Phe- $\psi$ -[CH<sub>2</sub>SO<sub>2</sub>]-DiFMU (**8**)

HATU (17.14 mg, 0.045 mmol) was added to a solution of peptidic backbone **2-b** (25 mg, 0.045 mmol) in  $\text{CH}_2\text{Cl}_2$  (241  $\mu\text{L}$ ) at 0 °C. The reaction mixture

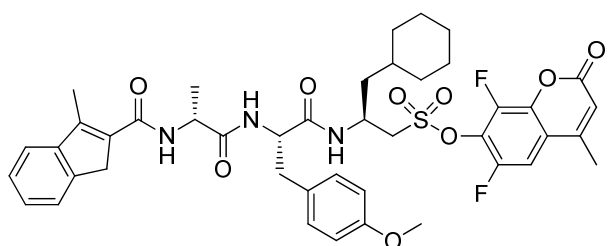
was stirred for 20 min before adding sulfonate headgroup **DiFMU-F-B** (18.3 mg, 0.041 mmol). Afterwards, the reaction mixture was stirred for 10 min at 0 °C and DIPEA (20.8  $\mu\text{L}$ , 0.119 mmol) was added dropwise. The reaction was then allowed to reach RT and was stirred overnight. After evaporation of the solvent the residue was dissolved in DMF (250  $\mu\text{L}$ ). Purification by RP-HPLC ( $t_R = 38$  min, linear gradient 20  $\rightarrow$  100% ACN/ $\text{H}_2\text{O}$  + 0.1% TFA in 90 min) and subsequent lyophilization yielded **8** (14 mg, 0.013 mmol, 32%) as a white powder.  $^1\text{H}$  NMR (500 MHz, DMSO- $d_6$ ):  $\delta = 10.22$  (s, 1H), 8.86 (s, 1H), 8.41 (d,  $J = 8.3$  Hz, 1H), 8.20 (d,  $J = 7.6$  Hz, 1H), 7.95 (d,  $J = 8.3$  Hz, 1H), 7.82 (dd,  $J = 10.5, 2.1$  Hz, 1H), 7.28 – 7.15 (m, 10H), 7.06 (d,  $J = 8.6$  Hz, 2H), 6.70 (d,  $J = 8.6$  Hz, 2H), 6.62 (d,  $J = 1.5$  Hz, 1H), 4.60 – 4.52 (m, 1H), 4.43 – 4.32 (m, 2H), 4.31 – 4.21 (m, 1H), 4.05 – 3.73 (m, 8H), 3.60 (s, 3H), 3.00 – 2.80 (m, 3H), 2.67 – 2.53 (m, 3H), 2.43 (d,  $J = 1.4$  Hz, 4H), 1.97 – 1.86 (m, 1H), 1.86 – 1.77 (m, 1H), 1.13 (d,  $J = 7.1$  Hz, 3H) ppm.  $^{13}\text{C}$  NMR (126 MHz, DMSO- $d_6$ ):  $\delta = 172.2$ , 171.0, 170.7, 158.3, 158.1, 152.7, 141.7, 139.2, 137.5, 130.5, 130.0, 129.7, 128.8, 128.8, 128.7, 127.0, 126.3, 120.1, 116.8, 113.8, 63.6, 55.4, 55.2, 54.5, 52.9, 52.3, 48.5, 46.7, 37.0, 34.6, 31.8, 18.8, 18.7 ppm.  $^{19}\text{F}$  NMR (471 MHz, DMSO- $d_6$ ):  $\delta = -132.54$  (d,  $J = 10.5$  Hz),  $-146.11$  ppm. HRMS (ESI):  $m/z$ : calcd. for  $\text{C}_{48}\text{H}_{54}\text{F}_2\text{N}_5\text{O}_{11}\text{S}$  [ $M+\text{H}^+$ ] 946.3503; found 946.3512.



**MorphAc-hPhe-Ala-Tyr(OMe)-  
3-cyclohexyl-L-Ala-ψ-  
[CH<sub>2</sub>SO<sub>2</sub>]-DiFMU (9)**

HATU (27.8 mg, 73.0 μmol) was added to a solution of peptidic backbone **2-b** (40.5 mg, 73.0 μmol) in CH<sub>2</sub>Cl<sub>2</sub> (390 μL) at

0 °C. The reaction mixture was stirred for 20 min before adding sulfonate headgroup **DiFMU-CyA-B** (30.0 mg, 66.4 μmol). Afterwards, the reaction mixture was stirred for 10 min at 0 °C and DIPEA (33.6 μL, 193 μmol) was added dropwise. The reaction was then allowed to reach RT and was stirred overnight. After evaporation of the solvent the residue was dissolved in DMF (300 μL). Purification by RP-HPLC (*t<sub>R</sub>* = 38 min, linear gradient 20 → 100% ACN/H<sub>2</sub>O + 0.1% TFA in 90 min) and subsequent lyophilization yielded **9** (10.5 mg, 10.01 μmol, 15%) as a white powder. **<sup>1</sup>H NMR** (500 MHz, DMSO-*d*<sub>6</sub>): δ = 10.22 (s, 1H), 8.85 (s, 1H), 8.22 (d, *J* = 7.5 Hz, 1H), 8.18 (d, *J* = 8.6 Hz, 1H), 8.10 (d, *J* = 8.3 Hz, 1H), 7.83 (dd, *J* = 10.5, 2.1 Hz, 1H), 7.30 – 7.23 (m, 2H), 7.20 – 7.13 (m, 3H), 7.10 (d, *J* = 8.7 Hz, 2H), 6.72 (d, *J* = 8.7 Hz, 2H), 6.62 (d, *J* = 1.5 Hz, 1H), 4.53 – 4.44 (m, 1H), 4.43 – 4.33 (m, 2H), 4.29 (p, *J* = 7.2 Hz, 1H), 4.06 – 3.68 (m, 8H), 3.61 (s, 3H), 3.46 – 3.07 (m, 4H), 2.87 (dd, *J* = 14.1, 4.9 Hz, 1H), 2.69 (dd, *J* = 14.1, 9.2 Hz, 1H), 2.60 – 2.52 (m, 2H), 2.43 (d, *J* = 1.4 Hz, 3H), 1.97 – 1.85 (m, 1H), 1.84 – 1.73 (m, 2H), 1.67 – 1.50 (m, 4H), 1.49 – 1.42 (m, 2H), 1.34 – 1.21 (m, 1H), 1.16 (d, *J* = 7.0 Hz, 3H), 1.09 (d, *J* = 10.1 Hz, 3H), 0.95 – 0.84 (m, 1H), 0.81 – 0.68 (m, 1H) ppm. **<sup>13</sup>C NMR** (126 MHz, DMSO-*d*<sub>6</sub>): δ = 172.3, 171.0, 170.7, 158.3, 158.1, 152.7 (t, *J* = 2.1 Hz), 150.2, 144.1, 141.7, 130.5, 130.0, 128.8, 128.7, 126.3, 120.0 (d, *J* = 9.1 Hz), 116.7, 113.8, 108.1 (dd, *J* = 22.0, 4.0 Hz), 63.5, 56.6, 55.2, 54.6, 52.9, 52.3, 48.5, 42.6, 41.5, 36.8, 34.6, 33.9, 33.4, 31.8, 31.8, 26.5, 26.2, 25.9, 18.8, 18.7 ppm. **<sup>19</sup>F NMR** (471 MHz, DMSO-*d*<sub>6</sub>): δ = -132.94, -146.56 ppm. **HRMS** (ESI): *m/z*: calcd. for C<sub>48</sub>H<sub>60</sub>F<sub>2</sub>N<sub>5</sub>O<sub>11</sub>S [*M*+*H*<sup>+</sup>] 952.3973; found 952.3980.



**3-MeIndAc-D-Ala-Tyr(OMe)-3-cyclohexyl-L-Ala-ψ-[CH<sub>2</sub>SO<sub>2</sub>]-DiFMU (7)**

HATU (41.6 mg, 110 μmol) was added to a solution of peptidic backbone **3-b** (46.3 mg, 110 μmol) in CH<sub>2</sub>Cl<sub>2</sub> (590 μL) at 0 °C and stirred for 20 min before adding sulfonate headgroup **DiFMU-CyA-B** (45.0 mg, 100 μmol). The reaction mixture was stirred at 0 °C for 10 min and DIPEA (50.4 μL, 37.3 μg, 289 μmol, 2.90 eq) was added dropwise, then the reaction was allowed to reach RT and was stirred overnight. After evaporation of the solvent the residue was dissolved in DMF (300 μL). Purification by RP-HPLC (*t<sub>R</sub>* = 65 min, linear gradient 20 → 100% ACN/H<sub>2</sub>O + 0.1% TFA in 90 min) and subsequent lyophilization yielded **7** (13.4 mg, 16.3 μmol, 36%) as a white powder. **<sup>1</sup>H NMR** (500 MHz, DMSO-*d*<sub>6</sub>): δ = 8.27 (d, *J* = 8.5 Hz, 1H), 8.15 (d, *J* = 8.7 Hz, 1H), 7.80 – 7.75 (m, 1H), 7.72 (d, *J* = 6.9 Hz, 1H), 7.48 (d, *J* = 7.2 Hz, 2H), 7.36 – 7.29 (m, 2H), 7.12 (d, *J* = 8.2 Hz, 2H), 6.74 (d, *J* = 8.2 Hz, 2H), 6.57 (s, 1H), 4.59 – 4.47 (m, 1H), 4.42 – 4.31 (m, 2H), 3.93 (dd, *J* = 14.5, 4.6 Hz, 1H), 3.77 (dd, *J* = 14.5, 7.7 Hz, 1H), 3.64 (s, 5H), 2.95 (dd, *J* = 14.1, 4.0 Hz, 1H), 2.69 (dd, *J* = 13.9, 10.4 Hz, 1H), 2.41 – 2.38 (m, 6H), 1.81 (d, *J* = 12.5 Hz, 1H), 1.67 – 1.42 (m, 7H), 1.40 – 1.30 (m, 1H), 1.28 – 0.96 (m, 8H), 0.95 – 0.85 (m, 1H), 0.82 – 0.70 (m, 1H) ppm. **<sup>13</sup>C NMR** (126 MHz, DMSO-*d*<sub>6</sub>): δ = 172.8, 171.1, 165.5, 158.9, 158.6, 158.3, 158.2, 152.6, 150.1, 145.7, 142.6, 139.2 (dd, *J* = 9.6, 2.7 Hz), 133.4, 130.6, 130.2, 127.3, 127.0, 124.2, 120.9, 119.9, 116.7, 113.8, 108.1 (dd, *J* = 21.2, 4.7 Hz), 56.5, 55.3, 54.7, 49.1, 42.8, 41.4, 38.6, 36.6, 33.9, 33.4, 31.9, 26.5, 26.2, 25.9, 18.7, 18.5, 12.3 ppm. **<sup>19</sup>F NMR** (471 MHz, DMSO-*d*<sub>6</sub>): δ = -131.69 (d, *J* = 10.7 Hz), -145.31 ppm. **HRMS** (ESI): *m/z*: calcd. for C<sub>43</sub>H<sub>48</sub>F<sub>2</sub>N<sub>3</sub>O<sub>9</sub>S [*M*+*H*<sup>+</sup>] 820.3074; found 820.3089.

## 5.4 References

- [1] M. Groll, T. Clausen, *Curr. Opin. Struct. Biol.* **2003**, *13*, 665–673.
- [2] A. F. Holleman, E. Wiberg, N. Wiberg, *Inorganic Chemistry*, Academic Press San Diego, **2001**.
- [3] A. F. Kisselev, Z. Songyang, A. L. Goldberg, *J. Biol. Chem.* **2000**, *275*, 14831–14837.
- [4] M. L. Stein, H. Cui, P. Beck, C. Dubiella, C. Voss, A. Krüger, B. Schmidt, M. Groll, *Angew. Chem. Int. Ed.* **2014**, *53*, 1679–1683.
- [5] C. Dubiella, H. Cui, M. Gersch, A. J. Brouwer, S. a. Sieber, A. Krüger, R. M. J. Liskamp, M. Groll, *Angew. Chem. Int. Ed.* **2014**, *53*, 11969–11973.
- [6] A. J. Brouwer, A. Jonker, P. Werkhoven, E. Kuo, N. Li, N. Gallastegui, J. Kemmink, B. I. Florea, M. Groll, H. S. Overkleeft, et al., *J. Med. Chem.* **2012**, *55*, 10995–11003.
- [7] R. K. Crossland, W. E. Wells, V. J. Shiner, *J. Am. Chem. Soc.* **1971**, *93*, 4217–4219.
- [8] A. Krantz, L. J. Copp, P. J. Coles, R. a Smith, S. B. Heard, *Biochemistry* **1991**, *30*, 4678–4687.
- [9] J. Bornholdt, K. Wilhemsen, J. Felding, J. Langgaard, *Tetrahedron* **2009**, *65*, 9280–9284.
- [10] J. Habermann, H. Kunz, *Tetrahedron Lett.* **1998**, *39*, 265–268.
- [11] T. B. Phan, M. Breugst, H. Mayr, *Angew. Chem. Int. Ed.* **2006**, *45*, 3869–3874.
- [12] F. Parlati, S. J. Lee, M. Aujay, E. Suzuki, K. Levitsky, J. B. Lorens, D. R. Micklem, P. Ruurs, C. Sylvain, Y. Lu, et al., *Blood* **2009**, *114*, 3439–3447.
- [13] N. Li, C.-L. Kuo, G. Paniagua, H. van den Elst, M. Verdoes, L. I. Willems, W. van der Linden, M. Ruben, E. van Genderen, J. Gubbens, et al., *Nat. Protoc.* **2013**, *8*, 1155–1168.
- [14] C. R. Berkers, M. Verdoes, E. Lichtman, E. Fiebiger, B. M. Kessler, K. C. Anderson, H. L. Ploegh, H. Ovaa, P. J. Galardy, *Nat. Methods* **2005**, *2*, 357–362.
- [15] L. K. Sharma, N. R. Lee, E. R. Jang, B. Lei, C. G. Zhan, W. Lee, K. B. Kim, *ChemBioChem* **2012**, *13*, 1899–1903.
- [16] W. a Sheppard, *J. Am. Chem. Soc.* **1970**, *92*, 5419–5422.
- [17] W. C. Sun, K. R. Gee, R. P. Haugland, *Bioorg. Med. Chem. Lett.* **1998**, *8*, 3107–3110.
- [18] M. L. Stein, H. Cui, P. Beck, C. Dubiella, C. Voss, A. Krüger, M. Groll, *Angew. Chem. Int. Ed.* **2014**, *53*, 1679–1683.
- [19] C. Hedberg, F. J. Dekker, M. Rusch, S. Renner, S. Wetzels, N. Vartak, C. Gerding-Reimers, R. S. Bon, P. I. H. Bastiaens, H. Waldmann, *Angew. Chem. Int. Ed.* **2011**, *50*, 9832–9837.
- [20] S. Welte, K.-H. Baringhaus, W. Schmider, G. Müller, S. Petry, N. Tennagels, *Anal. Biochem.* **2005**, *338*, 32–38.
- [21] K. R. Gee, W. C. Sun, M. K. Bhalgat, R. H. Upson, D. H. Klaubert, K. a Latham, R. P. Haugland, *Anal. Biochem.* **1999**, *273*, 41–48.

## 6 Abbreviations

Å	Ångström
Ac	Acetate/acetyl
ACN	acetonitrile
AMC	7-amino-4-methylcoumarin
AMP	adenosine monophosphate
ATP	adenosine triphosphate
Boc	<i>tert</i> -butyloxycarbonyl
BrAAP	branched chain amino acid preferring
°C	degree Celsius
CA	$\alpha$ -chloroacetamide
Cbz	carboxybenzyl
cCP	constitutive 20S proteasome
CD	cluster of differentiation
CFZ	carfilzomib
ChTL	chymotrypsin-like
CL	caspase-like
CP	core particle
CTL	cytotoxic T-lymphocytes
Da	Dalton
Dab	L-2,4-diaminobutyric acid
Dap	L-2,3-diaminopropionic acid
DiFMU	6,8-difluoro-4-methylumbelliferone
DIPEA	<i>N,N</i> -diisopropylethylamine
DMEM	Dulbecco's modified eagle medium
DMF	<i>N,N</i> -dimethylformamide
DMSO	dimethylsulfoxide
DNA	desoxyribonucleic acid
DUB	deubiquitinating enzymes
EA	ethyl acetate
ELISA	enzyme-linked immunosorbent assay
ER	endoplasmic reticulum
ERAP	endoplasmic reticulum aminopeptidases
ESI	electron spray ionisation
FCS	fetal calf serum
FDA	US Food and Drug Administration
Fmoc	fluoromethyloxycarbonyl
FMU	6-fluoro-4-methylumbelliferone
FPLC	fast protein liquid chromatography
h	hour(s)
HATU	1-[bis(dimethylamino)methylene]-1 <i>H</i> -1,2,3-triazolo[4,5- <i>b</i> ]pyridinium 3-oxid hexafluorophosphate

---

HBr	hydrobromic acid
HCl	hydrochloric acid
HCTU	<i>O</i> -(6-Chlorobenzotriazol-1-yl)- <i>N,N,N',N'</i> -tetramethyluronium hexafluorophosphate
HIC	hydrophobic interaction chromatography
HPLC	high performance liquid chromatography
HRMS	high resolution mass spectrometry
IC <sub>50</sub>	half maximal inhibitory concentration
iCP	20S immunoproteasome
IFN	interferon
IL	interleukin
K	Kelvin
kDa	kilo Dalton
KP	Kernpartikel
MDa	mega Dalton
MECL	multicatalytic endopeptidase complex-like
MeInd	methylindene
MES	2-( <i>N</i> -morpholino)ethanesulfonic acid
MHC	major histocompatibility complex
min	minute(s)
MorphAc	4-morpholinacetyl
MPD	2-methyl-2,4-pentenediol
mRNA	messenger ribonucleic acid
MS	mass spectrometry
MU	4-methylumbelliferone
MW	molecular weight
NF- $\kappa$ B	nuclear factor kappa-light-chain-enhancer of activated B cells
NMR	nuclear magnetic resonance
Ntn	N-terminal nucleophile
LC <sub>50</sub>	median lethal concentration
LG	leaving group
LMP	low-molecular mass polypeptide
LPS	lipopolysaccharides
PA	propionamide
PAGE	polyacrylamide gel electrophoresis
PBS	phosphate buffered saline
PCR	polymerase chain reaction
PDB	protein data bank
PE	petroleum ether
PEG	polyethylene glycol
PFP	pentafluorophenol
pK <sub>a</sub>	logarithmic acid dissociation constant
PPI	pyrophosphate
ppm	parts per million
PSE	peptide sulfonate ester

## 6. Abbreviations

---

PSF	peptido sulfonyl fluoride
PSM	proteasome (prosome, macropain) subunits
PyBOP	(Benzotriazol-1-yloxy)tripyrrolidinophosphonium hexafluorophosphate
rmsd	root mean square deviation
RPMI	Roswell Park Memorial Institute
RP-HPLC	reversed phase high-performance liquid chromatography
RT	room temperature
S	Svedberg
SDS	sodium dodecylsulfate
SLS	Swiss light source
SnAAP	small neutral amino acid preferring
SPPS	solid phase peptide synthesis
Suc	succinyl
TAP	transporter associated with antigen processing
tCP	20S thymoproteasome
TFA	trifluoro acetic acid
TFP	2,4,6-trifluorophenol
THF	tetrahydrofuran
TL	trypsin-like
TLC	thin-layer chromatography
TNF	tumor necrosis factor
$t_R$	retention time
Tris	tris(hydroxymethyl)-aminomethane
Ub	ubiquitin
UPS	ubiquitin-proteasome system
v/v	volume per volume
WT	wild type
w/v	weight per volume
yCP	yeast 20S proteasome
YPD	yeast extract peptone dextrose



## 7 Danksagung

Als erstes möchte ich meinem Betreuer Prof. Dr. Michael Groll für sein großes Vertrauen, seine vielfältige Unterstützung und sein stetes Interesse an meiner Arbeit danken. Dank der interdisziplinären Ausrichtung seines Lehrstuhls konnte ich zusammen mit einem großartigen Team ein Thema in seiner gesamten Komplexität bearbeiten, was mich über Jahre hinweg begeistern konnte. Dabei haben mich das hohe Maß an wissenschaftlicher Freiheit und Kreativität nachhaltig positiv beeinflusst, wofür ich sehr dankbar bin.

Allen Mitgliedern des Lehrstuhls danke ich für die angenehme Atmosphäre und den vielen schönen Erlebnissen bei gemeinsamen Aktivitäten. Besonders meinen Kollegen Haissi Cui, Bastian Bräuning, Philipp Baer, Eva Maria Huber, Marie-Theres Vielberg, Annika Frank, Camille Le Chapelain, Alois Bräuer, Hartmut Rauch und meinen Ex-Kollegen Dr. Philipp Beck, Dr. Ferdinand Alte, Dr. Martin Stein, Dr. Felix Qitterer, Dr. Andrea Kunfermann bin ich zu großem Dank verpflichtet. Ihre hilfreichen Handgriffe, Gespräche und ganz besonders ihr Sinn für Humor haben mir oft Freude bereiten können. Zudem möchte ich meinen Studenten Christian Fetzer, Anna-Lena Späth, Michael Heilmann, Matthias Rotheneder, Josef Braun und besonders Regina Baur für ihre hilfreiche Mitarbeit im Labor danken. Bei Richard Feicht möchte ich mich für die große Unterstützung durch die Vielzahl an Proteinaufreinigungen und Kristallansätze bedanken. Astrid König und Ute Kashoa danke ich für die Unterstützung bei administrativen Angelegenheiten und besonders für das Planen und Organisieren unserer schönen Ausfahrten.

Ebenfalls möchte ich meinen Kooperationspartnern dafür danken, dass sie mir Einblicke in andere Forschungsbereiche gewährt haben und meinen wissenschaftlichen Horizont durch ihre Methodenvielfalt erweitert haben. Nur durch ihr tatkräftiges Mitwirken konnten die komplexen Projekte erst realisiert werden. Dabei möchte ich mich im Besonderen bei Haissi Cui für ihren wertvollen Beitrag zu den Projekten bedanken. Eva Maria Huber danke ich für ihre vorangegangenen Arbeiten und die vielen hilfreichen Ratschläge. Danken möchte ich auch Prof. Achim Krüger, Dr. Malte Gersch, Prof. Dr. Stephan Sieber und Prof. Dr. Rob Liskamp und Florian Praetorius. Dr. Christine Groß und Dr. Sarah Krüger von der bayrischen Patentallianz danke ich für ihre freundliche und kompetente Unterstützung beim Verfassen der Patentanmeldung.

Abschließend möchte ich mich bei meiner Familie und meinen Freunden für die bedingungslose Unterstützung bedanken die diese Arbeit erst ermöglicht hat.



## **8 Declaration**

I, Christian Dubiella, hereby declare that I independently prepared the present thesis, using only the references and resources stated. This work has not been submitted to any examination board yet. Parts of this work have been or will be published in scientific journals.

Munich, 1.12.2015